INSIGHTS INTO THE BASIS FOR ATRIAL ELECTROPHYSIOLOGICAL REMODELLING AND ARRHYTHMOGENESIS IN HYPERTENSIVE HEART DISEASE, AGEING, AND FRAILTY

by

Hailey Janice Jansen

Submitted in partial fulfilment of the requirements
for the degree of Doctor of Philosophy

at

Dalhousie University
Halifax, Nova Scotia
November 2017

TABLE OF CONTENTS

LIST OF TABLES

LIST OF FIGURES

ABSTRACT

Atrial fibrillation (AF) is a major complication in heart disease and is linked to alterations in Angiotensin II (Ang II) signalling; however, the effects of Ang II on atrial electrophysiology is poorly understood. Natriuretic peptides (NPs) are a family of cardioprotective hormones that elicit their effects by binding to NP receptors denoted NPR-A, NPR-B, and NPR-C; however, their role in atrial arrhythmias and heart disease is poorly understood. In addition, the prevalence of cardiovascular disease increases with age; however, individuals age at different rates such that overall health status varies from fit to frail. Accordingly, the goals of this thesis were to characterize the effects of Ang II treatment on atrial electrophysiology and determine the role of NPR-C in modulating disease progression. The last goal of this thesis was to determine the effects of age and frailty on cardiac function *in vivo.* Ang II treated wildtype mice had an increased susceptibility to AF. Patch-clamp studies revealed Ang II treatment was associated with distinct patterns of electrical remodelling in right and left atrial myocytes. Ang II treatment in NPR-$C^{-/-}$ mice resulted in a more severe disease phenotype. Electrical remodelling was not different in right atrial myocytes and worsened in left atrial myocytes from Ang II treated NPR-$C^{-/-}$ vs. NPR-$C^{+/+}$ mice. Strikingly, mice co-treated with Ang II and cANF (a selective NPR-C agonist) had improvements in *in vivo* atrial function and a reduced susceptibility to AF. Electrical remodelling was normalized in Ang II with cANF treated right, but not left, atrial myocytes. There is a decline in SAN and atrial function with chronological age. By quantifying frailty (overall health status), this thesis demonstrates SAN and atrial function are correlated with frailty. Collectively, these findings demonstrate Ang II treatment is associated with distinct patterns of electrical remodelling in atrial myocytes and NPR-C plays a critical role in atrial disease progression. In fact, enhanced NPR-C signalling can be used as a therapeutic target for the treatment and prevention of AF. Frailty can be used as a powerful tool to predict SAN and atrial function, and should be considered when treating patients with cardiac disease.

LIST OF ABBREVIATIONS USED

4-AP	4-aminopyradine
ACE	Angiotensin converting enzyme
AERP	Atrial effective refractory period
AF	Atrial fibrillation
Ang II	Angiotensin II
ANOVA	Analysis of variance
ANP	Atrial natriuretic peptide
AP	Action potential
APD	Action potential duration
APD_{50}	Action potential duration at 50% repolarization
APD_{70}	Action potential duration at 70% repolarization
APD_{90}	Action potential duration at 90% repolarization
AT1R	Angiotensin type I receptor
AV	Atrioventricular
AVERP	Atrioventricular node effective refractory period
$BaCl_2$	Barium chloride
BNP	B-type natriuretic peptide
BSA	Bovine serum albumin
Ca^{2+}	Calcium
CaMKII	Ca^{2+}/calmodulin-dependent kinase II
cAMP	Cyclic adenosine monophosphate
cANF	$cANF_{4-23}$

Ca_V	Voltage-gated calcium channel
cGMP	Cyclic guanosine monophosphate
CNP	C-type natriuretic peptide
cSNRT	Corrected sinoatrial node recovery time
DAD	Delayed afterdepolarization
DAG	Diacylglycerol
DNP	*Dendroaspis* natriuretic peptide
DPP6	Diaminopeptidyl transferase-like protein 6
EAD	Early afterdepolarization
ECG	Electrocardiogram
ERK	Extracellular signal regulated kinase
ERP	Effective refractory period
ET	Endothelin
FGF	Fibroblast growth factor
FI	Frailty index
G	Chord conductance
GAPDH	Glyceraldehyde 3-phosphate dehydrogenase
$G_{i/o}$	Inhibitory G protein
GIRK	G protein inward rectifier potassium channel
G_{max}	Maximum conductance
G_s	Stimulatory G protein
HCN	Hyperpolarization-activated cyclic-nucleotide gated channel
I-V	Current-voltage

$I_{Ca,L}$	L-type calcium current
$I_{Ca,T}$	T-type calcium current
I_f	Hyperpolarization activated current
I_K	Potassium current
I_{K1}	Inward rectifier potassium current
I_{KAch}	Acetylcholine-sensitive potassium current
I_{Kr}	Rapidly activating delayed rectifier potassium current
I_{Ks}	Slowly activating delayed rectifier potassium current
I_{Kslow}	Slow inactivating potassium current
I_{Kss}	Steady-state non-inactivating outward potassium current
I_{Kur}	Ultra-rapid delayed rectifier potassium current
I_{Na}	Sodium current
I_{NCX}	Na^+/Ca^{2+} exchanger
IGF-1	Insulin-like growth factor 1
IP_3	Inositol triphosphate
I_{to}	Transient outward potassium current
JAK2	Janus kinase 2
k	Slope factor
K^+	Potassium
K_{2P}	Two-pore-domain potassium channel
KB	Kraft-Brühe
KChIP2	K_V channel interacting protein
K_{ir}	Inward rectifier potassium channel

K_V	Voltage-gated potassium channels
MAPK	Mitogen-activated protein kinase
Mg^{2+}	Magnesium
MI	Myocardial infarction
MiRP	MinkK related peptide
MMP	Matrix metalloproteinase
Na^+	Sodium
Na_V	Voltage-gated sodium channel
NF-κβ	Nuclear factor-kappa β
NFAT	Nuclear factor of activated T cells
NP	Natriuretic peptide
NPR	Natriuretic peptide receptor
NPR-A	Natriuretic peptide receptor A
NPR-B	Natriuretic peptide receptor B
NPR-C	Natriuretic peptide receptor C
PDE	Phosphodiesterase
PIP_2	Phosphatidyl inositol
PKA	Protein kinase A
PKC	Protein kinase C
PKG	Protein kinase G
PLC_β	Phospholipase C, β isoform
RAS	Renin-angiotensin system
RMP	Resting membrane potential

SAN	Sinoatrial node
SERCA	Sarcoplasmic reticulum Ca^{2+}-ATPase
SNRT	Sinoatrial node recovery time
TGF-β1	Transforming growth factor β1
TIMP	Tissue inhibitor of metalloproteinase
$V_{1/2(act)}$	Voltage required for 50% channel activation
VERP	Ventricular effective refractory period
V_{max}	Action potential upstroke velocity

ACKNOWLEDGEMENTS

First and foremost, I would like to extend my most sincere thanks to my supervisor Dr. Robert Rose. Thank you for the opportunity to pursue my doctoral training in your laboratory. Words alone could never express how grateful I am for your patience, guidance, help, encouragement, and mentorship over the last four years. Thank you for the opportunity to work on not only my thesis project, but to collaborate on other projects and scientific endeavors. I will undoubtedly cherish this experience for a lifetime.

I am eternally grateful to my committee members Dr. Susan Howlett and Dr. T. Alexander Quinn. Thank you for your insight, feedback, support, and encouragement throughout the years. I would also like to extend my thanks to Dr. Céline Fiset for being my external examiner.

Research advances best when individuals are part of an entangled network of scientists working together to unravel the mysteries behind a given series of questions. According, I would like to extend my appreciation and thanks to the current and former members of the Rose laboratory. In particular, I would like to thank Sara Rafferty for your friendship, help, support, and encouragement over the years, and for always being there to talk things through with. I would also like to thank Dr. Motahareh Moghtadaei, Dr. Iuliia Polina, Dr. Oleg Bogachev, Martin Mackasey, Kimberly Vella, and Loryn Bohne for your friendship and support.

I would also like to thank the members of the Howlett laboratory and the Cardiovascular Research Group for your support and help over the years. In addition, I would like to thank our collaborators and the Department of Physiology and Biophysics. In particular, I would like to thank Dr. Jiansong Qi for your friendship and mentorship and Dr. Yassine El Hiani for your many words of wisdom and encouragement over the years. I would also like to extend my thanks the members of the Physiology and Biophysics office for their assistance.

I am incredibly grateful for the funding I have personally received and the numerous grants that fund the Rose laboratory, without which these studies would not be possible. I was personally awarded with the Dalhousie Medical Research Foundation MacDonald Graduate Studentship 2016-2017 and a Nova Scotia Graduate Scholarship.

Lastly, to my closest friends and my loving family, to whom I express heartfelt thanks. To my parents, Kathleen and Derk, to Quinton and Patricia and your two beautiful daughters, and to Norman and Charmaine. Words alone could never encapsulate my appreciation and gratitude. Thank you for being my pillar of support when I needed it most and for being there to share my accomplishments with, no matter how small. Thank you for always believing in me and helping me achieve my goals. And in loving memory of Fritzy, whose own struggle with heart disease taught me in unimaginable ways the importance of cardiovascular research for both the patient and their loved ones, and why it's important to never give up.

CHAPTER 1
INTRODUCTION

1.1. Cardiac Electrophysiology

1.1.1. Cardiac Conduction and the Electrocardiogram

The cardiac conduction system is a series of highly specialized tissues in the heart that are responsible for the coordination of the heartbeat. There are three components to the cardiac conduction system including the sinoatrial node (SAN), the atrioventricular (AV) node, and the His-Purkinje system (Boyett, 2009; Dobrzynski *et al.*, 2013). The His-Purkinje system consists of the bundle of His, the bundle branches, and the Purkinje fibres. Electrical impulses propagate throughout the conduction system and spread across the atrial or ventricular myocardium between adjacent cells via gap junctions (Bartos *et al.*, 2015). This results in the rhythmic and coordinated contraction of the atria and ventricles. Myocytes within the cardiac conduction system display automaticity, with SAN myocytes demonstrating the highest level of automaticity; therefore, the SAN normally functions as the primary pacemaker of the heart. Abnormal activity in any of these regions can result in cardiac arrhythmias (Titus, 1973; Boyett, 2009; Dobrzynski *et al.*, 2013).

Under normal conditions, the heartbeat is initiated in the SAN and impulses propagate through the atrial myocardium where they activate the AV node. The AV node functions as the gateway to the ventricles as impulses traveling throughout the atrial myocardium must pass through the AV node in order to excite the His-Purkinje system (Boyett, 2009; Dobrzynski *et al.*, 2013). Once the His-Purkinje system is excited, the depolarizing wave spreads throughout the ventricular myocardium, ultimately resulting in ventricular contraction. Conduction in the AV node is slower than the atrial myocardium which results in a delay in impulse propagation to the His-Purkinje system. Functionally, this allows for sufficient filling of the ventricles before they contract (Boyett, 2009; Dobrzynski *et al.*, 2013).

In 1902 Willem Einthoven used a string galvanometer to record the electrical activities of the heart and revolutionized the field of cardiology. The electrocardiogram (ECG) is a powerful tool used by researchers and clinicians to gain valuable insight into electrical activities of heart (Fye, 1994; Barold, 2002; Becker, 2006; Woodrow, 2009). It should be noted that the electrical signals generated by the components of the cardiac conduction system are too small to be detected on a surface ECG and therefore deflections observed are representative of the electrical activity generated in the atrial and ventricular myocardium (Becker, 2006). Fig. 1.1 illustrates a representative mouse ECG with intervals and waves labelled. The first deflection observed on the ECG is the P wave and signifies depolarization of the atria (Fedorov *et al.*, 2012). Depolarization of the ventricular myocardium is represented by the QRS complex and ventricular repolarization by the T wave. The P-R interval can be used to assess conduction through the AV node as impulses must pass through the AV node to excite the ventricular myocardium (Becker, 2006; Woodrow, 2009). Furthermore, the isoelectric waveform between the P wave and QRS complex correlates with the slowing of conduction elicited by the AV node. Alterations to the electrical activity in the heart will ultimately manifest as abnormalities on ECG recordings.

1.1.2. The Sinoatrial Node

The SAN is the natural pacemaker of the heart and is located adjacent to the cristae terminalis within the intercaval region of the right atrium (Keith and Flack, 1907; Boyett *et al.*; 2003, Dobrzynski *et al.*, 2007; Liu *et al.*, 2007). The SAN is a heterogeneous structure that can be divided into the SAN center and the SAN periphery (Dobrzynski *et al.*, 2007; Jansen *et al.*, 2017a). Structurally, the SAN is comprised of SAN myocytes that are embedded in a network of connective tissue, blood vessels, and adipose tissue, which function to insulate the SAN from the surrounding atrial myocardium (Opthof, 1988; Boyett *et al.*, 2003; Dobrzynski *et al.*, 2007; Chandler *et al.*, 2009; Fedorov *et al.*, 2009; Fedorov *et al.*, 2012). The mouse SAN is comma shaped with a densely packed head region located near the superior vena cava and a loosely packed tail that runs adjacent to the cristae terminalis. In addition, the mouse SAN contains

Figure 1.1. Representative mouse ECG illustrating standard ECG parameters measured in a surface ECG recording.

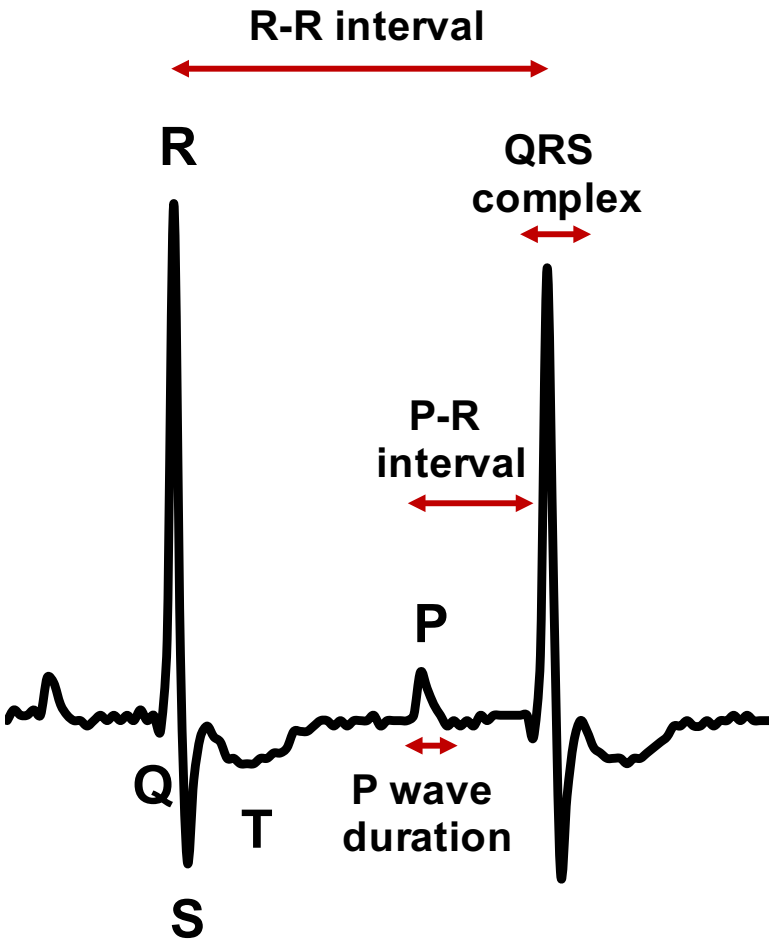

Figure 1.1

finger-like projections that extend into the surrounding atrial myocardium (Liu *et al.*, 2007).

The quintessential feature of SAN myocytes is the ability to generate spontaneous action potentials (APs), which initiate each heartbeat. These APs are characterized by a slow diastolic depolarization phase that occurs between successive APs and functions to gradually depolarize the cell until the threshold required to generate an AP is met (Mangoni and Nargeot, 2008). The diastolic depolarization slope is a major determinate of AP firing rate. Multiple ion currents contribute to the diastolic depolarization slope, including the hyperpolarization-activated current (I_f) and the L-type ($I_{Ca,L}$) and T-type ($I_{Ca,T}$) calcium currents as well as sarcoplasmic reticulum calcium (Ca^{2+}) release (Mangoni *et al.*, 2006; Mangoni and Nargeot, 2008). The initial breakthrough of electrical activity occurs at the leading pacemaker site (Dobrzynski *et al.*, 2007; Mangoni and Nargeot, 2008). It is estimated that the leading pacemaker site accounts for roughly 1% of the SAN in the rabbit heart (Bleeker *et al.*, 1980; Kodama and Boyett, 1985). The electrical signals generated here propagate towards the periphery of the SAN at the cristae terminalis and subsequently excite the atrial myocardium at distinct exit pathways (Fedorov *et al.*, 2012; Csepe *et al.*, 2015).

In the human and canine heart, excitation of the atrial myocardium occurs at distinct SAN conduction pathways (Fedorov *et al.*, 2012). The human and canine SAN is a three-dimensional structure that is 12-20 mm long and 2-6 mm wide and is insulated by structural and functional barriers that protect the SAN from the hyperpolarized atrial myocardium (Csepe *et al.*, 2015). This consists of a network of fat, connective tissue, and coronary arteries (Fedorov *et al.*, 2009; Fedorov *et al.*, 2012; Csepe *et al.,* 2015). Multiple SAN exit pathways have been identified and are located at the superior and inferior regions of the SAN. These exit pathways extend into the atrial myocardium and form SAN conduction pathways. Electrical activity originating in SAN pacemaker cells propagates throughout the SAN and into the SAN conduction pathways where the atrial myocardium is depolarized. Failure to excite the atrial myocardium at these regions results in SAN exit block (Fedorov *et al.*, 2009; Fedorov *et al.*, 2010; Fedorov *et al.*, 2012; Csepe *et al.*, 2015).

SAN dysfunction, also referred to as sick sinus syndrome, refers to the inability of the SAN to sustain heart rates sufficient for the physiological demands of an individual. Clinically, patients with SAN dysfunction present with bradycardia, an increased sinoatrial node recovery time (SNRT), sinus pauses, sinus arrest, syncope, and fatigue (Dobrzynski *et al.*, 2007; Bartos *et al.*, 2015; Choudhury *et al.*, 2015; Monfredi and Boyett, 2015). Furthermore, patients with SAN dysfunction are at increased risk for developing supraventricular arrhythmias, including atrial fibrillation (AF) (Choudhury *et al.*, 2015; Monfredi and Boyett, 2015). SAN dysfunction can be congenital or acquired and is the leading cause for pacemaker implantation (Dobrzynski *et al.*, 2007; Bartos *et al.*, 2015; Csepe *et al.*, 2015; Monfredi and Boyett, 2015).

SAN dysfunction arises when the delicate balance between SAN structure and electrophysiological function is compromised. In the healthy heart, specific patterns of collagen deposition function to electrically insulate the SAN from the surrounding atrial myocardium (Csepe *et al.*, 2015). However, in SAN dysfunction, increased levels of fibrosis results in slowed conduction across the SAN that can lead to SAN pauses and exit block (Csepe *et al.*, 2015). Electrical remodelling can also contribute to SAN dysfunction (Dobrzynski *et al.*, 2007; Morris and Kalman, 2014; Bartos *et al.*, 2015; Choudhury *et al.*, 2015). Reductions in hyperpolarization-activated cyclic-nucleotide gated (HCN) channel expression and I_f density have been demonstrated to occur with increasing age and in the presence of heart failure and AF (Morris and Kalman, 2014; Choudhury *et al.*, 2015). This results in a reduction in the automaticity of SAN myocytes, reduced AP firing rate, and in turn a reduction in heart rate. In addition, idiopathic SAN dysfunction is associated with a reduction in sodium current (I_{Na}) density at the periphery of the SAN. This results in slowed diastolic depolarization at the periphery of the SAN and is associated with SAN exit block (Morris and Kalman, 2014; Choudhury *et al.*, 2015; John and Kumar, 2016).

1.1.3. Autonomic Nervous System Regulation of Heart Rate

The SAN is highly innervated and its activity can be modulated by the release of neurotransmitters (Mangoni and Nargeot, 2008; Pauza *et al.*, 2013; Pauza *et al.*, 2014).

The autonomic nervous system is divided into two branches, the sympathetic nervous system and the parasympathetic nervous system (Mangoni and Nargeot, 2008). The sympathetic nervous system elicits a positive chronotropic effect whereas the parasympathetic nervous system elicits a negative chronotropic effect (Mangoni *et al.*, 2006). Thus, the resulting heart rate of an individual is based on the intrinsic function of the SAN as well as the interplay between the sympathetic and parasympathetic nervous systems.

The sympathetic nervous system increases heart rate through the release of catecholamines that activate β-adrenergic receptors. β-adrenergic receptors are coupled to stimulatory G proteins (G_s) and upon activation results in an increase in adenylyl cyclase activity (Mangoni and Nargeot, 2008; Triposkiadis *et al.*, 2009). Enhanced adenylyl cyclase activity increases intracellular cyclic adenosine monophosphate (cAMP) levels and activates protein kinase A (PKA). cAMP directly binds to HCN channels and produces a positive shift in the I_f activation curve that increases I_f. This in turn increases the diastolic depolarization slope and spontaneous firing rate of APs in SAN myocytes (DiFrancesco and Tortora, 1991; Irisawa *et al.*, 1993; Accili *et al.*, 2002; Mangoni and Nargeot, 2008). Furthermore, PKA phosphorylation of L-type calcium channels following β-adrenergic stimulation results in increased $I_{Ca,L}$ which can also increase diastolic depolarization slope and AP firing rate (Mangoni *et al.*, 2006; Mangoni and Nargeot, 2008). PKA targets a number of other proteins including ryanodine receptors, phospholamban, and troponin I (Triposkiadis *et al.*, 2009). Collectively, these downstream effects of β-adrenergic stimulation result in a positive chronotropic effect.

In contrast, heart rate is decreased following parasympathetic nervous system stimulation and the subsequent release of acetylcholine (Mangoni and Nargeot, 2008; Bartos *et al.*, 2015; Franciosi *et al.*, 2017). Acetylcholine binds to muscarinic receptors and results in the activation of inhibitory G proteins ($G_{i/o}$) that inhibit adenylyl cyclase activity and reduce intracellular cAMP (Irisawa *et al.*, 1993; Mangoni and Nargeot, 2008). In isolated SAN myocytes, the reduction in cAMP levels results in a negative shift in the activation curve for I_f and in turn a reduction in I_f (DiFrancesco and Borer, 2007; Mangoni and Nargeot, 2008; DiFrancesco, 2010). In addition, reduced intracellular

cAMP levels are associated with reductions in $I_{Ca,L}$ and sarcoplasmic reticulum Ca^{2+} release. Combined, these reductions decrease the diastolic depolarization slope and spontaneous AP frequency, ultimately reducing heart rate (Mangoni and Nargeot, 2008). Furthermore, the βγ subunits of $G_{i/o}$ proteins activate the G protein inward rectifier potassium (GIRK) channels that mediate I_{KACh} currents (Mangoni and Nargeot, 2008). Increased I_{KACh} results in a reduction in the diastolic depolarization slope and hyperpolarization of the maximum diastolic potential in SAN myocytes (Mangoni *et al.*, 2006). This results in slowing of spontaneous AP firing frequency. Combined, these effects demonstrate that stimulation of the parasympathetic nervous system produces a negative chronotropic effect.

1.2. Atrial Electrophysiology

1.2.1. The Cardiac Action Potential

The orchestrated movement of ions across the cellular membrane gives rise to the AP. There are five phases to the AP waveform, each of which is governed by different ion currents and designated a number from 0 to 4. A schematic representation of a mouse atrial AP is presented in Fig. 1.2. The AP is a key determinant of cardiomyocyte electrophysiology and represents membrane potential as a function of time (Nattel *et al.*, 2007). Accordingly, alterations in AP morphology at the different phases gives powerful insight into underlying ion channel function.

Phase 0 of the AP is the rapid depolarization phase. Depolarization is initiated when a depolarizing stimulus exceeds the threshold for the cell, which is at approximately -60 mV. Phase 0 of the AP is characterized by a rapid influx of sodium current (I_{Na}) (Nattel *et al.*, 2007; Grant, 2009; Iwasaki *et al.*, 2011). Phase 1 of the AP is the early repolarization phase. During this time, Na^+ channels are inactivated and the transient outward potassium current (I_{to}) is activated. This results in a rapid efflux of K^+ from the cell (Nerbonne and Kass, 2005; Nattel *et al.*, 2007; Schmitt *et al.*, 2014). Phase 2 of the AP is the plateau phase and is determined by the delicate balance of inward Ca^{2+} currents and outward K^+

Figure 1.2. Action potential waveform and underlying ion currents in mouse atrial myocytes.

Different phases of the AP are shown in red and adjacent labels represent the underlying ion currents responsible for that portion of the AP. Abbreviations: $I_{Ca,L}$, L-type calcium current; I_{K1}, inward rectifier potassium current; I_{Kslow}, slow inactivating potassium current; I_{Kss}, steady-state non-inactivating outward potassium current; I_{Kur}, ultra-rapid delayed rectifier potassium current; I_{Na}, sodium current; I_{to}, transient outward potassium current

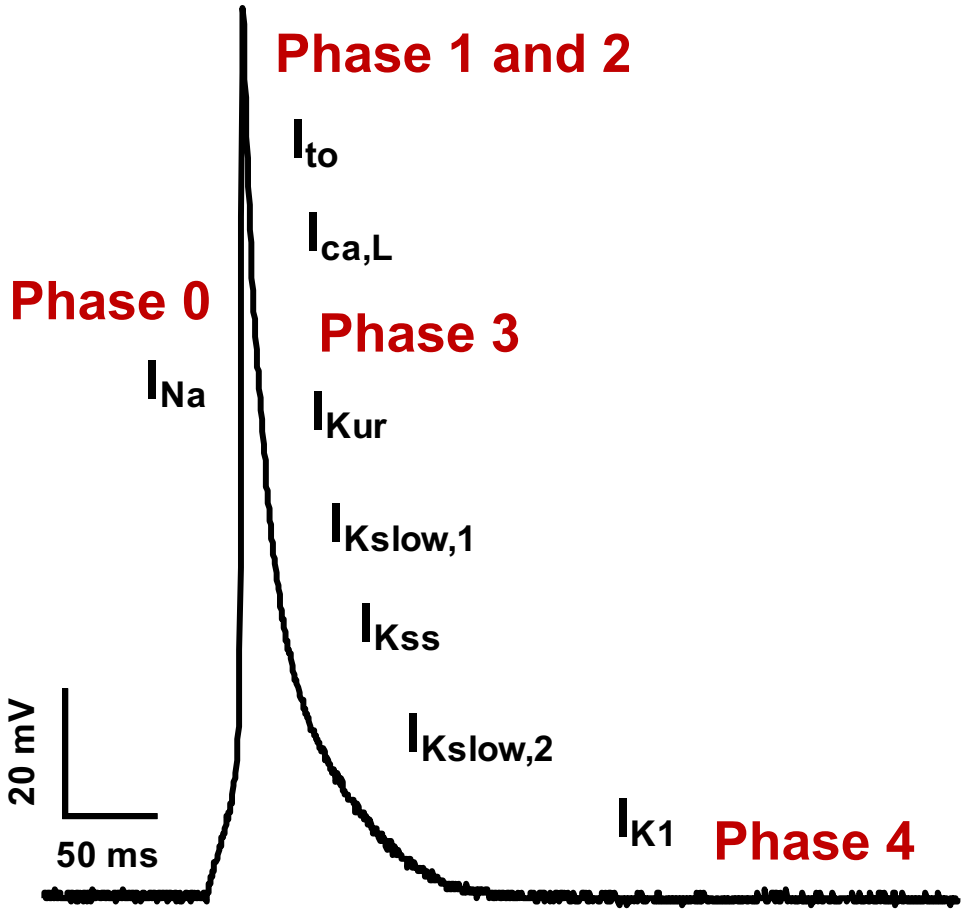
Phase 1 and 2
I_{to}
$I_{ca,L}$
Phase 0
Phase 3
I_{Na}
I_{Kur}
$I_{Kslow,1}$
I_{Kss}
$I_{Kslow,2}$
I_{K1}
Phase 4
20 mV
50 ms

Figure 1.2

currents (Nattel *et al.*, 2007; Grant *et al.* 2009; Schmitt *et al.*, 2014). Mouse atrial myocytes lack a clear plateau phase, which is attributed to high I_{to} densities and is important in maintaining high heart rates observed in mice (Niwa and Nerbonne, 2010). AP repolarization occurs in phase 3 of the AP. During this phase Ca^{2+} channels are inactivated and K^+ is extruded from the cell by multiple repolarizing K^+ currents. This ultimately restores the resting membrane potential to approximately -80 mV, which is phase 4 of the AP (Grant *et al.*, 2009).

1.2.2. Voltage-Gated Sodium Channels

Voltage-gated sodium channels (Na_V) are essential for electrical impulse propagation and are responsible for phase 0 of the AP. *SCN5a* encodes the pore forming α-subunit $Na_V1.5$, which is the main cardiac isoform responsible for sodium current (I_{Na}) (Schmitt *et al.*, 2014; Veerman *et al.*, 2015). *SCN5a* is a large and highly conserved gene that is expressed in many species including mice, humans, platypus, and birds (Veerman *et al.*, 2015). $Na_V1.5$ expression is higher in the working myocardium compared to the cardiac conduction system, which is consistent with the faster AP upstroke velocity and conduction velocity in the atria and ventricles (Schram *et al.*, 2002; Bartos *et al.*, 2015). Both the AP upstroke velocity and conduction velocity depend on the availability of $Na_V1.5$, which is the number of channels in the closed, but activatable state (Abriel, 2007).

Structurally, $Na_V1.5$ contains four homologous domains (DI-DIV) that are connected by intracellular linker loops (Abriel, 2010; Rook *et al.*, 2012; Veerman *et al.*, 2015). Each domain consists of six transmembrane segments denoted S1-S6, of which S4 functions as a voltage sensor that is required for activation and the Na^+ conducting pore is lined by S5 and S6. $Na_V1.5$ is part of a macromolecular complex that includes one or two β-subunits that each contain one transmembrane domain. These β-subunits function to modulate the biophysical properties of $Na_V1.5$ and are involved in membrane trafficking (Abriel, 2010; Veerman *et al.*, 2015). In addition, $Na_V1.5$ has numerous interacting proteins, including calmodulin, Ca^{2+}/calmodulin-dependent kinase II (CaMKII), Ankyrin-G, fibroblast growth factor homologous factor 1B, Nedd4-like ubiquitin ligases, and

syntrophin (Abriel, 2010; Rook *et al.*, 2012). These interacting proteins can further modulate $Na_V1.5$ activity.

Sodium channels exhibit voltage-dependent activation and therefore require a depolarizing current to open. In the atrium, this depolarizing current comes from adjacent cells coupled to each other by gap junctions. When a stimulus threshold is achieved, $Na_V1.5$ channels experience a conformational change, which results in a rapid influx of Na^+ ions for < 1ms (Veerman *et al.*, 2015). Almost immediately, fast inactivation of $Na_V1.5$ occurs and is characterized by a conformational change where the intracellular loop between DIII and DIV functions as a lid that occludes the channel pore (Grant, 2009; Veerman *et al.*, 2015; Ahern *et al.*, 2016). However, fast inactivation does not completely inactivate the channel, resulting in a persistent current that accounts for up to 1% of I_{Na} (Nerbonne and Kass, 2005; Schmitt *et al.*, 2014; Makielski, 2016). Late I_{Na} can persist during the AP plateau and slow AP repolarization, ultimately prolonging the AP (Zaza *et al.*, 2008; Belardinelli et el, 2015; Makielski, 2016).

1.2.3. Voltage-Gated Calcium Channels

Ca^{2+} plays pivotal role in a number of intracellular processes, including excitation-contraction coupling, regulation of enzyme activity, and regulating gene transcription (Caterall, 2011). The L-type calcium channels are critical for Ca^{2+} entry into the cell from the extracellular space. L-type calcium channels are heteromultimeric complexes consisting of pore forming α1-subunits and several accessory subunits. The heart expresses two α1-subunits, $Ca_V1.2$ and $Ca_V1.3$, which are encoded by *CACNA1c* and *CACNA1d*, respectively (Bodi *et al.*, 2005; Zhang *et al.*, 2005). $Ca_V1.2$ is expressed throughout the different regions of the heart whereas $Ca_V1.3$ is expressed in the SAN and atria (Mangoni *et al.*, 2003; Zhang *et al.*, 2005; Mangoni *et al.*, 2006; Tellez *et al.*, 2006).

Structurally, α1-subunits contain of four domains, DI-DIV, each with six transmembrane segments (S1-S6) that are connected by intracellular linkers. Each α1-subunit contains an ion selective pore lined by S5 and S6, a voltage sensor at S4, gating machinery, and binding sites for second messengers (Catterall, 2000; Bodi *et al.*, 2005).

In addition, accessory subunits, including α_2/γ and β, aid in trafficking and regulation of the α1-subunits (Bodi *et al.*, 2005).

$I_{Ca,L}$ functions during the AP plateau (phase 2). In the atrium, both $Ca_V1.2$ and $Ca_V1.3$ contribute to the L-type calcium current ($I_{Ca,L}$) and display voltage dependent activation (Mangoni *et al.*, 2006). $Ca_V1.2$ mediated $I_{Ca,L}$ exhibits a bell-shaped I-V relationship that activates positive to -40 mV and peaks between 0 and +10 mV (Koschak *et al.*, 2001; Xu and Lipscombe, 2001; Mesirca *et al.*, 2015). In contrast, $Ca_V1.3$ functions at hyperpolarized membrane potentials, activating at -60 mV and peaks between -10 and -20 mV (Koschak *et al.* 2001; Xu and Lipscombe, 2001; Mesirca *et al.*, 2015). $I_{Ca,L}$ is dependent on both voltage and Ca^{2+} dependent inactivation (Catterall, 2000; Mangoni *et al.*, 2006; Mesirca *et al.*, 2015). It is postulated that Ca^{2+} dependent inactivation via calmodulin is a protective mechanism to prevent Ca^{2+} overload. In addition, $I_{Ca,L}$ is regulated by CaMKII and cAMP-dependent phosphorylation pathways, including PKA (Mangoni *et al.*, 2006; Mesirca *et al.*, 2015). Furthermore, activation and inactivation curves for $I_{Ca,L}$ overlap which results in a "window current" that may play a role in the generation of proarrhythmic APs.

1.2.4. Potassium Channels

Multiple types of potassium channels are expressed in atrial myocytes and these currents are the main determinants of AP repolarization. These include voltage-gated potassium (K_V) channels that are voltage and time dependent as well as inward rectifier potassium (K_{ir}) channels which are not voltage gated. K_V channels can be subdivided into two categories: the transient outward potassium currents (I_{to}) which function during early AP repolarization and delayed rectifier potassium currents which function during the AP plateau (phase 2) and throughout AP repolarization (phase 3) (Nerbonne and Kass, 2005; Schmitt *et al.*, 2014; Bartos *et al.*, 2015). K_{ir} channels are active in phases 3 and 4 of the AP and function to repolarize the cell and maintain a stable resting membrane potential.

1.2.4.1. Transient outward potassium current and KChIP2

The transient outward potassium current (I_{to}) plays a key role in AP repolarization and functions to create a driving gradient for Ca^{2+} entry into the cell during the AP plateau (phase 2) (Grant, 2009; Schmitt *et al.*, 2014). In larger mammals, including humans, I_{to} functions during early repolarization of the AP (phase 1) and the AP plateau (phase 2) (Nerbonne and Kass, 2005). In comparison to larger mammals, the mouse AP lacks a clear phase 1 and displays an abbreviated APD which is attributed to high I_{to} densities (Niwa and Nerbonne, 2010, Bartos *et al.*, 2015). Accordingly, reductions in I_{to} can dramatically alter the AP waveform.

I_{to} can be divided into fast ($I_{to,f}$) and slow ($I_{to,s}$) components, both of which exhibit voltage dependent activation at membrane potentials positive to -30 mV (Nerbonne and Kass, 2005; Niwa and Nerbonne, 2010; Schmitt *et al.*, 2014). $I_{to,s}$ is conducted by $K_V1.4$ channels that are encoded by *KCNA4*. $I_{to,s}$ exhibits slower activation and recovery from inactivation kinetics compared to $I_{to,f}$ (Niwa and Nerbonne, 2010). Although $K_V1.4$ is detected in the mouse atrium, $I_{to,f}$ displays a prominent role in repolarization in the atria (Niwa and Nerbonne, 2010). I_{to} inactivation occurs by two mechanisms. The first is a "ball and chain" type, or N-type, inactivation where the N-terminal domain blocks the intracellular entrance to the pore. The second mechanism, C-type inactivation, involves a conformational change in the selectivity filter which restricts the pore size (Birnbaum *et al.*, 2004).

The pore-forming α-subunits for I_{to} in the mouse atrium are $K_V4.2$ and $K_V4.3$ and are encoded by *KCND2* and *KCND3*, respectively (Niwa and Nerbonne, 2010; Schmitt *et al.*, 2014). Functional I_{to} channels are macromolecular complexes consisting of four α-subunits and accessory β-subunits (Birnbaum *et al.*, 2004; Niwa and Nerbonne, 2010). The α-subunits contain six transmembrane helices (S1-S6), of which S4 serves as a voltage sensor, and a P loop between S5 and S6 functions as an ion selectivity filter. The α-subunits can assemble as homotetramers or heterotetromers, which results in regional heterogeneity in I_{to} density (Guo *et al.*, 2002; Birnbaum *et al.*, 2004; Niwa and Nerbonne, 2010). Multiple β-accessory subunits and interacting proteins have been identified and include $K_V\beta$ proteins, K_V channel interacting protein (KChIP2), diaminopeptidyl

transferase-like protein 6 (DPP6), and members of the MinK related peptide (MiRP) family (Birnbaum *et al.*, 2004; Niwa and Nerbonne, 2010). These β-subunits do not have transmembrane domains. Rather they are cytoplasmic proteins that modulate the biophysical properties of the K_V channels. There is also evidence to suggest phosphorylation by CaMKII, PKA, and PKC can further modulate I_{to} (Niwa and Nerbonne, 2010; Yang and Nerbonne, 2016)

KChIP2, encoded by *KCNIP2*, plays a critical role in I_{to} conductance (Nerbonne and Kass, 2005; Niwa and Nerbonne, 2010; McKinnon and Rosati, 2016). KChIP2 binds to the cytoplasmic N-terminal domain of K_V channels and co-precipitates with both K_V4.2 and K_V4.3 (An *et al.*, 2000; Guo *et al.*, 2002). A gradient of I_{to} exists across the ventricular myocardium in humans and dogs and is correlated with KChIP2 expression (Rosati *et al.*, 2001; Rosati *et al.*, 2003; Grubb *et al.*, 2015). In HEK-293 cells, co-expression of KChIP2 and K_V4.2 increases I_{to} compared to expression of K_V4.2 alone (Li *et al.*, 2005). In addition, I_{to} densities are significantly reduced in ventricular myocytes from *KCNIP2* knockout mice (Kuo *et al.*, 2001; Foeger *et al.*, 2013; Grubb *et al.*, 2014). Combined, these findings demonstrate that KChIP2 modulates I_{to} density. Furthermore, KChIP2 functions to induce proper ion channel folding, membrane trafficking, slows channel degradation, and shifts the voltage dependence of activation to more negative potentials (An *et al.*, 2000; Birnbaum *et al.*, 2004; Mezzano and Morley, 2015; McKinnon and Rosati, 2016). KChIP2 is also expressed in the atrial myocardium (Bosch *et al.*, 2003; Tellez *et al.*, 2006; Calloe *et al.*, 2011).

There is emerging evidence indicating the role of KChIP2 in the cardiomyocyte is not limited to I_{to}. $I_{Ca,L}$ is reduced in ventricular myocytes isolated from *KCNIP2* knockout mice (Thomsen *et al.*, 2009a; Foeger *et al.*, 2013; Grubb *et al.*, 2015). In these studies, Ca_V1.2 protein expression was either unchanged or increased in KChIP2 deficient mice. It is hypothesized that KChIP2 increases $I_{Ca,L}$ by binding to the N-terminal inhibitory module of Ca_V1.2, thereby relieving inhibition of channel conductance (Thomsen *et al.*, 2009a; Grubb *et al.*, 2012). In mouse ventricular myocytes, K_V1.5 and KChIP2 co-precipitate (Li *et al.*, 2005) and I_{Kur} densities are increased in ventricular myocytes from *KCNIP2* knockout mice (Thomsen *et al.*, 2009b; Grubb *et al.*, 2014). It is proposed that the increase in I_{Kur} is a compensatory mechanism in response to reduced I_{to} in these

animals. There is also evidence to suggest KChIP2 indirectly regulates *SCN5a* expression by modulating microRNA levels (Nassal *et al.*, 2017). These studies indicate KChIP2 can modulate $I_{Kur,}$ $I_{Ca,L}$, and I_{Na} in addition to its well-known effects on I_{to}, however the precise function of KChIP2 requires further investigation.

1.2.4.2. Ultra-rapid delayed rectifier potassium current

Delayed rectifier potassium currents function throughout AP repolarization. This family of outward potassium currents includes the ultra-rapid delayed rectifier potassium current (I_{Kur}), the rapidly activating delayed rectifier potassium current (I_{Kr}), and the slowly activating delayed rectifier potassium current (I_{Ks}). As their names suggest, each of these currents exhibits unique biophysical properties and are named according to the rate at which they activate. I_{Kr} and I_{Ks} play a more predominant role AP repolarization in larger mammalian species, including humans (Nerbonne and Kass, 2005; Bartos *et al.*, 2015). In the mouse heart, I_{Kr} contributes to AP repolarization in the SAN (Nerbonne *et al.*, 2001; Bartos *et al.*, 2015).

I_{Kur} is an essential repolarizing current during phases 1-3 in atrial myocytes in most species (Ravens and Odening, 2017). I_{Kur} is specific to the atrial myocardium in the human heart (Nattel, 2002). I_{Kur} is conducted by the α-subunit $K_V1.5$ and encoded by *KCNA5* (Nerbonne and Kass, 2005; Schmitt *et al.*, 2014; Ravens and Odening, 2017). Four of $K_V1.5$ α-subunits assemble to form the channel pore. In addition, β-subunits have been identified, including $K_V\beta1.2$, $K_V\beta1.3$, and $K_V\beta2.1$, and function in membrane trafficking, integration into the membrane, as well as modulation of activation and inactivation kinetics (Ravens and Wettwer, 2011). Activation of I_{Kur} occurs very rapidly, in the range of 1-10 ms, and at membrane potentials positive to 0 mV (Nattel *et al.*, 1999; Nerbonne and Kass, 2005; Ravens and Wettwer, 2011; Schmitt *et al.*, 2014). Inactivation is very slow, and includes both N-type inactivation via β-subunits and C-type inactivation.

1.2.4.3. Inwardly rectifying potassium current

Inwardly rectifying potassium currents (K_{ir}) contribute to AP repolarization and function to maintain a stable resting membrane potential. Unlike K_V channels, K_{ir} channels lack a voltage sensor (Schmitt *et al.*, 2014). These channels exhibit a strong voltage-dependent reduction in current during depolarization that produces a negative slope conductance during inward rectification (Lopatin and Nichols, 2001; Dhamoon and Jalife, 2005; Anumonwo and Lopatin, 2010). Furthermore, inward rectification is dependent on extracellular K^+ concentrations such that increasing concentrations corresponds to an increase in conductance, further contributing to the negative slope conductance following crossover (Lopatin and Nichols, 2001). The heart expresses multiple families of inwardly rectifying potassium channels, including the $K_{ir}2.x$, $K_{ir}3.x$, $K_{ir}6.x$ families (Bartos *et al.*, 2015)

The inward rectifier potassium current (I_{K1}) is conducted by the Kir2.x family of proteins, including $K_{ir}2.1$ (*KCNJ2*), $K_{ir}2.2$ (*KCNJ12*), $K_{ir}2.3$ (*KCNJ4*), and $K_{ir}2.4$ (*KCNJ14*) (Nerbonne and Kass, 2005; Schmitt *et al.*, 2014). The predominant cardiac isoform is $K_{ir}2.1$ and the resulting I_{K1} readily conducts ions at negative potentials (Lopatin and Nichols, 2001). Structurally, K_{ir} subunits contain two transmembrane domains with a pore loop between the two domains as well as cytoplasmic animo- and carboxy-terminal regions (Lopatin and Nichols, 2001; Dhamoon and Jalife, 2005). Within the pore region of I_{K1} are bindings sites for magnesium (Mg^{2+}) and polyamines, including spermine. K^+ current is accompanied by Mg^{2+} and polyamines that block outward I_{K1} current at membrane potentials positive to -20 mV (Grant, 2009; Schmitt *et al.*, 2014). Accordingly, I_{K1} does not contribute to phases 0, 1, and 2 of the AP. When membrane potentials are negative to -40 mV in phase 3 of the AP, Mg^{2+} and polyamines unbind from the channel pore, and I_{K1} conductance is recovered. I_{K1} is also active during phase 4 of the AP where it functions to stabilize the resting membrane potential.

The acetylcholine-sensitive potassium current (I_{KAch}) is a receptor activated K_{ir} channel that functions in modulating heart rate under physiological conditions. Vagal stimulation results in the release of acetylcholine which binds to muscarinic receptors and

results in the activation of I_{KAch} (Schmitt *et al.*, 2014; Yang and Nerbonne, 2016). I_{KAch} density is higher in right atrial myocytes compared to left atrial myocytes, and higher in the SAN than the atria (Lomax *et al.*, 2003a). I_{KAch} is conducted by the $K_{ir}3$ family of proteins, including $K_{ir}3.1$ and $K_{ir}3.4$, that are encoded by *KCNJ3* and *KCNJ5*, respectively (Anumonwo and Lopatin, 2010; Schmitt *et al.*, 2014). Once activated, I_{KAch} shortens the AP and hyperpolarizes the membrane potential (Lomax *et al.*, 2003a; Grant, 2009; Schotten *et al.*, 2011).

1.3. Atrial Fibrillation

1.3.1. Atrial Fibrillation

AF is the most common sustained cardiac arrhythmia and affects up to 4% of the population worldwide with the prevalence increasing with comorbidities (Nattel *et al.*, 2007; Rahman *et al.*, 2014). AF is characterized by rapid and uncoordinated patterns of electrical conduction in the atria (Grunnet *et al.*, 2011; Wakili *et al.*, 2011). Under physiological conditions the SAN maintains the heart rate at roughly 60 beats per minute at rest in humans. During AF, these atrial firing rates dramatically increase to 400-600 times per minute (Nattel, 2002). These high rates result in impaired atrial contraction whereby the atria quiver rather than contract (Nattel, 2002; Schoonderwoerd *et al.*, 2005). On the ECG, clear and distinct P waves followed by QRS complexes that occur during normal sinus rhythm are replaced by an undulating baseline and irregular R-R intervals (Wakili *et al.*, 2011).

Patients with AF have an increased risk for a reduced quality of life, morbidity, and mortality (Markides and Schilling, 2003; Mahajan *et al.*, 2017). Furthermore, patients with AF have a fivefold increase in the risk of stroke as blood pools and clots in the rapidly contracting atrial appendages during an AF episode (Grunnet *et al.*, 2011). In addition, the dyssnchryony between the atria and ventricles results in weakened ventricular contractions. Numerous risk factors for AF have been identified including age, genetics, hypertension, diabetes, sleep apnea, and obesity.

AF is a progressive disease. Paroxysmal AF is defined as short episodes of AF that spontaneously terminate within 7 days of onset (Allessie *et al.*, 2001; Markides and Schilling, 2003; Heijman *et al.*, 2014; Lau *et al.*, 2017). Persistent AF is characterized by the requirement of electrical or pharmacological cardioversion to terminate the AF episodes and the AF burden in these patients is approximately 53% (Allessie *et al.*, 2001; Iwasaki *et al.*, 2011; Lau *et al.*, 2017). In contrast, patients with permanent AF do not respond to treatment (Allessie *et al.*, 2001; Markides and Schilling, 2003; Heijman *et al.*, 2014). The progression from paroxysmal to more permanent types of AF is observed in patients with concomitant risk factors and is accompanied by atrial remodelling (Iwasaki *et al.*, 2011; Schotten *et al.*, 2011; Lau *et al.*, 2017; Mahajan *et al.*, 2017).

AF promotes the recurrence of AF through atrial remodelling, as first described in the ground-breaking study by Wijffels *et al.* (1995). In this study, 27 electrodes were placed in the right and left atrium of goats and connected to an external automatic fibrillator. This apparatus delivered rapid bursts of stimuli when goats were in sinus rhythm and was used to artificially maintain AF for up to two weeks. Inducibility and severity of AF was assessed immediately following termination of the electrically maintained AF. At the beginning of the experiment, high frequency burst pacing resulted in short, non-sustained periods of AF that lasted on average 6 seconds before spontaneously reverting to normal sinus rhythm (Wijffels *et al.*, 1995). When AF was artificially maintained for 24 hours before termination, the average duration of AF that followed increased to 132 seconds. After 48 hours of electrically maintained AF, the average AF duration during subsequent induction was 467 seconds. In addition, 2 out of 12 goats had sustained AF, which was defined as AF that lasted longer than 24 hours before reverting to normal sinus rhythm. After 2 weeks of maintaining AF, 9 out of 11 goats exhibited subsequent sustained AF. These data demonstrate that rapid atrial pacing results in an increase in AF duration, and therefore severity of AF. Furthermore, the prolongation in AF duration occurred in conjunction with a shortening of the atrial effective refractory period (AERP), thereby indicating that atrial electrical remodelling occurs as a direct result of AF. Furthermore, this indicates that AF promotes atrial remodelling that will further perpetuate AF, or as eloquently described by the authors “AF begets AF” (Wijffels *et al.*, 1995).

Electrical remodelling that occurs in AF is associated with a shortening of the AP and AERP (Brundel *et al.*, 2001; Dobrev and Ravens, 2003). Increased atrial rates lead to an accumulation of intracellular Ca^{2+} (Iwasaki *et al.*, 2011; Heijman *et al.*, 2014; Nattel and Harada, 2014). This results in Ca^{2+} overload which can be lethal to cardiomyocytes (Nattel, 2002). Increased intracellular Ca^{2+} results in activation of the Ca^{2+}-dependent phosphatase calcineurin which dephosphorylates the nuclear factor of activated T cells (NFAT) (Heijman *et al.*, 2014). As a result, NFAT translocates into the nucleus where it functions as a transcriptional repressor of *CACNA1c.* This in turn reduces $Ca_V1.2$ expression and $I_{Ca,L}$ density (Wakili *et al.*, 2011; Heijman *et al.*, 2014). However, reductions in $I_{Ca,L}$ reduce the AP plateau and abbreviate the AP. This reduces atrial ERPs and favours AF perpetuation (Nattel *et al.*, 2008; Iwasaki *et al.*, 2011). In addition to a reduction in $I_{Ca,L}$, chronic AF is associated with reductions in I_{to}, I_{Kur}, and I_{Ks} and increased I_{K1}, and constitutively active I_{KAch} in human and animal models (Van Wagoner *et al.*, 1997; Bosch *et al.*, 1999; Van Wagoner *et al.*, 1999; Yue *et al.*, 1999; Brundel *et al.*, 2001; Bosch *et al.*, 2003; Oh *et al.*, 2010; Voigt *et al.*, 2010).

There is a relationship between SAN dysfunction and AF. Epidemiology studies have shown that 40-70% of patients diagnosed with SAN dysfunction have pre-existing AF and up to 22% of patients with no history of AF at the time of SAN dysfunction diagnosis will develop AF at follow up (John and Kumar, 2016; Jackson *et al.*, 2017). In humans, pacing of the right atrium for 10 or 15 minutes results in an increase in cSNRT and SAN conduction time immediately following pacing compared to baseline measurements (Hadian *et al.*, 2002). In addition, sinus pauses lasting 3 to 10 seconds have been documented upon termination of paroxysmal AF (Hocini *et al.*, 2003). Interestingly, improved SAN function, as assessed by improved cSNRT and heart rates, is observed in some patients following cardioversion of AF (Hocini *et al.*, 2003; John and Kumar, 2016; Jackson *et al.*, 2017). Prolonged SNRT can also be used as an independent predictor of the recurrence of AF following radiofrequency catheter ablation in patients with persistent AF (Park *et al.*, 2013).

Experimental models have given some mechanistic insight to the connection between SAN dysfunction and AF. In a rabbit model of AF, 20% of atrial impulses during AF propagated into the SAN and successfully activated SAN pacemaker cells

(Kirchhof and Allessie, 1992). This was termed SAN entrance. In a dog model of AF, rapid pacing of the atria leads to a prolongation of the cSNRT, reduced SAN conduction time, and a reduction in intrinsic heart rate (Elvan *et al.*, 1996; Joung *et al.*, 2010; Zhao *et al.*, 2014; Choudhury *et al.*, 2015). This occurs in association with reduced HCN expression and I_f density in the SAN (Yeh *et al.*, 2009; Choudhury *et al.*, 2015). Electrophysiology studies have also demonstrated that rapid atrial pacing results in transient SAN exit block and therefore failure to excite the atrial myocardium (Fedorov *et al.*, 2009). On the other hand, AERP measurements were abbreviated in a dog model of SAN dysfunction (Li *et al.*, 2011). This occurred in association with increased susceptibility to AF and increased duration of AF. In addition, it has also been proposed that the structural barriers that insulate the human and dog SAN can create an anatomical obstacle that can promote re-entry (Fedorov *et al.*, 2010; Fedorov *et al.*, 2012). Combined, these data demonstrate a relationship between SAN dysfunction and AF, although the mechanisms are poorly understood.

1.3.2. Mechanisms of Atrial Fibrillation

AF is characterized by the erratic and rapid activation of the atria and is dysynchronous with the ventricles. AF requires both a trigger to induce arrhythmic activity and a substrate that promotes perpetuation of the arrhythmia (Allessie *et al.*, 2001; Allessie *et al.*, 2002; Nattel *et al*., 2007; Schotten *et al.*, 2011; Lau *et al.*, 2017). Triggers could include ectopic firing, altered atrial refractoriness, altered Ca^{2+} handling, and enhanced autonomic nervous system activation. Substrates include structural remodelling that create an anatomical obstacle or electrical remodelling of the atrial myocardium (Nattel, 2002; Grunnet *et al.*, 2011; Jalife and Kaur, 2015). Functionally, substrates create self-sustained excitation and continuous propagation of electrical activity throughout the atrial myocardium.

1.3.2.1. Electrical Remodelling

Electrical remodelling involves changes in ion channel function and can have profound effects on AP morphology. Both a prolongation and shortening of the APD are associated with AF and can result in triggered activity or an increased susceptibility to re-entry (Nattel, 2002; Dobrev and Ravens, 2003; Heijman *et al.*, 2014).

Alterations in AP morphology can result in ectopic activity that arise from increased automaticity or the generation of afterdepolarizations (Iwasaki *et al.*, 2011; Schotten *et al.*, 2011). Increased automaticity of atrial APs can facilitate the generation of spontaneous atrial APs. Under physiological conditions, I_{K1} maintains a stable resting membrane potential in atrial myocytes and I_f densities are low. Spontaneous APs can occur if an increase in I_f occurs with a corresponding reduction in I_{K1}. A spontaneous AP will be generated if the resulting depolarizing current is sufficient to meet the threshold to activate Na^+ channels (Nattel *et al.*, 2007; Iwasaki *et al.*, 2011; Schotten *et al.*, 2011).

Delayed afterdepolarizations (DAD) are characterized by the formation of an AP evoked by a premature membrane depolarization event during the diastolic interval of the AP (phase 4) (Nattel *et al.*, 2007; Schotten *et al.*, 2011). During the normal AP, free intracellular Ca^{2+} levels rapidly increase and are returned to baseline levels through two mechanisms. The first is uptake into the sarcoplasmic reticulum through the sarcoplasmic reticulum Ca^{2+}-ATPase (SERCA) (Iwasaki *et al.*, 2011; Schotten *et al.*, 2011). The second involves extrusion through the Na^+/Ca^{2+} exchanger (I_{NCX}) where 3 extracellular Na^+ ions are exchanged for 1 intracellular Ca^{2+} ion (Iwasaki *et al.*, 2011). DADs occur in conjunction with abnormal sarcoplasmic reticulum Ca^{2+} release, which can occur if ryanodine receptors are defective or if the sarcoplasmic reticulum is overloaded with Ca^{2+} (Nattel *et al.*, 2007; Iwasaki *et al.*, 2011; Bartos *et al.*, 2015). Increased intracellular Ca^{2+} levels result in activation of I_{NCX}, which functions to extrude these ions. This creates a net inward current that depolarizes the cellular membrane. An AP can be triggered if this depolarizing current exceeds the threshold to evoke an AP.

Early afterdepolarizations (EAD) are characterized by a slowing or reversal of AP repolarization during phase 2 or 3 of the AP (Weiss *et al.*, 2010; Iwasaki *et al.*, 2011; Schotten *et al.*, 2011). AP prolongation can be attributed to a reduction in K^+ currents,

including I_{to} and I_{Kur}, an increase in inward currents by $I_{Ca,L}$ or late I_{Na}, or a combination of the two (Burashnikov and Antzelevitch, 2006; Nattel *et al.*, 2007; Weiss *et al.*, 2010; Bartos *et al.*, 2015). The window current for $I_{Ca,L}$ is the overlap between steady-state activation and inactivation, and is typically between 30-90% repolarization at membrane potentials between -30 and 0 mV (Weiss *et al.*, 2010; Grunnet *et al.*, 2011). During this time, $I_{Ca,L}$ can reactivate, resulting in a depolarizing current. EADs can also arise from activation of I_{NCX} during phase 3 of the AP if intracellular Ca^{2+} levels are sufficiently high enough to activate I_{NCX} (Burashnikov and Antzelevitch, 2006; Weiss *et al.*, 2010; Bartos *et al.*, 2015). In addition, EADs can occur if late I_{Na} is increased, resulting in a depolarizing current during phase 2 of the AP (Belardinelli *et al.*, 2015; Makielski, 2016).

During AF, electrical activity is continuously propagated throughout the atrium through re-entry. Re-entry can occur in the setting of slowed electrical conduction or an increased path for impulse propagation such that the tissue regains excitability and therefore the ability to generate an AP (Grunnet *et al.*, 2011). The wavelength of re-entry is the minimum size of a functional re-entry circuit and is the product of the refractory period and conduction velocity (Dobrev and Ravens, 2003; Nattel *et al.*, 2007; Iwasaki *et al.*, 2011; Schotten *et al.*, 2011). Refractory period is determined by the APD whereas conduction velocity is determined by I_{Na} and the electrical coupling of cells by gap junctions. Re-entry is facilitated by a shortening of the refractory period and slowing of conduction (Markides and Schilling, 2003; Grunnet *et al.*, 2011; Berenfeld and Jalife, 2016). Shortening of the APD is associated with alterations in ion currents in the fibrillating atria that can include a reduction in $I_{Ca,L}$ and enhanced I_{K1} and I_{KAch} (Allessie *et al.*, 2001; Allessie *et al.*, 2002; Nattel *et al.*, 2007; Iwasaki *et al.*, 2011). This shortening facilitates both the acceleration and stabilization of sustained re-entry. Furthermore, shorter wavelengths can be associated with an increase in the number of re-entry circuits, which makes it more difficult to terminate AF (Allessie *et al.*, 2002).

1.3.2.2. Structural Remodelling

In persistent and paroxysmal AF, both electrical and structural remodelling create a substrate for AF. Structural remodelling involves alterations to the architecture of the

atria. This includes atrial enlargement, fibrosis, adipose tissue deposits, hypertrophy, and myocyte apoptosis (Morillo *et al.*, 1995; Allessie *et al.*, 2001; Schotten *et al.*, 2011; Lau *et al.*, 2016; Lau *et al.* 2017). Structural remodelling results in local conduction disturbances and conduction blocks, both of which promote re-entry. In addition, increased levels of fibrosis can fragment the propagating wave front, which can facilitate the perpetuation of AF.

Cardiac fibroblasts play an essential role in cardiac function. Under physiological conditions, cardiac fibroblasts are involved in many processes including maintenance of the extracellular matrix and secretion of cytokines and growth factors (Souders *et al.*, 2009; Fan *et al.*, 2012). In response to pathological stimuli, cardiac fibroblasts proliferate, differentiate, and increase synthesis of extracellular matrix proteins, including collagens (Camelliti *et al.*, 2005; Yue *et al.*, 2011; Fan *et al.*, 2012). Furthermore, cardiac fibroblasts secrete cytokines which promote fibrosis. Cardiac fibrosis is extremely common in AF and can be reparative or reactive. Reparative fibrosis replaces cardiomyocyte loss with a structural scar to maintain structural integrity. On the other hand, reactive fibrosis occurs in response to myocardial dysfunction and results in the physical separation of muscle fibres within the atrium. Increased fibrosis results in conduction abnormalities, myocardial stiffness, and diastolic dysfunction, and can be an important contributor to the development of a substrate for AF (Allessie *et al.*, 2001; Iwasaki *et al.*, 2011; Schotten *et al.*, 2011; Jalife and Kaur, 2015).

1.3.3. Pathophysiology of Atrial Fibrillation

AF is associated with adverse structural and electrical remodelling of the atria (Wijffels *et al.*, 1995; Morillo *et al.*, 1995; Allessie *et al.*, 2002; Nattel *et al.*, 2007; Seccia *et al.*, 2016). This remodelling promotes the sustained disorganized activity that potentiates AF. However, the underlying mechanisms that create a substrate that gives rise to AF is poorly understood. In addition, AF is a highly diverse cardiac arrhythmia that can be acquired in different disease states. These include hypertension, hypertrophy, and heart failure (Nattel, 2002). In addition, the incidence of AF exponentially increases

with age (Monfredi and Boyett, 2015; Nattel *et al.*, 2007). These factors will be described below.

1.3.3.1. Hypertension

Hypertension is a disease of the cardiovascular system that manifests from an increase in blood pressure. Patients with hypertensive heart disease have an increased risk of developing arrhythmias (including AF), coronary artery disease, and heart failure. Hypertension affects nearly a quarter of the Canadian population and the prevalence increases with age (Mensah *et al.*, 2003; Leung *et al.*, 2017). Annually, hypertension causes 7.1 million deaths, which equates to 13% of all deaths (Georgiopoulou *et al.*, 2010). It is estimated between 60-80% of patients with AF are also diagnosed with hypertension (Kirchhof and Schotten, 2006; Schotten *et al.*, 2011). In addition, hypertension is the most common comorbidity associated with AF, however the underlying mechanisms that promote the genesis of AF are relatively unknown.

Prolonged increases in blood pressure cause alterations in cardiac structure and function due to increased afterload. The resulting changes in myocardial structure, coronary vasculature, and cardiac conduction are collectively referred to as hypertensive heart disease. These alterations include concentric left ventricular hypertrophy, cardiomyocyte hypertrophy, and increased interstitial fibrosis (Georgiopoulou *et al.*, 2010; Messerli *et al.* 2017). Initially these alterations serve as a compensatory mechanism to preserve cardiac function in response to increased peripheral vascular resistance. However, over time they become maladaptive and severely compromise cardiac performance (Izzo and Gradman, 2004; Prisant, 2005).

Clinically, hypertension is a progressive disease that can be divided into four categories (Messerli *et al.*, 2017). Degree I is characterized by left ventricular diastolic dysfunction without hypertrophy. Degree II is characterized by left ventricular dysfunction and concentric left ventricular hypertrophy. Degree III is clinical heart failure with preserved ejection fraction. Lastly, Degree IV is heart failure that is characterized by dilated cardiomyopathy with reduced ejection fraction.

Although poorly understood, the effects of chronic hypertension are not limited to the ventricular myocardium. Concentric left ventricular hypertrophy results in a reduction in the elastic properties of the ventricles. This diminishes the ability of the ventricles to fill with blood during diastole. Rather, the left ventricle becomes dependent on atrial systole (Prisant, 2005). The increased pressures exerted on the left atrium result in left atrial enlargement as well as adverse effects on the pulmonary circulation (Mensah *et al.*, 2003; Prisant, 2005; Abhayaratna *et al.*, 2006). Left atrial enlargement is an early manifestation of hypertension and is characterized by an increase in P wave duration. Furthermore, left atrial enlargement predisposes patients to AF and stroke (Abhayaratna *et al.*, 2006; Beigel *et al.*, 2014). Hypertension is also associated with increased levels atrial fibrosis (Kistler *et al.*, 2006; Lau *et al.*, 2010).

Hypertension is associated with alterations in atrial electrophysiology. In patients with a history of hypertension, right atrial conduction velocity is significantly reduced (Medi *et al.*, 2011). In hypertensive sheep, P wave duration (a measure of atrial conduction time) is increased and conduction velocity is reduced in the right and left atrial appendage compared to normotensive controls (Kistler *et al.*, 2006; Lau *et al.*, 2010). These alterations occurred in conjunction with an increase in AERP. In addition, hypertensive sheep have an increased susceptibility and severity of AF (Kistler *et al.*, 2006; Lau *et al.*, 2010). The underlying changes to ion currents are poorly understood.

Although hypertension is the initial stimulus in hypertensive heart disease, the renin-angiotensin system (RAS) plays a critical role in cardiac remodelling. RAS is a key modulator of blood pressure and blood volume (van Kats *et al.*, 2001; Patel *et al.*, 2017). The key effector molecule is Angiotensin (Ang) II. Briefly, angiotensinogen is cleaved into Ang I by renin, which is released from the kidneys. Ang I is then converted into the biologically active peptide Ang II by angiotensin converting enzyme (ACE) (Wollert and Drexler, 1999; De Mello and Danser, 2000). In the heart, Ang II exerts its effects by binding to Ang II type I receptors (AT1R) (De Mello and Danser, 2000; Schotten *et al.*, 2011). Ang II is also detected in the effluent collected from Langendorff-perfused rat hearts, indicating that the heart locally synthesizes and secretes Ang II (Lindpainter *et al.*, 1990). Locally synthesized Ang II modulates cardiac structure and function (Wollert and Drexler, 1999; De Mello, 2011; Kim and Iwao, 2011).

Ang II is a potent regulator of cellular function in both cardiomyocytes and cardiac fibroblasts (Mehta and Griendling, 2007; Kim and Iwao, 2011). Ang II modulates a number of intracellular pathways including the mitogen-activated protein kinase (MAPK), extracellular signal regulated kinases (ERK), janus kinase 2 (JAK2), transforming growth factor β1 (TGF-β1), and nuclear factor-kappa β (NF-κβ) pathways (Wollert and Drexler, 1999; Mehta and Griendling, 2007; Kim and Iawo, 2011). Furthermore, Ang II signalling is associated with an increase in the generation of reactive oxygen species as well as increased inflammation. In cardiomyocytes, increased Ang II signalling via AT1R is associated with increased cellular hypertrophy, altered gene expression patterns, and increased cell death. In cardiac fibroblasts, Ang II signalling increases cellular proliferation and expression of pro-fibrotic genes, including collagen I and collagen III (Bernardo *et al.*, 2010; Kim and Iwao, 2011, Prabhu *et al.*, 2017). Collectively, enhanced Ang II signalling results in remodelling that favours the onset and perpetuation of AF (Seccia *et al.*, 2016).

Previous studies have demonstrated that Ang II modulates ion currents. Tissue culture experiments in H9c2 cells have demonstrated that Ang II exposure reduced peak I_{Na} and increased late I_{Na} (Shang *et al.*, 2008). This occurred in association with a reduction in *SCN5a* mRNA expression that was mediated by NADPH oxidase signalling and NF-κβ activation (Shang *et al.*, 2008). Experiments using a genetic model of increased Ang II/AT1R signalling demonstrated that I_{Na} was reduced independently of altered *SCN5a* mRNA or $Na_V1.5$ protein expression in ventricular myocytes (Mathieu *et al.*, 2016). Rather, the reduction in I_{Na} was attributed to enhanced PKCα signalling (Mathieu *et al.*, 2016). In contrast, another study demonstrated that acute exposure to Ang II increased I_{Na} in ventricular cardiomyocytes (Wagner *et al.*, 2014). In this study, the increase in I_{Na} was attributed to PKA and CaMKII signalling. The effects of chronic Ang II treatment on I_{Na} in the atria remains poorly understood.

Ang II signalling has been shown to affect $I_{Ca,L}$. An increase in $I_{Ca,L}$ density has been demonstrated following acute exposure to Ang II in human right atrial myocytes (Gassanov *et al.*, 2006). In HL-1 cells and ventricular myocytes, Ang II treatment increased $I_{Ca,L}$ in association with an increase in $Ca_V1.2$ subunit expression (Tsai *et al.*, 2007; Gu *et al.*, 2013 Ma *et al.*, 2016). In another study, acute exposure to Ang II resulted

in an increase in $I_{Ca,L}$ density that was attributed to NOX2 and PKA signalling in ventricular myocytes (Wagner *et al.*, 2014). In contrast, $I_{Ca,L}$ was not altered in ventricular myocytes isolated from Ang II treated mice for 28 days (Markandeya *et al.*, 2015). Although poorly understood, these data demonstrate that acute exposure to Ang II can increase $I_{Ca,L}$ however chronic exposure does not affect $I_{Ca,L}$. The effects of chronic Ang II treatment on $I_{Ca,L}$ in atrial myocytes is an area requiring further investigation.

Previous studies have investigated the effects of acute Ang II exposure on K^+ currents. In human right atrial myocytes, acute exposure to Ang II resulted in a reduction in I_{to} density without alterations in I_{Kur} or I_{K1} (Gassanov *et al.*, 2006). Ang II mediated reductions in I_{to} density have also been demonstrated in ventricular myocytes (Caballero *et al.*, 2004). Neither mRNA nor protein expression were quantified in those studies. Acute exposure to Ang II in guinea pig ventricular myocytes results in a reduction in both I_{Kr} and I_{Ks} densities and is attributed to PKC and PKA signalling (Si *et al.*, 2013; Wang *et al.*, 2008; Liu *et al.*, 2017). In neonatal rat atrial myocytes, treatment with Ang II for 24 hours resulted in an increase in $K_V1.5$ protein expression (Lu *et al.*, 2014; Lu *et al.*, 2017). This was attributed to increased levels of reactive oxygen species that increased P-ERK1/2 and Smad2/3 signalling. I_{Kur} was not recorded in those studies. The effects of chronic Ang II signalling on K^+ currents in atrial myocytes remains poorly understood.

Plasma and intracardiac Ang II levels are significantly increased in patients with AF and in animal models of cardiovascular disease (Sadoshima *et al.*, 1993; Iwai *et al.*, 1995; Nattel *et al.*, 2007; Tsai *et al.*, 2008; Adam *et al.*, 2011; Schotten *et al.*, 2011; Tadevosyan *et al.*, 2017). Increased cardiac Ang II levels are attributed to an increase in plasma renin that is sequestered by the heart as well as cardiac expression of ACE (Wollert and Drexler, 1999; De Mello and Danser, 2000; De Mello, 2011). In addition, local Ang II synthesis is increased under pathological conditions.

In the clinical setting, both the incidence of AF and new onset AF is reduced in patients receiving ACE inhibitors or Ang II receptor blockers (Healey *et al.*, 2005; Ehrlich *et al.*, 2006; Naccarellie and Peacock, 2009; Seccia *et al.*, 2016; Ferrario and Mullick, 2017). Mechanistically, it is proposed these beneficial effects against AF are attributed to improved left ventricular hemodynamics, reduced atrial stretch, suppressed Ang II-induced fibrosis, as well as direct modulation of ion channel function.

In rodents, subcutaneous perfusion of Ang II results in hypertension, cardiac hypertrophy, and increased interstitial fibrosis (van Kats *et al.*, 2001; Ichihara *et al.*, 2001; Wakisaka *et al.*, 2007; Fukui *et al.*, 2013; Purohit *et al.*, 2013; Tsukamoto *et al.*, 2013). In addition, Ang II treated mice have bradycardia and SAN dysfunction, as well as an increased susceptibility to AF (Swaminathan *et al.*, 2011; Fukui *et al.*, 2013; Purohit *et al.*, 2013). However, the mechanisms underlying SAN dysfunction and AF in Ang II treated animals remains poorly understood.

Chronic Ang II treatment results in an increase in susceptibility to AF (Purohit *et al.*, 2013). AP recordings have demonstrated that chronic Ang II treatment is associated with the generation of DADs in isolated atrial myocytes. This was attributed to an increase in the number of spontaneous Ca^{2+} sparks released from the sarcoplasmic reticulum (Purohit *et al.*, 2013). In optical mapping experiments, conduction velocity was reduced in the left atria of Ang II treated mice (Swaminathan *et al.*, 2011). Combined, these findings indicate that Ang II treatment is associated with electrical remodelling of the atria. However, very little is known about the effects of chronic Ang II treatment on ion channel function in the atria.

1.3.3.2. Cardiac Hypertrophy

Cardiac hypertrophy is a process in which the heart increases in mass and is an independent predictor of cardiovascular morbidity and mortality (Gradman and Alfayoumi, 2006). Hypertrophy can be physiological or pathological and occurs as a result of increased haemodynamic demand (Barry *et al.*, 2008). Physiological hypertrophy is observed during postnatal growth, pregnancy, and chronic exercise and is characterized by normal or enhanced function with proportional chamber enlargement (Bernardo *et al.*, 2010; Shimizu and Minamino, 2016). On the other hand, pathological cardiac hypertrophy occurs in response to abnormal haemodynamic stress and is associated with structural abnormalities and cardiac dysfunction (Bernardo *et al.*, 2010; Shimizu and Minamino, 2016). Initially, pathological hypertrophy is an adaptive response to maintain cardiac function, however over time it becomes maladaptive and is associated with adverse cardiac remodelling that can lead to heart failure. In both

physiological and pathological hypertrophy, growth occurs as a result of an increase in cardiomyocyte size rather than cell division as proliferation rates in cardiomyocytes rapidly decline after birth (Agrawal *et al.*, 2010; Bernardo *et al.*, 2010).

Cardiac hypertrophy can be classified as either concentric or eccentric. In concentric hypertrophy, increased pressure overload leads to an increase in cell width as sarcomeres are added in parallel. This results in an increase in the thickness of the ventricular myocardium (Agrawal *et al.*, 2010; Bernardo *et al.*, 2010). On the other hand, eccentric hypertrophy occurs in response to increased volume overload. Cardiomyocytes increase in length as sarcomeres are added in series in response to increased diastolic wall stress. Eccentric hypertrophy is associated with dilation of the ventricular myocardium (Agrawal *et al.*, 2010; Bernardo *et al.*, 2010).

Underlying changes in gross morphology of the heart are alterations in gene expression patterns, energy metabolism, and increased rates of protein synthesis (Agrawal *et al.*, 2010; Bernardo *et al.*, 2010). The fetal gene program is activated in pathological hypertrophy and promotes synthesis of proteins required to increase cardiomyocyte size and alter energy metabolism (Barry *et al.*, 2008). These genes include fetal isoforms of proteins involved in contractility, Ca^{2+} handling, and energy metabolism as well as natriuretic peptides (Dirkx *et al.*, 2013). In addition, multiple signal transduction cascades are activated and include the MAPK, TGF-β, fibroblast growth factor (FGF), PKC, NFAT, and RAS pathways (Barry *et al.*, 2008; Agrawal *et al.*, 2010; Shimizu and Minamino, 2016). Many of these pathways are regulated by Ang II signalling, which is increased in the hypertrophic heart. Structural remodelling also occurs in pathological hypertrophy and is associated with increased cell apoptosis, fibrosis, and cardiomyocyte hypertrophy (Bernardo *et al.*, 2010). Combined, these changes result in stiffening of the ventricular myocardium and impaired diastolic filling from the atrium (Vaidya *et al.*, 2017).

Epidemiology studies indicate AF is highly prevalent in patients with cardiac hypertrophy, affecting approximately 20% of patients with hypertrophic cardiomyopathy (Olivotto *et al.*, 2001; Siontis *et al.*, 2014; Zegkos *et al.*, 2017). In addition, concomitant AF is a strong predictor of increased mortality in these patients. In fact, patients diagnosed with both hypertrophic cardiomyopathy and AF have a 50% increased risk of

mortality resulting from heart failure or thromboembolic stroke (Siontis *et al.*, 2014; Zegkos *et al.*, 2017).

Atrial remodelling occurs in the setting of cardiac hypertrophy. Structural remodelling in patients with cardiac hypertrophy includes increased levels of fibrosis and increased atrial diameter (Olivotto *et al.*, 2001; Ozdemir, 2004; Siontis *et al.*, 2014; Vaidya *et al.*, 2017). These morphological changes create a substrate for AF. In addition, left atrial diameter and an increase in P wave duration are independent predictors of AF in patients with cardiac hypertrophy (Ozdemir, 2004; Zegkos *et al.*, 2017). Consistent with these clinical findings, the AP is prolonged in right and left atrial myocytes from rabbits with left ventricular hypertrophy (Guo *et al.*, 2010). In this study, EADs and spontaneous APs were recorded in left, but not right, atrial myocytes from hypertrophic rabbits. The proarrhythmic activity was attributed to an increase in late I_{Na} in left atrial myocytes (Guo *et al.*, 2010). However, the effects of cardiac hypertrophy on atrial electrical remodelling is poorly understood.

1.3.3.3. Heart Failure

Heart failure affects 2% of the population and the prevalence increases with age (Metra *et al.*, 2017; Prabhu *et al.*, 2017). Heart failure is a clinical syndrome that is characterized by left ventricular dysfunction resulting from prolonged systolic and/or diastolic dysfunction (Tilman, 2014; Messerli *et al.*, 2017; Prabhu *et al.*, 2017). Heart failure occurs when the heart can no longer provide adequate blood flow and/or pressure to the body in order to meet the physiological demands of an individual. This results from structural or functional impairments in ventricular filling or ejection of blood (Ziaeian and Fonarow, 2016).

Heart failure results from multiple aetiologies, of which ischaemic heart disease, chronic obstructive pulmonary disease, hypertensive heart disease, and rheumatic heart disease are the most common. In fact, hypertension is an independent risk factor for the development of heart failure and it is estimated 91% of patients with hypertension will develop heart failure within 20 years of diagnosis (Gradman and Alfayoumi, 2006; Ziaeian and Fonarow, 2016; Messerli *et al.*, 2017).

AF and heart failure are interconnected. Epidemiology studies indicate that patients with AF have a four-fold increased risk of developing heart failure compared to those without AF (Miyasaka *et al.*, 2006; Pandey *et al.*, 2017). Conversely, AF is diagnosed in 30-40% of patients with heart failure (Schotten *et al.*, 2011; Pandey *et al.*, 2017). Heart failure is more common in patients with persistent AF and AF is observed in 50% of patients with severe heart failure (Tilman, 2014). AF promotes heart failure through the loss of atrial contraction and irregular ventricular rhythm that results in reduced systolic function. On the other hand, heart failure promotes AF as impaired ventricular function increases atrial pressures and volume. This in turn promotes atrial remodelling, including atrial enlargement, increased fibrosis, and hypertrophy, all of which create a substrate for AF (Maisel and Stevenson, 2003; Prabhu *et al.*, 2017). In addition, heart failure is associated with increased neurohormonal activity, including the RAS system, which further promotes atrial remodelling (Sanders *et al.*, 2003; Nattel *et al.*, 2007).

Although poorly understood, electrical remodelling occurs in the atrial myocardium of failing hearts. In patients with heart failure, P wave duration is prolonged in conjunction with an increase in atrial conduction time and AERP (Sanders *et al.*, 2003). Rapid ventricular tachypacing in dogs is a commonly used experimental model of heart failure. In this model, dogs with heart failure have an increase in the susceptibility and severity of AF (Li *et al.*, 2000; Stambler *et al.*, 2003; Cha *et al.*, 2003; Cha *et al.*, 2004). Electrophysiology studies demonstrate P wave duration and AERP are increased whereas conduction velocity is reduced in animals with heart failure (Morillo *et al.*, 1995; Cha *et al.*, 2003; Stamber *et al.*, 2003). Atrial structural remodelling includes increased levels of atrial fibrosis and left atrial area. In isolated atrial myocytes, AP is significantly prolonged in dogs with heart failure and is attributed to reductions in I_{to} and I_{Ks} as well as an increase in I_{NCX} (Li *et al.*, 2000; Stambler *et al.*, 2003; Cha *et al.*, 2004). In addition, a reduction in $I_{Ca,L}$ has been demonstrated in atrial myocytes isolated from rats with heart failure (Boixel *et al.*, 2001; Bond *et al.*, 2017). The reduction in $I_{Ca,L}$ occurred independently of $Ca_V1.2$ expression and was attributed to alterations in intracellular second messengers. However, the effects of heart failure on atrial electrophysiology remains an area requiring further investigation.

1.3.3.4. Ageing and Frailty

The incidence of cardiovascular disease, including hypertension, increases with chronological age (Monfredi and Boyett, 2015; Nattel *et al.*, 2007; Rahman *et al.*, 2014). In the clinical setting, SAN dysfunction affects 1 in 600 patients over 65 years old with an increase in prevalence among patients with pre-existing heart disease (Monfredi and Boyett, 2015; Csepe *et al.*, 2015; Dobrzynski *et al.*, 2007). The incidence of supraventricular arrhythmias also increases with age and it is predicted that over 13% of the population over 80 years of age will be diagnosed with AF (Rahman *et al.*, 2014). In addition, epidemiology studies indicate a progression from paroxysmal to persistent AF is associated with increased age (Mirza *et al.*, 2012). In fact, 50% of elderly patients diagnosed with paroxysmal AF either developed persistent AF or passed away in a Canadian 10-year follow-up study (Padfield *et al.*, 2017). In addition, the incidence of heart failure increases with age and it is estimated to affect more than 10% of the population over the age of 80 years (Ziaeian and Fonarow, 2016).

Although relatively poorly understood, SAN function declines with age. In the human SAN, collagen content increases from approximately 24% at birth to 70% in the adult heart. By the age of 75 years, it is estimated the number of functional pacemaker SAN myocytes is reduced to 10% compared to young adults (Mirza *et al.*, 2012; Csepe *et al.*, 2015). Electrophysiology studies have demonstrated a prolongation of SNRT with age (Kistler *et al.*, 2004; Dobrzynski *et al.*, 2007; Choudhury *et al.*, 2015). Studies in aged rodents have revealed a reduction in AP firing rate in isolated SAN myocytes (Larson *et al.*, 2013; Sharpe *et al.*, 2017). This occurs in conjunction with reductions in I_f and $I_{Ca,L}$ density (Larson *et al.*, 2013; Sharpe *et al.*, 2017). In addition, studies have demonstrated a reduction in HCN1, HCN2, HCN4, and $Ca_V1.2$ expression in the aged SAN (Tellez *et al.*, 2011; Huang *et al.*, 2007; Jones *et al.*, 2007; Larson *et al.*, 2013; Sharpe *et al.*, 2017). I_{Na} at the periphery of the SAN is reduced with age and can result in SAN exit block (Dobrzynski *et al.*, 2007; Huo *et al.*, 2011; Choudhury *et al.*, 2015; John and Kumar, 2016). Combined, these alterations contribute to SAN dysfunction and a reduction in intrinsic heart rate.

Although poorly understood, there are changes to the structure and electrophysiology in the aged atria. Gross morphology of the senescent atria demonstrates an age-related reduction in the number of myocytes, increased abundance of cardiac fibroblasts, increased levels of interstitial fibrosis, cardiomyocyte hypertrophy, and increased epicardial adipose tissue deposits (Liu *et al.*, 2004; Dobrzynski *et al.*, 2007; Mirza *et al.*, 2012, Csepe *et al.*, 2015, Lin *et al.*, 2017). Electrophysiology studies have revealed an increase in refractoriness, prolonged conduction time, and an increase in P wave duration with age (Kistler *et al.*, 2004; Liu *et al.*, 2004; Gan *et al.*, 2013; Choudhury *et al.*, 2015). In aged dogs in sinus rhythm, AP recordings in the whole atria demonstrate a reduction in V_{max} and a prolongation in APD_{90} (Anyukhovsky *et al.*, 2002; Anyukhovsky *et al.*, 2005; Gan *et al.*, 2013; Xu *et al.*, 2013). In contrast, other studies have demonstrated that V_{max} and APD are not altered in aged left atrial myocytes (Wongcharoen *et al.*, 2007; Tellez *et al.*, 2011). There is evidence to suggest ion currents are altered in the senescent atria. These include a reduction in $I_{Ca,L}$ and increase in I_{to} density in aged right atrial myocytes (Dun *et al.*, 2003; Dun and Boyden, 2009; Gan *et al.*, 2013). An increase in I_{Na} and $Na_V1.5$ protein expression has also been demonstrated in aged atria (Baba *et al.*, 2006; Tellez *et al.*, 2011). However, the effects of age on atrial electrophysiology remains poorly understood.

As we age, deficits accumulate in cells and result in altered cellular and molecular function. Over time, the gradual accumulation of these deficits results in impaired tissue and organ function that ultimately affect the overall health of an individual. Frailty is reflective of the biological age of an individual and is characterized by an increased state of vulnerability to adverse health outcomes (Rockwood and Mitnitski, 2007; Rockwood and Mitnitski, 2011; Kane *et al.*, 2017). Importantly, there is heterogeneity in the rate at which deficits accumulate such that two individuals of the same chronological age can vary in overall health status from very fit to very frail (Mitnitski *et al.*, 2002; Rockwood and Mitnitski, 2011). Furthermore, the rate of deficit accumulation exponentially increases with increasing age and in individuals with poor health status (Rockwood and Mitnitski, 2011; Mitnitski *et al.*, 2013). Accordingly, there is a relationship between age and frailty in both humans (Mitnitski *et al.*, 2002; Rockwood and Mitnitski, 2007) and animals (Parks *et al.*, 2011; Whitehead *et al.*, 2014; Rockwood *et al.*, 2017).

In both the clinical and laboratory setting, frailty can be quantified in individuals using a frailty index (FI) (Rockwood and Mitnitski, 2007; Searle *et al.*, 2008; Whitehead *et al.* 2014; Feridooni *et al.*, 2015; Rockwood *et al.*, 2017). The FI score of an individual is proportionate to the number of age-related deficits present in a given individual. Deficits are defined as health-related signs, symptoms, diseases, disabilities, and laboratory abnormalities (Kane *et al.*, 2017). The FI score of an individual is calculated by counting the total number of deficits present in an individual and dividing this value by the total number of deficits measured. This gives an FI score between 0 and 1 where 0 indicates there are no deficits present and 1 indicates all deficits are present. Our lab has adopted a non-invasive 31 item clinical frailty index (Whitehead *et al.*, 2014). Using this frailty index, clinical assessments are made for the integument, muscoskeletal, vestibulocochlear, auditory, ocular, nasal, digestive, urogenital, and respiratory systems (Whitehead *et al.*, 2014). Animals are also observed for signs of discomfort. Previous studies have demonstrated that FI scores rarely exceed 0.5 in humans and 0.4 in mice (Rockwood *et al.*, 2017). This indicates there is a maximal limit to the number of health deficits an individual can accumulate and maintain survival. Importantly, deficit accumulation in mice reflects observations made in the clinical setting (Whitehead *et al.*, 2014). Accordingly, the FI can be used as a powerful tool to investigate the effects of overall health on cardiovascular function.

In the clinical setting, frail individuals have an increased risk of adverse health outcomes compared to non-frail patients of the same chronological age (Afilalo *et al.*, 2009; McNallen *et al.*, 2013; Maden *et al.*, 2016; Nguyen *et al.*, 2016; Kim *et al.*, 2017). In one study, frail patients that underwent cardiac surgery had a 2-3.5 increased risk of mortality within 1 year of surgery (Lytwyn *et al.*, 2017). In addition, frail patients are more susceptible to having 3 or more cardiovascular disease comorbidities, including hypertension, AF, and heart failure (McNallen *et al.*, 2013; Frisoli *et al.*, 2015). AF is more prevalent in the frail population compared to non-frail patients of the same chronological age (Polidoro *et al.*, 2013; Nguyen *et al.*, 2016). In fact, frailty can be used as a predictor of mortality in aged patients with AF (Nguyen *et al.*, 2016; Maden *et al.*, 2016; Kim *et al.*, 2017). However, the relationship between FI score and SAN and atrial function is poorly understood.

1.4. Natriuretic Peptides and Natriuretic Peptide Receptors

1.4.1. Natriuretic Peptides

Natriuretic peptides (NPs) are a group of cardioprotective hormones that play a vital role in regulating cardiovascular function. In a landmark study, de Bold *et al.* (1981) discovered that intravenous infusion of atrial homogenates results in a rapid reduction in blood pressure accompanied by natriuresis and diuresis. This study led to the discovery of atrial natriuretic peptide (ANP). Soon thereafter, B-type natriuretic peptide (BNP) (Sudoh *et al.*, 1988) and C-type natriuretic peptide (CNP) (Sudoh *et al.*, 1990) were purified from porcine brain matter and both peptides exhibited potent relaxant properties on smooth muscle. A fourth member, *Dendroaspis* natriuretic peptide (DNP) was discovered in the venom of the green mamba snake and has relaxant effects on contracted aortic strips (Schweitz *et al.*, 1992). All of these NPs are expressed in the myocardium and are detected in the circulation (Moghtadaei *et al.*, 2016a).

Structurally, NPs are characterized by a distinctive ring structure that is formed by a disulphide bridge between two cysteine resides that flank a highly conserved 17 amino acid sequence (Pandey, 2008; Potter *et al.*, 2009; Jansen and Rose, 2015; Moghtadaei *et al.*, 2016a). This peptide ring is essential for biological activity (Potter *et al.*, 2006). Structural variability between NPs occurs within the ring and the amino- and carboxyl-terminal extensions (Fig. 1.3). CNP lacks a C-terminal extension and is the most highly conserved NP between species (Pandey, 2008; Potter *et al.*, 2009).

NPs are transcribed as pre-pro-hormones that are transformed into biologically active NPs by post transcriptional processing. ANP is encoded by the *Nppa* gene and is transcribed as a 151 amino acid pre-pro-ANP polypeptide that is cleaved into a 126 amino acid pro-ANP molecule. Pro-ANP is stored in granules located in the atrial myocardium (Pandey, 2008; Potter *et al.*, 2009). Pro-ANP is cleaved by the serine protease corin to yield a biologically active ANP that consists of 28 amino acids. ANP is released into the coronary sinus, enabling it to circulate throughout the body as an endocrine factor. Plasma levels of ANP are 3.2-19.5 pmol/L in healthy subjects (Ogawa and de Bold, 2004). In healthy humans, the ANP concentration is 9600 pmol/g and 37 pmol/g in the atrium and ventricles, respectively. ANP levels increase as a result of atrial

Figure 1.3. Schematic representation of the amino acid sequence and ring structure of natriuretic peptides.

Abbreviations: ANP: Atrial natriuretic peptide; BNP: B-type natriuretic peptide; CNP: C-type natriuretic peptide; cANF: a synthetic NPR-C agonist; DNP: *Dendroaspis* natriuretic peptide.

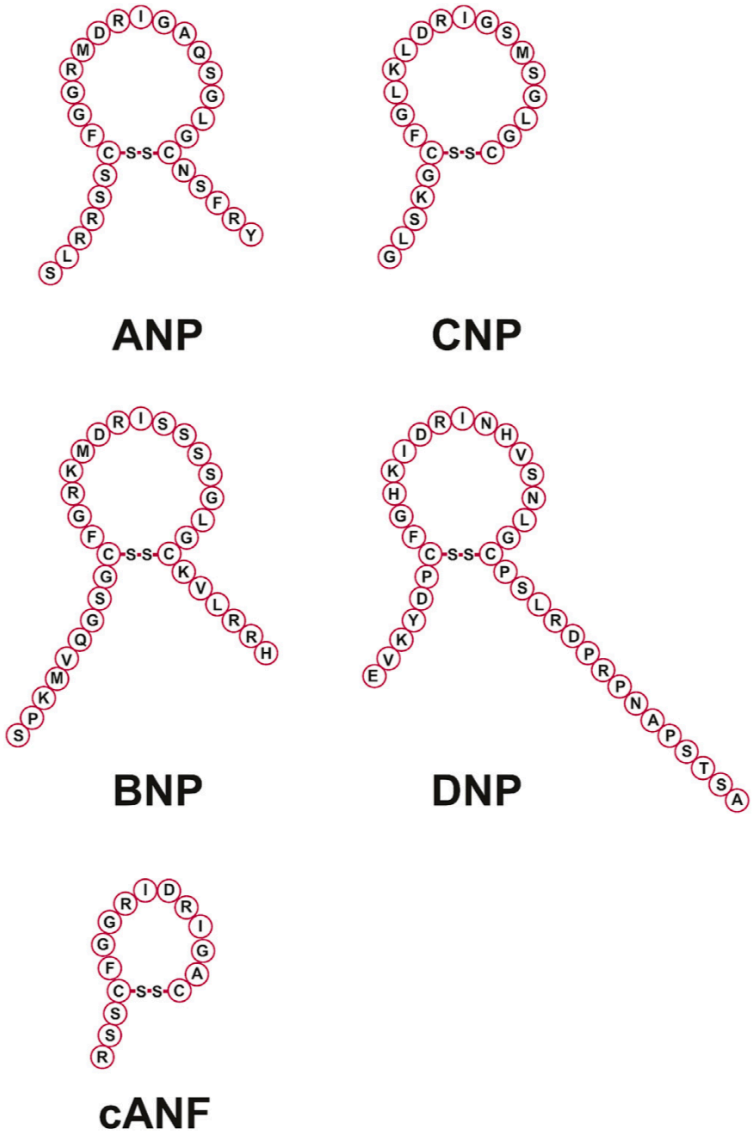

Figure 1.3

distension, as in the case of hypertension (Pandey, 2005; Volpe *et al.*, 2016). In addition, circulating levels of ANP increase by 10-30 fold in patients with congestive heart failure (Cody *et al.*, 1986; Mukoyama *et al.*, 1991; Wei *et al.*, 1993; Volpe *et al.*, 2016).

BNP is encoded by *Nppb* which yields a 134 amino acid pre-pro-BNP polypeptide that is cleaved to form a 108 amino acid pro-BNP molecule. Biologically active BNP is 32 amino acids in humans, dogs, and pigs whereas BNP in mice and rats is slightly longer at 45 amino acids (Potter *et al.*, 2006). Low levels of pro-BNP are stored in granules in atrial myocytes alongside pro-ANP (Pandey, 2008; Potter *et al.*, 2006). In healthy humans, plasma levels of BNP are 1.4-14.5 pmol/L and tissue levels are 250 pmol/g in the atria and 18 pmol/g in the ventricles (Ogawa and de Bold, 2004). BNP has the longest half-life of NPs at approximately 20 minutes, compared to 2-3 minutes for ANP and CNP (Potter *et al.*, 2006).

In the ventricular myocardium, BNP is transcriptionally regulated and expression is increased in response to wall stretch resulting from volume overload (Ogawa *et al.*, 1991; D'Souza *et al.*, 2004; Bricca and Lantelme, 2011). Accordingly, patients with cardiac hypertrophy or congestive heart failure have a 200-300 fold increase in circulating BNP levels, with levels circulating levels 10-50 times higher than ANP (Wei *et al.*, 1993; Del Ry *et al.*, 2013). BNP is used as a biomarker for left ventricular dysfunction and can be used as a predictor for the deterioration of cardiac function, morbidity, and mortality (Rubattu *et al.*, 2008; Geske *et al.*, 2013).

CNP is encoded by *Nppc*. CNP is not stored in granules, rather secretion is stimulated by cytokines and shear stress in endothelial cells (Pandey, 2008; Potter *et al.*, 2009). Pre-pro-CNP is a 126 amino acid sequence that is cleaved into a 103 amino acid pro-CNP. The intracellular serine endoprotease furin cleaves pro-CNP into a 53 amino acid CNP (CNP-53) molecule. CNP-53 is biologically active in cardiac tissue whereas a smaller molecule, CNP-22, is detected in the circulatory system (Potter *et al.*, 2006; Potter *et al.*, 2009). Circulating levels of CNP are very low at 1-6 pmol/L in healthy humans (Ogawa and de Bold, 2004). CNP levels in the human atrium are approximately 0.11pmol/g. Circulating CNP levels are increased in patients with congestive heart failure (Potter *et al.*, 2009; Del Ry *et al.*, 2013). It is thought that CNP functions as a paracrine molecule.

Much less is known about DNP. Structurally, DNP is a 38 amino acid molecule that has both an amino- and carboxyl- terminal extension (D'Souza *et al.*, 2004). DNP is detected in the mammalian circulatory system and the myocardium, with higher levels in the atria (Schirger *et al.*, 1999; Lisy *et al.*, 2001; Park *et al.*, 2015). Both circulating and tissue levels of DNP are increased in heart failure. The physiological and pathophysiological roles of DNP are poorly understood.

NPs are cleared from the circulatory system by two mechanisms. The first involves enzymatic digestion by neprilysin, a neutral endopeptidase that is expressed on the plasma membrane (Potter *et al.*, 2009; Volpe *et al.*, 2016). The primary cleavage sites are located within the peptide ring and cleavage in this region opens the ring structure, thereby inactivating the NP. Human BNP is more resistant to neprilysin degradation than ANP (Smith *et al.*, 2000). The second mechanism of NP degradation involves ligand-mediated internalization. In this mechanism, NP-NPR complexes are internalized and NPs are degraded. A small pool of receptors is recycled back into the membrane (Volpe *et al.*, 2016).

1.4.2. Natriuretic Peptide Receptors

NPs elicit their physiological effects by binding to specific natriuretic peptide receptors (NPRs). A schematic representation of NPRs, their respective ligands, and downstream signalling pathways is presented in Fig. 1.4. There are three NPRs denoted NPR-A, NPR-B, and NPR-C, which are encoded by *Npr1*, *Npr2*, and *Npr3*, respectively. NPRs are expressed in both cardiomyocytes and cardiac fibroblasts (Potter *et al.*, 2006; Jansen and Rose, 2015). NPR-A has affinity for both ANP and BNP, although it has greater affinity for ANP (Nakao *et al.*, 1992). NPR-B has specific affinity for CNP (Pandey, 2008; Moghtadaei *et al.*, 2016a). NPR-A and NPR-B are coupled to intracellular particulate guanylyl cyclase enzymes and upon activation results in an increase in intracellular cGMP levels. cGMP functions as a second messenger, activating protein kinase G (PKG), cyclic nucleotide-gated ion channels, and modulates phosphodiesterase (PDE) activity (Potter *et al.*, 2006; Pandey., 2008; Moghtadaei *et al.*, 2016a). In particular, NPR-A/B activation results in activation of phosphodiesterase 2 (PDE2) and

Figure 1.4. Schematic representation of natriuretic peptide receptors and their downstream signalling pathways.

Abbreviations: ANP: Atrial natriuretic peptide; BNP: B-type natriuretic peptide; CNP: C-type natriuretic peptide; cANF: a synthetic NPR-C agonist; DNP: *Dendroaspis* natriuretic peptide; NPR-A: natriuretic peptide receptor A; NPR-B: natriuretic peptide receptor B; NPR-C: natriuretic peptide receptor C; cAMP: cyclic adenosine monophosphate; cGMP: cyclic guanosine monophosphate; G_i: inhibitory G protein.

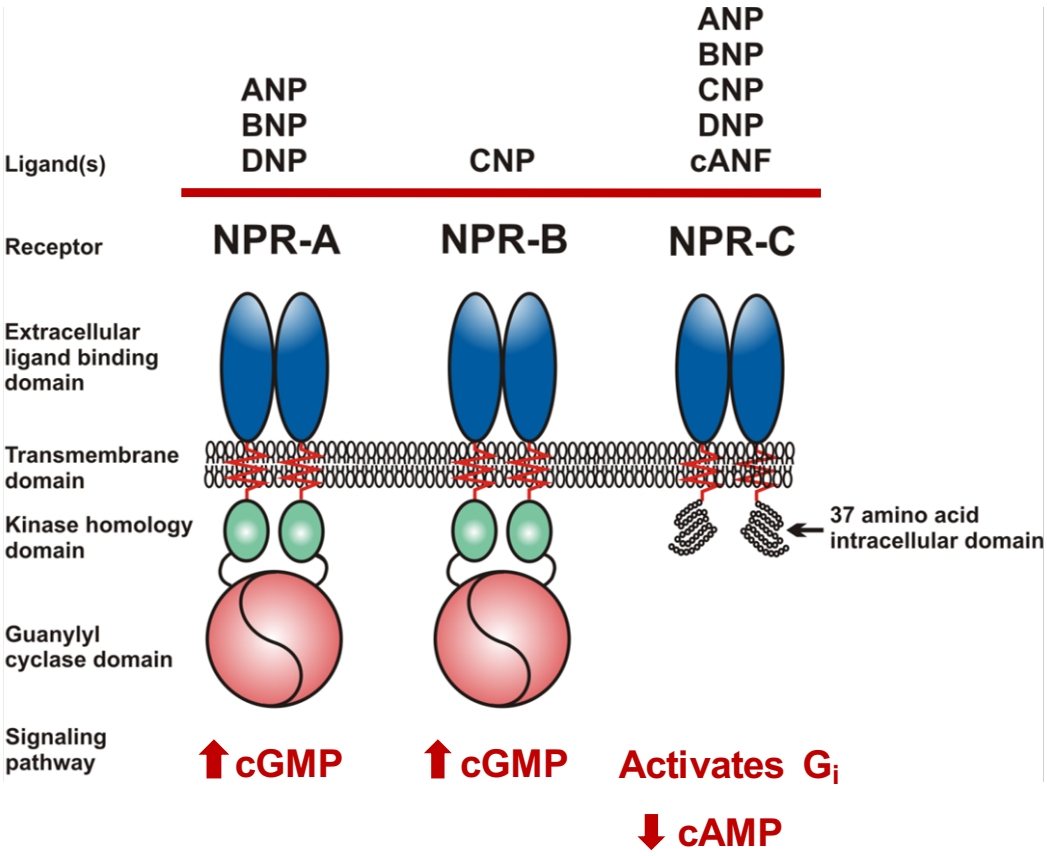
Ligand(s)
ANP
BNP
DNP
CNP
ANP
BNP
CNP
DNP
cANF
Receptor
NPR-A
NPR-B
NPR-C
Extracellular ligand binding domain
Transmembrane domain
Kinase homology domain
37 amino acid intracellular domain
Guanylyl cyclase domain
Signaling pathway
cGMP
cGMP
Activates G_i
cAMP

Figure 1.4

inhibition of phosphodiesterase 3 (PDE3). PKG phosphorylates a number of targets, including ion channels (Potter *et al.*, 2006).

In contrast, NPR-C binds all NPs with comparable affinity. NPR-C lacks a guanylyl cyclase domain (Anand-Srivastava, 2005; Rose and Giles, 2008; Moghtadaei *et al.*, 2016a). Rather, NPR-C has a 37 amino acid cytoplasmic domain that is coupled to a pertussis toxin sensitive inhibitory G protein (G_i). Upon activation, this results in inhibition of adenylyl cyclase and in turn a reduction in cAMP levels and protein kinase A (PKA) activity. In addition, the βγ subunit of G_i activates phospholipase C (PLC_β) and results in the generation of inositol triphosphate (IP_3) and diacylglycerol (DAG) from phosphatidyl inositol bisphosphate (PIP_2) (Zhou and Murthy, 2003; Anand-Srivastava, 2005; Rose and Giles, 2008; Moghtadaei *et al.*, 2016a). NPR-C is the most highly expressed NPR in the heart, and the atria has higher expression of NPRs compared to the ventricular myocardium (Anand-Srivastava *et al.*, 1993; Egom *et al.*, 2015; Hua *et al.*, 2015).

cANF is a synthetic NPR-C agonist (Maack *et al.*, 1987; Anand-Srivastava *et al.*, 1990; Anand-Srivastava, 2005). Structurally, cANF is a ring deleted analogue of ANP. Functionally, cANF application results in inhibition of adenylyl cyclase and a reduction in cAMP levels without any alterations in cGMP (Anand-Srivastava *et al.*, 1990). Exposure to pertussis toxin abolishes these effects, indicating that cANF has specific affinity for NPR-C and not NPR-A or NPR-B.

Upon activation, the NP system modulates physiological processes by altering intracellular cGMP and cAMP levels. cGMP is a ubiquitous second messenger that is synthesized by two types of guanylyl cyclases. The first is a particulate guanylyl cyclase domain that is coupled to NPR-A and NPR-B and the second is a soluble guanylyl cyclase that is activated by nitric oxide (Fischmeister *et al.*, 2006; Tsai and Kass, 2009). cGMP exerts its effects by activating PKG and PDEs. PDEs are a family of enzymes that degrade cyclic nucleotides into inactive 5'-nucleotide monophosphates (Fischmeister *et al.*, 2006; Potter *et al.* 2006). The heart expresses PDE1-5, PDE7, and PDE8, of which the activities of PDE2 and PDE3 are modulated by NPR-A and NPR-B activation. PDE2 and PDE3 can hydrolyze both cAMP and cGMP, however PDE3 has higher affinity for cGMP than cAMP (Boswell-Smith *et al.* 2006). Interestingly, cGMP functions as both a

substrate and an allosteric modulator of PDEs such that cGMP inhibits PDE3 and cGMP increases the activity of PDE2, thereby promoting cAMP hydrolysis (Boswell-Smith *et al.*, 2006; Zaccolo and Movsesian, 2007). In addition, activation of NPR-C inhibits adenylyl cyclase which results in a reduction in cAMP levels (Anand-Srivastava, 2005). This ultimately leads to a highly dynamic crosstalk between the cAMP and cGMP pathways, resulting in a compartmentalization of these two second messengers within cardiomyocytes.

1.4.3. Electrophysiological Effects of Natriuretic Peptides in the Heart

1.4.3.1. Effects of Natriuretic Peptides on Heart Rate and the Sinoatrial Node

NPs modulate heart rate by binding to NPRs. In Langendorff-perfused mouse hearts, exposure to BNP and CNP results in an increase in heart rate under baseline conditions. In contrast, exposure to the selective NPR-C agonist cANF does not alter heart rate under baseline conditions (Azer *et al.*, 2012; Springer *et al.*, 2012). Combined, these data indicate NPR-A/B signalling elicits a positive chronotropic response under baseline conditions.

In the presence of β-adrenergic receptor stimulation using isoproterenol, heart rate is increased in both wildtype and NPR-$C^{-/-}$ mice. In wildtype mice, this increase in heart rate was reduced by subsequent application of BNP or CNP (Azer *et al.*, 2012). In contrast to baseline conditions, subsequent application of cANF also reduced the heart rate in the presence of isoproterenol. The NPR-A blocker A71915 was used to further elucidate the role of the different NPRs. Application of BNP in the presence of isoproterenol and A71915 (results in only NPR-C activation by BNP) resulted in a reduction in heart rate. Combined, these data demonstrate that NPR-C modulates heart rate following β-adrenergic stimulation. Furthermore, these data demonstrate that activation of the NPR-A/B pathway has a stimulatory effect on heart rate whereas the NPR-C pathway has an inhibitory effect on heart rate.

The role of NPs on SAN function has been further interrogated using high resolution optical mapping in isolated preparations. BNP and CNP increase conduction velocity

across the SAN under basal conditions whereas cANF does not evoke a change in conduction velocity across the SAN (Azer *et al.*, 2014). NPR-A blockade using A71915 abolished the effects of BNP on conduction velocity, demonstrating that the effects are mediated by NPR-A, not NPR-C, under baseline conditions. Following β-adrenergic stimulation, subsequent application of BNP, CNP, or cANF slowed conduction velocity in the SAN (Azer *et al.*, 2014). The inhibitory effect was greatest with cANF and was abolished in the presence of NPR-C blockade, indicating the inhibitory effects are dependent on NPR-C activation. In NPR-$C^{-/-}$ mice, BNP application in the presence of isoproterenol increased conduction velocity, indicating that NPR-A is activated (Azer *et al.*, 2014). When taken together, these data unravel the complexity of the NP system in the SAN as the resulting conduction velocity is dependent on the contributions of the opposing NPR-A/B and NPR-C signalling cascades.

In isolated SAN myocytes, BNP and CNP increase AP firing rate under baseline conditions (Springer *et al.*, 2012). This is attributed to an increase in diastolic depolarization slope resulting from increases in I_f and $I_{Ca,L}$. In NPR-$C^{-/-}$ mice, AP firing frequency was increased in the presence of BNP (only NPR-A would be activated) and CNP (only NPR-B would be activated) with corresponding increases in I_f and $I_{Ca,L}$. In contrast, pharmacological blockade of NPR-A with A71915 abolished the effects of BNP in SAN myocytes. Application of the PDE3 inhibitor milrinone increased AP firing frequency, diastolic depolarization, I_f, and $I_{Ca,L}$ in the presence of BNP and CNP and occluded the effects of BNP and CNP indicating that PDE3 is a key mediator of the effects of these NP (Springer *et al.*, 2012). In the presence of isoproterenol, CNP and cANF reduce $I_{Ca,L}$ in isolated SAN myocytes without altering I_f (Rose *et al.*, 2004). This effect is dependent on NPR-C as a reduction in $I_{Ca,L}$ was observed when a G_i activator peptide was dialysed into the cell, therefore mimicking NPR-C activation. Combined these data demonstrate that under baseline conditions, NPs can potently increase SAN activity though NPR-A/B signalling. However, in the presence of β-adrenergic stimulation, NPR-C is activated and reduces SAN activity.

1.4.3.2. Effects of Natriuretic Peptides on Atrial Electrophysiology

NPs modulate atrial electrophysiology. Optical mapping studies have revealed that BNP and CNP increase conduction velocity across the atrial myocardium under baseline conditions (Azer *et al.*, 2014). On the other hand, cANF does not alter conduction velocity, indicating these effects are not mediated by NPR-C. In addition, blockade of NPR-A using A71915 followed by application of BNP does not change conduction velocity. Collectively, these findings indicate that BNP and CNP increase atrial conduction velocity by binding to NPR-A/B, and not NPR-C. In the presence of β-adrenergic stimulation, subsequent application of BNP and CNP results in a reduction in conduction velocity across the atria (Azer et a, 2014). A greater reduction in conduction velocity is observed in the presence of cANF, indicating activation of NPR-C. In atrial preparations from NPR-$C^{-/-}$ mice, conduction velocity is increased following BNP application in the presence of isoproterenol, indicating that NPR-A is activated (Azer *et al.*, 2014). Combined, these findings indicate that in the presence of β-adrenergic stimulation, not only are multiple NPR subtypes activated but the resulting conduction velocity is dependent on the balance between the stimulatory effects of NPR-A/B and the inhibitory effects of NPR-C.

The effects of NPs have also been investigated in isolated atrial myocytes. Under basal conditions, ANP, BNP, and CNP do not alter AP morphology in isolated mouse atrial myocytes (Springer *et al.*, 2012; Hua *et al.*, 2015). Following β-adrenergic stimulation with isoproterenol, ANP and BNP increase APD in wildtype mice (Springer *et al.*, 2012; Hua *et al.*, 2015). In atrial myocytes isolated from NPR-$C^{-/-}$ mice, ANP and BNP increase $I_{Ca,L}$ indicating the response is not mediated by NPR-C activation. Furthermore, in the presence of PDE3 inhibition, thereby mimicking NPR-A/B activation, subsequent application of ANP or BNP increases $I_{Ca,L}$ whereas the NPR-A antagonist A71915 abolishes this effect. Combined, these data demonstrate NPR-A/B, not NPR-C, enhance $I_{Ca,L}$ in the presence of β-adrenergic stimulation.

To date, the majority of the effects of NPs on atrial electrophysiology have been attributed to $I_{Ca,L}$. Although limited, there is limited evidence to indicate NPs can modulate the activity of other ion currents. In human atrial myocytes, ANP reduces I_{to}

(Le Grand *et al.*, 1992). In rat ventricular myocytes, BNP and CNP inhibit the ATP-sensitive K^+ channel (Burley *et al.*, 2014). In contrast, ANP does not affect I_{Na} in the presence of isoproterenol in mouse atrial myocytes (Hua *et al.*, 2015). This is an area requiring further investigation.

1.4.3.3. Effects of Natriuretic Peptides on Blood Pressure and Structural Remodelling

As their name suggests, NPs are known for their role in regulating blood pressure. ANP and NPR-A knockout mice are hypertensive (Lopez *et al.*, 1995; Oliver *et al.*, 1997; Feng *et al.*, 2003), whereas overexpression of ANP or BNP in mice results in hypotension (Stienhelper *et al.*, 1990; Barbee *et al.*, 1994; Ogawa *et al.*, 1994). ANP and BNP are secreted into the circulation in response to atrial and ventricular distension and regulate blood pressure by binding to NPR-A (Woods, 2004; Volpe *et al.*, 2016). In addition, circulating ANP levels are inversely correlated with blood pressure (Rubattu *et al.*, 2008). In the kidneys, ANP promotes natriuresis and diuresis (Potter *et al.*, 2006). ANP also induces vasodilation which in turn reduces preload and afterload (Rubattu *et al.*, 2008; Calzetta *et al.*, 2016). In addition, ANP and BNP inhibit the pressor hormones renin, aldosterone, and arginine vasopressin (Woods, 2004; Volpe *et al.*, 2016). Lastly, CNP functions as a paracrine factor to regulate vascular tone and inhibit vascular remodelling.

NPs are potent regulators of cardiac structure. Cardiac fibrosis levels are significantly increased in BNP, NPR-A, and NPR-C knockout mice (Oliver *et al.*, 1997; Tamura *et al.*, 2000; Egom *et al.*, 2015). In addition, ANP and NPR-A knockout mice have enlarged cardiomyocytes and cardiac hypertrophy (Oliver *et al.* 1997; Kishimoto *et al.*, 2000; Knowles *et al.*, 2001; Feng *et al.*, 2003; Wang *et al.*, 2003). In contrast, overexpression of ANP and NPR-A results in a reduction in heart size and cardiomyocyte size (Barbee *et al.*, 1994; Kishimoto *et al.*, 2000). These genetic phenotypes demonstrate the NP system has antifibrotic and antihypertrophic properties.

Tissue culture experiments have investigated the effects of NPs on cardiac fibroblast function. Growth hormones and growth factors including Ang II, TGF-β1, FGF,

endothelin (ET), insulin-like growth factor 1 (IGF-1) are involved in increasing cardiac fibroblast proliferation, hypertrophy, collagen expression, and extracellular matrix remodelling (Calvieri *et al.*, 2012; Jansen and Rose, 2015). In cultured cardiac fibroblasts stimulated with these proliferative agents, subsequent application of ANP, BNP, or CNP potently reduces the rate of DNA synthesis and cellular proliferation (Cao and Gardner, 1995; Kapoun *et al.*, 2004; Glenn *et al.*, 2009). Furthermore, ANP, BNP, and CNP inhibit collagen mRNA synthesis and secretion by modulating the Ang II and TGF-β1 signalling pathways (Redondo *et al.*, 1998; Horio *et al.*, 2003; Kapoun *et al.*, 2004; Li *et al.*, 2008; Parthasarathy *et al.*, 2013). These effects are concentration dependent and attributed to increased cGMP levels resulting from activation of NPR-A and NPR-B (Redondo *et al.*, 1998; Horio *et al.*, 2003; Li *et al.*, 2008). Combined, these data demonstrate NPs are potent regulators of cell proliferation, hypertrophy, and fibrosis.

Experimental models of cardiovascular disease have further demonstrated a cardioprotective role for NPs in structural remodelling. Aortic constriction in ANP, BNP, or NPR-A knockout mice results in severe ventricular fibrosis in conjunction with increased collaged and TGF-β mRNA expression (Tamura *et al.*, 2000; Wang *et al.*, 2003; Franco *et al.*, 2004; Li *et al.*, 2008) and in NPR-A knockout mice results in more severe left ventricular hypertrophy (Knowles *et al.* 2001). Conversely, chronic NP infusion following myocardial infarction (MI) is cardioprotective in rats. One study treated rats with either a low dose (5 µg/kg/day) or a high (15 µg/kg/day) dose of BNP for 8 weeks following MI (He *et al.*, 2009). In this study, rats treated with the higher dose of BNP had significantly lower levels of TGF-β1 and left ventricular fibrosis compared to the vehicle controls (He *et al.*, 2009). Another study examined the effects of CNP (0.1 µg/kg/min) treatment for two weeks post MI in rats (Soeki *et al.*, 2005). Rats treated with CNP had drastically less fibrosis at both the remote and border regions compared to vehicle treated controls. Cardiomyocytes in the left ventricle were also smaller in CNP treated animals. The role of the NP system in regulating atrial structural remodelling *in vivo* is poorly understood.

1.4.3.4. The Natriuretic Peptide System in Cardiovascular Disease

NP levels significantly increase in cardiovascular disease. Plasma ANP and BNP levels are significantly increased in patients with hypertension, hypertrophy, and heart failure (Takemura *et al.*, 1991; Hasegawa *et al.*, 1993; Nishikimi *et al.*, 1996; Berger *et al.*, 2002; Macheret *et al.*, 2012). ANP and BNP levels in atrial and ventricular cardiomyocytes are also increased in patients with heart disease (Takemura *et al.*, 1991; Hasegawa *et al.*, 1993; Inoue *et al.*, 2000). In addition, patients with both hypertension and concentric hypertrophy exhibit a greater increase in plasma ANP and BNP levels compared to hypertensive patients alone (Nishikimi *et al.*, 1996). Furthermore, plasma ANP and BNP levels are 3-fold higher in patients with AF (Inoue *et al.*, 2000; Siontis *et al.*, 2014; Wozakowska-Kaplon, 2009). Following cardioversion, plasma NP levels are reduced. Plasma BNP levels are used as a biomarker for heart failure as increased levels are correlated with an increased severity of heart failure (Wettersten and Maisel, 2016). Plasma BNP levels can also be used as a predictor of hospital readmission and sudden death in patients with hypertrophic cardiomyopathy or chronic heart failure (Berger *et al.*, 2002; Wright and Struthers, 2006; Boerrigter *et al.*, 2009; Geske *et al.*, 2013; Gandhi and Pinney, 2014; Maisel *et al.*, 2015). Collectively, these findings indicate NPs are biomarkers for cardiovascular disease and are powerful predictors of the severity of disease.

Mutations in the NPs or NPRs are associated with an increased susceptibility to AF. An autosomal dominant gene mutation in *NPPA* (encodes ANP) is associated with AF in a European family (Hodgson-Zingman *et al.*, 2008). This mutation results in the formation of mutant ANP (mANP). Genetic studies have revealed that mANP contains a two base pair mutation in the *NPPA* gene that abolishes a stop codon in exon 3. Structurally, this frameshift mutation results in a 12 amino acid extension on the C-terminal extension of ANP (Dickey *et al.*, 2009). In addition, mANP is resistant to proteolytic degradation. Circulating levels of mANP are 5-10 times higher than ANP in affected family members. All affected family members are heterozygous for this gene mutation and have been diagnosed with AF.

The basis for AF in these patients has been unravelled in a series of electrophysiology experiments. In this study, ANP exposure resulted in an increase in AP upstroke velocity (V_{max}) and APD following β-adrenergic stimulation (Hua *et al.*, 2015). In contrast, subsequent exposure to mANP had the opposite effect and reduced V_{max} and APD. Next, the effects of ANP and mANP were examined on $I_{Ca,L}$ following β-adrenergic stimulation. ANP increased $I_{Ca,L}$ whereas mANP reduced $I_{Ca,L}$ in wildtype mice. In NPR-$C^{-/-}$ mice, ANP increased $I_{Ca,L}$ whereas the effects of mANP were abolished. In contrast, the effects of ANP were abolished in the presence of the NPR-A blocker A71915. The opposing effects of ANP and mANP on $I_{Ca,L}$ were also observed in human atrial myocytes (Hua *et al.*, 2015). Combined, these data demonstrate ANP and mANP elicit their effects by activating different NPR subtypes whereby ANP activates NPR-A and mANP activates NPR-C.

The effects of mANP were further examined in optical mapping experiments of atrial preparations in the presence of β-adrenergic stimulation. Application of ANP resulted in an increase in conduction velocity across both the right and left atrium (Hua *et al.*, 2015). In contrast, mANP reduced conduction velocity across the atria. Next, atrial pacing was used to ascertain the susceptibility to arrhythmias in the presence of either ANP or mANP. Strikingly, application of mANP induced arrhythmias in 62.5% of preparations whereas ANP exposure did not induce any arrhythmias in paced preparations following β-adrenergic stimulation (Hua *et al.*, 2015). Collectively, these data demonstrate that mANP is proarrhythmic whereas ANP is antiarrhythmic.

In another study, the cardiac phenotype of NPR-$C^{-/-}$ mice was characterized. NPR-$C^{-/-}$ mice contain a 36 base pair deletion that results in the formation of a non-functional NPR-C protein that is truncated in the extracellular domain (Jaubert *et al.*, 1999). NPR-C deficient mice are characterized by SAN dysfunction and an increased susceptibility to AF. Structurally, echocardiography experiments demonstrate that atrial size is not different in NPR-$C^{-/-}$ mice compared to NPR-$C^{+/+}$ mice (Egom *et al.*, 2015). In addition, blood pressure is not altered in NPR-$C^{-/-}$ mice compared to wildtype controls.

Baseline heart rate was not different in anaesthetized NPR-$C^{-/-}$ mice compared to NPR-$C^{+/+}$ mice. However, heart rate is significantly reduced in NPR-$C^{-/-}$ mice in the presence of autonomic nervous system blockade (Egom *et al.*, 2015). cSNRT is

prolonged in NPR-C$^{-/-}$ mice, which is consistent with a reduction in intrinsic heart rate. In addition, optical mapping experiments of the SAN demonstrate that NPR-C$^{-/-}$ mice have an increase in cycle length and a reduction in SAN conduction velocity compared to NPR-C$^{+/+}$ mice (Egom *et al.*, 2015). Patch-clamp experiments have revealed there are no differences in AP morphology in isolated SAN myocytes from NPR-C$^{-/-}$ mice compared to NPR-C$^{+/+}$ mice. Combined, these data demonstrate SAN dysfunction in NPR-C$^{-/-}$ mice.

Atrial function is also impaired in NPR-C$^{-/-}$ mice. In intracardiac programmed stimulation experiments, approximately 50% of NPR-C$^{-/-}$ mice were induced into AF compared to 6% of NPR-C$^{+/+}$ mice (Egom *et al.*, 2015). In addition, AF duration ranged from 1.1 to 116.5 seconds in NPR-C$^{-/-}$ mice that were induced into AF. Under baseline conditions, AERP was prolonged in NPR-C$^{-/-}$ mice and P wave duration was increased in the presence of autonomic nervous system blockade compared to NPR-C$^{+/+}$ mice (Egom *et al.*, 2015). Optical mapping studies demonstrated that conduction velocity is reduced in the right and left atria of NPR-C$^{-/-}$ mice compared to NPR-C$^{+/+}$ mice. Patch-clamp studies revealed there were no differences in AP morphology in right atrial myocytes from NPR-C$^{-/-}$ mice compared to NPR-C$^{+/+}$ mice. On the other hand, atrial fibrosis and collagen expression is increased in NPR-C$^{-/-}$ mice compared to NPR-C$^{+/+}$ mice. Collectively, these findings indicate the increased susceptibility to AF and reduction in conduction velocity in NPR-C$^{-/-}$ mice is attributed to enhanced fibrosis.

In contrast to the SAN and atria, ventricular function is not altered in NPR-C$^{-/-}$ mice. In anaesthetized mice, QRS duration, Q-T interval, and VERP measurements were not different between NPR-C$^{-/-}$ and NPR-C$^{+/+}$ mice (Egom *et al.*, 2015). In addition, ventricular arrhythmias could not be induced in either genotype using high frequency burst pacing of the right ventricle. Studies also revealed there are no differences in interstitial fibrosis nor collagen mRNA expression in NPR-C$^{-/-}$ mice compared to NPR-C$^{+/+}$ mice (Egom *et al.*, 2015). This is consistent with the finding that NPR-C is more highly expressed in the supraventricular regions of the heart.

1.5. Thesis Objectives

AF is a highly prevalent cardiac arrhythmia. Epidemiology studies have demonstrated the prevalence of AF increases in patients with concomitant hypertension, hypertrophy, heart failure (Allessie *et al.*, 2001; Gradman and Alfayoumi, 2006; Schotten *et al.*, 2011; Ziaeian and Fonarow, 2016). Hypertensive heart disease leads to both cardiac hypertrophy and heart failure (Messerli *et al.*, 2017), however the effects on atrial electrophysiology remain poorly understood. Even less is known about the comparative effects of heart disease on right and left atrial myocytes. Chronic Ang II treatment in mice results in hypertension and hypertrophy. In addition, previous studies have demonstrated that Ang II treatment is associated with SAN dysfunction and an increased susceptibility to AF (Swaminathan *et al.*, 2011; Purohit *et al.*, 2013). However, the underlying mechanisms remain poorly understood. Accordingly, the first goal of my thesis was to determine the effects of chronic Ang II treatment on SAN and atrial function *in vivo.* The second goal of my thesis was to characterize electrical remodelling in right and left atrial myocytes from Ang II treated wildtype mice. These data are presented in Chapters 3 and 4.

NPs are powerful cardioprotective hormones that have profound effects on electrical function in the SAN and atria. NP expression is increased in patients with AF, hypertension, hypertrophy, and heart failure (Macheret *et al.*, 2012; Sergeeva and Christoffels, 2013; Gandhi and Pinney, 2014). In addition, dysregulation of the NP system is associated with AF. In particular, mANP is associated with familial AF (Hodgson-Zingman *et al.*, 2008) and has opposing effects on atrial electrophysiology compared to ANP (Hua *et al.*, 2015). In addition, NPR-C$^{-/-}$ mice have an increased susceptibility to AF (Egom *et al.*, 2015). However, the role of NPs in heart disease is poorly understood. Accordingly, the third goal of my thesis is to characterize the effects of Ang II treatment in NPR-C$^{-/-}$ mice and to determine if chronic NPR-C activation is protective against electrical remodelling in Ang II treated mice. The effects of Ang II treatment in NPR-C deficient mice and the effects of co-treatment with the NPR-C agonist cANF in Ang II treated mice are presented in Chapter 5.

There is an age-related increase in the prevalence of SAN dysfunction and AF (Rahman *et al.*, 2014; Monfredi and Boyett, 2015; Ziaeian and Fonarow, 2016; Padfield *et al.*, 2017). However, individuals age at different rates such that the overall health status of two individuals of the same chronological age varies from fit to frail. Accordingly, the goal of Chapter 6 was to determine the effects of age and frailty on SAN and atrial function *in vivo*.

CHAPTER 2
MATERIALS AND METHODS

2.1. Experimental Animals

This study used wildtype (C57BL/6; Charles River Laboratories) and NPR-$C^{-/-}$ male mice. NPR-$C^{-/-}$ mice were initially obtained from Jackson Laboratory (strain: B6;C-$Npr3^{lgj}$/J) then backcrossed with C57BL/6 mice for more than 15 generations in the animal care facility before being used for experiments. The NPR-$C^{-/-}$ mice contain an in-frame 36 base pair deletion. This mutation results in the formation of a non-functional NPR-C protein product that is truncated by 12 amino acids in the extracellular domain (Jaubert *et al.*, 1999).

Mice were housed in our animal care facility until used experimentally. Mice used in the Ang II project (Chapters 3, 4, and 5) were used between the ages of 10 and 15 weeks. Mice used in the ageing and frailty project (Chapter 6) were purchased and housed in our animal care facility until experimental use. Mice were housed at a maximum of 5 mice per cage and had *ad libitum* access to food (mouse chow) and water. Animals were maintained on a 12-hour light/dark cycle. All experimental protocols performed in this study were approved by the Dalhousie University Committee for Laboratory Animals and were in accordance with the regulations of The Canadian Council on Animal Care.

2.2. Surgical Procedures and Blood Pressure Measurements

Mice were implanted with subcutaneous miniosmotic pumps (Alzet model 1004) to allow for the continuous delivery of saline, Ang II (3 mg/kg/day; Bachem H-1705), or Ang II with cANF (Bachem H-3134) for three weeks. Saline was used as a vehicle control. Briefly, mice were anaesthetized with 2% isoflurane inhalation and an incision was made on their lateral side. A miniosmotic pump was inserted and the incision was sutured or stapled closed. Mice were administered a dose of the analgesic ketoprofen.

Mice were monitored following surgery and throughout the treatment period until used experimentally.

Blood pressure measurements were taken in conscious restrained mice using a tail-cuff apparatus (IITC Life Sci, Woodland Hills, CA, USA). Mice were trained in the blood pressure apparatus for two days before any measurements were taken. Baseline blood pressure measurements were taken prior to miniosmotic pump insertion and the final blood pressure measurements were taken at the end of the three week treatment period, before mice were used experimentally.

2.3. *In vivo* Electrophysiology and Intracardiac Programmed Electrical Stimulation

Mice were anaesthetized with 3% isoflurane inhalation and three 30-gauge subdermal needle electrodes (Grass Technologies) were used to record surface ECGs in a lead II confirmation with a grounding electrode. Body temperature was continuously recorded using a rectal thermometer and maintained at 37 ± 0.5ºC using a heating pad. To record intracardiac ECGs and perform intracardiac programmed electrical stimulation protocols, a 1.2 French octapolar electrophysiology catheter (Transonic Scisence Inc, London, Ontario) was inserted into the right heart via the jugular vein. Correct catheter placement was achieved by obtaining a predominantly atrial signal in the proximal lead and ventricular signals in the distal lead. Once correct placement was achieved, anesthetic was lowered and maintained at 2% isoflurane for the remainder of the experiment. Surface and intracardiac ECGs were acquired using a Gould ACQ-7700 amplifier and Ponemah Physiology Platform software (Data Sciences International, St. Paul, MN, USA) and stored for offline analysis.

Surface ECG recordings were used to calculate standard ECG parameters including the R-R interval, P wave duration, and P-R interval. The R-R interval was defined as the time between the peak of two successive R waves. P wave duration was measured from the start to the end of the P wave. P-R interval was calculated as the time between the start of the P wave to the peak of the R wave. An average of 4 heart beats was used to determine the value for each ECG parameter for a given mouse.

Intracardiac programmed electrical stimulation was used to measure sinoatrial node recover time (SNRT), atrial effective refractory period (AERP), and atrioventricular node effective refractory period (AVERP). Stimulation pulses were given at 3 V for 2 ms using a cycle length of 100 ms to ensure continuous capture and drive of cardiac conduction using the neuro/Craft^{TM} StimPulse Stimulator (FHC, Bowdoin, ME, USA). SNRT was measured by delivering a 12 stimulus drive train at a fixed cycle length of 100 ms. SNRT was defined as the time interval between the last stimulated beat and the start of the first intrinsic heartbeat, as defined as the beginning of the P wave. To correct for variability in heart rate between animals, corrected SNRT (cSNRT) was calculated as the difference between SNRT and the pre-stimulus R-R interval (cSNRT = SNRT – R-R). ERP measurements were determined using a S1-S2 protocol where an 8 stimulus drive train (S1) at a fixed cycle length of 100 ms was delivered followed by an extra stimulus (S2) at a progressively shorter cycle length. ERPs were defined as the shortest S1-S2 interval that allowed for capture of the region of interest. This was defined as the P wave for AERP measurements and a dropped QRS complex for AVERP measurements.

Rapid burst pacing of the right atrium was used to determine susceptibility to AF in a subset of mice, as we have previously described (Egom *et al.*, 2015). Briefly, mice were given multiple high frequency bust pace stimulations with a 2 min rest period between each stimulation. AF was defined as a rapid and irregular atrial rhythm in association with irregular R-R intervals that persisted for at least 1 second. AF duration was quantified for each mouse and defined as the time from the last burst pace stimulus to the time the mouse reverted back into normal sinus rhythm. AF duration was defined as brief (<5 seconds), non-sustained (5-25 seconds), and sustained (>25 seconds).

The autonomic nervous system was blocked in a subset of animals using atropine and propranolol to block muscarinic and β-adrenergic receptors, respectively. For these experiments, stock solutions were made daily by dissolving atropine sulfate salt hydrate and propranolol hydrochloride in milliQ water. Once heart rates were stable, mice were administered with a combined intraperitoneal injection of atropine and propranolol at a dose of 10 mg/kg. These compounds were allowed to circulate for 25 min.

2.4. Atrial Myocyte Isolation

Atrial myocytes were isolated as described previously (Egom *et al.*, 2015; Hua *et al.*, 2015). Briefly, mice were anaesthetized using isoflurane inhalation then sacrificed by cervical dislocation. The right or left atrial appendage was removed and placed in 35ºC Tyrode's solution containing (in mM): 140 NaCl, 5.4 KCl, 1.2 KH_2PO_4, 1.0 $MgCl_2$, 1.8 $CaCl_2$, 5.55 glucose, and 5 HEPES adjusted to pH 7.4 with NaOH. Heparin was added to the Tyrode's solution to prevent blood clotting and all steps were performed at 35ºC. The right or left atrial appendage was cut into strips then transferred to in a 'low Ca^{2+}, Mg^{2+} free' solution for 5 min followed by two brief washes. The 'low Ca^{2+}, Mg^{2+} free' solution contained (in mM): 140 NaCl, 5.4 KCl, 1.2 KH_2PO_4, 0.07 $CaCl_2$, 50 taurine, 18.5 glucose, 5 HEPES, and 1 mg/mL bovine serum albumin (BSA) adjusted to pH 6.9 with NaOH. Next, atrial strips were enzymatically digested in 5 mL of 'low Ca^{2+}, Mg^{2+} free' solution containing 1064 units collagenase (type II, Worthington Biochemical Corporation), 9 units elastase (from porcine pancreas, Worthington Biochemical Corporation), and 62.5 µL of a 1 mg/µL protease from *Streptomyces griseus* (type XIV, Sigma) solution dissolved in water. Tissue strips were digested for 30 min at 35ºC with occasional agitation. Following the completion of enzymatic digestion, tissue strips were washed 3 times in 5 mL of modified Kraft-Brühe (KB) solution containing (in mM): 100 K-glutamate, 10 K-aspartate, 25 KCl, 10 KH_2PO_4, 2 $MgSO_4$, 20 taurine, 5 creatine, 0.5 EGTA, 20 glucose, 5 HEPES, and 0.1% BSA adjusted to pH 7.2 with KOH. Tissue strips were transferred to 2.5 mL of modified KB solution and allowed to rest for 5 min. Digested tissue strips were gently triturated using a wide-bore glass pipet to mechanically isolate individual atrial myocytes. Right or left atrial myocytes were stored in approximately 5 mL of modified KB solution at room temperature and used for electrophysiology experiments within 6 hours of isolation.

2.5. Solutions and Electrophysiology Protocols

In this study, APs and ion currents were recorded in isolated atrial myocytes using the current clamp or voltage clamp configuration of the patch-clamp technique.

Microelectrode pipets were pulled from borosilicate glass (with filament, 1.5 mm OD, 0.75 mm ID; Sutter Instrument Company) using a Flaming/Brown pipette puller (model p-87; Sutter Instrument Company). Microelectrodes were positioned within the recording chamber using a micromanipulator (Burleigh PCS-5000 system) which was mounted on the stage of an inverted microscope (Olympus IX71). A flow rate of ~ 2 mL/min was used for solutions superfused over the recording chamber and a grounding electrode was placed in a 3 M KCl, 2% agarose bridge in the recording chamber. Once filled with internal solution the access resistance of the microelectrodes was 4-5 MΩ. Gigaohm (GΩ) seals were made between the microelectrode and the extracellular membrane of the atrial myocyte. All ion currents were recorded in the whole-cell configuration of the patch-clamp technique and APs were recorded using either the whole-cell or perforated patch configuration. Data sets were combined if AP recordings for a given treatment group were generated using both the whole-cell and perforated patch-clamp configuration as there were no differences in the resulting AP parameters. When in the whole-cell configuration, series resistance was typically below 15 MΩ following rupture and series resistance compensation was adjusted to ~ 85% using an Axopatch 200B amplifier (Molecular Devices). For all patch-clamp experiments, data was acquired using Digidata 1440 and pCLAMP 10 software (Molecular Devices), and stored for offline analysis. Patch-clamp recordings were obtained from right or left atrial myocytes isolated from a minimum of 3 mice. Most data sets include recordings from at least 5 mice.

Stimulated APs were recorded with a normal Tyrode's solution consisting of (in mM): 140 NaCl, 5.4 KCl, 1 $MgCl_2$, 1 $CaCl_2$, 10 HEPES, and 5.5 glucose and adjusted to pH 7.4 with NaOH. The pipet filling solution contained (in mM): 5 NaCl, 140 KCl, 1 $MgCl_2$, 0.2 $CaCl_2$, 10 HEPES, 5 EGTA, 4 Mg-ATP, 0.3 Na-GTP, and 6.6 Na-phosphocreatine and adjusted to pH 7.2 with KOH. Amphotericin B (200 ug/mL) was added to the pipet filling solution for APs recorded using the perforated patch-clamp technique. Once a GΩ seal was formed between the myocyte and microelectrode (filled with Amphotericin B), cells were monitored for the appearance of capacitative transients as the access resistance lowered. APs were recorded once the access resistance was below 30 MΩ, which was typically achieved within 5 min of sealing onto the cell. To record APs, a small amount of depolarizing current was injected for 20 ms into the cell every 5

seconds. The amount of depolarizing current injected was optimized for each cell to ensure the stimulus threshold was met to generate an AP without producing a stimulus artifact. Typically, right atrial myocytes and saline treated left atrial myocytes received ~0.05 nA, whereas Ang II treated left atrial myocytes were injected with ~0.1 nA of depolarizing current.

I_{Na} was recorded in atrial myocytes using a modified Tyrode's solution. This solution contained (in mM): 5 NaCl, 130 CsCl, 5.4 TEA-Cl, 1 $MgCl_2$, 1 $CaCl_2$, 10 HEPES, and 5.5 glucose and adjusted to pH 7.4 with CsOH. Nifedipine (10 μM) was added to block $I_{Ca,L}$. The pipette solution contained (in mM): 5 NaCl, 130 CsCl, 1 $MgCl_2$, 0.2 $CaCl_2$, 10 HEPES, 5 BAPTA, 5 Mg-ATP, and 0.3 Na-GTP and adjusted to pH 7.2 with CsOH. The voltage clamp protocol used to record I_{Na} was a series of 50 ms steps from -100 to +50 mV in 10 mV increments from a holding potential of -120 mV.

A modified, sodium-free Tyrode's solution was used to record $I_{Ca,L}$. This solution contained (in mM): 145.5 TEA-Cl, 1 $MgCl_2$, 2 $CaCl_2$, 10 HEPES, and 5.5 glucose adjusted to pH 7.4 with CsOH. The internal pipette solution used to record $I_{Ca,L}$ contained (in mM): 5 NaCl, 135 CsCl, 1 $MgCl_2$, 0.2 $CaCl_2$, 10 HEPES, 5 EGTA, 4 Mg-ATP, 0.3 Na-GTP, and 6.6 Na-phosophocreatine and adjusted to pH 7.2 with CsOH. The voltage clamp protocol used to record $I_{Ca,L}$ was a series of voltage clamp steps from -60 to +80 mV in 10 mV increments for 250 ms that returned to a holding potential of -70 mV between each step.

I_{Na} and $I_{Ca,L}$ were measured as the difference between the peak inward current and the steady state current measured at the end of the voltage step (before returning to the holding potential), and normalized to cell capacitance. Activation kinetics were analyzed for both I_{Na} and $I_{Ca,L}$ by calculating chord conductance (G), using the equation $G=I/(V_m-V_{rev})$. $V_{1/2}$ of activation ($V_{1/2(act)}$) and slope factor (k) were calculated by fitting the chord conductance with the Boltzmann equation in Origin 6.0.

Potassium currents were recorded in the whole-cell configuration of the patch-clamp technique using a normal Tyrode's solution and the same pipette filling solution as used to record APs. To record total potassium currents (no pre-pulse), cells were held at a holding potential of -80 mV then I_K was recorded using voltage clamp steps (500 ms duration) from -120 to +80 mV in 10 mV increments. To record potassium currents with

an inactivating pre-pulse (to inactivate I_{to}), cells were given a 200 ms pre-pulse to -40 mV immediately followed by 500 ms voltage clamp steps from -120 to +80 mV from a holding potential of -80 mV. For both the no pre-pulse and with pre-pulse recordings, I_K was measured at the peak current for each voltage step and current was normalized to cell capacitance. I_{to} was calculated as the difference in current between the no pre-pulse and with pre-pulse voltage clamp protocols at each membrane potential (Kuo *et al.*, 2001; Lomax *et al.*, 2003b).

4-aminopyradine (4-AP) sensitivity was used to determine I_{Kur} (Wang *et al.*, 1993; London *et al.*, 2001). In this set of experiments, the following voltage step protocol was used: cells received a pre-pulse to -40mV for 200 ms to inactivate I_{to} immediately followed by a 500 ms step to +30 mV before returning to a holding potential of -80 mV. Cells were superfused with normal Tyrode's solution to measure baseline current, then 100 μM 4-AP in normal Tyrode's solution was superfused over the recording chamber. Once current was stabilized in the presence of 4-AP, the solution was switched back to normal Tyrode's solution. Currents at baseline, in the presence of 4-AP, and after washout were measured as the peak current for each time point and normalized to cell capacitance. I_{Kur} is sensitive to micromolar concentrations of 4-AP (Wang *et al.*, 1993; Nattel *et al.*, 1999; London *et al.*, 2001; Lomax *et al.*, 2003b). Accordingly, I_K sensitivity in the presence of 4-AP can be used to assess the level of I_{Kur} in myocytes. 4-AP sensitive current was calculated as the percent reduction in I_K using the formula: Percent reduction in $I_K = (1-(I_{K(4\text{-}AP)}/I_{K(baseline)}))*100$.

In a separate set of experiments, barium sensitive potassium current was measured. Barium chloride ($BaCl_2$) is a selective I_{K1} blocker (Lomax *et al.*, 2003b). In this set of experiments, cells were superfused with normal Tyrode's solution to establish a baseline I_K then 100 μM $BaCl_2$ in normal Tyrode's solution was perfused over cells until I_K stabilized before switching back to normal Tyrode's solution for washout. The patch-clamp protocol used for this set of experiments consisted of a 1 second voltage ramp between +50 mV and -120 mV from a holding potential of -80 mV. Inward I_K was measured at -100 mV at baseline, in the presence of $BaCl_2$, and following washout. Barium sensitive current was based off of the percent reduction in I_K measured at -100

mV and calculated for each cell using the following formula: Percent reduction in I_K = (1 – ($I_{K(BaCl2)}$/$I_{K(baseline)}$))*100.

2.6. Quantitative PCR

Total RNA was isolated from the right or left atrial appendage using the PureZOL™ RNA Isolation Reagent and the Aurum™ Total RNA Fatty and Fibrous Tissue Kit (Bio-Rad Laboratories) as per kit instructions. RNA samples were eluted from the spin column in 40 µL elution buffer. RNA yield and purity were assessed using a NanoDrop™ Lite Spectrophotometer (ThermoFisher Scientific). All samples had a A_{260}/A_{280} ratio over 2.0, indicating samples were free of DNA contamination. RNA integrity was assessed by observing 28S and 18S rRNA subunits using the Experion RNA StdSens Analysis Kit (Bio-Rad Laboratories). Next, cDNA (20 ng/µL) was synthesized using the iScript™ cDNA Synthesis Kit (Bio-Rad Laboratories). Reactions were performed in a Bio-Rad MyCycler thermal cycler using the following protocol: 5 min of priming at 25ºC followed by reverse transcription for 30 min at 42ºC then 5 min at 85ºC to inactivate reverse transcriptase.

All qPCR reactions were run in duplicate in 10 µL reactions that contained the following: 4 µL sample cDNA, 5.6 µL GoTaq® qPCR Master Mix (Promega), and 0.4 µL primers. Primers were reconstituted to a final concentration of 100 µM with nuclease free water and stored at -20ºC until use. RT-qPCR reactions were performed in the CFX396 Touch™ Real-Time PCR Detection System (Bio-Rad) using the following protocol: Taq polymerase was activated for 2 min at 95ºC followed by 39 cycles of denaturing for 15 s at 95ºC, annealing for 30 s at 60ºC, and extension for 30 s at 72ºC. This was followed by melt curve analysis from 65-95ºC in 0.5ºC increments. Data were analyzed using the $2^{-\Delta\Delta C_T}$ method using the CFX Manager Software version 3.1 (Bio-Rad). Gene expression was normalized to both GAPDH and β-actin.

Primer sequences were designed and validated for all ion channel proteins used in this study. Primer sequences for the references genes, GAPDH and β-actin, and for NPR-A (*Npr1)*, NPR-B (*Npr2)*, NPR-C (*Npr3)*, and ANP (*Nppa*) were previously designed and validated in the Rose laboratory. Candidate primer sequences were run through the NCBI

Primer-BLAST software to determine sequence specificity. Next, cDNA was pooled from right and left atrial appendages from 8 wildtype mice. This pooled cDNA was used to validate all candidate primer sets using a concentration gradient that consisted of 7 serial dilutions between 20 ng/μL and 0.31 ng/μL. Validated primers had a copy efficiency of 90 – 110% per cycle and did not form primer dimers during melt curve analysis. A concentration of 2.5 ng/μL of cDNA was used to assess gene expression patterns in saline and Ang II treated mice. Primer sequences used in this study are provided in Table 2.1.

2.7. Frailty Assessment in Wildtype Mice

Frailty was assessed in mice immediately prior to experimental use using a non-invasive 31 item clinical frailty index (FI; Table 2.2) (Whitehead *et al.*, 2014). Clinical assessments were made for the integument, muscoskeletal, vestibulocochlear/auditory, ocular/nasal, digestive/urogenital, and respiratory systems. Mice were also observed for signs of discomfort. Measurements were also obtained for body surface temperature and body mass. Surface body temperature was measured using an infrared temperature probe (La Crosse Technology, La Crosse, WI) that was directed towards the lower abdomen and averaged for three measurements. Each of the 31 items was given a value of 0 (deficit is absent), 0.5 (mild deficit), or 1 (severe deficit). Deficits in body mass and temperature were based on standard deviations from average values measured in young or aged mice. To generate an FI score for each mouse, the sum of all traits for a given mouse was divided by the total number of items measured (i.e. 31). This gives a value between 0 and 1, where 0 is least frail and 1 is most frail.

2.8. Statistical Analysis

Summary data are presented as mean ± SEM. Data were analyzed using Student's *t*-test, Mann-Whitney rank sum test, one-way ANOVA with Tukey's post hoc test, two-way ANOVA with Tukey's post hoc test, or two-way repeated measures ANOVA with Tukey's post hoc test as indicated in each Figure legend. Fischer's exact test was used to

Table 2.1. Quantitative PCR primer sequences

Gene of interest	Gene product	Primer Sequence (5'→ 3')	Amplicon length (bp)
SCN5a	$Na_V1.5$	Forward: GGAGTACGCCGACAAGATGT Reverse: ATCTCGGCAAAGCCTAAGGT	171
CACNA1c	$Ca_V1.2$	Forward: ATGATTCGGGCCTTTGTTCAG Reverse: TGGAGTAGGGATGTGCTCG	228
CACNA1d	$Ca_V1.3$	Forward: TGAAGGAGAAGATTGCGCCC Reverse: TTGCGGAATGAGTGGCTACG	190
KCND2	$K_V4.2$	Forward: GCAAGCGGAATGGGCTAC Reverse: TGGTTTTCTCCAGGCAGTG	126
KCND3	$K_V4.3$	Forward: CCTAGCTCCAGCGGACAAGA Reverse: CCACTTACGTTGAGGACGATCA	60
KCNIP2	KChIP2	Forward: AACTATCCACGGTGTGCCAC Reverse: GGACATTCGTTCTTGAAGCCT	112
KCNA5	$K_V1.5$	Forward: TTATTCTTATGGCTGACGAGTGC Reverse: AAGGCACCAATAGTACATCCCAG	204
Npp1	NPR-A	Forward: CGAAGCTTCCAAGGTGTGACAGG Reverse: GACACAGCCATCAGCTCCTGGG	152
Npp2	NPR-B	Forward: GGGGACTTTCAGCCCGCAGC Reverse: GTGGAGTTTTATCACAGGATGGGTCG	150
Npp3	NPR-C	Forward: CGAGCGAGTGGTGATCATGTGTG Reverse: CTCCACGAGCCATCTCCGTAGG	147
Nppa	ANP	Forward: CAAGAACCTGCTAGACCACCTGGAG Reverse: AGAGGTGGGTTGACCTCCCCAGTCC	153
GAPDH	GAPDH	Forward: AATGGGGTGAGGCCGGTGCT Reverse: CACCCTTCAAGTGGGCCCCG	87
β-*actin*	β-actin	Forward: CACCCTTCAAGTGGGCCCCG Reverse: CACCCTTCAAGTGGGCCCCG	227

Table 2.2. Mouse frailty assessment form

Date: _____

Mouse #: _____ **Date of Birth:** _____ **Sex:** F M
Body weight (g): _____ **Body surface temperature (°C):** _____

Rating: 0 = absent 0.5 = mild 1 = severe

➢ **Integument:**					**NOTES:**
❖ Alopecia	**0**	**0.5**	**1**	_____
❖ Loss of fur colour	**0**	**0.5**	**1**	_____
❖ Dermatitis	**0**	**0.5**	**1**	_____
❖ Loss of whiskers	**0**	**0.5**	**1**	_____
❖ Coat condition	**0**	**0.5**	**1**	_____
➢ **Physical/Musculoskeletal:**				
❖ Tumours	**0**	**0.5**	**1**	_____
❖ Distended abdomen	**0**	**0.5**	**1**	_____
❖ Kyphosis	**0**	**0.5**	**1**	_____
❖ Tail stiffening	**0**	**0.5**	**1**	_____
❖ Gait disorders	**0**	**0.5**	**1**	_____
❖ Tremor	**0**	**0.5**	**1**	_____
❖ Forelimb grip strength	**0**	**0.5**	**1**	_____
❖ Body condition score	**0**	**0.5**	**1**	_____
➢ **Vestibulocochlear/Auditory:**				
❖ Vestibular disturbance	**0**	**0.5**	**1**	_____
❖ Hearing loss	**0**	**0.5**	**1**	_____
➢ **Ocular/Nasal:**				
❖ Cataracts	**0**	**0.5**	**1**	_____
❖ Corneal opacity	**0**	**0.5**	**1**	_____
❖ Eye discharge/swelling	**0**	**0.5**	**1**	_____
❖ Microphthalmia	**0**	**0.5**	**1**	_____
❖ Vision loss	**0**	**0.5**	**1**	_____
❖ Menace reflex	**0**	**0.5**	**1**	_____
❖ Nasal discharge	**0**	**0.5**	**1**	_____
➢ **Digestive/Urogenital:**				
❖ Malocclusions	**0**	**0.5**	**1**	_____
❖ Rectal prolapse	**0**	**0.5**	**1**	_____
❖ Vaginal/uterine/penile prolapse	**0**	**0.5**	**1**	_____
❖ Diarrhoea	**0**	**0.5**	**1**	_____
➢ **Respiratory system:**				
❖ Breathing rate/depth	**0**	**0.5**	**1**	_____
➢ **Discomfort:**				
❖ Mouse Grimace Scale	**0**	**0.5**	**1**	_____
❖ Piloerection	**0**	**0.5**	**1**	_____
❖ **Temperature score:** _____				
❖ **Body weight score:** _____				

Total Score/ Max Score:

This table was previously published in Whitehead *et al.*, 2014.

perform statistical analysis on the incidence of AF and AV node block. For linear regression analysis presented in Chapter 6, correlation coefficients were obtained using Pearson's correlation. In all instances, $P < 0.05$ was considered statistically significant.

CHAPTER 3
EFFECTS OF ANG II TREATMENT ON SINOATRIAL NODE FUNCTION, ATRIAL FUNCTION, AND SUSCEPTIBILITY TO ATRIAL FIBRILLATION *IN VIVO*

3.1. Effects of Ang II treatment on cardiac electrophysiology and susceptibility to atrial fibrillation *in vivo*

Previous studies have demonstrated that chronic hypertension results in impaired cardiac electrophysiology *in vivo* (Swaminathan *et al.*, 2011; Purohit *et al.*, 2013). Accordingly, the goal of the first study was determine the effects of Ang II treatment on *in vivo* cardiac function by recording surface ECGs in conjunction with intracardiac programmed electrical stimulation in anaesthetized wildtype mice. Summary data for ECG intervals and intracardiac ECG parameters measured in this study are located in Appendix A.

Systolic blood pressure was measured in saline and Ang II treated mice before surgery and at the end of the 3 week treatment period, as summarized in Appendix B. Baseline blood pressure measurements were not different ($P = 0.10$) between saline and Ang II treated mice. In addition, there were no differences ($P = 0.35$) between baseline and endpoint blood pressure measurements in saline treated mice. In contrast, endpoint blood pressure was increased ($P < 0.001$) in Ang II treated mice compared to baseline measurements.

Representative ECG recordings from a saline and Ang II treated mouse are shown in Fig. 3.1A and 3.1B. Summary data illustrate that baseline heart rate was reduced ($P = 0.049$; Fig. 3.1C) in Ang II treated mice compared to saline treated mice. To determine if the reduction in heart rate occurred in association with a decline in SAN function, cSNRT was measured using the intracardiac programmed electrical stimulation technique in anaesthetized mice. Representative ECG recordings are presented in Fig. 3.2A and 3.2B. Summary data (Fig. 3.2C) demonstrate that cSNRT was prolonged ($P < 0.001$) in Ang II

Figure 3.1. Effects of Ang II treatment on heart rate in anaesthetized wildtype mice.

A. and **B**. Representative ECG recordings in saline (A) and Ang II (B) treated mice.

C. Summary data illustrating the effects of Ang II treatment on heart rate in mice. **P*<0.05 vs. saline. Data analyzed by Student's *t*-test; *n* = 23 saline and 33 Ang II treated mice.

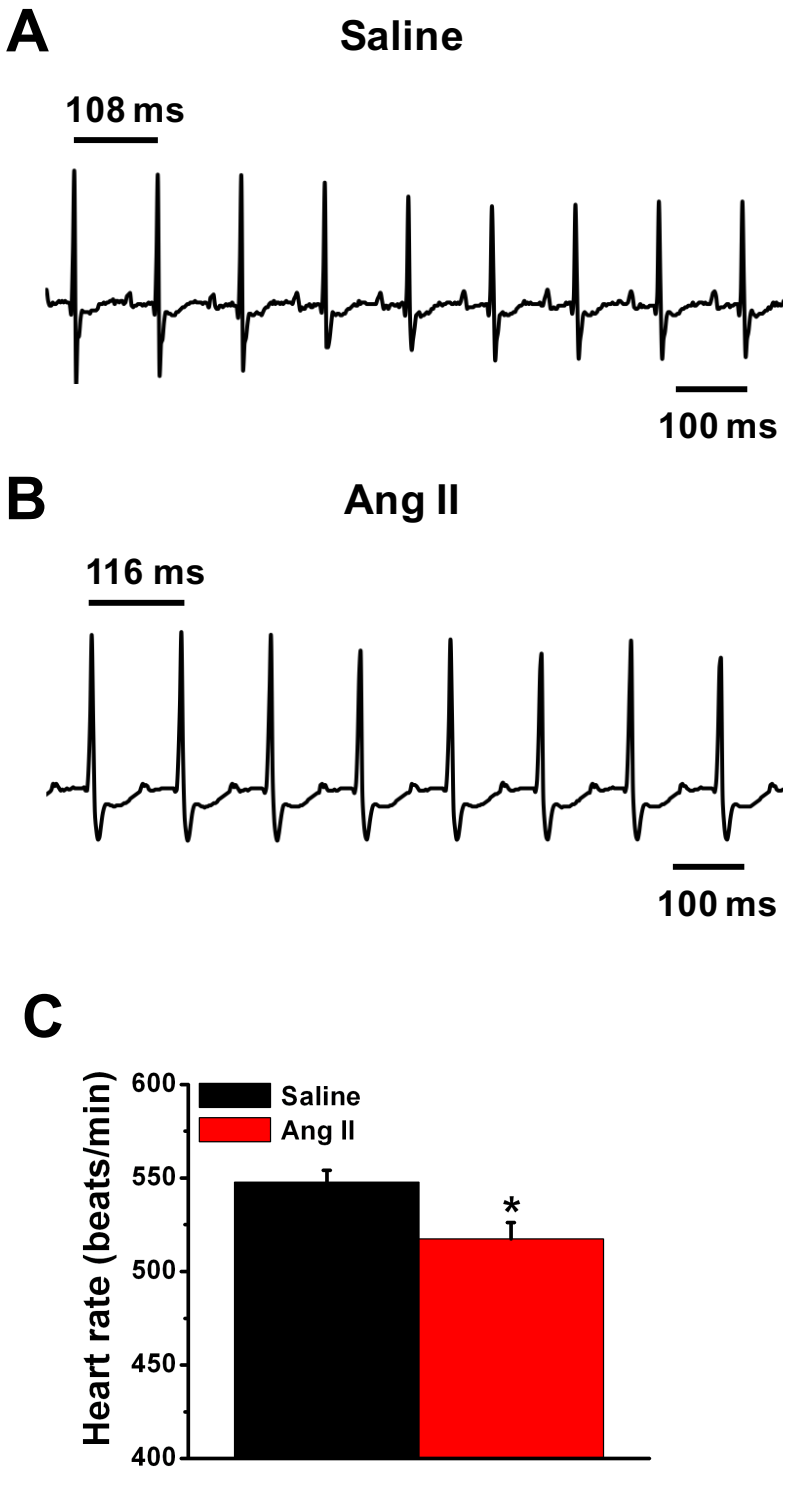
A
Saline
108 ms
100 ms
B
Ang II
116 ms
100 ms
C
Heart rate (beats/min)
600
550
500
450
400
Saline
Ang II
*

Figure 3.1

Figure 3.2. Effects of Ang II treatment on sinoatrial node recovery time in anaesthetized wildtype mice.

A. and **B**. Representative ECG recordings during intracardiac programmed electrical stimulation in saline (A) and Ang II (B) treated mice. Sinoatrial node recovery time (SNRT) was measured as described in the Methods. **C**. Summary data illustrating the effects of Ang II treatment on corrected SNRT (cSNRT) in mice. **P*<0.05 vs. saline. Data analyzed by Student's *t*-test; *n* = 23 saline and 24 Ang II treated mice.

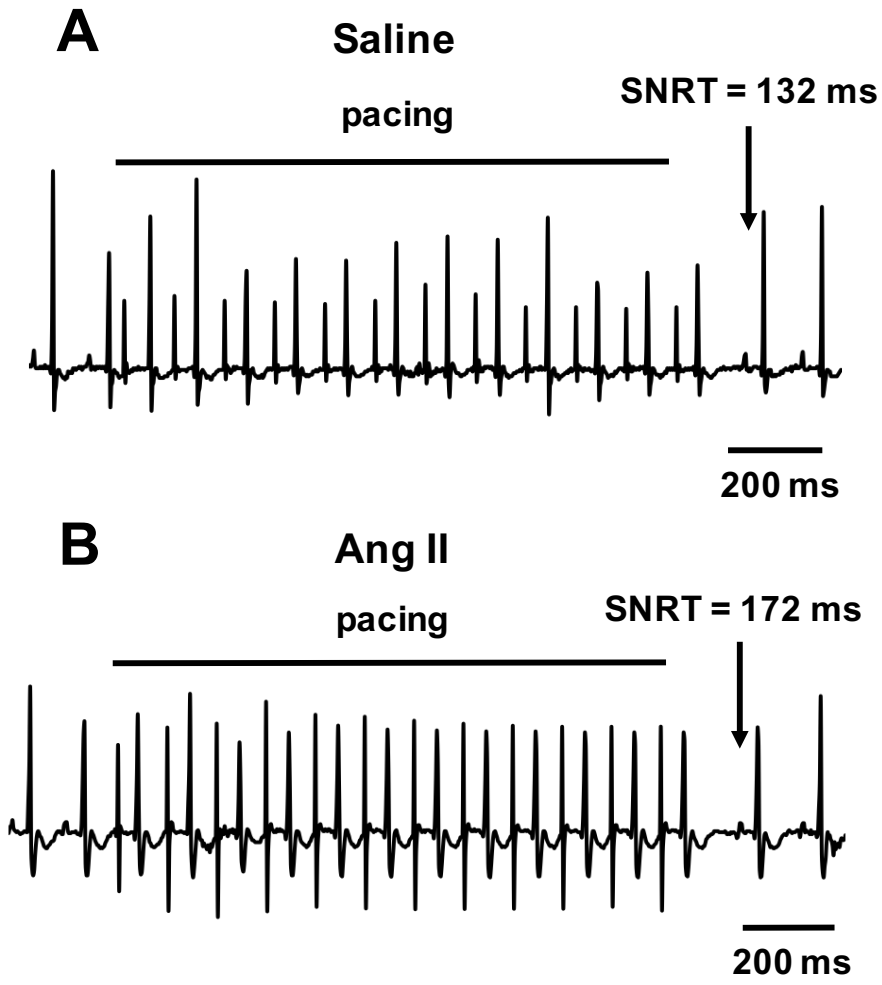
A
Saline
pacing
SNRT = 132 ms
200 ms
B
Ang II
pacing
SNRT = 172 ms
200 ms
C
Saline
Ang II
*
cSNRT (ms)
60
45
30
15
0

Figure 3.2

treated mice. Thus, SAN function is impaired in Ang II treated mice and is consistent with the reduction in heart rate observed in Ang II treated mice.

Next, the effects of Ang II treatment on the inducibility to AF was measured in saline and Ang II treated wildtype mice. Fig. 3.3A and 3.3B show representative surface and intracardiac atrial ECG recordings of a saline and Ang II treated mouse following burst pacing of the right atrium. Summary data (Fig. 3.3C) demonstrates the incidence of AF was significantly higher ($P = 0.001$) in Ang II treated mice (15/30) compared to saline treated mice (2/25). Further scrutiny of the data revealed a difference in the duration of AF (Table 3.1). In saline treated mice, AF lasted less than 5 seconds before reverting back into normal sinus rhythm in all cases. In Ang II treated mice, AF duration was less than 5 seconds in 60% of Ang II treated mice. In fact, AF duration was longer than 25 seconds in 13% of Ang II treated mice and lasted 800 seconds in one Ang II treated mouse before spontaneously reverting to normal sinus rhythm. These data demonstrate that Ang II treated mice have a higher incidence of AF and when induced AF is more severe.

To determine if Ang II treatment affects conduction times across the atria and through the AV node, P wave duration and P-R intervals were measured using ECG recordings from anaesthetized saline and Ang II treated mice. P wave duration was prolonged ($P < 0.001$) in Ang II treated mice (Fig. 3.4A) indicating conduction is slowed across the atrial myocardium. Similarly, P-R interval was prolonged ($P < 0.001$) in Ang II treated animals (Fig. 3.4B), demonstrating that conduction through the AV node is also slowed following Ang II treatment.

Atrial and AV node electrical function were further studied by measuring AERP and AVERP in Ang II treated mice using the intracardiac programmed electrical stimulation technique. Both AERP ($P < 0.001$; Fig. 3.4C) and AVERP ($P = 0.042$; Fig. 3.4D) were prolonged in Ang II treated mice. These data are consistent with the prolongation in conduction times across the atria and through the AV node and are indicative of electrical remodelling in these regions.

Figure 3.3. Susceptibility to induced atrial fibrillation in anaesthetized wildtype mice. **A.** and **B.** Representative surface (top) and intracardiac atrial (bottom) ECG recordings from saline (A) and Ang II (B) treated mice. AF was induced as described in the Methods. The saline treated mouse was not induced into AF whereas the Ang II treated mouse remained in AF for 8.1 seconds before reverting to normal sinus rhythm. **C.** Summary data for the inducibility of AF in saline and Ang II treated mice following burst pacing. Numbers in parenthesis indicate the number of mice induced into AF following burst pacing. $^{*}P <$ 0.05 vs. saline. Data analyzed by Fisher's exact test. $n = 25$ saline and 30 Ang II treated mice. Data collected from H. Jansen and other members of the Rose laboratory.

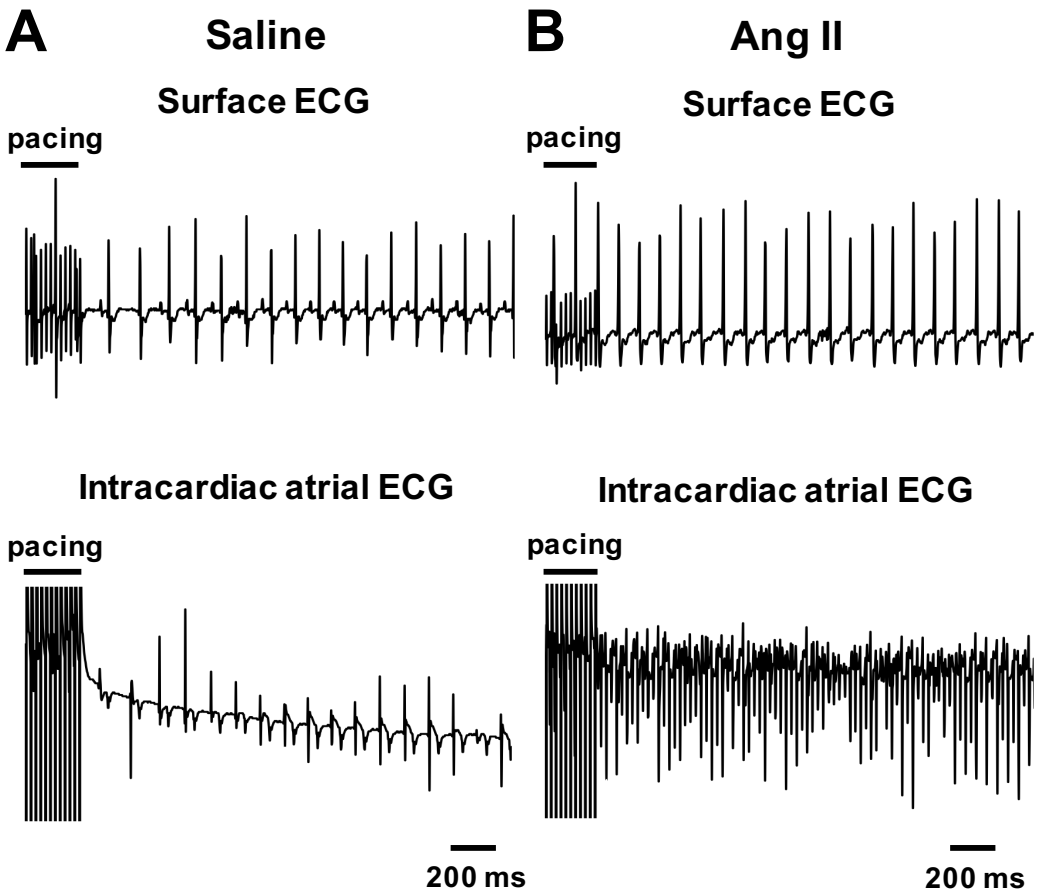
A
Saline
Surface ECG
pacing
B
Ang II
Surface ECG
pacing
Intracardiac atrial ECG
pacing
Intracardiac atrial ECG
pacing
200 ms
200 ms
C
Saline
Ang II
Induced AF (%)
60
40
20
0
(2/25)
*
(15/30)

Figure 3.3

Table 3.1. Duration of arrhythmia in saline and Ang II treated mice that were induced into atrial fibrillation.

Duration (s)	Saline	Ang II
< 5	100% (2/2)	60% (9/15)
5 – 25		27% (4/15)
> 25		13% (2/15)

Numbers in parenthesis indicate the number of mice in each group.

Figure 3.4. Effects of Ang II treatment on atrial and atrioventricular node conduction and electrical function in anaesthetized wildtype mice.

A. and **B.** Summary data illustrating the effects of Ang II treatment on P wave duration (A) and P-R interval (B) in mice. *n* = 23 saline and 33 Ang II treated mice. **C.** Summary data illustrating the effects of Ang II treatment on atrial effective refractory period (AERP) in mice. *n* = 16 saline and 22 Ang II treated mice. **D.** Summary data illustrating the effects of Ang II treatment on atrioventricular node effective refractory period (AVERP) in mice. *n* = 7 saline and 13 Ang II treated mice. **P*<0.05 vs. saline. Data analyzed by Student's *t*-test.

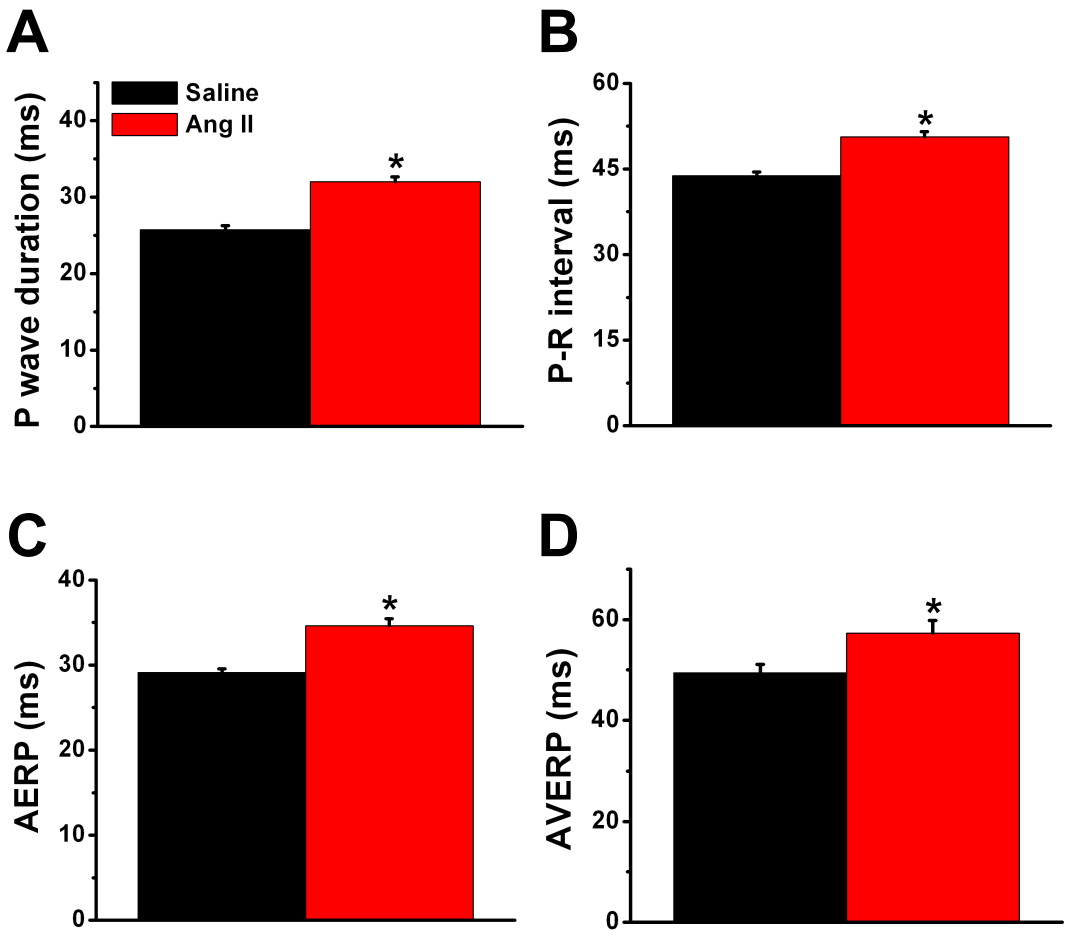
A
Saline
Ang II
P wave duration (ms)
0
10
20
30
40
*
B
P-R interval (ms)
0
15
30
45
60
*
C
AERP (ms)
0
10
20
30
40
*
D
AVERP (ms)
0
20
40
60
*

Figure 3.4

3.2. Effects of autonomic nervous system blockade on heart rate, P wave duration, and P-R interval in saline and Ang II treated anaesthetized mice

The next set of experiments investigated the effects of autonomic nervous system blockade on heart rate, P wave duration, and P-R interval in saline and Ang II treated anaesthetized wildtype mice. Heart rate is modulated by the intrinsic activity of the SAN and the autonomic nervous system (DiFrancesco and Borer, 2007; Mangoni and Nargeot, 2008). Furthermore, the atria and AV node are innervated by parasympathetic and sympathetic neurons and therefore their function can be modulated by the autonomic nervous system. By blocking the autonomic nervous system with pharmacological agents, we can determine if the observations made in section 3.1 are attributed to alterations in the intrinsic activity of the heart and/or resulting from altered autonomic nervous system activity. Accordingly, a combined intraperitoneal injection of atropine (a parasympathetic nervous system antagonist; 10 mg/kg) and propranolol (a sympathetic nervous system antagonist; 10 mg/kg) was used to block muscarinic and β-adrenergic receptors, respectively, in a subset of saline and Ang II treated mice.

The effects of autonomic nervous system blockade on heart rate in saline and Ang II treated mice is summarized in Fig. 3.5. Representative ECG recordings (Figs. 3.5A and 3.5B) as well as summary data (Fig. 3.5C) show that, consistent with the data in Fig. 3.1, heart rate was lower ($P = 0.008$) in Ang II treated mice under baseline conditions (measured immediately before autonomic nervous system blockade) in this subset of mice. Atropine and propranolol treatment reduced heart rate in both saline ($P < 0.001$) and Ang II ($P < 0.001$) treated mice over the 25 min treatment period (Fig. 3.5C). This is consistent with the observation that mice have a higher level of sympathetic tone compared to parasympathetic tone (Gehrmann *et al.*, 2000; Just *et al.*, 2000; Janssen and Smits, 2002). Surprisingly, saline and Ang II treated animals exhibited the same reduction in heart rate ($P = 0.684$) in the presence of atropine and propranolol indicating that under these conditions autonomic tone is not altered in Ang II treated mice. On the other hand, Ang II treated mice had a lower heart rate compared to saline treated mice at all time points throughout the autonomic nervous system blockade experiment ($P < 0.05$;

Figure 3.5. Effects of autonomic nervous system blockade on heart rate, P wave duration, and P-R interval in saline and Ang II treated wildtype anesthetized mice. **A.** and **B.** Representative ECG recordings at baseline and following combined intraperitoneal injection of atropine and propranolol (10 mg/kg) to block the autonomic nervous system in saline (A) and Ang II (B) treated mice. **C**. Summary data illustrating the effects of autonomic nervous system blockade on heart rate in saline and Ang II treated mice. Atropine and propranolol were injected at 0 min. **D.** and **E.** Summary data for P wave duration (D) and P-R interval (E) at baseline (0 min) and 25 minutes after injection of atropine and propranolol (blockade) in saline and Ang II treated mice. *$P<0.05$ vs. baseline; $^{+}P<0.05$ vs. saline. Data analyzed by two-way repeated measures ANOVA with Tukey's post-hoc test; $n = 6$ saline and 11 Ang II treated mice.

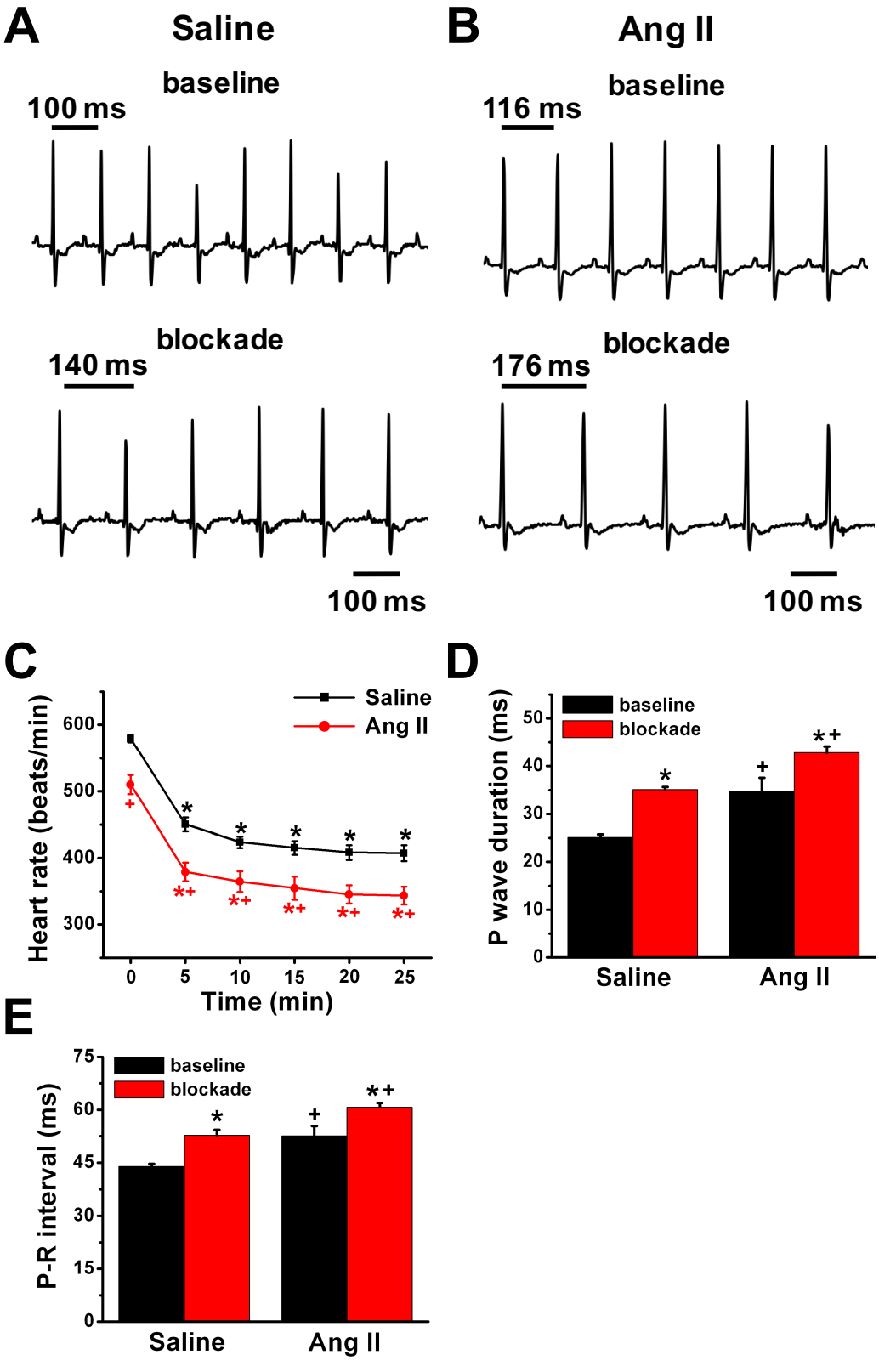
A
Saline
baseline
100 ms
blockade
140 ms
100 ms
B
Ang II
baseline
116 ms
blockade
176 ms
100 ms
C
Saline
Ang II
Heart rate (beats/min)
600
500
400
300
0
5
10
15
20
25
Time (min)
D
baseline
blockade
P wave duration (ms)
50
40
30
20
10
0
Saline
Ang II
E
baseline
blockade
P-R interval (ms)
75
60
45
30
15
0
Saline
Ang II

Figure 3.5

Fig. 3.5C), which supports the conclusion that Ang II treated mice have a lower intrinsic heart rate (i.e. impaired intrinsic SAN function). This is consistent with the prolongation in cSNRT observed in Fig. 3.2 and indicates the reduced heart rate observed in Ang II treated mice is attributed to changes in the intrinsic function of the SAN independent of autonomic nervous system activity.

Next, the effects of autonomic nervous system blockade on P wave duration and P-R interval in saline and Ang II treated mice were examined. Consistent with the data presented in Fig. 3.4, both P wave duration ($P = 0.005$; Fig. 3.5D) and P-R interval ($P = 0.009$; Fig. 3.5E) were prolonged in Ang II treated mice under baseline conditions in this subset of mice. Following application of atropine and propranolol, P wave duration was prolonged in both saline ($P = 0.013$) and Ang II ($P = 0.006$) treated mice (Fig. 3.5D) compared to baseline measurements. Similarly, P-R interval was also prolonged in the presence of atropine and propranolol in saline ($P = 0.010$) and Ang II ($P = 0.001$) treated mice (Fig. 3.5E). Further investigation of the data indicates that both P wave duration ($P = 0.015$) and P-R interval ($P = 0.010$) were prolonged to a greater extent in Ang II treated mice compared to saline treated mice in the presence of atropine and propranolol. Combined, these data provide further evidence that conduction in the atrial myocardium and through AV node is slowed in Ang II treated mice, and that this occurs independently of the autonomic nervous system.

CHAPTER 4
EFFECTS OF ANG II TREATMENT ON RIGHT AND LEFT ATRIAL MYOCYTE ELECTROPHYSIOLOGY

4.1. Effects of Ang II treatment on action potential morphology in right and left atrial myocytes from wildtype mice

The results presented in Chapter 3 demonstrate *in vivo* cardiac electrophysiology is altered following Ang II treatment in anaesthetized wildtype mice. In particular, both P wave duration and AERP were prolonged in Ang II treated mice, indicating remodelling within the atrium. Accordingly, the goal of this chapter was to determine if Ang II treatment is associated with electrical remodelling in right and left atrial myocytes.

Cell capacitance, an indirect measure of cell size, was measured in right and left atrial myocytes during patch-clamp experiments as shown in Fig. 4.1. Ang II treatment did not affect cell capacitance in the right atrial myocytes ($P = 0.26$; Fig. 4.1A). In contrast, cell capacitance was increased ($P < 0.001$; Fig. 4.1A) in Ang II treated left atrial myocytes. There were no differences ($P = 0.15$) in cell capacitance between saline treated right and left atrial myocytes.

To determine if Ang II treatment alters atrial electrophysiology at the cellular level, AP morphology was assessed in right and left atrial myocytes isolated from Ang II treated mice and saline treated controls. Representative recordings and summary data illustrating the effects of Ang II treatment on AP morphology are presented in Fig. 4.2. There were no differences ($P = 0.61$) in resting membrane potential (RMP; Fig. 4.2C) between Ang II treated right and left atrial myocytes compared to saline controls. Therefore, Ang II treatment does not affect membrane excitability in the right and left atria.

Next, the effects of Ang II treatment on AP maximum upstroke velocity (V_{max}) and AP overshoot were investigated in right and left atrial myocytes. In the right atria,

Figure 4.1. Effects of Ang II treatment on cell capacitance in right and left atrial myocytes from wildtype mice.

A. Summary data illustrating the effects of Ang II treatment on cell capacitance in right and left atrial myocytes from wildtype mice. **P*<0.05 vs. saline within atrial region; $^{+}$*P*<0.05 vs. right atrium within treatment group. Data analyzed by two-way ANOVA with Tukey's post hoc test. Right atrium: *n* = 41 saline and 39 Ang II treated myocytes; Left atrium: *n* = 25 saline and 30 Ang II treated myocytes.

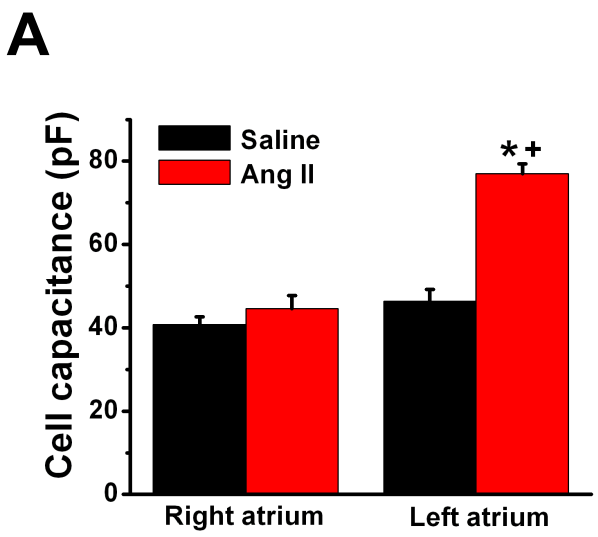
A
Cell capacitance (pF)
0
20
40
60
80
Saline
Ang II
*+
Right atrium
Left atrium

Figure 4.1

Figure 4.2. Effects of Ang II treatment on action potential morphology in right and left atrial myocytes from wildtype mice.

A. and **B.** Representative right and left atrial action potentials (APs) from saline or Ang II treated mice. Dashed lines are at 0 mV. **C – H**. Summary data illustrating the effects of Ang II treatment on resting membrane potential (RMP; C), AP upstroke velocity (V_{max}; D), AP overshoot (E), AP duration (APD) at 50% (APD_{50}; F), 70% (APD_{70}; G), and 90% (APD_{90}; H) repolarization in right and left atrial myocytes. There was no difference (P = 0.61) in RMP between treatment groups. There was no difference in V_{max} (P = 0.61) and AP overshoot (P = 0.51) in the right atrial myocytes following Ang II treatment. *P<0.05 vs. saline within atrial region; ^{+}P<0.05 vs. right atrium within treatment group. Data analyzed by two-way ANOVA with Tukey's post hoc test; Right atrium: n = 19 saline and 15 Ang II treated myocytes; Left atrium: n = 14 saline and 15 Ang II treated myocytes.

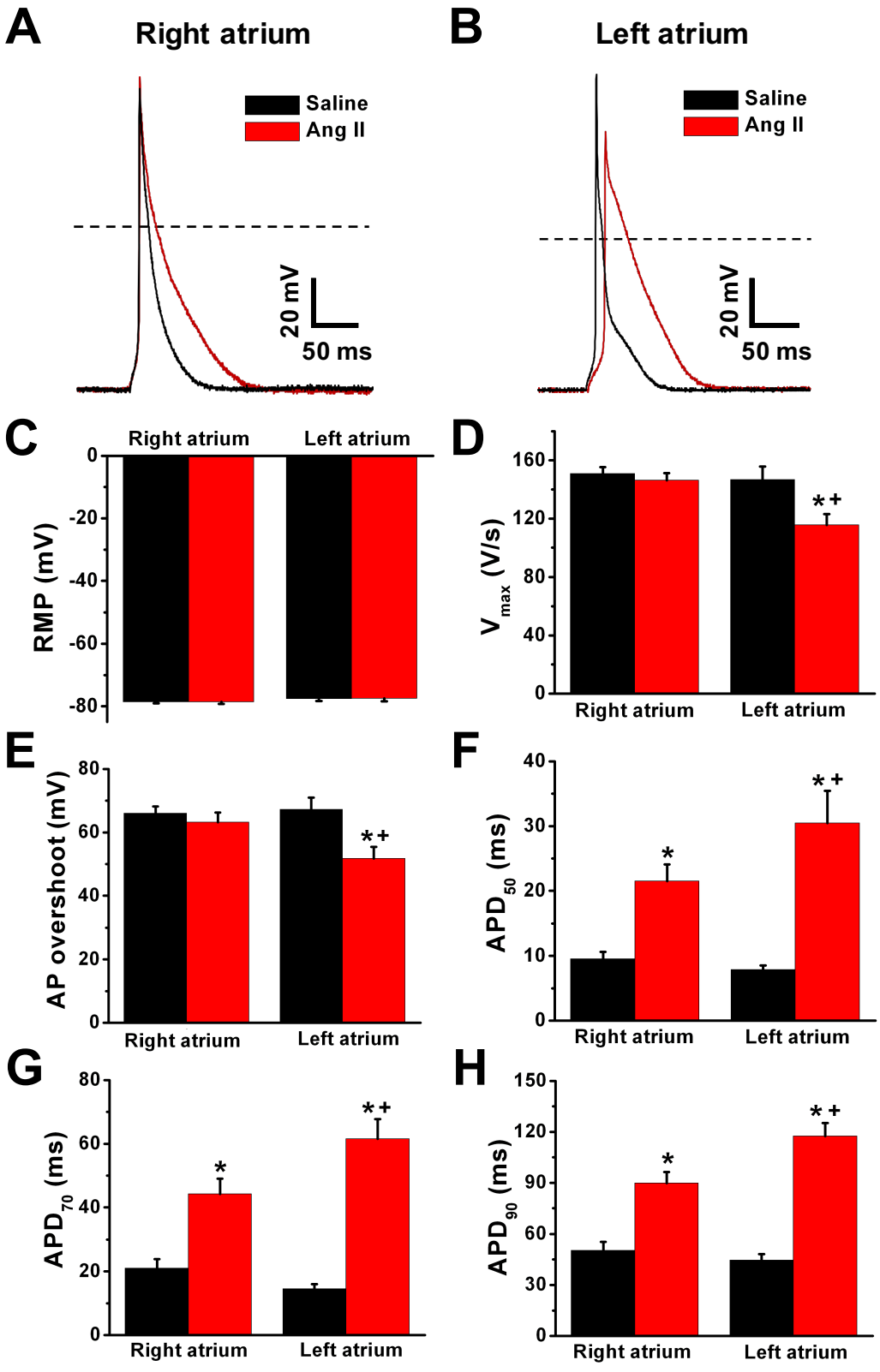
A
Right atrium
Saline
Ang II
20 mV
50 ms
B
Left atrium
Saline
Ang II
20 mV
50 ms
C
Right atrium
Left atrium
RMP (mV)
0
-20
-40
-60
-80
D
V_{max} (V/s)
160
120
80
40
0
*+
Right atrium
Left atrium
E
AP overshoot (mV)
80
60
40
20
0
*+
Right atrium
Left atrium
F
APD_{50} (ms)
40
30
20
10
0
*
*+
Right atrium
Left atrium
G
APD_{70} (ms)
80
60
40
20
0
*
*+
Right atrium
Left atrium
H
APD_{90} (ms)
150
120
90
60
30
0
*
*+
Right atrium
Left atrium

Figure 4.2

neither V_{max} ($P = 0.61$; Fig. 4.2D) nor AP overshoot ($P = 0.51$; Fig. 4.2E) were different in saline vs. Ang II treated myocytes. In contrast, both V_{max} ($P = 0.002$; Fig. 4.2D) and AP overshoot ($P = 0.001$; Fig. 4.2E) were reduced in Ang II treated left atrial myocytes compared to saline treated controls. There were no differences in V_{max} ($P = 0.65$) and AP overshoot ($P = 0.76$) between saline treated right vs. left atrial myocytes however both V_{max} ($P = 0.002$) and AP overshoot ($P = 0.011$) were reduced in Ang II treated left vs. right atrial myocytes.

To determine if Ang II treatment affects AP repolarization, AP duration (APD) was measured at 50% (APD_{50}), 70% (APD_{70}), and 90% (APD_{90}) repolarization in right and left atrial myocytes. In right atrium, APD_{50} ($P < 0.001$; Fig. 4.2F), APD_{70} ($P < 0.001$; Fig. 4.2G), and APD_{90} ($P < 0.001$; Fig. 4.2H) were prolonged in Ang II treated myocytes compared to saline controls. Ang II treatment also prolonged APD_{50} ($P < 0.001$; Fig. 4.2F), APD_{70} ($P < 0.001$; Fig. 4.2G), and APD_{90} ($P < 0.001$; Fig. 4.2H) in left atrial myocytes. Strikingly, the extent of AP prolongation at APD_{50} ($P = 0.015$), APD_{70} ($P = 0.006$), and APD_{90} ($P = 0.002$) was greater in left vs. right atrial myocytes from Ang II treated mice. There were no differences in APD_{50} ($P = 0.63$), APD_{70} ($P = 0.27$) and APD_{90} ($P = 0.50$) between saline treated right and left atrial myocytes.

The alterations in AP morphology described in this section indicate Ang II treatment is associated with distinct patterns of electrical remodelling (i.e. changes in ion currents) in right and left atrial myocytes. Accordingly, the next set of experiments were focused on the measurement of key ionic currents that could underlie this electrical remodelling.

4.2. Effects of Ang II treatment on sodium current in right and left atrial myocytes from wildtype mice

AP upstroke velocity is determined by sodium currents (I_{Na}). The AP data presented in Fig. 4.2D demonstrates that V_{max} is unchanged in right atrial myocytes yet is reduced in Ang II treated left atrial myocytes. Accordingly, the goal of the next set of experiments was to measure I_{Na} in Ang II treated myocytes.

Representative I_{Na} recordings from a saline and Ang II treated right atrial myocyte are shown in Figs. 4.3A and 4.3B. Summary Na^+ I-V relationships (Fig. 4.3E) demonstrate that Ang II does not affect ($P = 0.25$) I_{Na} in right atrial myocytes compared to saline controls. There were also no differences ($P = 0.65$) in I_{Na} activation kinetics as assessed by I_{Na} conductance density plots (Fig. 4.4A). Specifically, maximum conductance (G_{max}; $P = 0.14$; Fig. 4.4C), slope factor (k; $P = 0.31$; Fig. 4.4E), and $V_{1/2(activation)}$ ($V_{1/2(act)}$; $P = 0.38$; Fig. 4.4G) were not different in right atrial myocytes from Ang II treated mice. These data are consistent with the current-clamp data demonstrating that Ang II treatment does not affect V_{max} (Fig. 4.2D) in right atrial myocytes.

Figs. 4.3C and 4.3D show representative voltage-clamp recordings for I_{Na} in saline and Ang II treated left atrial myocytes. Summary Na^+ I-V relationships (Fig. 4.3F) demonstrate I_{Na} was reduced in Ang II treated myocytes at membrane potentials between -50 mV ($P = 0.028$) and +10 mV ($P = 0.008$), which is consistent with a reduction in AP V_{max}. Analysis of I_{Na} activation kinetics in Ang II left atrial myocytes demonstrates a reduction in G_{max} ($P < 0.001$; Figs. 4.4B and 4.4D), without changes in slope factor ($P = 0.12$; Fig. 4.4F) and $V_{1/2(act)}$ ($P = 0.37$; Fig. 4.4H).

4.3. Effects of Ang II treatment on calcium currents in right and left atrial myocytes from wildtype mice

The next set of experiments sought to characterize the L-type calcium current ($I_{Ca,L}$) in Ang II treated myocytes as a possible mechanism for the APD prolongation described in section 4.1. Representative $I_{Ca,L}$ recordings for saline and Ang II treated right atrial myocytes are shown in Figs. 4.5A and 4.5B and for saline and Ang II treated left atrial myocytes in Figs. 4.5C and 4.5D. Summary Ca^{2+} I-V relationships demonstrate Ang II does not affect $I_{Ca,L}$ in right ($P = 0.53$; Fig. 4.5D) or left ($P = 0.80$; Fig. 4.5E) atrial myocytes compared to saline controls. Furthermore, Ang II treatment does not affect $I_{Ca,L}$ conductance density in right ($P = 0.52$; Fig. 4.6A) or left ($P = 0.74$; Fig. 4.6B) atrial myocytes. In agreement with this, G_{max} ($P = 0.30$; Fig. 4.6C), slope factor ($P = 0.68$; Fig. 4.6E), and $V_{1/2(act)}$ ($P = 0.38$; Fig. 4.6G) were not different in Ang II treated right atrial

Figure 4.3. Effects of Ang II treatment on sodium current (I_{Na}) in right and left atrial myocytes from wildtype mice.

A. and **B.** Representative I_{Na} recordings from saline (A) and Ang II (B) treated right atrial myocytes. **C.** and **D.** Representative I_{Na} recordings from saline (C) and Ang II (D) treated left atrial myocytes. **E.** and **F.** Summary Na^+ I-V relationships demonstrating the effects of Ang II treatment on I_{Na} in right (E) and left (F) atrial myocytes. **P*<0.05 vs. saline at each membrane potential. Data analyzed by two-way repeated measures ANOVA with Tukey's post hoc test. Right atrium: *n* = 13 saline and 12 Ang II treated myocytes; Left atrium: *n* = 8 saline and 8 Ang II treated myocytes.

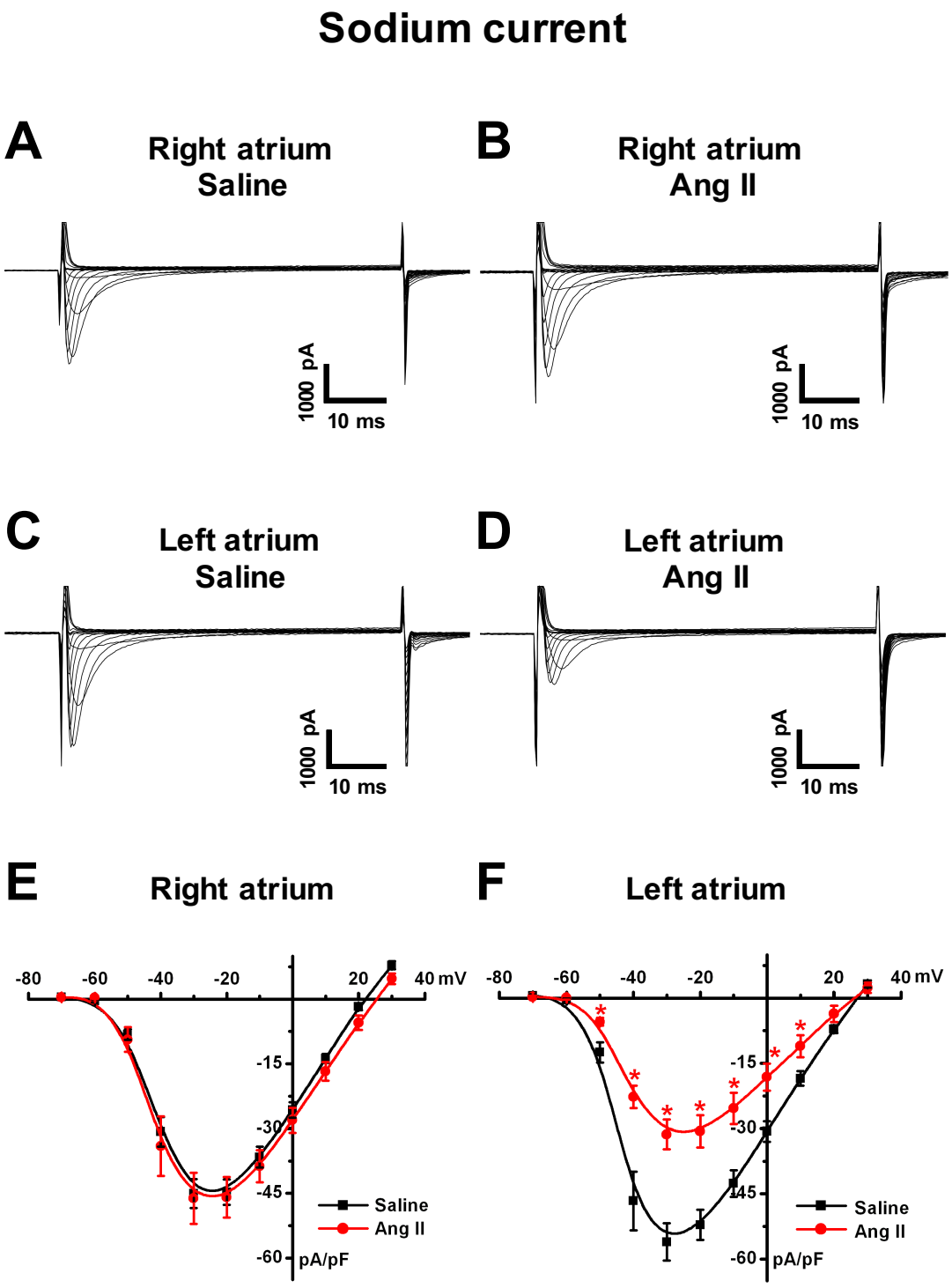
Sodium current
A
Right atrium
Saline
1000 pA
10 ms
B
Right atrium
Ang II
1000 pA
10 ms
C
Left atrium
Saline
1000 pA
10 ms
D
Left atrium
Ang II
1000 pA
10 ms
E
Right atrium
-80
-60
-40
-20
20
40 mV
-15
-30
-45
-60
pA/pF
Saline
Ang II
F
Left atrium
-80
-60
-40
-20
20
40 mV
-15
-30
-45
-60
pA/pF
Saline
Ang II

Figure 4.3

Figure 4.4. Effects of Ang II treatment on I_{Na} conductance in right and left atrial myocytes from wildtype mice.

A. and **B.** Summary I_{Na} conductance density plots demonstrating the effects of Ang II treatment on I_{Na} conductance in right (A) and left (B) atrial myocytes. **P*<0.05 vs. saline at each membrane potential. Data analyzed by two-way repeated measures ANOVA with Tukey's post hoc test. **C.** and **D.** Summary data demonstrating the effects of Ang II treatment on maximum conductance (G_{max}) in right (C) and left (D) atrial myocytes. There were no differences in G_{max} in the right atrium (*P* = 0.14). **E.** and **F.** Summary data of the effects of Ang II treatment on slope factor (k) in right (E) and left (F) atrial myocytes. There were no differences in slope factor (right atrium: *P* = 0.31; left atrium: *P* = 0.12) following Ang II treatment. **G.** and **H.** Summary of the effects of Ang II treatment on $V_{1/2(activation)}$ ($V_{1/2(act)}$) in right (G) and left (H) atrial myocytes. There were no differences in $V_{1/2(act)}$ (right atrium: *P* = 0.38; left atrium: *P* = 0.37) following Ang II treatment. **P*<0.05 vs. saline within atrial region. Data analyzed by Student's *t*-test. Right atrium: *n* = 13 saline and 12 Ang II treated myocytes; Left atrium: *n* = 8 saline and 8 Ang II treated myocytes.

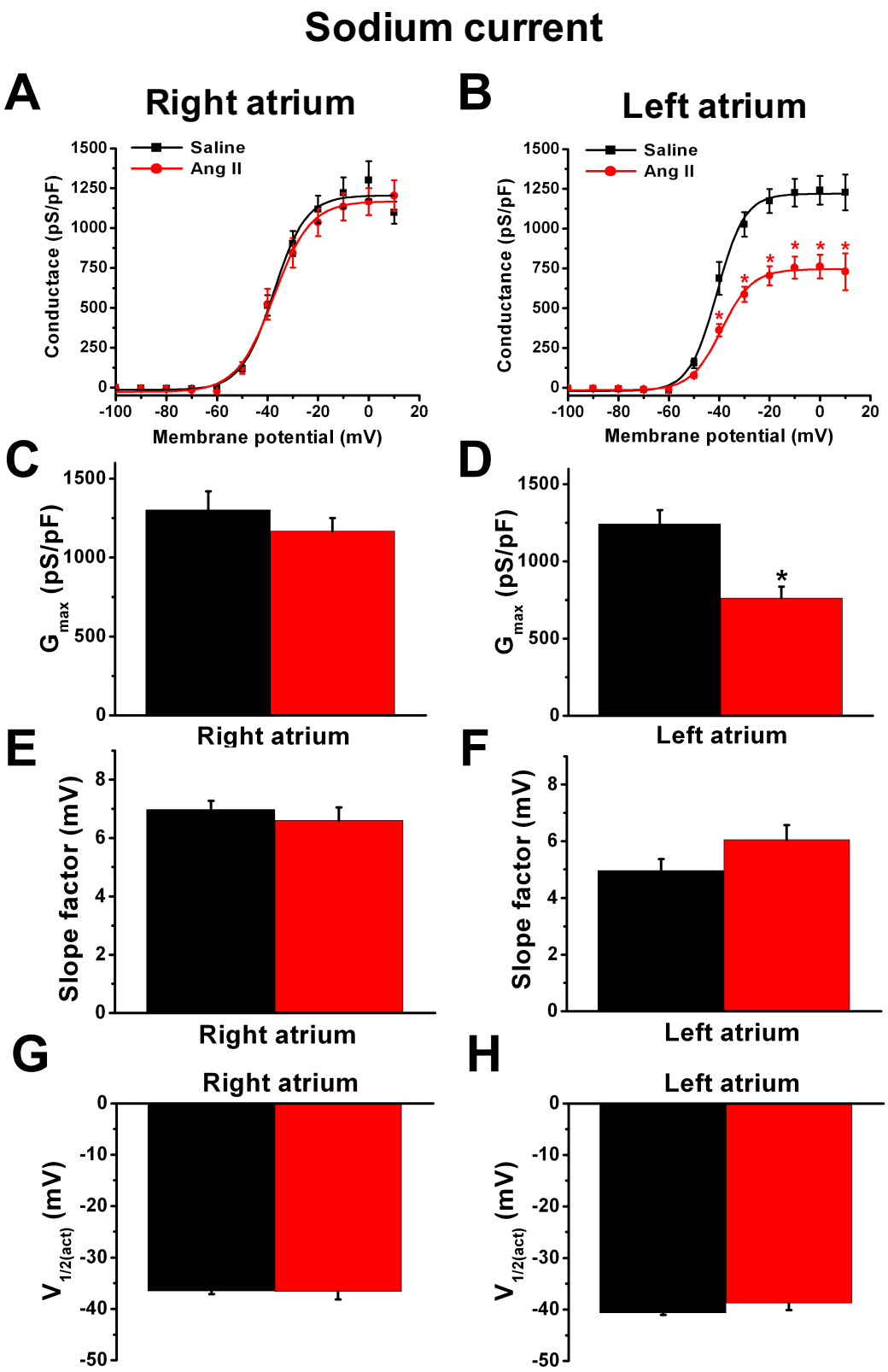
Sodium current
A
Right atrium
Saline
Ang II
Conductace (pS/pF)
Membrane potential (mV)
B
Left atrium
Saline
Ang II
Conductance (pS/pF)
Membrane potential (mV)
C
G_{max} (pS/pF)
Right atrium
D
G_{max} (pS/pF)
Left atrium
E
Slope factor (mV)
Right atrium
F
Slope factor (mV)
Left atrium
G
Right atrium
$V_{1/2(act)}$ (mV)
H
Left atrium
$V_{1/2(act)}$ (mV)

Figure 4.4

Figure 4.5. Effects of Ang II treatment on L-type calcium current ($I_{Ca,L}$) in right and left atrial myocytes from wildtype mice.

A. and **B.** Representative $I_{Ca,L}$ recordings from saline (A) and Ang II (B) treated right atrial myocytes. **C.** and **D.** Representative $I_{Ca,L}$ recordings from saline (C) and Ang II (D) treated left atrial myocytes. **E.** and **F.** Summary Ca^{2+} I-V relationships demonstrating the effects of Ang II treatment on $I_{Ca,L}$ in right (E) and left (F) atrial myocytes. There were no differences in $I_{Ca,L}$ in Ang II treated right ($P = 0.53$) or left ($P = 0.80$) atrial myocytes vs. saline controls. Data analyzed by two-way repeated measures ANOVA with Tukey's post hoc test. Right atrium: $n = 13$ saline and 15 Ang II treated myocytes; Left atrium: $n = 11$ saline and 10 Ang II treated myocytes.

Calcium current

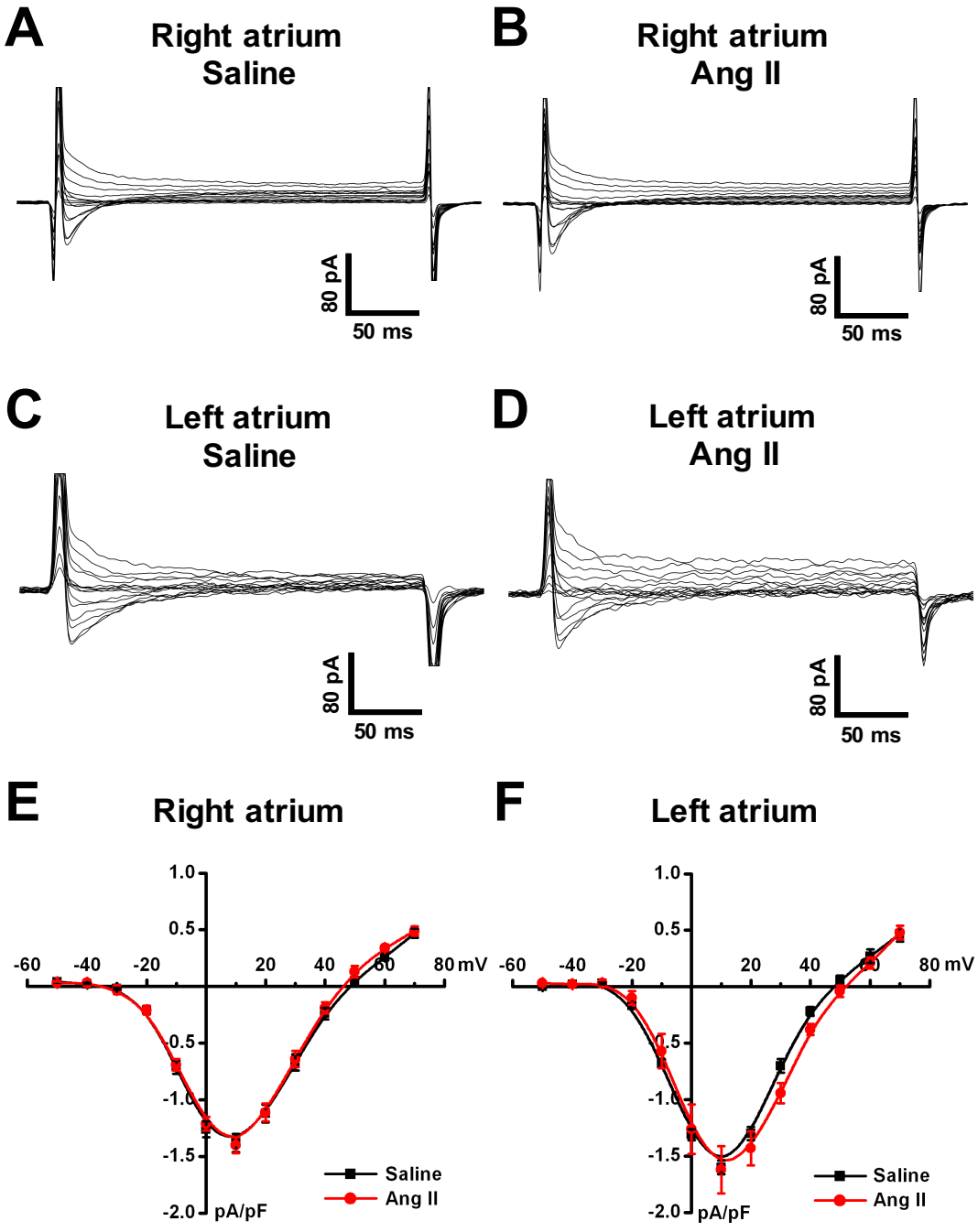

Figure 4.5

Figure 4.6. Effects of Ang II treatment on $I_{Ca,L}$ conductance in right and left atrial myocytes from wildtype mice.

A. and **B**. Summary $I_{Ca,L}$ conductance density plots demonstrating the effects of Ang II treatment on $I_{Ca,L}$ activation kinetics in right (A) and left (B) atrial myocytes. Data analyzed by two-way repeated measures ANOVA with Tukey's post hoc test. **C.** and **D.** Summary data demonstrating the effects of Ang II treatment on maximum conductance (G_{max}) in right (C) and left (D) atrial myocytes. There were no differences in G_{max} (right atrium: P = 0.30; left atrium: P = 0.74) following Ang II treatment. **E.** and **F.** Summary data of the effects of Ang II treatment on slope factor (k) in right (E) and left (F) atrial myocytes. There were no differences on slope factor (right atrium: P = 0.68; left atrium: P = 0.86) following Ang II treatment. **G.** and **H.** Summary of the effects of Ang II treatment on $V_{1/2(act)}$ in right (G) and left (H) atrial myocytes. There were no differences on $V_{1/2(act)}$ (right atrium: P = 0.38; left atrium: P = 0.15) following Ang II treatment. Data analyzed by Student's *t*-test. Right atrium: n = 13 saline and 15 Ang II treated myocytes; Left atrium: n = 11 saline and 10 Ang II treated myocytes.

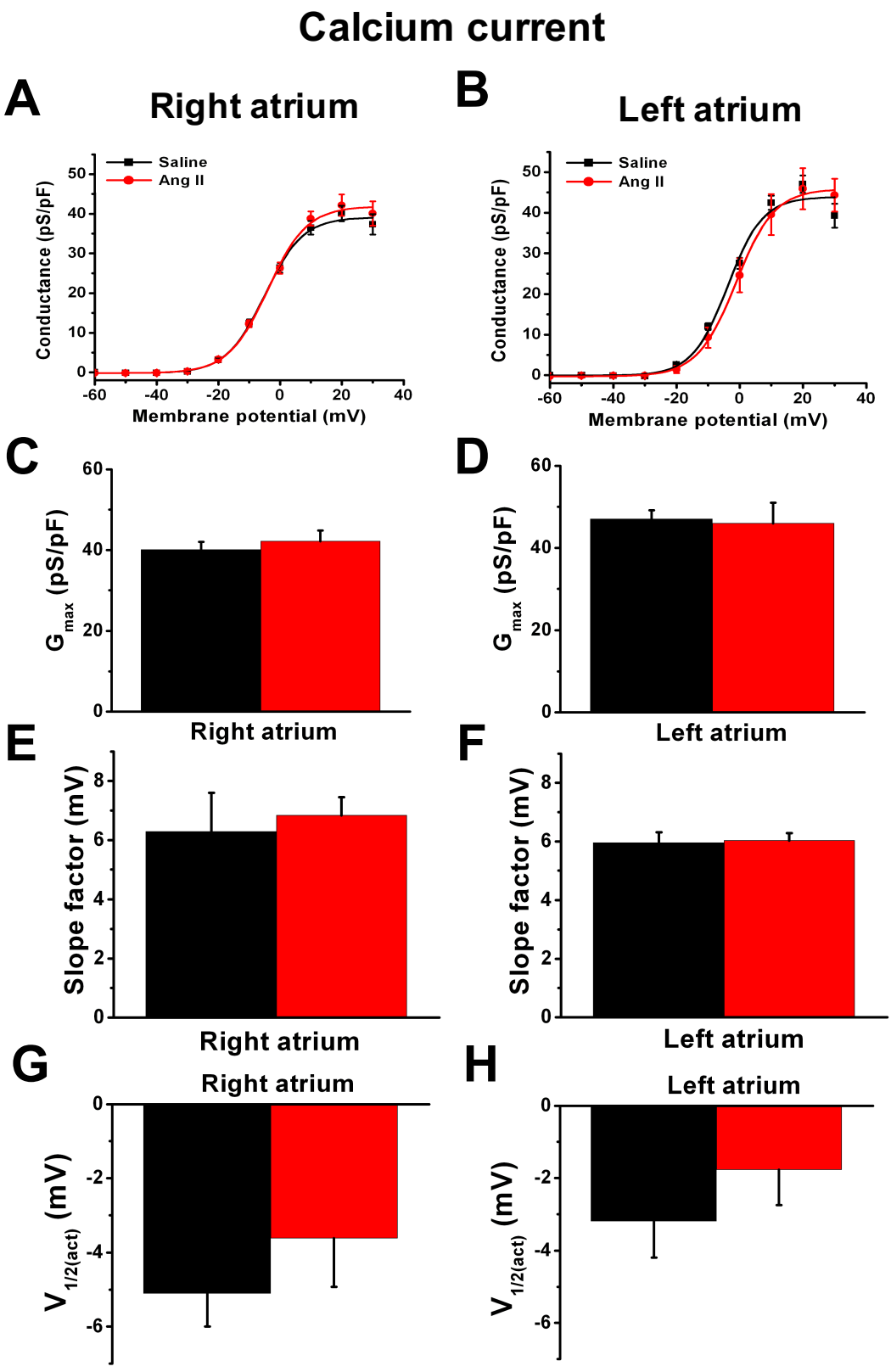
Calcium current
A
Right atrium
B
Left atrium
Saline
Ang II
Conductance (pS/pF)
Membrane potential (mV)
C
D
G_{max} (pS/pF)
Right atrium
Left atrium
E
F
Slope factor (mV)
G
H
$V_{1/2(act)}$ (mV)

Figure 4.6

myocytes. Similarly, G_{max} ($P = 0.74$; Fig. 4.6D), slope factor ($P = 0.86$; Fig. 4.6F), and $V_{1/2(act)}$ ($P = 0.15$; Fig. 4.6H) were not different in Ang II treated left atrial myocytes. Combined, these data demonstrate Ang II treatment does not affect $I_{Ca,L}$ suggesting that $I_{Ca,L}$ does not contribute to APD prolongation observed in Ang II treated myocytes.

4.4. Effects of Ang II treatment on repolarizing potassium currents in right and left atrial myocytes from wildtype mice

The AP data presented in section 4.1 demonstrates APD is prolonged at all repolarization times in Ang II treated right and left atrial myocytes. Accordingly, the goal of the next set of experiments was to characterize the effects of Ang II treatment on repolarizing K^+ currents in right and left atrial myocytes.

Total K^+ currents were measured in right and left atrial myocytes using a no pre-pulse voltage-clamp protocol between -120 and +80 mV from a holding potential of -80 mV. Representative recordings for a family of total K^+ currents in saline and Ang II treated right atrial myocytes are shown in Figs. 4.7A and 4.7B. As shown in the summary K^+ I-V relationship in Fig. 4.7E, outward K^+ currents are reduced ($P < 0.001$) in Ang II treated right atrial myocytes at membrane potentials between -10 mV and +80 mV. These data are consistent with the APD prolongation in Ang II treated right atrial myocytes.

Representative recordings for a family of total K^+ currents from a saline and Ang II treated left atrial myocyte are shown in Figs. 4.7C and 4.7D and the summary K^+ I-V relationship is shown in Fig. 4.7F. Outward K^+ currents were reduced ($P < 0.001$) between membrane potentials -20 mV and +80 mV and inward K^+ currents negative to -100 mV in Ang II treated left atrial myocytes. These data are consistent with the APD prolongation in Ang II treated left atrial myocytes.

The reduction in I_K elicited by Ang II treatment was greater in the left atrium. I_K at +50 mV was compared between the right and left atrial myocytes shown in Fig. 4.8. There was no difference ($P = 0.052$) in I_K between saline treated right and left atrial myocytes. Strikingly, I_K was reduced to a greater extent ($P = 0.050$) in Ang II treated left

Figure 4.7. Effects of Ang II treatment on potassium currents in right and left atrial myocytes from wildtype mice.

A. and **B.** Representative patch-clamp recordings showing a family of total K^+ currents (no pre-pulse) recorded from saline (A) and Ang II (B) treated right atrial myocytes. **C.** and **D.** Representative patch-clamp recordings showing a family of K^+ currents recorded from saline (C) and Ang II (D) treated left atrial myocytes. **E.** and **F.** Summary K^+ I-V relationships illustrating the effects of Ang II treatment on K^+ currents (no pre-pulse) in right (E) and left (F) atrial myocytes. Currents measured at the peak current for each membrane potential. *$P<0.05$ vs. saline at each membrane potential. Data analyzed by two-way repeated measures ANOVA with Tukey's post hoc test. Right atrium: $n = 29$ saline and 28 Ang II treated myocytes; Left atrium: $n = 10$ saline and 17 Ang II treated myocytes.

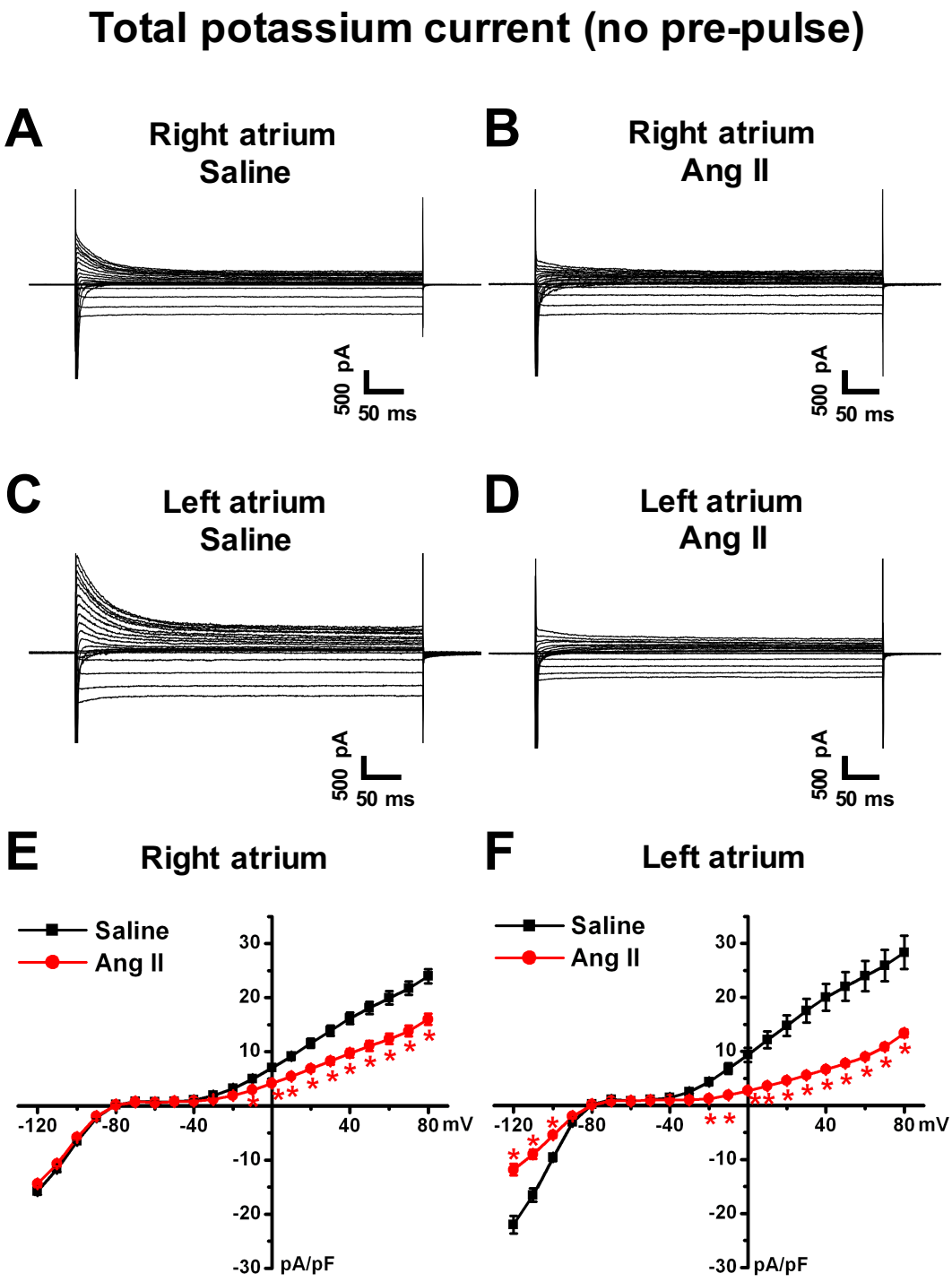
Total potassium current (no pre-pulse)
A
Right atrium
Saline
500 pA
50 ms
B
Right atrium
Ang II
500 pA
50 ms
C
Left atrium
Saline
500 pA
50 ms
D
Left atrium
Ang II
500 pA
50 ms
E
Right atrium
Saline
Ang II
30
20
10
-10
-20
-30
-120
-80
-40
40
80 mV
pA/pF
F
Left atrium
Saline
Ang II
30
20
10
-10
-20
-30
-120
-80
-40
40
80 mV
pA/pF

Figure 4.7

Figure 4.8. Comparison of the effects of Ang II treatment on potassium current densities in right and left atrial myocytes from wildtype mice.

A. Summary data comparing the effects of Ang II treatment on total K^+ currents (no pre-pulse) measured at +50 mV in right and left atrial myocytes. **P*<0.05 vs. saline within atrial region; ^+P<0.05 vs. right atrium within treatment group. Data analyzed by two-way ANOVA with Tukey's post hoc test. Right atrium: *n* = 29 saline and 28 Ang II treated myocytes; Left atrium: *n* = 10 saline and 17 Ang II treated myocytes.

Total potassium current (no pre-pulse)

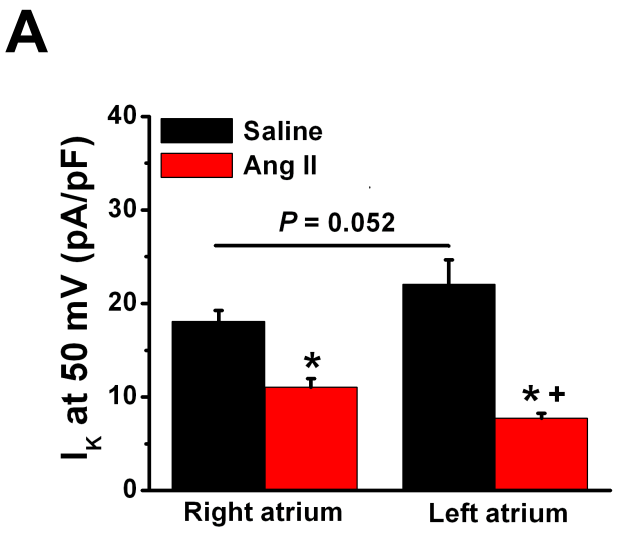

Figure 4.8

atrial myocytes compared to Ang II treated right atrial myocytes. This corresponds to a 64% reduction in the left atrium and 38% in the right atrium compared to saline controls. These data demonstrate the reduction in total K^+ currents is greater in Ang II treated left atrial myocytes, and is consistent with the greater prolongation in APD observed in these cells.

In the next set of experiments, K^+ currents were measured following a pre-pulse to -40 mV to inactivate the transient outward potassium current (I_{to}) (Kuo *et al.*, 2001; Lomax *et al.*, 2003b). Representative patch-clamp recordings for a saline and Ang II treated right atrial myocyte are shown in Figs. 4.9A and 4.9B. As illustrated in the summary K^+ I-V relationship (Fig. 4.9E), outward K^+ currents are reduced between 0 mV ($P = 0.018$) and +80 mV ($P < 0.001$) in Ang II treated right atrial myocytes. Representative recordings for a saline and Ang II treated left atrial myocyte are presented in Figs. 4.9C and 4.9D. Summary K^+ I-V relationships (Fig. 4.9F) demonstrate a reduction in outward K^+ currents from -20 mV ($P = 0.009$) to +80 mV ($P < 0.001$) and inward currents ($P < 0.001$) from -120 to -100 mV in Ang II treated left atrial myocytes. Combined, these data demonstrate outward K^+ currents are reduced in Ang II treated myocytes, independent of I_{to}.

Fig. 4.10 compares I_K density at +50 mV following an inactivating pre-pulse in right and left atrial myocytes of saline and Ang II treated mice. Consistent with the I-V relationships, I_K is reduced in Ang II treated right ($P = 0.001$) and left ($P < 0.001$) atrial myocytes compared to saline controls. I_K was larger ($P < 0.001$; Fig. 4.10A) in saline treated left atrial myocytes compared to saline treated right atrial myocytes. There were no differences ($P = 0.56$; Fig. 4.10A) in Ang II treated right vs. left atrial myocytes. Although there are no differences in I_K at +50 mV (with inactivating pre-pulse) in right vs. left Ang II treated myocytes, left atrial myocytes elicited a greater reduction (approximately 56%) in I_K compared to saline controls. In the right atrium, the reduction in I_K was approximately 26%.

I_{to} was measured as the difference current with and without a pre-pulse to -40 mV. Representative I_{to} recordings at a membrane potential of +50 mV for saline and Ang II treated right atrial myocytes are shown in Figs. 4.11A and 4.11B and from a saline and Ang II treated left atrial myocyte in Figs. 4.11C and 4.11D. Summary I-V relationships

Figure 4.9. Effects of Ang II treatment on potassium currents following a pre-pulse to -40 mV in right and left atrial myocytes from wildtype mice.

A. and **B.** Representative patch-clamp recordings showing a family of K^+ currents recorded from saline (A) and Ang II (B) treated right atrial myocytes following a pre-pulse to -40 mV to inactivate the transient outward potassium current (I_{to}). **C.** and **D.** Representative patch-clamp recordings showing a family of K^+ currents recorded from saline (C) and Ang II (D) treated left atrial myocytes following a pre-pulse to -40 mV to inactivate I_{to}. **E.** and **F.** Summary K^+ I-V relationships illustrating the effects of Ang II treatment on K^+ currents in right (E) and left (F) atrial myocytes with a pre-pulse to -40 mV. Currents measured from the peak current at each membrane potential. **P*<0.05 vs. saline at each membrane potential. Data analyzed by two-way repeated measures ANOVA with Tukey's post hoc test. Right atrium: *n* = 29 saline and 28 Ang II treated myocytes; Left atrium: *n* = 10 saline and 17 Ang II treated myocytes.

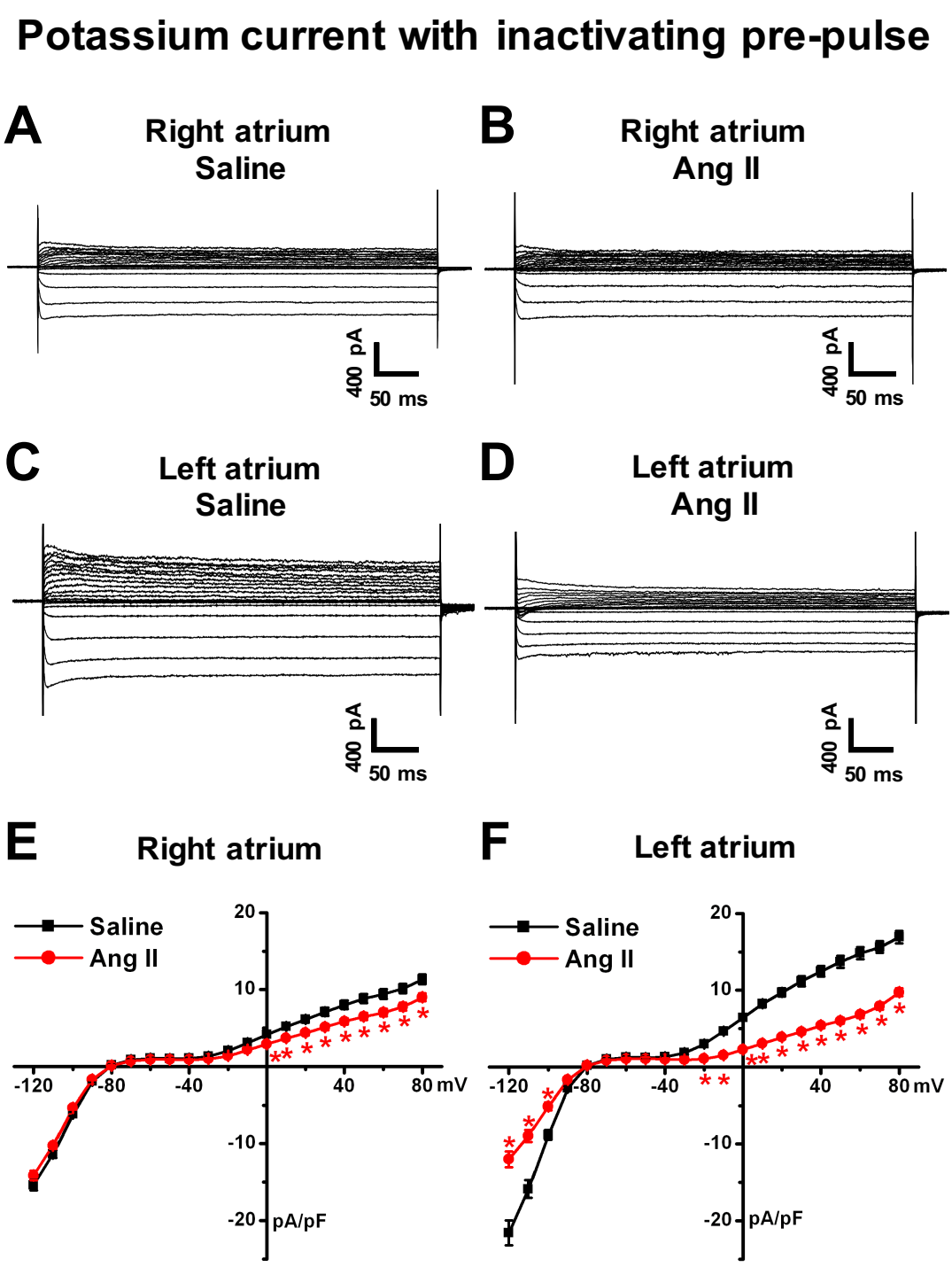
Potassium current with inactivating pre-pulse
A
Right atrium
Saline
B
Right atrium
Ang II
400 pA
50 ms
C
Left atrium
Saline
D
Left atrium
Ang II
E
Right atrium
F
Left atrium
Saline
Ang II
20
10
-10
-20
pA/pF
-120
-80
-40
40
80 mV

Figure 4.9

Figure 4.10. Comparison of the effects of Ang II treatment on potassium current density following a pre-pulse to -40 mV in right and left atrial myocytes from wildtype mice.

A. Summary data comparing the effect Ang II treatment on K^+ currents at +50 mV in right and left atrial myocytes following a pre-pulse to -40 mV to inactivate I_{to}. **P*<0.05 vs. saline within atrial region; ^+P<0.05 vs. right atrium within treatment group. Data analyzed by two-way ANOVA with Tukey's post hoc test. Right atrium: *n* = 29 saline and 28 Ang II treated myocytes; Left atrium: *n* = 10 saline and 17 Ang II treated myocytes.

Potassium current with inactivating pre-pulse

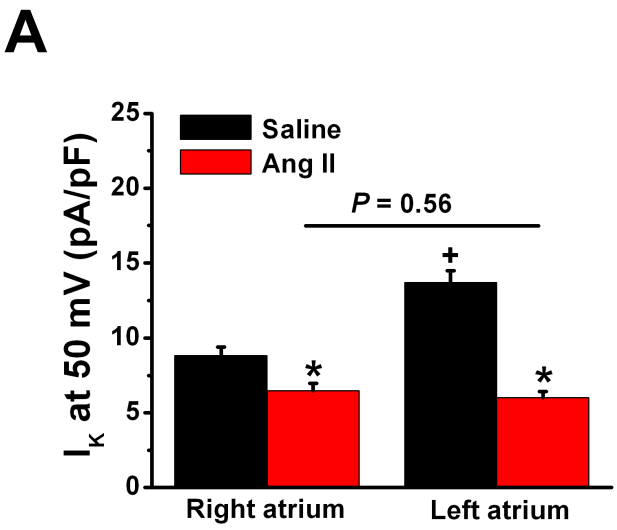

Figure 4.10

Figure 4.11. Effects of Ang II treatment on the transient outward potassium current (I_{to}) in right and left atrial myocytes from wildtype mice.

A. and **B.** Representative patch-clamp recordings showing I_{to} from saline (A) and Ang II (B) treated right atrial myocytes. Representative recordings at +50 mV as measured from the difference current with and without a pre-pulse to -40 mV. **C.** and **D.** Representative patch-clamp recordings showing I_{to} from saline (C) and Ang II (D) treated left atrial myocytes. Representative recordings were obtained from the difference in current with and without a pre-pulse to -40 mV at a membrane potential of +50 mV. **E.** and **F.** Summary K^+ I-V relationships illustrating the effects of Ang II treatment on I_{to} in right (E) and left (F) atrial myocytes. **P*<0.05 vs. saline at each membrane potential. Data analyzed by two-way repeated measures ANOVA with Tukey's post hoc test. Right atrium: *n* = 29 saline and 28 Ang II treated myocytes; Left atrium: *n* = 10 saline and 17 Ang II treated myocytes.

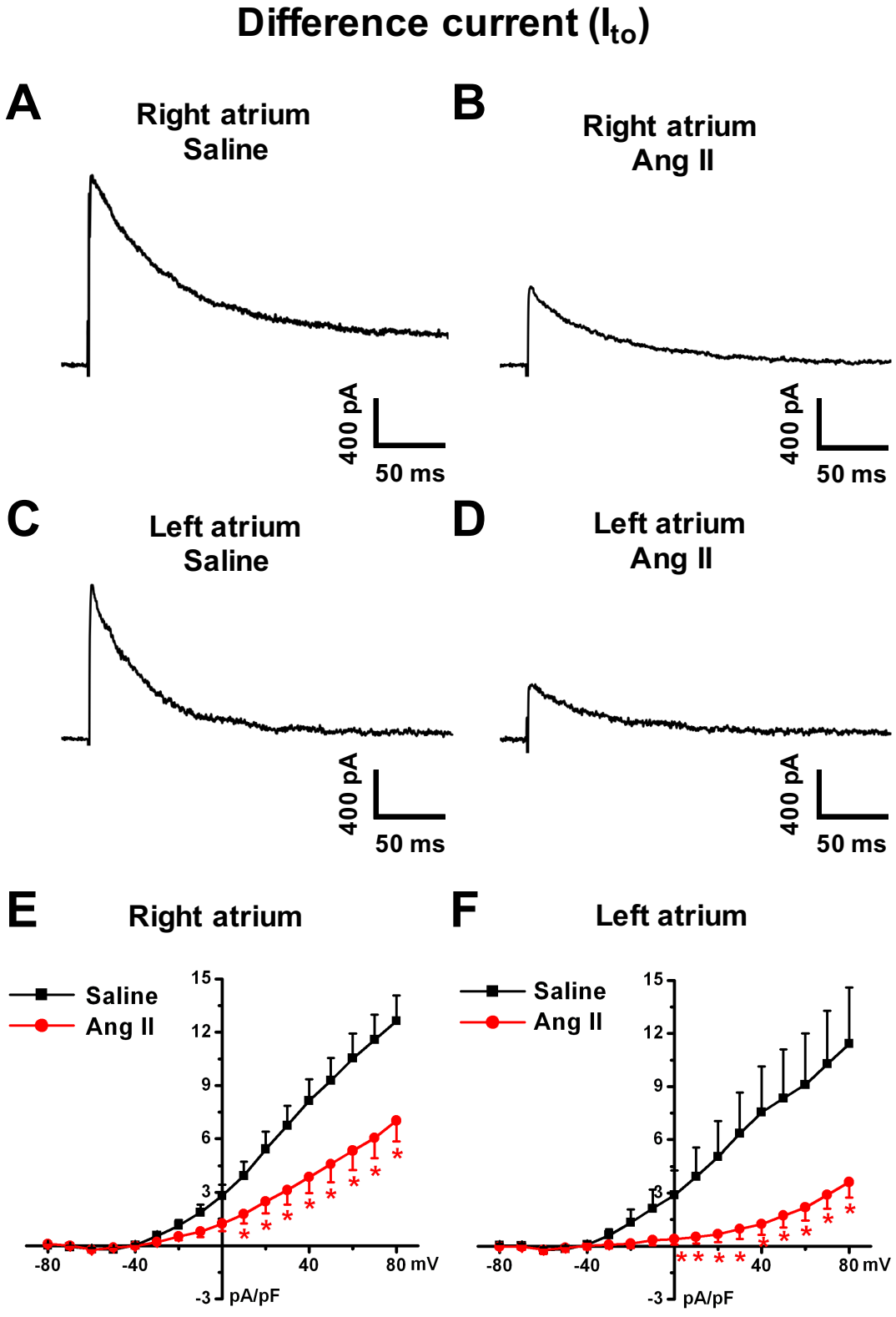
Difference current (I_{to})
A
Right atrium
Saline
400 pA
50 ms
B
Right atrium
Ang II
400 pA
50 ms
C
Left atrium
Saline
400 pA
50 ms
D
Left atrium
Ang II
400 pA
50 ms
E
Right atrium
Saline
Ang II
15
12
9
6
3
-3
-80
-40
40
80 mV
pA/pF
F
Left atrium
Saline
Ang II
15
12
9
6
3
-3
-80
-40
40
80 mV
pA/pF

Figure 4.11

demonstrate a clear reduction in I_{to} in Ang II treated right ($P < 0.001$; Fig. 4.11E) and left ($P < 0.001$; Fig. 4.11F) atrial myocytes. Comparison of the effects of Ang II treatment on I_{to} in right and left atrial myocytes is presented in Fig. 4.12. There were no differences ($P = 0.57$) in I_{to} between saline treated right and left atrial myocytes. Consistent with the I-V relationships, I_{to} was reduced following Ang II treatment in right ($P < 0.001$) and left ($P < 0.001$) atrial myocytes compared to saline controls. Left atrial myocytes exhibited a greater reduction ($P = 0.045$) in I_{to} following Ang II treatment compared to right atrial myocytes. This is consistent with the total K^+ current data demonstrating a greater reduction in I_K in Ang II treated left atrial myocytes.

Next, the effects of Ang II treatment on I_{Kur} was assessed in the right and left atrium. I_{Kur} is sensitive to micromolar concentrations of 4-aminopyradine (4-AP) (Lomax *et al.*, 2003b) and can be quantified based on the reduction in I_K in the presence of 4-AP compared to baseline current. In this set of experiments, I_{to} was inactivated with a pre-pulse to -40 mV and I_K was measured at +30 mV. As demonstrated in the representative patch-clamp recordings, application of 4-AP (100 μM) reduced I_K in right (Figs. 4.13A and 4.13B) and left (Figs. 4.13C and 4.13D) atrial myocytes and was reversible upon washout. The effects of 4-AP were blunted in Ang II treated right ($P = 0.016$; Fig. 4.13E) and left ($P = 0.006$; Fig. 4.13F) atrial myocytes compared to saline controls. There were no differences in 4-AP sensitivity between saline ($P = 0.08$) and Ang II ($P = 0.60$) right vs. left atrial myocytes. Combined, these data demonstrate I_{Kur} is reduced following Ang II treatment, and the magnitude of reduction is the same in right and left atrial myocytes.

The K^+ I-V relationships in Figs. 4.7 and 4.9 demonstrate a reduction in inward K^+ current negative to -100 mV in Ang II treated left atrial myocytes, which could indicate a reduction in the inward rectifier potassium current (I_{K1}). Accordingly, sensitivity to barium chloride ($BaCl_2$), a selective I_{K1} blocker (Lomax *et al.*, 2003b), was assessed in saline and Ang II treated myocytes. Inward K^+ current was measured at -100 mV from a voltage ramp between +50 mV and -120 mV. Representative recordings for saline and Ang II treated right atrial myocytes are shown in Figs. 4.14A and 4.14B and left atrial myocytes are shown in Figs. 4.14C and 4.14D. Superfusion of $BaCl_2$ (100 μM)

Figure 4.12. Comparison of the effects of Ang II treatment on I_{to} in right and left atrial myocytes from wildtype mice.

A. Summary data comparing the reduction in I_{to} measured at +50 mV following Ang II treatment in right and left atrial myocytes. **P*<0.05 vs. saline within atrial region; $^{+}$*P*<0.05 vs. right atrium within treatment group. Data analyzed by two-way ANOVA with Tukey's post hoc test. Right atrium: *n* = 29 saline and 28 Ang II treated myocytes; Left atrium: *n* = 10 saline and 17 Ang II treated myocytes.

Difference current (I_{to})

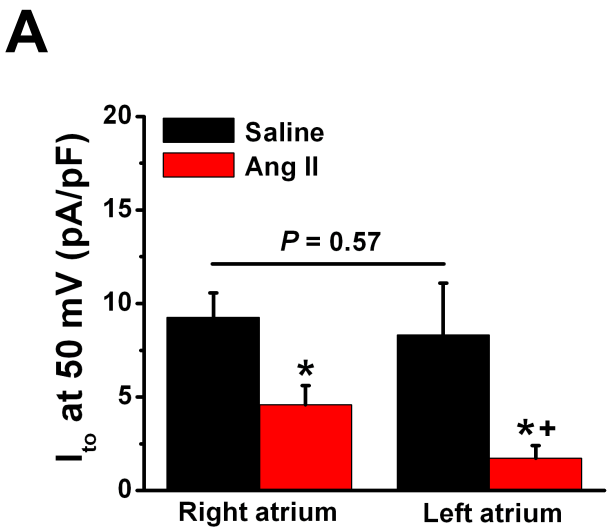

Figure 4.12

Figure 4.13. Effects of Ang II treatment on 4-aminopyradine (4-AP) sensitive potassium current in right and left atrial myocytes from wildtype mice.

A. and **B.** Representative recordings demonstrating the effects of 4-AP (100 μM) on potassium currents (I_K) recorded from saline (A) and Ang II (B) treated right atrial myocytes. **C.** and **D.** Representative recordings demonstrating the effects of 4-AP (100 μM) on I_K recorded from saline (C) and Ang II (D) treated left atrial myocytes. **E.** and **F.** Summary data illustrating the percent reduction in I_K following application of 4-AP (100 μM) in right (E) and left (F) atrial myocytes. **P*<0.05 vs. saline. Data analyzed by Student's *t*-test. Right atrium: *n* = 22 saline and 14 Ang II treated myocytes; Left atrium: *n* = 12 saline and 9 Ang II treated myocytes.

4-Aminopyradine sensitive potassium current

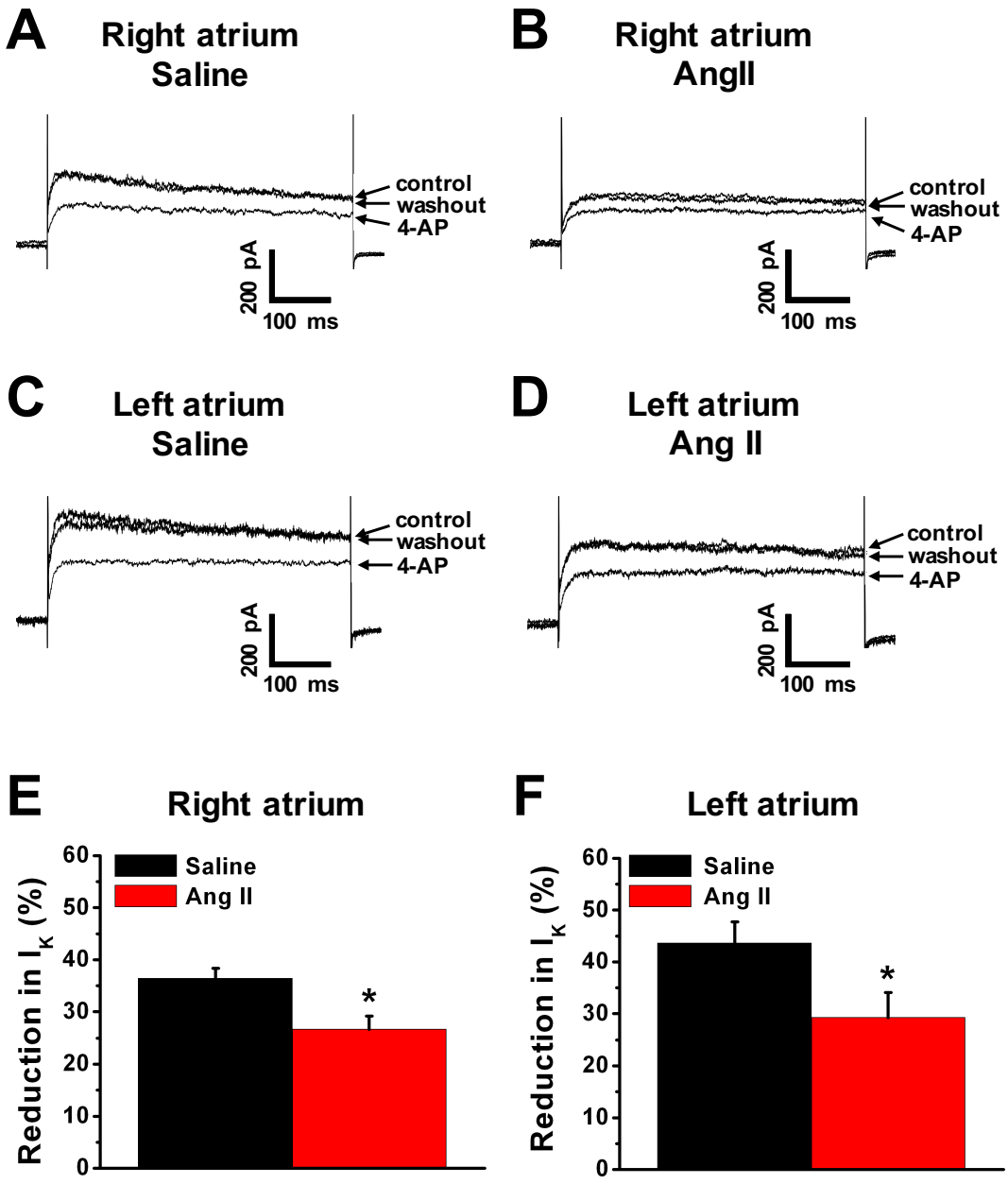

Figure 4.13

Figure 4.14. Effects of barium on potassium currents in saline and Ang II treated right and left atrial myocytes from wildtype mice.

A. and **B.** Representative recordings demonstrating the effects of barium chloride ($BaCl_2$; 100 μM) on potassium current (I_K) recorded from saline (A) and Ang II (B) treated right atrial myocytes using a voltage ramp between +50 mV and -120 mV. **C.** and **D.** Representative recordings demonstrating the effects of $BaCl_2$ (100 μM) on I_K recorded from saline (C) and Ang II (D) treated left atrial myocytes. **E.** and **F.** Summary data illustrating the reduction in I_K measured at -100 mV following application of $BaCl_2$ (100 μM) in right (E) and left (F) atrial myocytes. $BaCl_2$ was applied to selectively block the inward rectifier potassium current (I_{K1}). There were no differences in the effects of $BaCl_2$ on I_k between saline and Ang II treated myocytes in the right ($P = 0.55$) or left ($P = 0.29$) atrium. Data analyzed by Student's *t*-test. Right atrium: $n = 8$ saline and 7 Ang II treated myocytes; Left atrium: $n = 7$ saline and 9 Ang II treated myocytes.

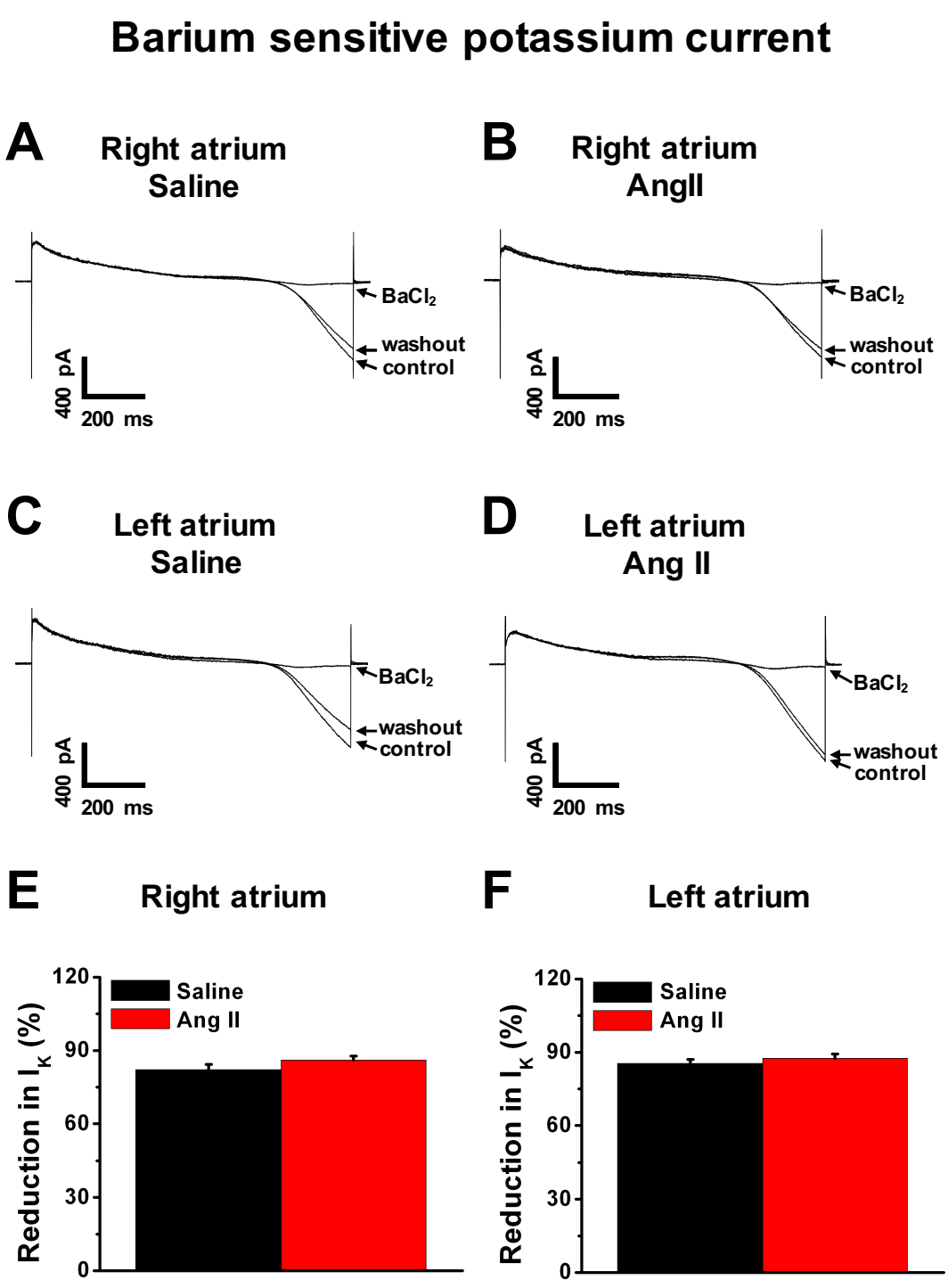
Barium sensitive potassium current
A
Right atrium
Saline
BaCl2
washout
control
400 pA
200 ms
B
Right atrium
AngII
BaCl2
washout
control
400 pA
200 ms
C
Left atrium
Saline
BaCl2
washout
control
400 pA
200 ms
D
Left atrium
Ang II
BaCl2
washout
control
400 pA
200 ms
E
Right atrium
Reduction in IK (%)
120
90
60
30
0
Saline
Ang II
F
Left atrium
Reduction in IK (%)
120
90
60
30
0
Saline
Ang II

Figure 4.14

reduced I_K in right ($P < 0.001$) and left ($P < 0.001$) atrial myocytes and was reversible upon washout. There were no differences in the reduction in I_K in right ($P = 0.55$; Fig. 4.14E) or left ($P = 0.29$; Fig. 4.14F) atrial myocytes from saline vs. Ang II treated mice. Therefore, I_{K1} is not altered following Ang II treatment.

4.5. Effects of Ang II treatment on ion channel expression in the right and left atrium of wildtype mice

The patch-clamp data presented in sections 4.2 and 4.4 demonstrate profound changes in ion currents in Ang II treated right and left atrial myocytes. To gain insight to the underlying mechanisms responsible for these alterations, mRNA levels were quantified in a series of qPCR experiments to determine if these changes were attributed to altered gene expression patterns for ion channel subunits. All gene expression data was normalized to both GAPDH and β-actin.

Expression of the I_{Na} α-subunit $Na_V1.5$ (*SCN5a*) was quantified in the right and left atrium as summarized in Fig. 4.15A. In the right atrium, *SCN5a* mRNA expression was not different ($P = 0.97$) in saline vs. Ang II treated mice. Similarly, there were no differences ($P = 0.83$) in *SCN5a* mRNA expression in the left atrium of Ang II treated mice compared to saline controls. This is consistent with the patch-clamp data in the right, but not the left, atrial myocytes from Ang II treated mice.

Next, the effects of Ang II treatment on the α1-C subunit $Ca_V1.2$ (*CACNA1c*) and the α1-D subunit $Ca_V1.3$ (*CACNA1d*) were quantified in the right and left atrium. There were no differences ($P = 0.58$) in *CACNA1c* (Fig. 4.15B) mRNA expression in the right and left atrium of Ang II treated mice. Similarly, *CACNA1d* (Fig. 4.15C) mRNA expression was not different in the right ($P = 0.26$) or left ($P = 0.15$) atrium of Ang II treated mice compared to saline controls. These data are consistent with the patch-clamp data demonstrating $I_{Ca,L}$ is not altered in Ang II treated mice. In addition, *CACNA1d* mRNA expression was lower in the left atrium of saline ($P = 0.003$) and Ang II ($P < 0.001$) treated mice compared to the right atrium.

The patch-clamp data presented in Fig. 4.11 shows a significant reduction in I_{to} in Ang II treated right and left atrial myocytes. To determine if altered gene expression

Figure 4.15. Quantitative mRNA expression of ion channel subunits following Ang II treatment in the right and left atrium.

A – G. Summary data illustrating the effects of Ang II treatment on mRNA expression levels for the I_{Na} α-subunit $Na_V1.5$ (*SCN5a*; A), the $I_{Ca,L}$ α1-C subunit $Ca_V1.2$ (*CACNA1c*; B), the α1-D subunit $Ca_V1.3$ (*CACNA1d*; C), the I_{to} subunits $K_V4.2$ (*KCND2*; D) and $K_V4.3$ (*KCND3*; E), the I_{Kur} subunit $K_V1.5$ (*KCNA5*; F), the accessory β-subunit KChIP2 (*KCNIP2*; G) in the right and left atrium. mRNA expression was normalized to GAPDH and β-actin. $*P<0.05$ vs. saline within atrial region; $^{+}P<0.05$ vs. right atrium within treatment group. Data analyzed by two-way ANOVA with Tukey's post hoc test. Right atrium: $n = 7$ saline and 8 Ang II treated hearts; Left atrium: $n = 8$ saline and 8 Ang II treated hearts.

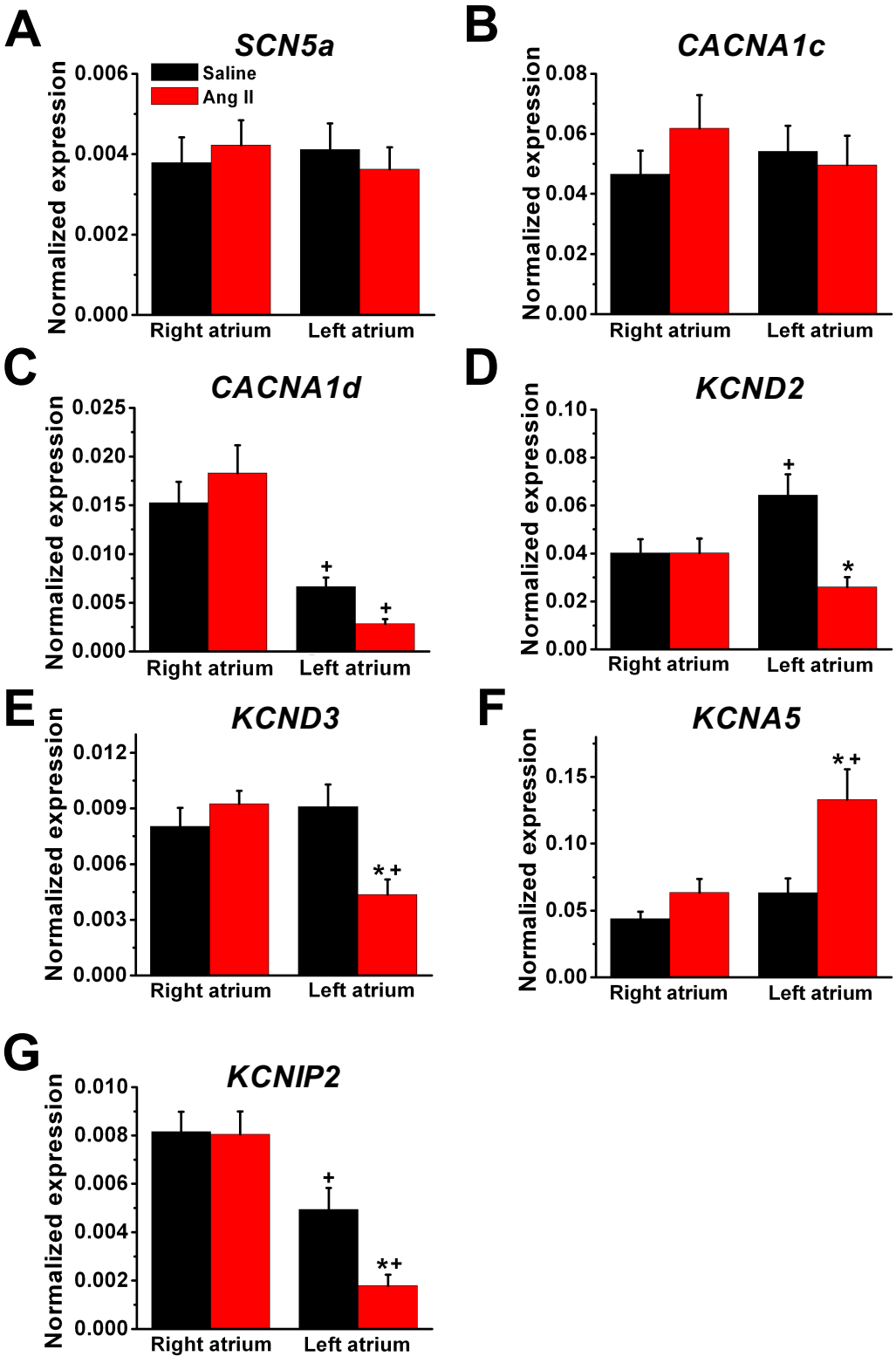
A
SCN5a
Saline
Ang II
Normalized expression
0.006
0.004
0.002
0.000
Right atrium
Left atrium
B
CACNA1c
Normalized expression
0.08
0.06
0.04
0.02
0.00
Right atrium
Left atrium
C
CACNA1d
Normalized expression
0.025
0.020
0.015
0.010
0.005
0.000
+
+
Right atrium
Left atrium
D
KCND2
Normalized expression
0.10
0.08
0.06
0.04
0.02
0.00
+
*
Right atrium
Left atrium
E
KCND3
Normalized expression
0.012
0.009
0.006
0.003
0.000
*+
Right atrium
Left atrium
F
KCNA5
Normalized expression
0.15
0.10
0.05
0.00
*+
Right atrium
Left atrium
G
KCNIP2
Normalized expression
0.010
0.008
0.006
0.004
0.002
0.000
+
*+
Right atrium
Left atrium

Figure 4.15

patterns contributed to this reduction, mRNA expression was quantified for the I_{to} α-subunits $K_V4.2$ (*KCND2*) and $K_V4.3$ (*KCND3*). In the right atrium, there were no differences in *KCND2* ($P = 1.00$; Fig. 4.15D) nor *KCND3* ($P = 0.38$; Fig. 4.15E) mRNA expression in saline vs. Ang II treated mice. Therefore, altered gene expression patterns do not contribute to a reduction in I_{to} in the right atrium. In contrast, both *KCND2* ($P = 0.015$; Fig. 4.15D) and *KCND3* ($P = 0.002$; Fig. 4.15E) mRNA expression were reduced in the left atrium of Ang II treated mice compared to saline controls. *KCND2* mRNA expression was higher in the left atrium of saline ($P = 0.015$), but not Ang II ($P = 0.13$), treated hearts compared to the right atrium. There were no left-right differences ($P = 0.45$) in *KCND3* mRNA expression in saline treated mice; however, *KCND3* mRNA expression was lower ($P = 0.001$) in the left vs. right atrium of Ang II treated mice. Combined, the reductions in *KCND2* and *KCND3* mRNA expression in the left atrium can contribute to the reduction in I_{to} densities in Ang II treated left atrial myocytes.

The I_{Kur} pore forming α-subunit, $K_V1.5$, is encoded by *KCNA5*. There were no differences ($P = 0.35$; Fig. 4.15F) in *KCNA5* mRNA expression in the right atrium of saline vs. Ang II treated mice. Surprisingly, *KCNA5* mRNA expression was increased ($P = 0.002$; Fig. 4.15F) in the left atrium of Ang II treated mice. Comparison of *KCNA5* mRNA expression between the regions indicates there were no differences ($P = 0.35$) between saline treated right vs. left atria, however expression was higher ($P = 0.002$) in Ang II treated left vs. right atria. These data indicate the reduction in I_{Kur} observed in patch-clamp experiments is not attributed to altered gene expression patterns of *KCNA5*.

KChIP2, encoded by *KCNIP2*, is an accessory β-subunit for K_V4 channels with emerging roles in regulating I_{Na} and $I_{Ca,L}$ (Mezzano and Morley, 2015). In the right atrium, there were no differences ($P = 0.92$; Fig. 4.15G) in *KCNIP2* mRNA expression in saline vs. Ang II treated mice. In contrast, *KCNIP2* mRNA expression was reduced ($P = 0.010$; Fig. 4.15G) in the left atrium of Ang II treated mice. Compared to the right atrium, *KCNIP2* mRNA expression was lower in the saline ($P = 0.010$) and Ang II ($P < 0.001$) treated left atrium.

CHAPTER 5
EFFECTS OF NPR-C ON SINOATRIAL NODE FUNCTION AND ATRIAL ELECTROPHYSIOLOGY IN ANG II TREATED MICE

5.1. Effects of Ang II treatment on cardiac electrophysiology in anaesthetized NPR-C$^{+/+}$ and NPR-C$^{-/-}$ mice

Recently, our lab characterized cardiac function in NPR-C$^{-/-}$ mice (Egom *et al.*, 2015) and demonstrated that NPR-C$^{-/-}$ mice have SAN dysfunction and an increased susceptibility to AF under baseline conditions. This was attributed to structural remodelling (i.e. fibrosis) rather than electrical remodelling (i.e. ion channel function) of the SAN and atrium. These data demonstrate a cardioprotective role for NPR-C in the heart. The next set of experiments aimed at investigating the role of NPR-C in the progression of heart disease induced by Ang II treatment. It should be noted that *in vivo* and patch-clamp data from saline and Ang II treated wildtype mice was previously presented in Chapters 3 and 4 and used as controls in this chapter.

Summary systolic blood pressure measurements are presented in Appendix C. Systolic blood pressure was not different in saline treated NPR-C$^{+/+}$ ($P = 0.35$) and NPR-C$^{-/-}$ ($P = 0.96$) mice during the 3 week treatment period. Ang II treatment increased systolic blood pressure in both NPR-C$^{+/+}$ ($P < 0.001$) and NPR-C$^{-/-}$ ($P < 0.001$) mice compared to baseline measurements. There were no differences ($P = 0.57$) in systolic blood pressure measured at the 3 week time point between Ang II treated NPR-C$^{+/+}$ and NPR-C$^{-/-}$ mice.

Representative ECG recordings from saline and Ang II treated NPR-C$^{+/+}$ mice are shown in Figs. 5.1A and 5.1B. Representative recordings from saline and Ang II treated NPR-C$^{-/-}$ mice are presented in Figs. 5.1C and 5.1D. Summary data for ECG intervals and intracardiac ECG parameters measured in NPR-C$^{+/+}$ and NPR-C$^{-/-}$ mice are located in Appendix D. Summary data shown in Fig. 5.1E illustrates that baseline heart rate is reduced in Ang II treated NPR-C$^{+/+}$ ($P = 0.014$) and NPR-C$^{-/-}$ ($P = 0.006$) mice compared to saline controls. Furthermore, heart rate in Ang II treated NPR-C$^{-/-}$ mice was

Figure 5.1. Effects of Ang II treatment on heart rate in anaesthetized NPR-C$^{+/+}$ and NPR-C$^{-/-}$ mice.

A. and **B.** Representative ECG recordings in anesthetized saline (A) and Ang II (B) treated NPR-C$^{+/+}$ mice. **C.** and **D.** Representative ECG recordings in anesthetized saline (C) and Ang II (D) treated NPR-C$^{-/-}$ mice. **E.** Summary data illustrating the effects of Ang II treatment on heart rate in NPR-C$^{+/+}$ and NPR-C$^{-/-}$ mice. There was no difference in heart rate (P = 0.41) between saline treated NPR-C $^{+/+}$ and NPR-C$^{-/-}$ mice. *P<0.05 vs. saline within genotype. ^{+}P<0.05 vs. NPR-C $^{+/+}$ within treatment group. Data analyzed by two-way ANOVA with Tukey's post hoc test. NPR-C$^{+/+}$: n = 23 saline and 33 Ang II treated mice; NPR-C$^{-/-}$: n = 14 saline and 15 Ang II treated mice.

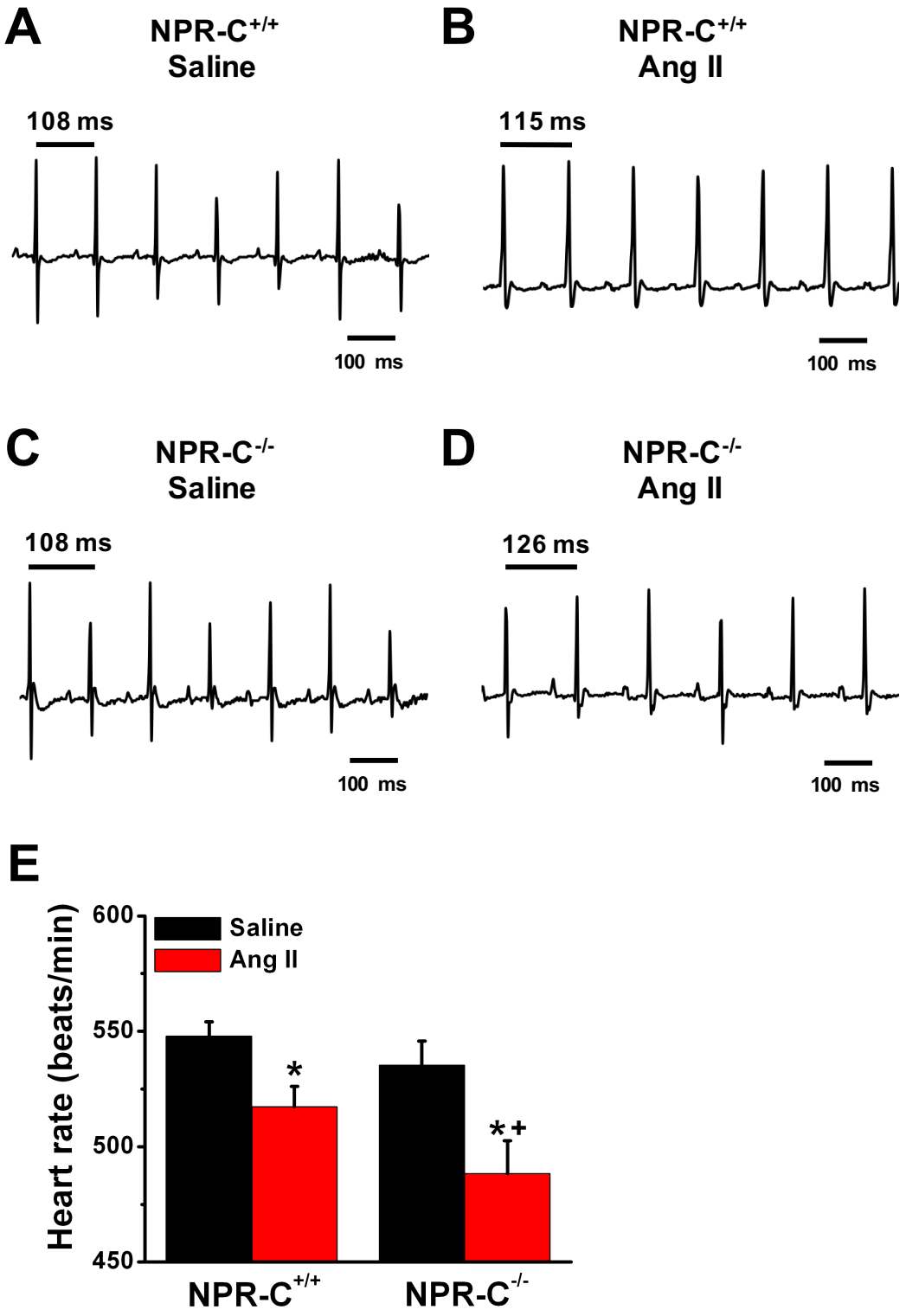
A
NPR-C+/+
Saline
108 ms
100 ms
B
NPR-C+/+
Ang II
115 ms
100 ms
C
NPR-C-/-
Saline
108 ms
100 ms
D
NPR-C-/-
Ang II
126 ms
100 ms
E
Heart rate (beats/min)
600
550
500
450
Saline
Ang II
*
*+
NPR-C+/+
NPR-C-/-

Figure 5.1

significantly lower ($P = 0.041$) compared to Ang II treated NPR-$C^{+/+}$ mice. There were no differences ($P = 0.41$) in heart rate between saline treated NPR-$C^{+/+}$and NPR-$C^{-/-}$ mice. To determine if the reduction in heart rate was correlated with impaired SAN function, cSNRT was measured in anaesthetized mice. Representative ECG recordings during intracardiac programmed electrical stimulation are presented in Figs. 5.2A and 5.2B for NPR-$C^{+/+}$ mice and Figs. 5.2C and 5.2D for NPR-$C^{-/-}$ mice. Summary data (Fig. 5.2E) demonstrates that cSNRT is prolonged following Ang II treatment in both NPR-$C^{+/+}$ ($P < 0.001$) and NPR-$C^{-/-}$ ($P < 0.001$) mice. Strikingly, this prolongation was greater ($P < 0.001$) in Ang II treated NPR-$C^{-/-}$ mice compared to NPR-$C^{+/+}$ mice. cSNRT was also prolonged ($P < 0.001$) in saline treated NPR-$C^{-/-}$ vs. NPR-$C^{+/+}$ mice. Combined, these data demonstrate that Ang II treatment in NPR-$C^{-/-}$ mice results in a greater reduction in heart rate compared to NPR-$C^{+/+}$ mice and this is attributed to a greater impairment of SAN function *in vivo*.

NPR-$C^{-/-}$ mice had an increased susceptibility to induced AF, as demonstrated in Fig. 5.3A and Table 5.1. In saline treated mice, AF was induced in 8% of NPR-$C^{+/+}$ (2/25) mice and 56% of NPR-$C^{-/-}$ (18/32) mice. Ang II treatment increased the incidence of AF in both NPR-$C^{+/+}$ (15/30; $P = 0.001$) and NPR-$C^{-/-}$ (27/33; $P = 0.033$) mice. Strikingly, Ang II treatment in NPR-$C^{-/-}$ mice resulted in a higher ($P = 0.015$) incidence of AF compared to Ang II treatment in NPR-$C^{+/+}$ mice. In fact, 82% of Ang II treated NPR-$C^{-/-}$ mice were induced into AF compared to 50% of Ang II treated NPR-$C^{+/+}$ mice. Further scrutiny of the data revealed that Ang II treated NPR-$C^{-/-}$ mice were induced into more severe forms of AF, as shown in Table 5.1. AF lasted longer than 5 seconds in 56% of Ang II treated NPR-$C^{-/-}$ mice and longer than 25 seconds in 30% of mice before spontaneously reverting back to normal sinus rhythm. In comparison, 13% of Ang II treated NPR-$C^{+/+}$ mice and 17% of saline treated NPR-$C^{-/-}$ mice were induced into AF that lasted longer than 25 seconds. This demonstrates that not only does Ang II treatment in NPR-$C^{-/-}$ mice increase the susceptibility to AF, but when induced AF is long lasting and more severe.

Next, the effects of Ang II treatment on conduction time across the atria and through the AV node were assessed in anaesthetized NPR-$C^{+/+}$ and NPR-$C^{-/-}$ mice. Summary data (Fig. 5.4A) demonstrates P wave duration is prolonged in Ang II treated

Figure 5.2. Effects of Ang II treatment on sinoatrial node recovery time in anaesthetized NPR-C$^{+/+}$ and NPR-C$^{-/-}$ mice.

A. and **B.** Representative ECG recordings during intracardiac programmed electrical stimulation in anesthetized saline (A) and Ang II (B) treated NPR-C$^{+/+}$ mice. Sinoatrial node recovery time (SNRT) was measured as described in the Methods. **C.** and **D.** Representative ECG recordings during intracardiac programmed electrical stimulation in anesthetized saline (C) and Ang II (D) treated NPR-C$^{-/-}$ mice. **E**. Summary data illustrating in the effects of Ang II treatment on corrected SNRT (cSNRT) in NPR-C$^{+/+}$ and NPR-C$^{-/-}$ mice. **P*<0.05 vs. saline within genotype; $^{+}$*P*<0.05 vs. NPR-C$^{+/+}$ mice within treatment group. Data analyzed by two-way ANOVA with Tukey's post hoc test. NPR-C$^{+/+}$: *n* = 23 saline and 24 Ang II treated mice; NPR-C$^{-/-}$: *n* = 14 saline and 12 Ang II treated mice.

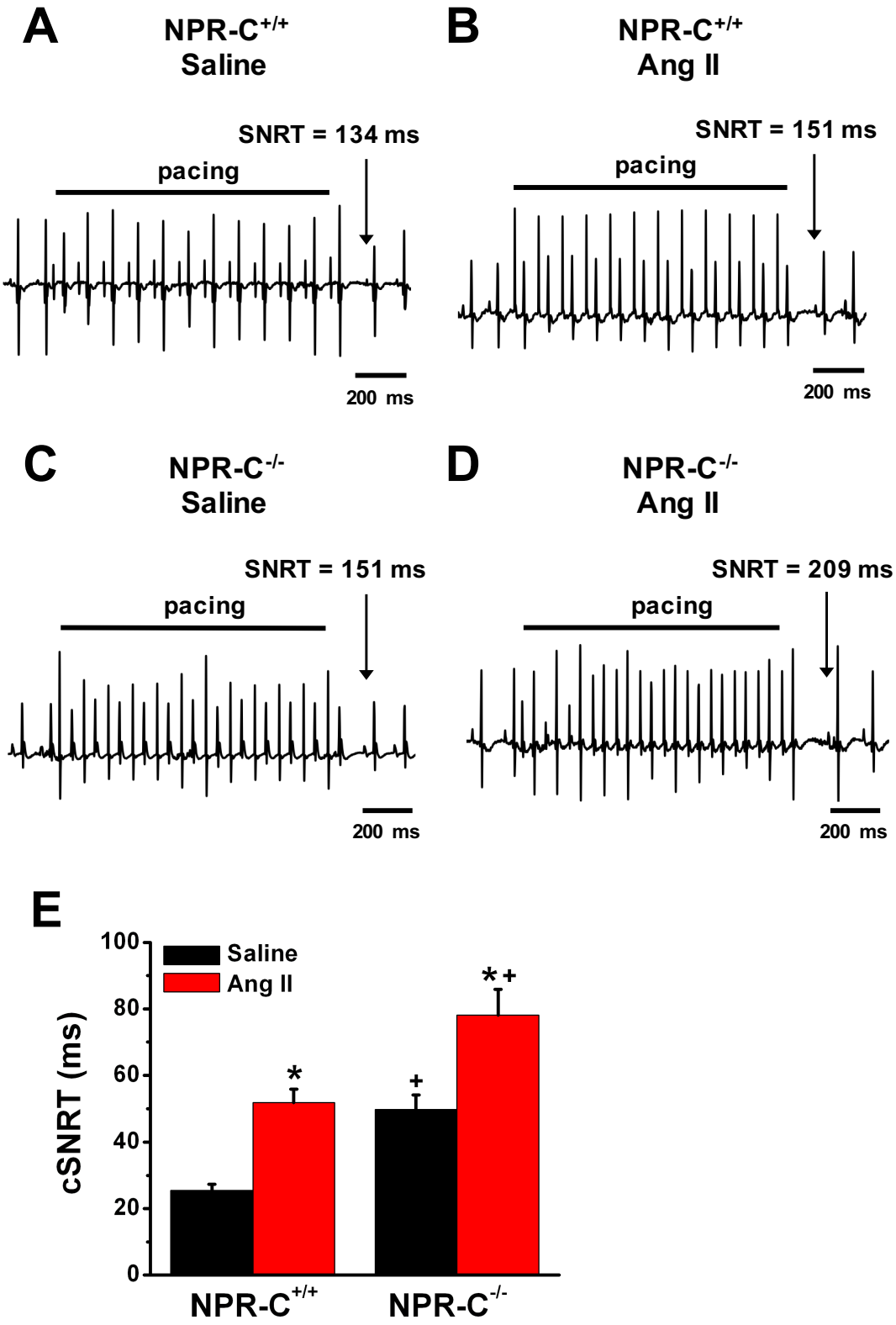
A
NPR-C+/+
Saline
SNRT = 134 ms
pacing
200 ms
B
NPR-C+/+
Ang II
SNRT = 151 ms
pacing
200 ms
C
NPR-C-/-
Saline
SNRT = 151 ms
pacing
200 ms
D
NPR-C-/-
Ang II
SNRT = 209 ms
pacing
200 ms
E
Saline
Ang II
cSNRT (ms)
100
80
60
40
20
0
*
+
*+
NPR-C+/+
NPR-C-/-

Figure 5.2

Figure 5.3. Susceptibility to induced atrial fibrillation in anaesthetized NPR-C$^{+/+}$ and NPR-C$^{-/-}$ mice treated with Ang II.

A. Summary data for the inducibility of AF in saline and Ang II treated NPR-C$^{+/+}$ and NPR-C$^{-/-}$ mice. Numbers in parenthesis indicate the number of mice induced into AF following burst pacing. $^{*}P < 0.05$ vs. saline. $^{+}P < 0.05$ vs. NPR-C$^{+/+}$ mice within treatment group. Data analyzed by Fisher's exact test. NPR-C$^{+/+}$: $n = 25$ saline and 30 Ang II treated mice; NPR-C$^{-/-}$: $n = 32$ saline and 33 Ang II treated mice. Data collected from H. Jansen and other members of the Rose laboratory.

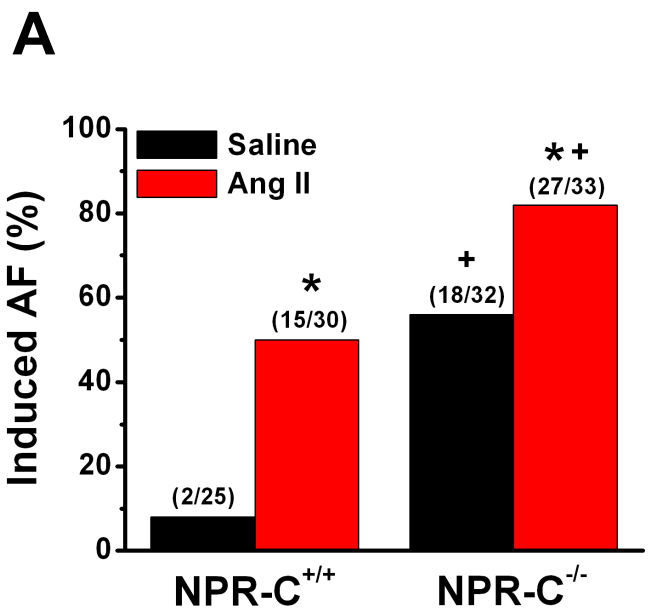
A
Induced AF (%)
100
80
60
40
20
0
Saline
Ang II
(2/25)
*
(15/30)
+
(18/32)
* +
(27/33)
NPR-C+/+
NPR-C-/-

Figure 5.3

Table 5.1. Duration of arrhythmia in NPR-C$^{+/+}$ and NPR-C$^{-/-}$ mice treated with Ang II.

	NPR-C$^{+/+}$		NPR-C$^{-/-}$	
Duration (s)	**Saline**	**Ang II**	**Saline**	**Ang II**
< 5	100% (2/2)	60% (9/15)	61% (11/18)	44% (12/27)
5 – 25		27% (4/15)	22% (4/18)	26% (7/27)
> 25		13% (2/15)	17% (3/18)	30% (8/27)

Numbers in parenthesis indicate the number of mice in each group.

Figure 5.4. Effects of Ang II treatment on atrial and atrioventricular node conduction and electrical function in anaesthetized NPR-C$^{+/+}$ and NPR-C$^{-/-}$ mice.

A. and **B.** Summary data illustrating the effects of Ang II treatment on P wave duration (A) and P-R interval (B) in NPR-C$^{+/+}$ and NPR-C$^{-/-}$ mice. NPR-C$^{+/+}$: n = 23 saline and 33 Ang II treated mice; NPR-C$^{-/-}$: n = 14 saline and 15 Ang II treated mice. **C.** Summary data illustrating the effects of Ang II treatment on atrial effective refractory period (AERP) in NPR-C$^{+/+}$ and NPR-C$^{-/-}$ mice. NPR-C$^{+/+}$: n = 16 saline and 22 Ang II treated mice; NPR-C$^{-/-}$: n = 11 saline and 8 Ang II treated mice. **D.** Summary data illustrating the effects of Ang II treatment on atrioventricular node effective refractory period (AVERP) in NPR-C$^{+/+}$ and NPR-C$^{-/-}$ mice. There was no difference in AVERP (P = 0.30) between saline treated NPR-C$^{+/+}$ vs. NPR-C$^{-/-}$ mice. NPR-C$^{+/+}$: n = 7 saline and 13 Ang II treated mice; NPR-C$^{-/-}$: n = 9 saline and 8 Ang II treated mice. *P<0.05 vs. saline within genotype; ^{+}P<0.05 vs. NPR-C$^{+/+}$ mice within treatment group. Data analyzed by two-way ANOVA with Tukey's post hoc test.

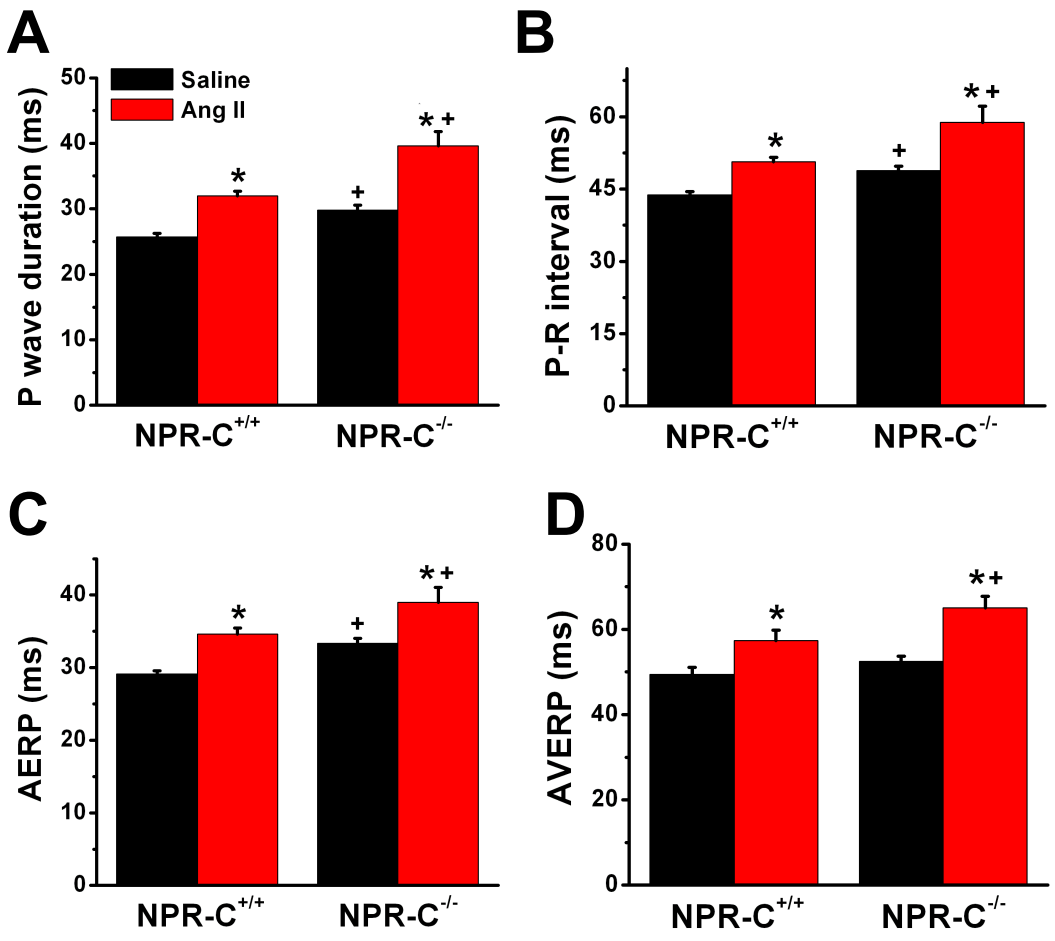
A
Saline
Ang II
P wave duration (ms)
50
40
30
20
10
0
*
+
*+
NPR-C+/+
NPR-C-/-
B
P-R interval (ms)
60
45
30
15
0
*
+
*+
NPR-C+/+
NPR-C-/-
C
AERP (ms)
40
30
20
10
0
*
+
*+
NPR-C+/+
NPR-C-/-
D
AVERP (ms)
80
60
40
20
0
*
*+
NPR-C+/+
NPR-C-/-

Figure 5.4

NPR-C$^{+/+}$ ($P < 0.001$) and NPR-C$^{-/-}$ ($P < 0.001$) mice and this effect was greater ($P < 0.001$) in NPR-C$^{-/-}$ mice. Similarly, P-R interval (Fig. 5.4B) was prolonged in Ang II treated NPR-C$^{+/+}$ ($P < 0.001$) and NPR-C$^{-/-}$ ($P < 0.001$) mice, and was prolonged to a greater extent ($P < 0.001$) in NPR-C$^{-/-}$ mice. P wave duration ($P = 0.010$) and P-R interval ($P = 0.027$) were prolonged in saline treated NPR-C$^{-/-}$ vs. NPR-C$^{+/+}$ mice. Collectively, these data demonstrate that conduction across the atrium and through the AV node is slowed to a greater extent in Ang II treated NPR-C$^{-/-}$ mice compared to NPR-C$^{+/+}$ mice. The effects of Ang II treatment in NPR-C$^{-/-}$ mice was further investigated by measuring AERP and AVERP using intracardiac programmed electrical stimulation in anaesthetized mice. Summary data demonstrates that AERP (Fig. 5.4C) was prolonged in Ang II treated NPR-C$^{+/+}$ ($P < 0.001$) and NPR-C$^{-/-}$ ($P = 0.001$) mice compared to saline controls. Compared to NPR-C$^{+/+}$ mice, AERP was prolonged in both saline ($P = 0.004$) and Ang II ($P = 0.008$) treated NPR-C$^{-/-}$ mice. AVERP (Fig. 5.4D) was prolonged in Ang II treated NPR-C$^{+/+}$ ($P = 0.021$) and NPR-C$^{-/-}$ ($P < 0.001$) mice compared to saline controls. Furthermore, AVERP was prolonged to a greater extent ($P = 0.019$) in Ang II treated NPR-C$^{-/-}$ vs. NPR-C$^{+/+}$ mice. There were no differences ($P = 0.30$) in AVERP between saline treated NPR-C$^{+/+}$ and NPR-C$^{-/-}$ mice. Combined, these data indicate conduction time is prolonged to a greater extent in Ang II treated NPR-C$^{-/-}$ mice and occurs in association with an increase in AERP and AVERP.

5.2. Effects of Ang II treatment on action potential morphology in isolated right and left atrial myocytes from NPR-C$^{+/+}$ and NPR-C$^{-/-}$ mice

The data presented in section 5.1 demonstrates a severe impairment in *in vivo* cardiac electrophysiology in Ang II treated NPR-C$^{-/-}$ mice. Furthermore, the data presented in Chapter 4 demonstrates that Ang II treatment is associated with electrical remodelling in atrial myocytes. Specifically, in right atrial myocytes Ang II treatment resulted in APD prolongation without alterations in V_{max} or AP overshoot compared to saline controls. In contrast, Ang II treatment was associated with reductions in V_{max} and AP overshoot as well as a greater prolongation of the APD at all repolarization times in left atrial myocytes. Accordingly, the next set of experiments sought to characterize

electrical remodelling in right and left atrial myocytes of NPR-$C^{-/-}$ mice following Ang II treatment.

Ang II treatment increased ($P < 0.001$) cell capacitance in right atrial myocytes (Fig. 5.5A) from NPR-$C^{-/-}$ mice, but not NPR-$C^{+/+}$ ($P = 0.58$) mice. In contrast, cell capacitance in left atrial myocytes (Fig. 5.5B) was increased in NPR-$C^{+/+}$ ($P < 0.001$) and NPR-$C^{-/-}$ ($P < 0.001$) mice following Ang II treatment. This increase in cell capacitance was not different ($P = 0.11$) between genotypes in left atrial myocytes. Cell capacitance was also increased ($P < 0.001$) in saline treated left atrial myocytes from NPR-$C^{-/-}$ mice compared to saline treated NPR-$C^{+/+}$ mice.

Representative right atrial APs are presented in Figs. 5.6A and 5.6B for saline and Ang II treated right atrial myocytes from NPR-$C^{+/+}$ and NPR-$C^{-/-}$ mice. Summary data demonstrates that Ang II treatment does not affect RMP ($P = 0.42$; Fig. 5.6C), V_{max} ($P = 0.90$; Fig. 5.6D), or AP overshoot ($P = 0.92$; Fig. 5.6E) in right atrial myocytes from NPR-$C^{-/-}$ mice. APD_{50} ($P < 0.001$; Fig. 5.6F), APD_{70} ($P < 0.001$; Fig. 5.6G), and APD_{90} ($P < 0.001$; Fig. 5.6H) were prolonged in Ang II treated NPR-$C^{-/-}$ right atrial myocytes vs. saline controls. Comparison of the effects of Ang II treatment between genotypes indicates there were no differences in RMP ($P = 0.41$; Fig. 5.6C), V_{max} ($P = 0.41$; Fig. 5.6D), AP overshoot ($P = 0.35$; Fig. 5.6E), APD_{50} ($P = 0.62$; Fig. 5.6F), APD_{70} ($P = 0.45$; Fig. 5.6G), and APD_{90} ($P = 0.22$; Fig. 5.6H) between Ang II treated NPR-$C^{+/+}$ and NPR-$C^{-/-}$ mice. Combined, these findings suggest the extent of electrical remodelling, as assessed by AP morphology, is similar in Ang II treated right atrial myocytes from NPR-$C^{+/+}$ and NPR-$C^{-/-}$ mice.

Representative left atrial APs are presented in Figs. 5.7A and 5.7B. Summary data (Fig. 5.7C) demonstrates that RMP is depolarized in Ang II treated left atrial myocytes from NPR-$C^{-/-}$ compared to saline controls ($P = 0.042$) and Ang II treated NPR-$C^{+/+}$ mice ($P = 0.008$). Both V_{max} ($P < 0.001$; Fig. 5.7D) and AP overshoot ($P = 0.001$; Fig. 5.7E) were reduced in Ang II treated left atrial myocytes vs. saline controls in NPR-$C^{-/-}$ mice. Comparison between genotypes indicates a greater reduction in V_{max} ($P = 0.018$) but not AP overshoot ($P = 0.08$) in Ang II treated NPR-$C^{-/-}$ vs. NPR-$C^{+/+}$ mice. There were no differences in RMP ($P = 0.38$), V_{max} ($P = 0.23$), and AP overshoot ($P = 0.07$) in saline treated NPR-$C^{+/+}$ vs. NPR-$C^{-/-}$ mice.

Figure 5.5. Effects of Ang II treatment on cell capacitance in right and left atrial myocytes from NPR-C$^{+/+}$ and NPR-C$^{-/-}$ mice.

A. Summary data illustrating the effects of Ang II treatment on cell capacitance in right atrial myocytes from NPR-C$^{+/+}$ and NPR-C$^{-/-}$ mice. **B.** Summary data illustrating the effects of Ang II treatment on cell capacitance in left atrial myocytes from NPR-C$^{+/+}$ and NPR-C$^{-/-}$ mice. *P<0.05 vs. saline within genotype. ^{+}P<0.05 vs. NPR-C $^{+/+}$ within treatment group. Data analyzed by two-way ANOVA with Tukey's post hoc test. Right atrium: n = 41 saline and 39 Ang II treated myocytes from NPR-C$^{+/+}$ mice; n = 35 saline and 43 Ang II treated myocytes from NPR-C$^{-/-}$ mice; Left atrium: n = 25 saline and 30 Ang II treated myocytes from NPR-C$^{+/+}$ mice; n = 32 saline and 28 Ang II treated myocytes from NPR-C$^{-/-}$ mice.

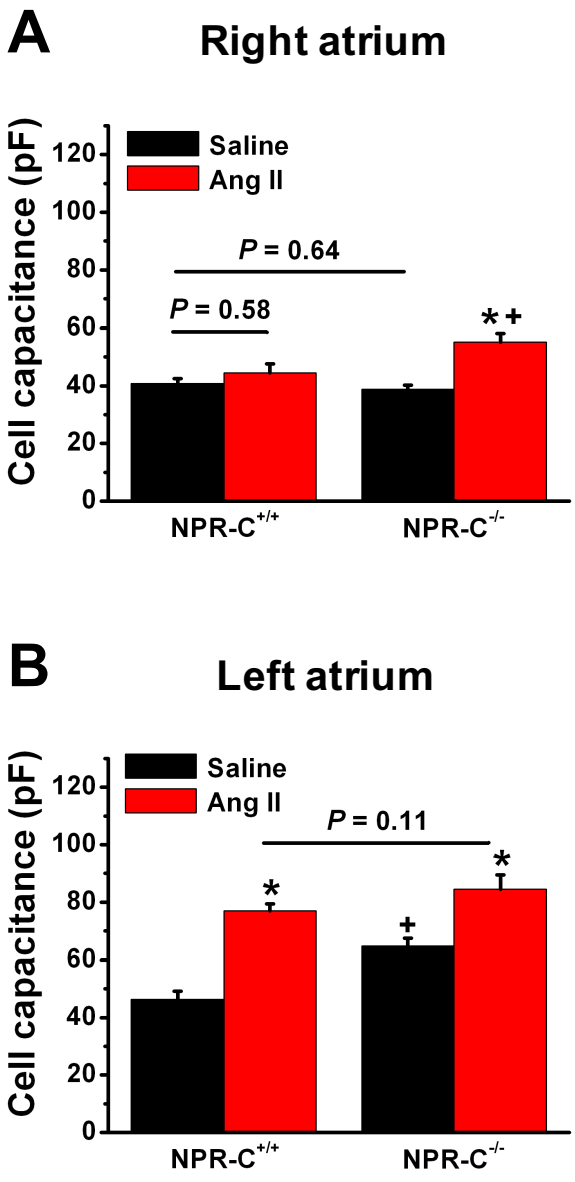
A
Right atrium
Cell capacitance (pF)
Saline
Ang II
P = 0.64
P = 0.58
* +
NPR-C+/+
NPR-C-/-
B
Left atrium
Cell capacitance (pF)
Saline
Ang II
P = 0.11
*
*
+
NPR-C+/+
NPR-C-/-

Figure 5.5

Figure 5.6. Effects of Ang II treatment on action potential morphology in right atrial myocytes from NPR-C$^{+/+}$ and NPR-C$^{-/-}$ mice.

A. and **B.** Representative right atrial APs from saline or Ang II treated NPR-C$^{+/+}$ (A) and NPR-C$^{-/-}$ (B) mice. Dashed lines are at 0 mV. **C – H**. Summary data illustrating the effects of Ang II treatment on RMP (C), V_{max} (D), AP overshoot (E), APD_{50} (F), APD_{70} (G), and APD_{90} (H) in NPR-C$^{+/+}$ and NPR-C$^{-/-}$ mice. *P<0.05 vs. saline within genotype. Data analyzed by two-way ANOVA with Tukey's post hoc test. NPR-C$^{+/+}$: n = 19 saline and 15 Ang II treated myocytes; NPR-C$^{-/-}$: n = 23 saline and 27 Ang II treated myocytes.

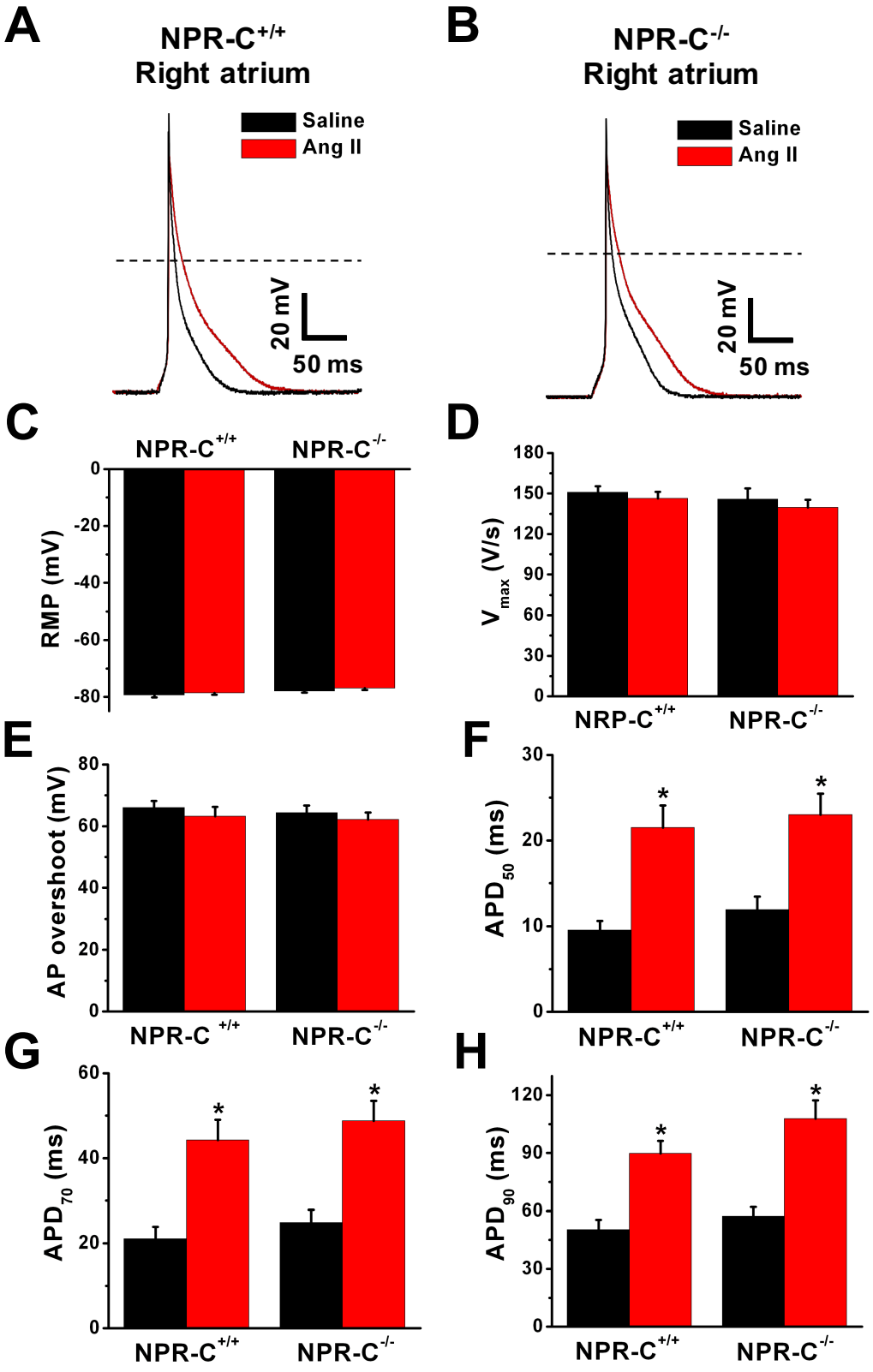
A
NPR-C+/+
Right atrium
Saline
Ang II
20 mV
50 ms
B
NPR-C-/-
Right atrium
Saline
Ang II
20 mV
50 ms
C
NPR-C+/+
NPR-C-/-
RMP (mV)
0
-20
-40
-60
-80
D
Vmax (V/s)
180
150
120
90
60
30
0
NRP-C+/+
NPR-C-/-
E
AP overshoot (mV)
80
60
40
20
0
NPR-C +/+
NPR-C-/-
F
APD50 (ms)
30
20
10
0
*
*
NPR-C+/+
NPR-C-/-
G
APD70 (ms)
60
40
20
0
*
*
NPR-C+/+
NPR-C-/-
H
APD90 (ms)
120
90
60
30
0
*
*
NPR-C+/+
NPR-C-/-

Figure 5.6

Figure 5.7. Effects of Ang II treatment on action potential morphology in left atrial myocytes from NPR-C$^{+/+}$ and NPR-C$^{-/-}$ mice.

A. and **B.** Representative left atrial APs from saline or Ang II treated NPR-C$^{+/+}$ and NPR-C$^{-/-}$ mice. Dashed lines are at 0 mV. **C – H.** Summary data illustrating the effects of Ang II treatment on RMP (C), V_{max} (D), AP overshoot (E), APD_{50} (F), APD_{70} (G), and APD_{90} (H) in NPR-C$^{+/+}$ and NPR-C$^{-/-}$ mice. *P<0.05 vs. saline within genotype; ^{+}P<0.05 vs. NPR-C$^{+/+}$ mice. Data analyzed by two-way ANOVA with Tukey's post hoc test. NPR-C$^{+/+}$: n = 14 saline and 15 Ang II treated myocytes; NPR-C$^{-/-}$: n = 18 saline and 15 Ang II treated myocytes.

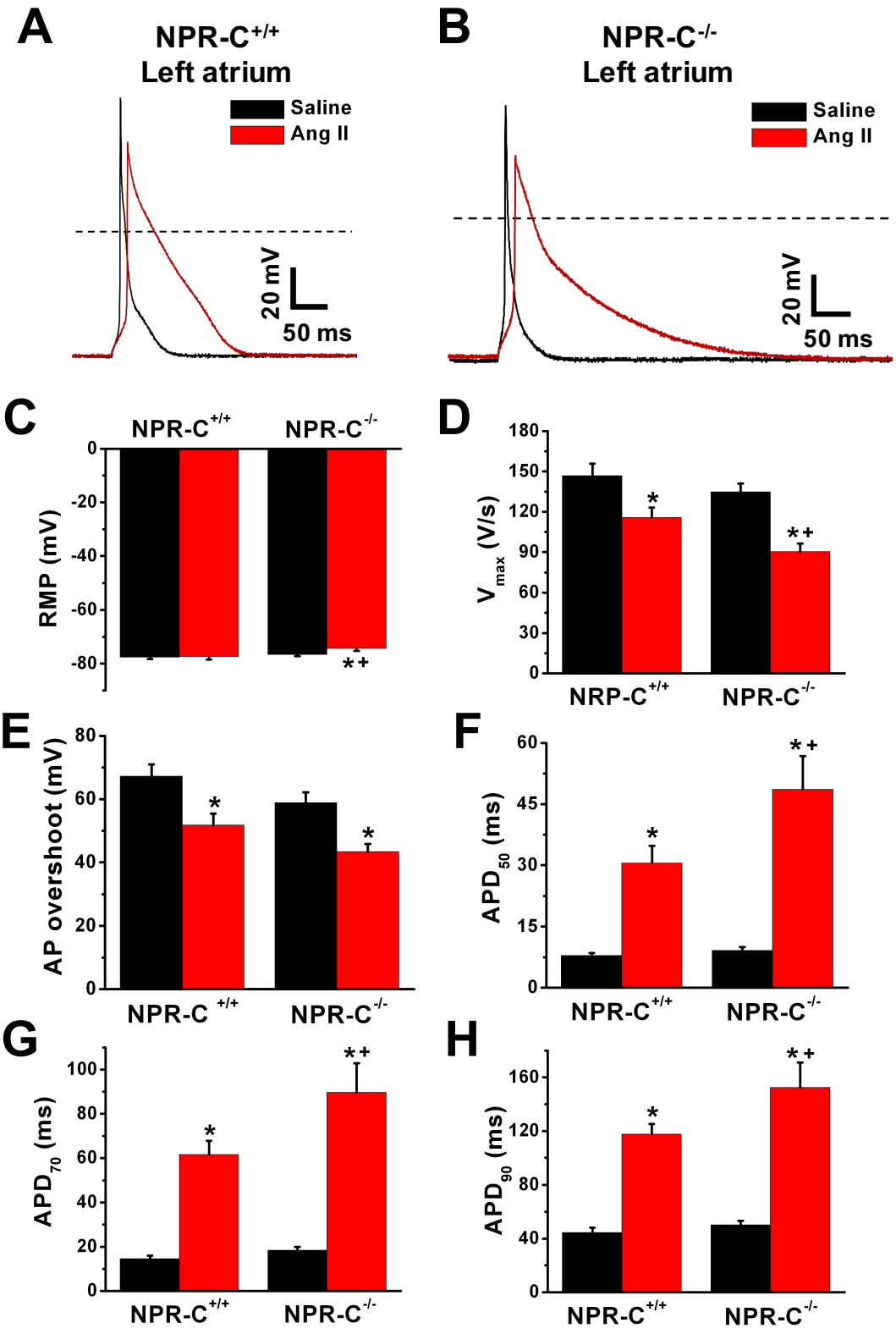
A
NPR-C+/+
Left atrium
Saline
Ang II
20 mV
50 ms
B
NPR-C-/-
Left atrium
Saline
Ang II
20 mV
50 ms
C
NPR-C+/+
NPR-C-/-
RMP (mV)
0
-20
-40
-60
-80
*+
D
Vmax (V/s)
180
150
120
90
60
30
0
*
*+
NRP-C+/+
NPR-C-/-
E
AP overshoot (mV)
80
60
40
20
0
*
*
NPR-C +/+
NPR-C-/-
F
APD50 (ms)
60
45
30
15
0
*
*+
NPR-C+/+
NPR-C-/-
G
APD70 (ms)
100
80
60
40
20
0
*
*+
NPR-C+/+
NPR-C-/-
H
APD90 (ms)
160
120
80
40
0
*
*+
NPR-C+/+
NPR-C-/-

Figure 5.7

Next, the effects of Ang II treatment on AP repolarization was assessed in left atrial myocytes from NPR-$C^{-/-}$ mice. APD_{50} ($P < 0.001$; Fig. 5.7F), APD_{70} ($P < 0.001$; Fig. 5.7G), and APD_{90} ($P < 0.001$; Fig. 5.7H) were prolonged in Ang II treated NPR-$C^{-/-}$ mice compared to saline controls. Strikingly, NPR-$C^{-/-}$ mice exhibited a greater prolongation of APD_{50} ($P = 0.007$; Fig. 5.7F), APD_{70} ($P = 0.008$; Fig. 5.7G), and APD_{90} ($P = 0.019$; Fig. 5.7H) compared to Ang II treated left atrial myocytes from NPR-$C^{+/+}$ mice. There were no differences ($P > 0.05$) in APD_{50}, APD_{70}, and APD_{90} in saline treated NPR-$C^{+/+}$ vs. NPR-$C^{-/-}$ mice. These data demonstrate that electrical remodelling, as assessed by AP morphology, is exacerbated in Ang II treated left atrial myocytes from NPR-$C^{-/-}$ mice.

5.3. Effects of Ang II treatment on potassium currents in right and left atrial myocytes from NPR-$C^{+/+}$ and NPR-$C^{-/-}$ mice

The data presented in section 4.4 demonstrates a reduction in K^+ currents in Ang II treated myocytes from wildtype mice. The AP data described above demonstrates APD prolongation at all repolarization times in Ang II treated right and left atrial myocytes from NPR-$C^{-/-}$ mice. Furthermore, Ang II treated left atrial myocytes from NPR-$C^{-/-}$ mice demonstrated a greater increase in APD prolongation compared to Ang II treated myocytes from NPR-$C^{+/+}$ mice. Accordingly, the goal of this section was to characterize the effects of Ang II treatment on K^+ currents in right and left atrial myocytes from NPR-$C^{+/+}$ and NPR-$C^{-/-}$ mice.

Representative recordings showing a family of total K^+ currents (measured from a holding potential of -80 mV and with no pre-pulse) in right atrial myocytes treated with saline or Ang II are presented in Figs. 5.8A and 5.8B for NPR-$C^{+/+}$ mice and Figs. 5.8C and 5.8D for NPR-$C^{-/-}$ mice. Summary K^+ I-V relationships (Fig. 5.8E) illustrate a reduction ($P < 0.05$) in outward K^+ currents at membrane potentials positive to -10 mV in Ang II treated right atrial myocytes from NPR-$C^{+/+}$ mice. Similarly, outward K^+ currents were reduced ($P < 0.05$) in Ang II treated myocytes from NPR-$C^{-/-}$ mice at membrane potentials positive to -10 mV as summarized in Fig. 5.8F. Inward K^+ currents were

Figure 5.8. Effects of Ang II treatment on potassium currents in right atrial myocytes from NPR-C$^{+/+}$ and NPR-C$^{-/-}$ mice.

A. and **B.** Representative recordings showing a family of total K^+ currents (no pre-pulse) recorded from saline (A) and Ang II (B) treated right atrial myocytes isolated from NPR-C$^{+/+}$ mice. **C.** and **D.** Representative recordings showing a family of total K^+ currents recorded from saline (C) and Ang II (D) treated right atrial myocytes isolated from NPR-C$^{-/-}$ mice. **E.** and **F.** Summary K^+ I-V relationships illustrating the effects of Ang II treatment on K^+ currents (no pre-pulse) in NPR-C$^{+/+}$ (E) and NPR-C$^{-/-}$ (F) mice. Currents were measured at the peak current at each membrane potential. *****P<0.05 vs. saline at each membrane potential. Data analyzed by two-way repeated measures ANOVA with Tukey's post hoc test. NPR-C$^{+/+}$: n = 29 saline and 28 Ang II treated right atrial myocytes; NPR-C$^{-/-}$: n = 16 saline and 23 Ang II treated right atrial myocytes.

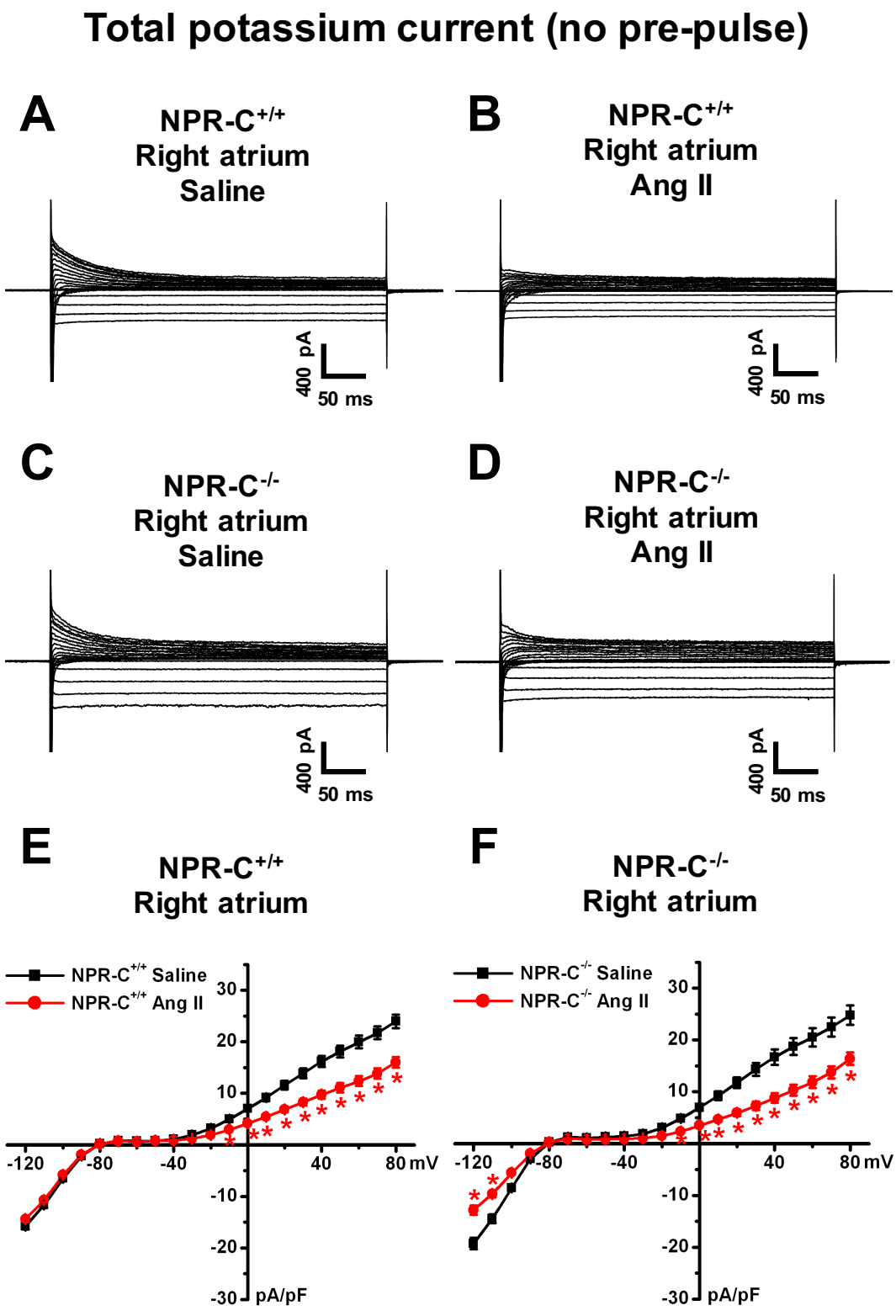
Total potassium current (no pre-pulse)
A
NPR-C+/+
Right atrium
Saline
400 pA
50 ms
B
NPR-C+/+
Right atrium
Ang II
400 pA
50 ms
C
NPR-C-/-
Right atrium
Saline
400 pA
50 ms
D
NPR-C-/-
Right atrium
Ang II
400 pA
50 ms
E
NPR-C+/+
Right atrium
NPR-C+/+ Saline
NPR-C+/+ Ang II
30
20
10
-10
-20
-30
-120
-80
-40
40
80 mV
pA/pF
F
NPR-C-/-
Right atrium
NPR-C-/- Saline
NPR-C-/- Ang II
30
20
10
-10
-20
-30
-120
-80
-40
40
80 mV
pA/pF

Figure 5.8

reduced ($P < 0.05$) in Ang II treated right atrial myocytes at -110 and -120 mV in NPR-C$^{-/-}$ mice. Representative patch-clamp recordings showing a family of total K^+ currents (no pre-pulse) in left atrial myocytes from saline or Ang II treated NPR-C$^{+/+}$ and NPR-C$^{-/-}$ mice are shown in Figs. 5.9A-D. Summary K^+ I-V relationships (Fig. 5.9E) demonstrates a reduction ($P < 0.05$) in K^+ currents at membrane potentials negative to -100 mV and positive to -20 mV in left atrial myocytes from NPR-C$^{+/+}$ mice. In NPR-C$^{-/-}$ mice (Fig. 5.9F), total K^+ current densities were reduced ($P < 0.05$) at membrane potentials negative to -110 mV and positive to -10 mV in Ang II treated left atrial myocytes compared to saline controls.

Comparison of I_K density measured at +50 mV between genotypes is summarized in Fig. 5.10. In right atrial myocytes (Fig. 5.10A), there were no differences in I_K density between in saline ($P = 0.70$) and Ang II ($P = 0.65$) treated NPR-C$^{+/+}$ vs. NPR-C$^{-/-}$ mice. Similarly, in left atrial myocytes (Fig. 5.10B), there were no differences in I_K measured at +50 mV between saline ($P = 0.43$) and Ang II ($P = 0.14$) treated NPR-C$^{+/+}$ vs. NPR-C$^{-/-}$ mice. These data demonstrate Ang II treatment reduces total I_K (no pre-pulse) in a similar fashion in right and left atrial myocytes from NPR-C$^{+/+}$ and NPR-C$^{-/-}$ mice.

In the next set of experiments, the effects of Ang II treatment on K^+ currents following an inactivating pre-pulse to -40 mV was assessed in NPR-C$^{+/+}$ and NPR-C$^{-/-}$ mice. Representative patch-clamp recordings for saline and Ang II treated right atrial myocytes are presented in Figs. 5.11A and 5.11B for NPR-C$^{+/+}$ mice and in Figs. 5.11C and 5.11D for NPR-C$^{-/-}$ mice. Summary K^+ I-V relationships illustrate a reduction ($P < 0.05$) in outward K^+ currents at membrane potentials positive to 0 mV in NPR-C$^{+/+}$ mice (Fig. 5.11E) and positive to -20 mV in NPR-C$^{-/-}$ mice (Fig. 5.11F). Ang II treated right atrial myocytes from NPR-C$^{-/-}$ mice also exhibited a reduction ($P < 0.05$) in inward K^+ currents at -110 mV and -120 mV (Fig. 5.11F).

Representative recordings showing K^+ currents following a pre-pulse to -40 mV in left atrial myocytes from saline and Ang II treated NPR-C$^{+/+}$ and NPR-C$^{-/-}$ mice are shown in Figs. 5.12A-D. Summary K^+ I-V relationships demonstrate that K^+ currents were reduced following Ang II treatment in both NPR-C$^{+/+}$ (Fig. 5.12E) and NPR-C$^{-/-}$ (Fig. 5.12F) mice compared to saline controls. In particular, K^+ current densities were reduced between -100 mV and -120 mV and at membrane potentials positive to -20 mV

Figure 5.9. Effects of Ang II treatment on potassium currents in left atrial myocytes from NPR-C$^{+/+}$ and NPR-C$^{-/-}$ mice.

A. and **B.** Representative recordings showing a family of total K^+ currents (no pre-pulse) recorded from a saline (A) and Ang II (B) treated left atrial myocyte isolated from a NPR-C$^{+/+}$ mouse. **C.** and **D.** Representative recordings showing a family of total K^+ currents recorded from a saline (C) and Ang II (D) treated left atrial myocyte isolated from a NPR-C$^{-/-}$ mouse. **E.** and **F.** Summary K^+ I-V relationships illustrating the effects of Ang II treatment on K^+ currents (no pre-pulse) in NPR-C$^{+/+}$ (E) and NPR-C$^{-/-}$ (F) mice. Currents were measured at the peak current at each membrane potential. *****P<0.05 vs. saline at each membrane potential. Data analyzed by two-way repeated measures ANOVA with Tukey's post hoc test. NPR-C$^{+/+}$: n = 10 saline and 17 Ang II treated left atrial myocytes; NPR-C$^{-/-}$: n = 17 saline and 13 Ang II treated left atrial myocytes.

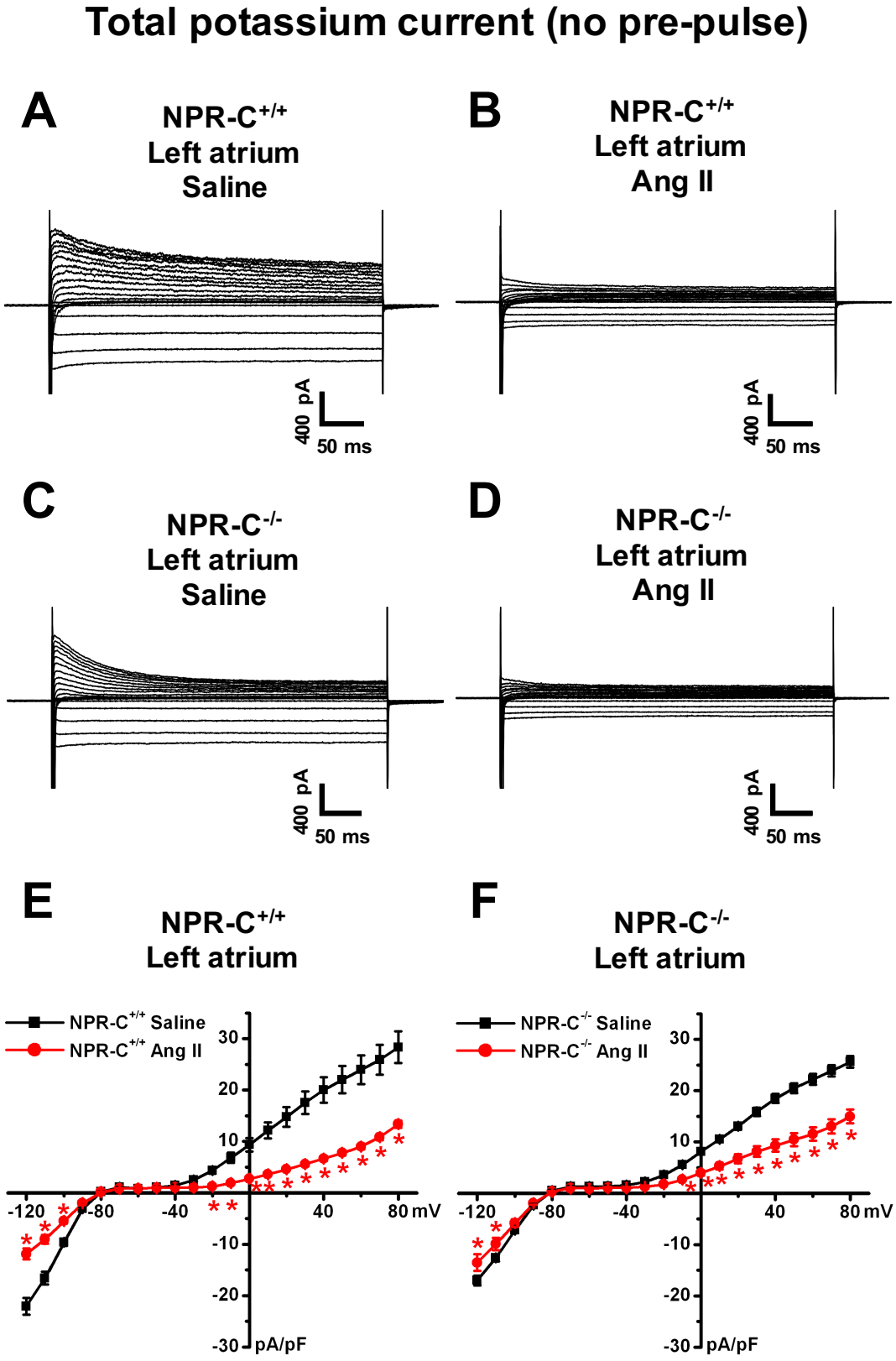
Total potassium current (no pre-pulse)
A
NPR-C+/+
Left atrium
Saline
B
NPR-C+/+
Left atrium
Ang II
400 pA
50 ms
C
NPR-C-/-
Left atrium
Saline
D
NPR-C-/-
Left atrium
Ang II
E
NPR-C+/+
Left atrium
F
NPR-C-/-
Left atrium
NPR-C+/+ Saline
NPR-C+/+ Ang II
NPR-C-/- Saline
NPR-C-/- Ang II
30
20
10
-10
-20
-30
-120
-80
-40
40
80 mV
pA/pF

Figure 5.9

Figure 5.10. Comparison of the effects of Ang II treatment on potassium current densities in right and left atrial myocytes from NPR-C$^{+/+}$ and NPR-C$^{-/-}$ mice.

A. and **B.** Summary data comparing the effects of Ang II treatment on total K^+ currents (no pre-pulse) measured at +50 mV in right (A) and left (B) atrial myocytes from NPR-C$^{+/+}$ and NPR-C$^{-/-}$mice. *P<0.05 vs. saline within genotype; ^+P<0.05 vs. NPR-C$^{+/+}$ mice within treatment. Data analyzed by two-way ANOVA with Tukey's post hoc test. Right atrium: n = 29 saline and 28 Ang II treated myocytes from NPR-C$^{+/+}$ mice, n = 16 saline and 23 Ang II treated myocytes from NPR-C$^{-/-}$ mice; Left atrium: n = 10 saline and 17 Ang II treated myocytes from NPR-C$^{+/+}$ mice, n = 17 saline and 13 Ang II treated myocytes from NPR-C$^{-/-}$ mice.

Total potassium current (no pre-pulse)

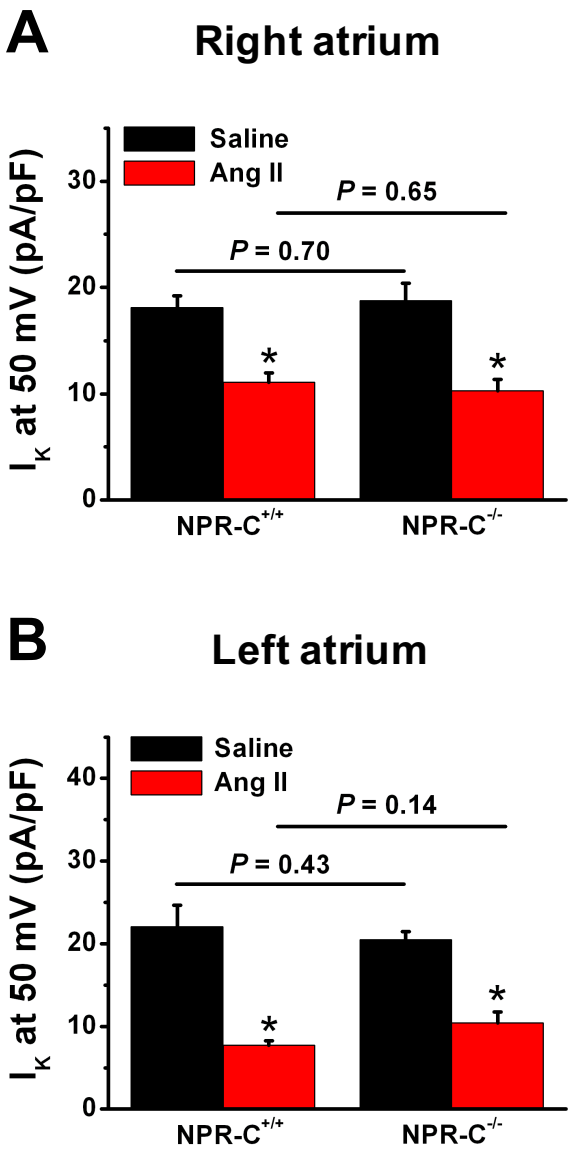

Figure 5.10

Figure 5.11. Effects of Ang II treatment on potassium currents following a pre-pulse to -40 mV in right atrial myocytes from NPR-C$^{+/+}$ and NPR-C$^{-/-}$ mice.

A. and **B.** Representative patch-clamp recordings showing a family of K^+ currents recorded from saline (A) and Ang II (B) treated right atrial myocytes following a pre-pulse to -40 mV to inactivate I_{to} in NPR-C$^{+/+}$ mice. **C.** and **D.** Representative patch-clamp recordings showing a family of K^+ currents recorded from saline (C) and Ang II (D) treated right atrial myocytes following a pre-pulse to -40 mV to inactivate I_{to} in NPR-C$^{-/-}$ mice. **E.** and **F.** Summary K^+ I-V relationships illustrating the effects of Ang II treatment on K^+ currents in NPR-C$^{+/+}$ (E) and NPR-C$^{-/-}$ (F) mice following a pre-pulse to -40 mV. Currents measured at the peak current at each membrane potential. $^{*}P<0.05$ vs. saline at each membrane potential. Data analysed by two-way repeated measures ANOVA with Tukey's post hoc test. NPR-C$^{+/+}$: $n = 29$ saline and 28 Ang II treated right atrial myocytes; NPR-C$^{-/-}$: $n = 16$ saline and 23 Ang II treated right atrial myocytes.

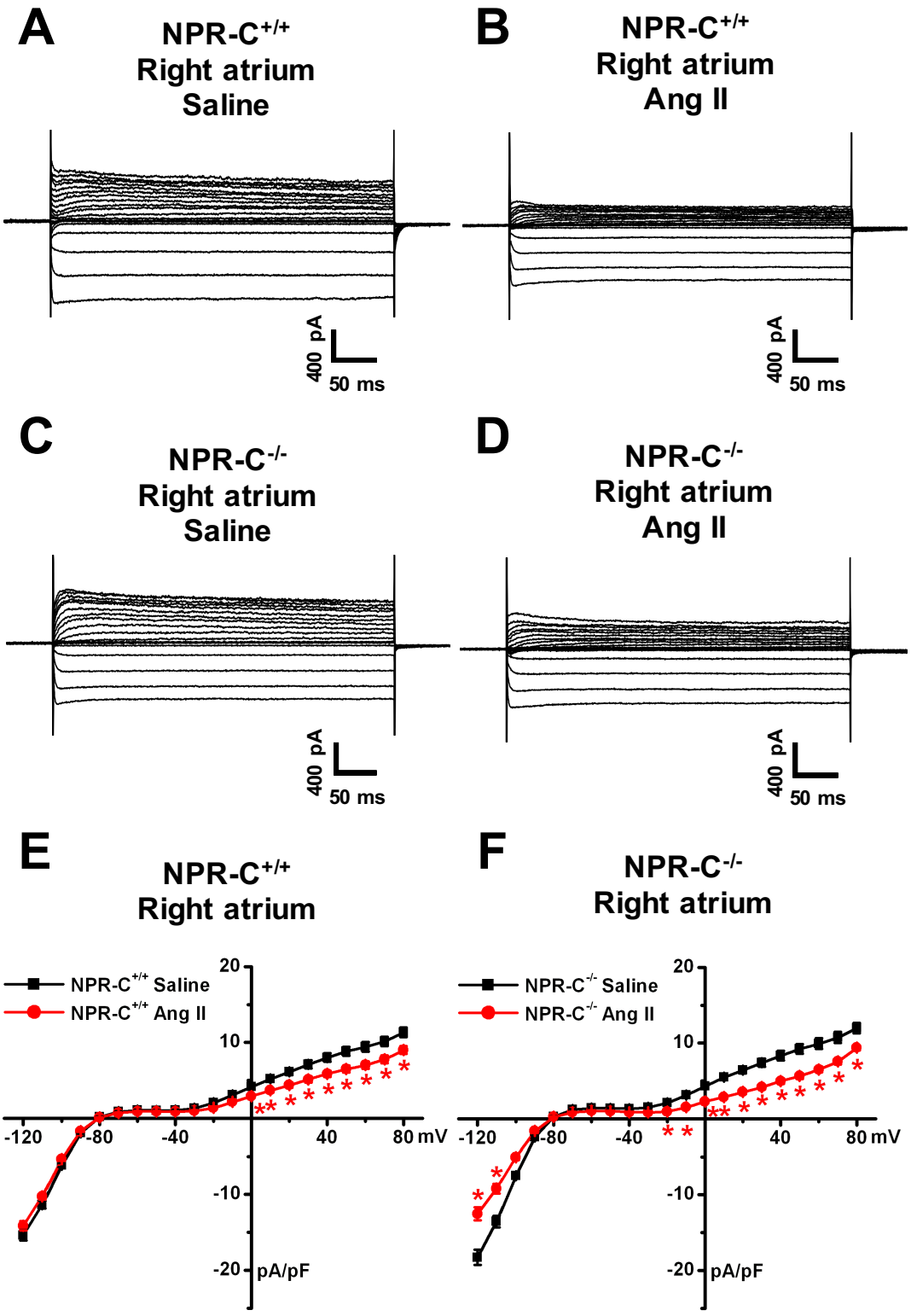
Potassium current with inactivating pre-pulse
A
NPR-C+/+
Right atrium
Saline
B
NPR-C+/+
Right atrium
Ang II
400 pA
50 ms
C
NPR-C-/-
Right atrium
Saline
D
NPR-C-/-
Right atrium
Ang II
E
NPR-C+/+
Right atrium
F
NPR-C-/-
Right atrium
NPR-C+/+ Saline
NPR-C+/+ Ang II
NPR-C-/- Saline
NPR-C-/- Ang II
20
10
-10
-20
-120
-80
-40
40
80 mV
pA/pF

Figure 5.11

Figure 5.12. Effects of Ang II treatment on potassium currents following a pre-pulse to -40 mV in left atrial myocytes from NPR-C$^{+/+}$ and NPR-C$^{-/-}$ mice.

A. and **B.** Representative patch-clamp recordings showing a family of K^+ currents recorded from saline (A) and Ang II (B) treated left atrial myocytes following a pre-pulse to -40 mV to inactivate I_{to} in NPR-C$^{+/+}$ mice. **C.** and **D.** Representative patch-clamp recordings showing a family of K^+ currents recorded from saline (C) and Ang II (D) treated left atrial myocytes following a pre-pulse to -40 mV to inactivate I_{to} in NPR-C$^{-/-}$ mice. **E.** and **F.** Summary K^+ I-V relationships illustrating the effects of Ang II treatment on K^+ currents in NPR-C$^{+/+}$ (E) and NPR-C$^{-/-}$ (F) mice following a pre-pulse to -40 mV. Currents were measured at the peak current at each membrane potential. $^{*}P<0.05$ vs. saline at each membrane potential. Data analysed by two-way repeated measures ANOVA with Tukey's post hoc test. NPR-C$^{+/+}$: n = 10 saline and 17 Ang II treated left atrial myocytes; NPR-C$^{-/-}$: n = 17 saline and 13 Ang II treated left atrial myocytes.

Potassium current with inactivating pre-pulse

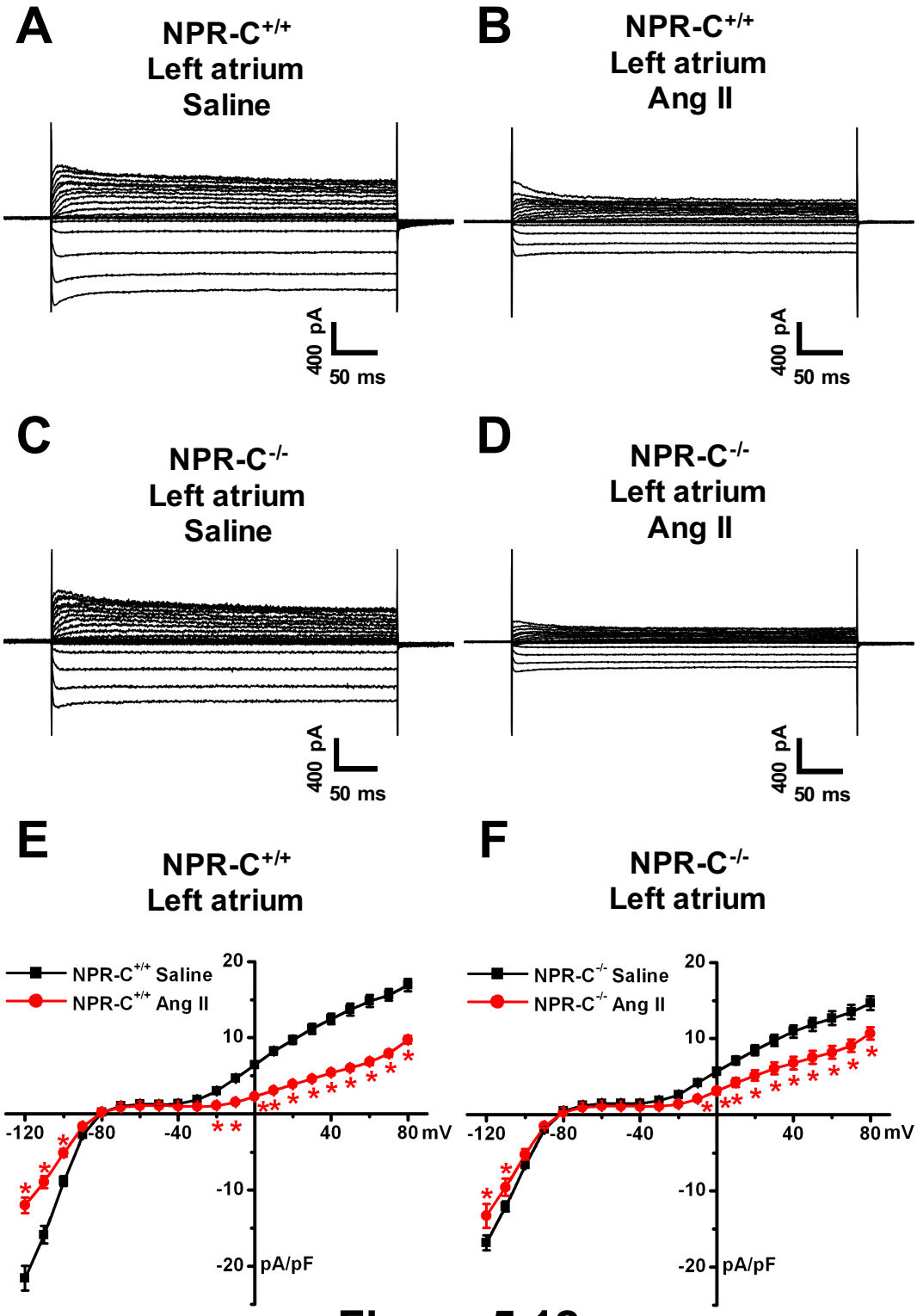

Figure 5.12

in Ang II treated left atrial myocytes from NPR-$C^{+/+}$ mice. In NPR-$C^{-/-}$ mice, this reduction was observed at -110 mV and -120 mV and positive to -10 mV in Ang II treated mice compared to saline controls.

Comparison of I_K density at +50 mV following a pre-pulse to -40 mV between genotypes and treatment groups is summarized in Fig. 5.13. In right atrial myocytes (Fig. 5.13A), Ang II treatment reduced I_K density in both NPR-$C^{+/+}$ ($P < 0.001$) and NPR-$C^{-/-}$ ($P < 0.001$) mice treated with Ang II vs. saline controls. Comparison between genotypes demonstrates there were no differences in I_K density between saline ($P = 0.62$) and Ang II ($P = 0.21$) treated right atrial myocytes from NPR-$C^{+/+}$ vs. NPR-$C^{-/-}$ mice. In left atrial myocytes (Fig. 5.13B), Ang II treatment reduced I_K density in both NPR-$C^{+/+}$ ($P < 0.001$) and NPR-$C^{-/-}$ ($P < 0.001$) mice vs. saline controls. Comparison between the genotypes demonstrate there were no differences in I_K density measured at +50 mV between saline ($P = 0.11$) and Ang II ($P = 0.15$) treated left atrial myocytes from NPR-$C^{+/+}$ and NPR-$C^{-/-}$ mice. Combined, these data demonstrate a similar reduction in I_K (with pre-pulse) following Ang II treatment in NPR-$C^{+/+}$ and NPR-$C^{-/-}$ mice.

Next, the effects of Ang II treatment on I_{to} was assessed. I_{to} was measured as the difference current with and without a pre-pulse to -40 mV in NPR-$C^{+/+}$ and NPR-$C^{-/-}$ mice. Representative patch-clamp recordings for I_{to} measured at +50 mV from right atrial myocytes are presented in Figs. 5.14A-D. In NPR-$C^{+/+}$ mice, summary I-V relationships (Fig. 5.14E) demonstrate a reduction ($P < 0.05$) in I_{to} at membrane potentials positive to +10 mV in Ang II treated right atrial myocytes. In NPR-$C^{-/-}$ mice, I_{to} was reduced ($P < 0.05$) at membrane potentials positive to +20 mV (Fig. 5.14F) in Ang II treated right atrial myocytes vs. saline controls. Representative I_{to} recordings measured at +50 mV in saline and Ang II treated left atrial myocytes from NPR-$C^{+/+}$ and NPR-$C^{-/-}$ mice are presented in Figs. 5.15A-D. Summary I-V relationships demonstrate a reduction ($P < 0.05$) in I_{to} at membrane potentials positive to 0 mV in Ang II treated left atrial myocytes from NPR-$C^{+/+}$ mice (Fig. 5.15E). In NPR-$C^{-/-}$ mice, I_{to} density was also reduced ($P < 0.05$) at membrane potentials positive to 0 mV in Ang II vs. saline treated myocytes, as summarized in Fig. 5.15F.

A comparison of I_{to} measured at +50 mV between saline and Ang II treated NPR-$C^{+/+}$ and NPR-$C^{-/-}$ mice is presented in Fig. 5.16. In saline treated mice, there were no

Figure 5.13. Comparison of the effects of Ang II treatment on potassium current density following a pre-pulse to -40 mV in right and left atrial myocytes from NPR-$C^{+/+}$ and NPR-$C^{-/-}$ mice.

A. and **B.** Summary data comparing the effects of Ang II treatment on K^+ currents following a pre-pulse to -40 mV in right (A) and left (B) atrial myocytes from NPR-$C^{+/+}$ and NPR-$C^{-/-}$ mice. I_K was measured at +50 mV. **P*<0.05 vs. saline within genotype; $^+$*P*<0.05 vs. NPR-$C^{+/+}$ mice within treatment. Data analyzed by two-way ANOVA with Tukey's post hoc test. Right atrium: *n* = 29 saline and 28 Ang II treated myocytes from NPR-$C^{+/+}$ mice, *n* = 16 saline and 23 Ang II treated myocytes from NPR-$C^{-/-}$ mice; Left atrium: *n* = 10 saline and 17 Ang II treated myocytes from NPR-$C^{+/+}$ mice, *n* = 17 saline and 13 Ang II treated myocytes from NPR-$C^{-/-}$ mice.

Potassium current with inactivating pre-pulse

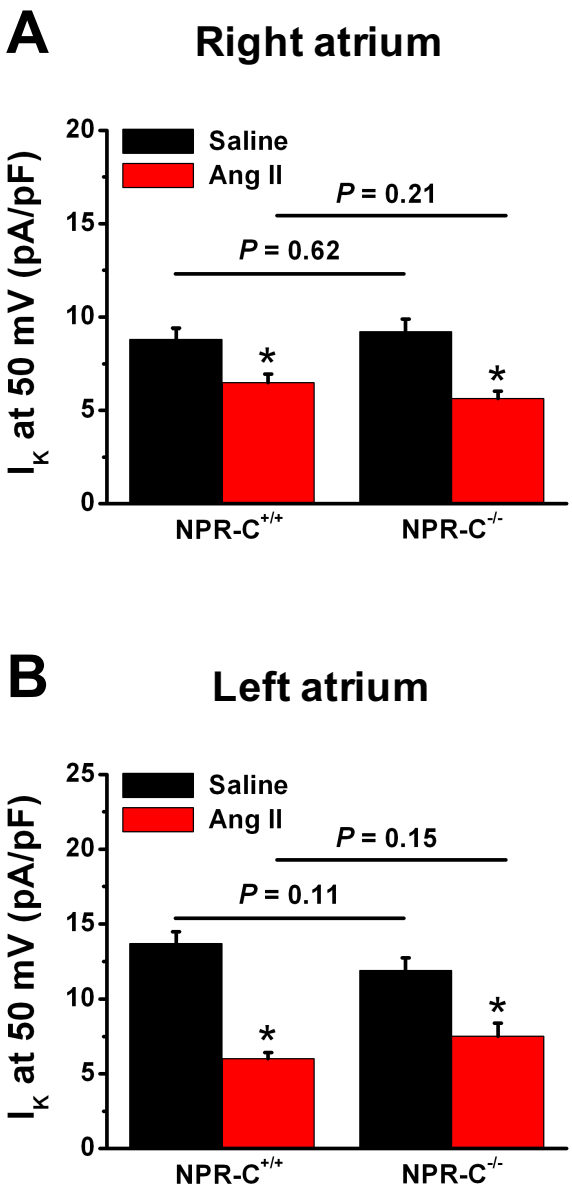

Figure 5.13

Figure 5.14. Effects of Ang II treatment on transient outward potassium current (I_{to}) in right atrial myocytes from NPR-$C^{+/+}$ and NPR-$C^{-/-}$ mice.

A. and **B.** Representative patch-clamp recordings showing I_{to} from saline (A) and Ang II (B) treated right atrial myocytes from NPR-$C^{+/+}$ mice. Representative recordings are at +50 mV as measured from the difference current with and without a pre-pulse to -40 mV. **C.** and **D.** Representative patch-clamp recordings showing I_{to} from saline (C) and Ang II (D) treated right atrial myocytes from NPR-$C^{-/-}$ mice. **E.** and **F.** Summary I-V relationships illustrating the effects of Ang II treatment on I_{to} in right atrial myocytes from NPR-$C^{+/+}$ (E) and NPR-$C^{-/-}$ (F) mice. $^{*}P<0.05$ vs. saline at each membrane potential. Data analyzed by two-way repeated measures ANOVA with Tukey's post hoc test. NPR-$C^{+/+}$: $n = 29$ saline and 28 Ang II treated right atrial myocytes; NPR-$C^{-/-}$: $n = 16$ saline and 23 Ang II treated right atrial myocytes.

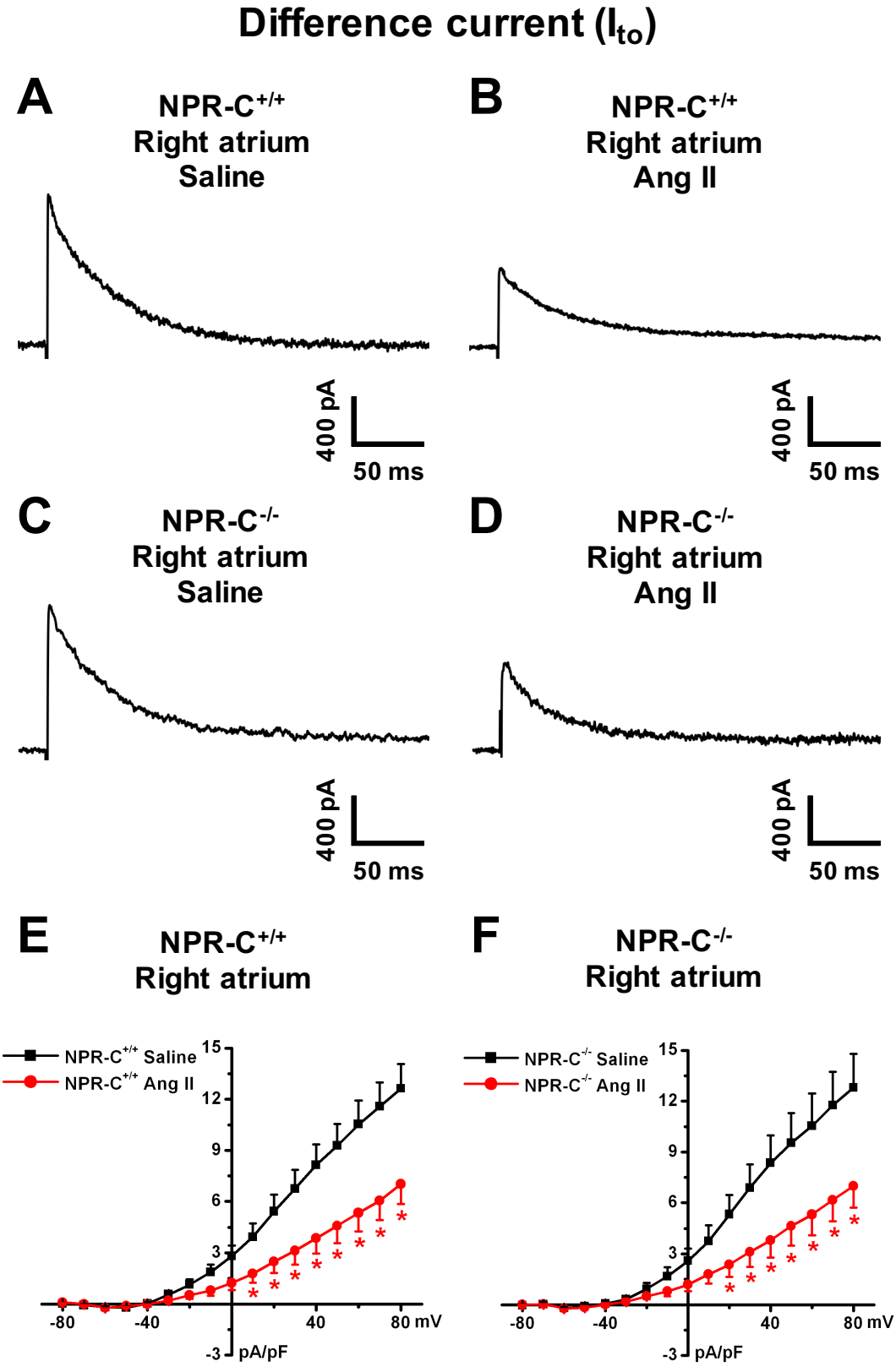
Difference current (I_{to})
A
NPR-C+/+
Right atrium
Saline
B
NPR-C+/+
Right atrium
Ang II
400 pA
50 ms
C
NPR-C-/-
Right atrium
Saline
D
NPR-C-/-
Right atrium
Ang II
E
NPR-C+/+
Right atrium
F
NPR-C-/-
Right atrium
NPR-C+/+ Saline
NPR-C+/+ Ang II
NPR-C-/- Saline
NPR-C-/- Ang II
15
12
9
6
3
-3
-80
-40
40
80 mV
pA/pF

Figure 5.14

Figure 5.15. Effects of Ang II treatment on transient outward potassium current (I_{to}) in left atrial myocytes from NPR-$C^{+/+}$ and NPR-$C^{-/-}$ mice.

A. and **B.** Representative patch-clamp recordings showing I_{to} from saline (A) and Ang II (B) treated left atrial myocytes from NPR-$C^{+/+}$ mice. Representative recordings are at +50 mV as measured from the difference current with and without a pre-pulse to -40 mV. **C.** and **D.** Representative patch-clamp recordings showing I_{to} from saline (C) and Ang II (D) treated left atrial myocytes from NPR-$C^{-/-}$ mice. **E.** and **F.** Summary I-V relationships illustrating the effects of Ang II treatment on I_{to} in left atrial from NPR-$C^{+/+}$ (E) and NPR-$C^{-/-}$ (F) mice. $^{*}P<0.05$ vs. saline at each membrane potential. Data analyzed by two-way repeated measures ANOVA with Tukey's post hoc test. NPR-$C^{+/+}$: n = 10 saline and 17 Ang II treated left atrial myocytes; NPR-$C^{-/-}$: n = 17 saline and 13 Ang II treated left atrial myocytes.

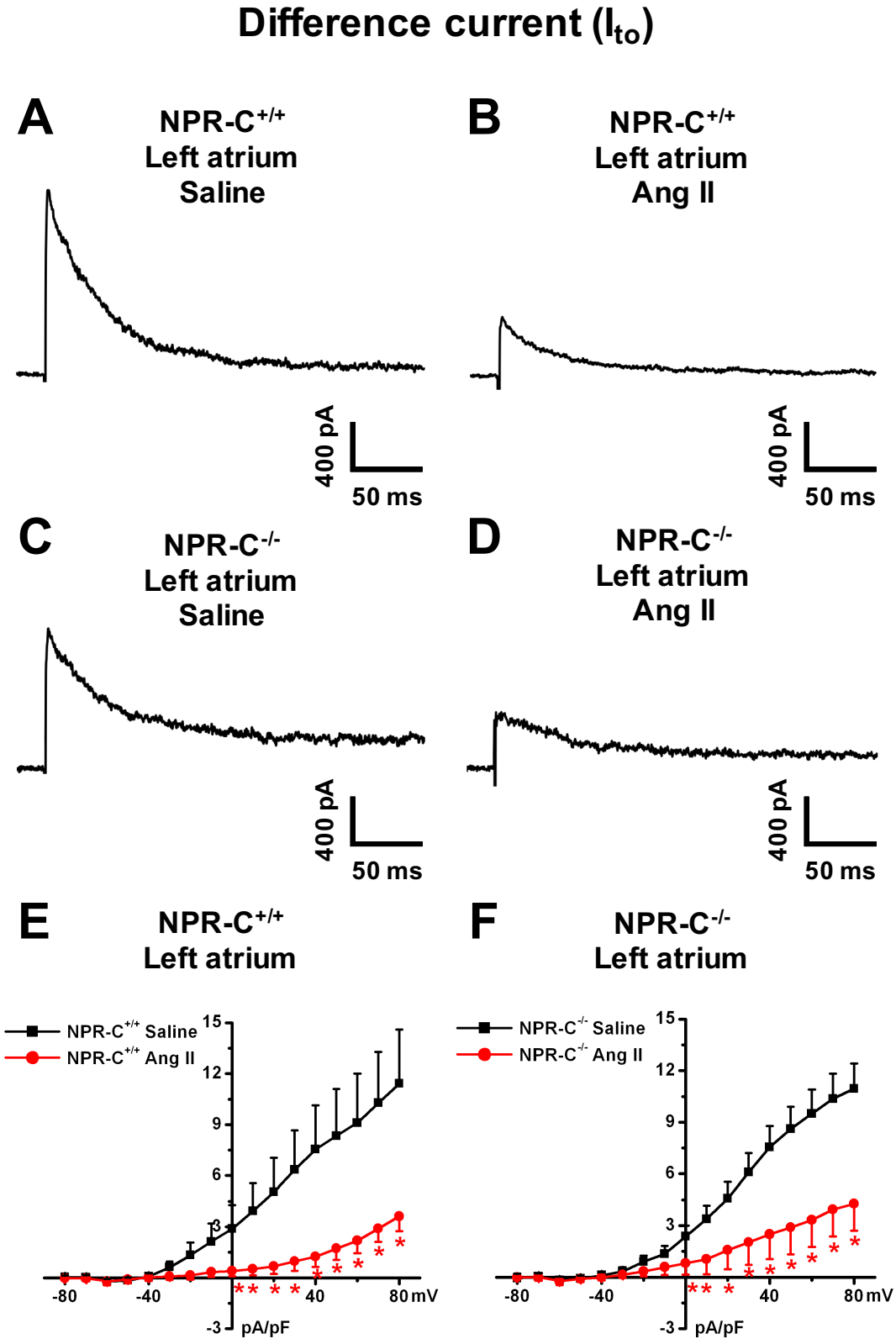
Difference current (I_{to})
A
NPR-C+/+
Left atrium
Saline
400 pA
50 ms
B
NPR-C+/+
Left atrium
Ang II
400 pA
50 ms
C
NPR-C-/-
Left atrium
Saline
400 pA
50 ms
D
NPR-C-/-
Left atrium
Ang II
400 pA
50 ms
E
NPR-C+/+
Left atrium
NPR-C+/+ Saline
NPR-C+/+ Ang II
15
12
9
6
3
-3
-80
-40
40
80 mV
pA/pF
F
NPR-C-/-
Left atrium
NPR-C-/- Saline
NPR-C-/- Ang II
15
12
9
6
3
-3
-80
-40
40
80 mV
pA/pF

Figure 5.15

Figure 5.16. Comparison of the effects of Ang II treatment on I_{to} in right and left atrial myocytes from NPR-$C^{+/+}$ and NPR-$C^{-/-}$ mice.

A. and **B.** Summary data comparing the reduction in I_{to} following Ang II treatment in right (A) and left (B) atrial myocytes from NPR-$C^{+/+}$ and NPR-$C^{-/-}$ mice. **P*<0.05 vs. saline within genotype; ^{+}P<0.05 vs. NPR-$C^{+/+}$ mice within treatment. Data analyzed by two-way ANOVA with Tukey's post hoc test. Right atrium: *n* = 29 saline and 28 Ang II treated myocytes from NPR-$C^{+/+}$ mice, *n* = 16 saline and 23 Ang II treated myocytes from NPR-$C^{-/-}$ mice; Left atrium: *n* = 10 saline and 17 Ang II treated myocytes from NPR-$C^{+/+}$ mice, *n* = 17 saline and 13 Ang II treated myocytes from NPR-$C^{-/-}$ mice.

Difference current (I_{to})

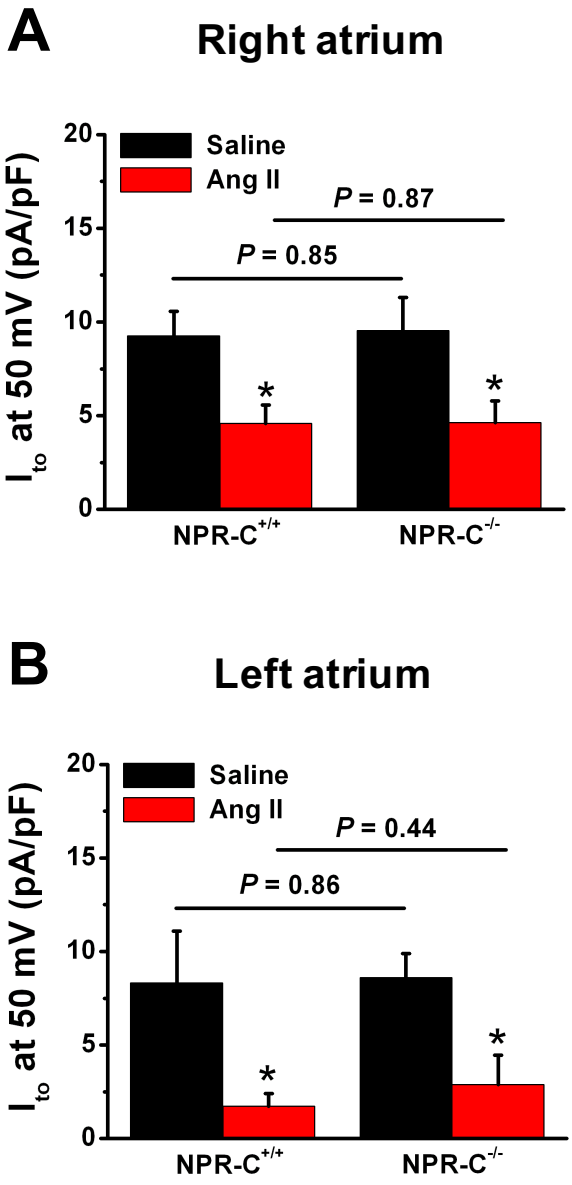

Figure 5.16

differences in I_{to} density measured at +50 mV between right ($P = 0.85$; Fig. 5.16A) and left ($P = 0.86$; Fig. 5.16B) atrial myocytes from NPR-$C^{+/+}$ and NPR-$C^{-/-}$ mice. There were no differences in I_{to} density in Ang II treated right ($P = 0.87$) and left ($P = 0.44$) atrial myocytes between genotypes. These data demonstrate Ang II treatment reduces I_{to} to a similar extent in right and left atrial myocytes in NPR-$C^{+/+}$ and NPR-$C^{-/-}$ mice.

5.4. Effects of the NPR-C agonist cANF on cardiac electrophysiology in anaesthetized wildtype mice treated with Ang II

The aforementioned data demonstrate that Ang II treatment in NPR-$C^{-/-}$ mice results in more severe impairment of cardiac function *in vivo* relative to wildtype mice and suggests that NPR-C may be a therapeutic target. cANF is a selective NPR-C agonist (Anand-Srivastava *et al.*, 1990) and can be used to characterize the role of chronic NPR-C activation in disease progression elicited by Ang II treatment. Accordingly, the goal of the next series of experiments was to determine the effects of the NPR-C agonist cANF on cardiac electrophysiology *in vivo* in Ang II treated wildtype mice. Mice receiving cANF were co-treated with Ang II for the entire 3 week treatment period. Two doses were used for this study, a lower dose of 0.05 mg/kg/min and a higher dose of 0.1 mg/kg/min.

Summary data demonstrating the effects of cANF treatment on systolic blood pressure in Ang II treated mice is shown in Appendix E. Systolic blood pressure was increased in Ang II ($P < 0.001$), Ang II with cANF (0.05 mg/kg/min; $P < 0.001$), and Ang II with cANF (0.1 mg/kg/min; $P < 0.001$) treated mice compared to baseline measurements. There were no differences ($P > 0.05$) in blood pressure between Ang II, Ang II with cANF (0.05 mg/kg/min), and Ang II with cANF (0.1 mg/kg/min) treated mice at the end of the treatment period. Therefore, co-treatment with cANF does not alter blood pressure in Ang II treated mice.

Representative ECG recordings are presented for saline, Ang II, Ang II with cANF (0.05 mg/kg/min), and Ang II with cANF (0.1 mg/kg/min) treated anaesthetized wildtype mice in Figs. 5.17A-D. Summary data (Fig. 5.17E) demonstrates a reduction in heart rate in Ang II ($P = 0.034$) and Ang II with cANF (0.05 mg/kg/min; $P = 0.007$)

Figure 5.17. Effects of the NPR-C agonist cANF on heart rate in anaesthetized wildtype mice treated with Ang II.

A – D. Representative ECG recordings in anaesthetized wildtype mice treated with saline (A), Ang II (B), Ang II with cANF (0.05 mg/kg/min; C), and Ang II with cANF (0.1 mg/kg/min; D). Mice receiving cANF were co-treated with Ang II for three weeks. **E.** Summary data illustrating the effects of cANF on heart rate in Ang II treated mice. There were no differences in heart rate between saline vs. Ang II with cANF (0.1 mg/kg/min; $P = 1.00$) and Ang II vs. Ang II with cANF (0.05 mg/kg/min $P = 0.80$) treated mice. $^{*}P<0.05$ vs. saline; $^{+}P<0.05$ vs. Ang II. Data analyzed by one-way ANOVA with Tukey's post hoc test. $n = 23$ saline, 33 Ang II, 20 Ang II with cANF (0.05 mg/kg/min), 22 Ang II with cANF (0.1 mg/kg/min) treated mice.

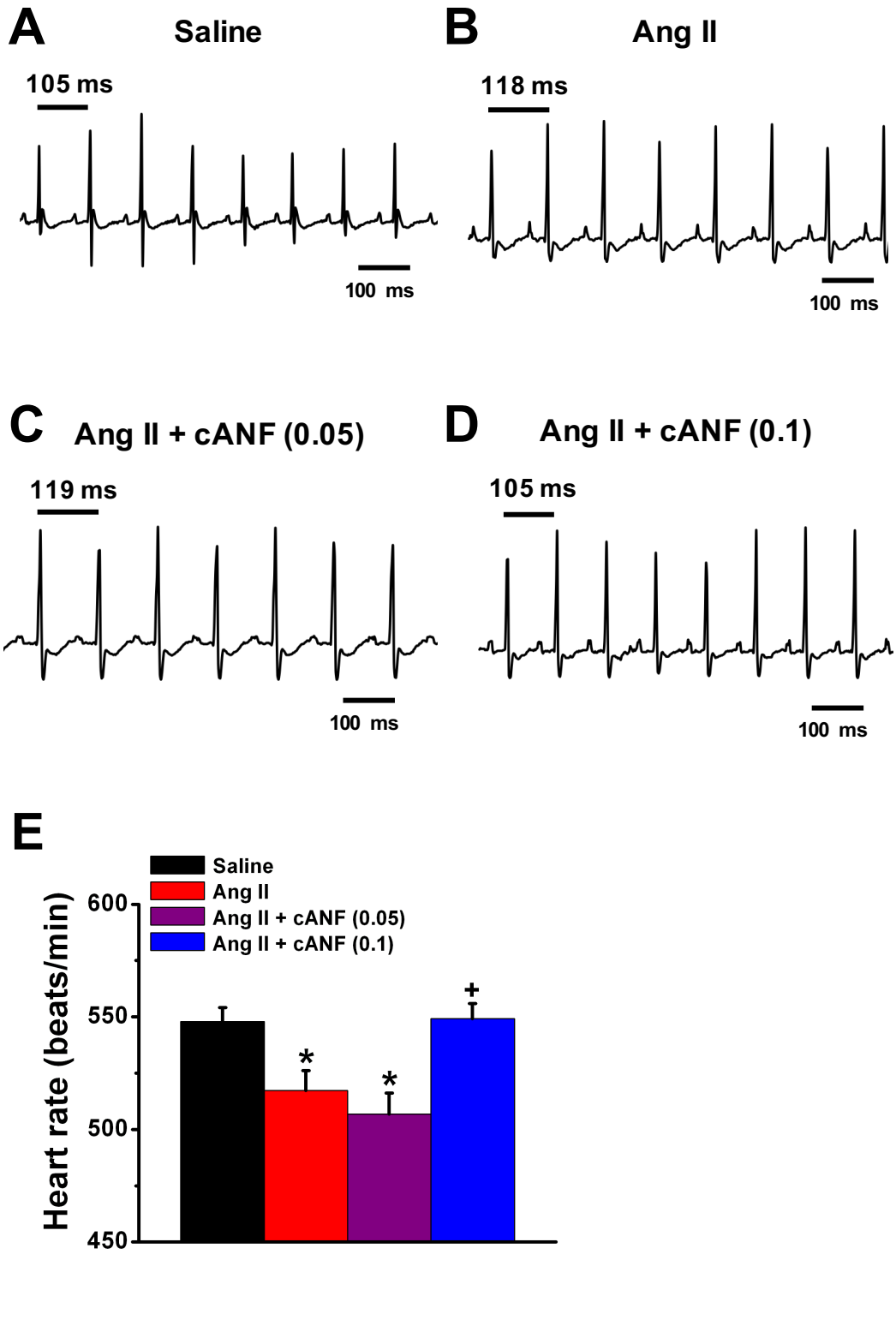
A
Saline
105 ms
100 ms
B
Ang II
118 ms
100 ms
C
Ang II + cANF (0.05)
119 ms
100 ms
D
Ang II + cANF (0.1)
105 ms
100 ms
E
Saline
Ang II
Ang II + cANF (0.05)
Ang II + cANF (0.1)
Heart rate (beats/min)
600
550
500
450
*
*
+

Figure 5.17

treated mice compared to saline controls. There were no differences ($P = 0.80$) in heart rate between Ang II with cANF (0.05 mg/kg/min) and Ang II treated mice. Heart rate was increased in Ang II with cANF (0.1 mg/kg/min; $P = 0.027$) compared to Ang II treated mice and was not different ($P = 1.00$) compared to saline treated mice. In addition, heart rate was increased ($P = 0.006$) in Ang II with cANF (0.1 mg/kg/min) compared to Ang II with cANF (0.05 mg/kg/min) treated mice, highlighting the importance cANF dosage in eliciting an effect in these experiments. Combined, these data demonstrate that co-treatment with cANF at a higher dose (0.1 mg/kg/min) can attenuate the reduction in heart rate elicited by Ang II treatment whereas co-treatment with a lower dose of cANF (0.05 mg/kg/min) does not. Summary data for ECG intervals and intracardiac ECG parameters measured in this study is located in Appendix F.

To determine if cANF could attenuate impaired SAN function in Ang II treated mice, cSNRT was measured in anaesthetized mice. Representative ECG recordings during intracardiac programmed electrical stimulation are presented in Figs. 5.18A-D. Summary data (Fig. 5.18E) demonstrates there were no differences ($P = 0.51$) in cSNRT between Ang II with cANF (0.05 mg/kg/min) and Ang II treated mice. On the other hand, cSNRT was reduced ($P < 0.001$) in Ang II with cANF (0.1 mg/kg/min) vs. Ang II treated mice and there were no differences ($P = 0.33$) in cSNRT between Ang II with cANF (0.1 mg/kg/min) and saline treated mice. cSNRT was reduced in Ang II with cANF (0.1 mg/kg/min) vs. Ang II with cANF (0.05 mg/kg/min) although this did not reach statistical significance ($P = 0.064$). Combined, these data are consistent with the heart rate data and indicate that co-treatment with cANF (0.1 mg/kg/min) can improve SAN function in Ang II treated mice.

Next, the effects of co-treatment with cANF (0.1 mg/kg/min) on the susceptibility and severity of AF in Ang II treated mice was assessed by burst pacing the right atrium using the intracardiac programmed stimulation technique. Summary data for the susceptibility to AF is shown in Fig. 5.19A and AF durations are presented in Table 5.2. The incidence of AF was higher ($P = 0.001$) in Ang II (15/30) treated mice compared to saline (2/25) treated mice. In fact, AF was induced in 50% of Ang II treated mice compared to 8% of saline treated mice. Mice co-treated with Ang II and cANF (0.1

Figure 5.18. Effects of the NPR-C agonist cANF on sinoatrial node recovery time in anaesthetized wildtype mice treated with Ang II.

A – D. Representative ECG recordings during intracardiac programmed electrical stimulation in anaesthetized wildtype mice treated with saline (A), Ang II (B), Ang II with cANF (0.05 mg/kg/min; C), and Ang II with cANF (0.1 mg/kg/min; D). Mice receiving cANF were co-treated with Ang II for three weeks. **E.** Summary data illustrating the effects of cANF on cSNRT in Ang II treated mice. There was no difference in cSNRT between saline vs. Ang II with cANF (0.1 mg/kg/min; $P = 0.33$) and Ang II vs. Ang II with cANF (0.05 mg/kg/min; $P = 0.51$) treated mice. $^{*}P<0.05$ vs. saline; $^{+}P<0.05$ vs. Ang II. Data analyzed by one-way ANOVA with Tukey's post hoc test. $n = 23$ saline, 24 Ang II, 19 Ang II with cANF (0.05 mg/kg/min), 22 Ang II with cANF (0.1 mg/kg/min) treated mice.

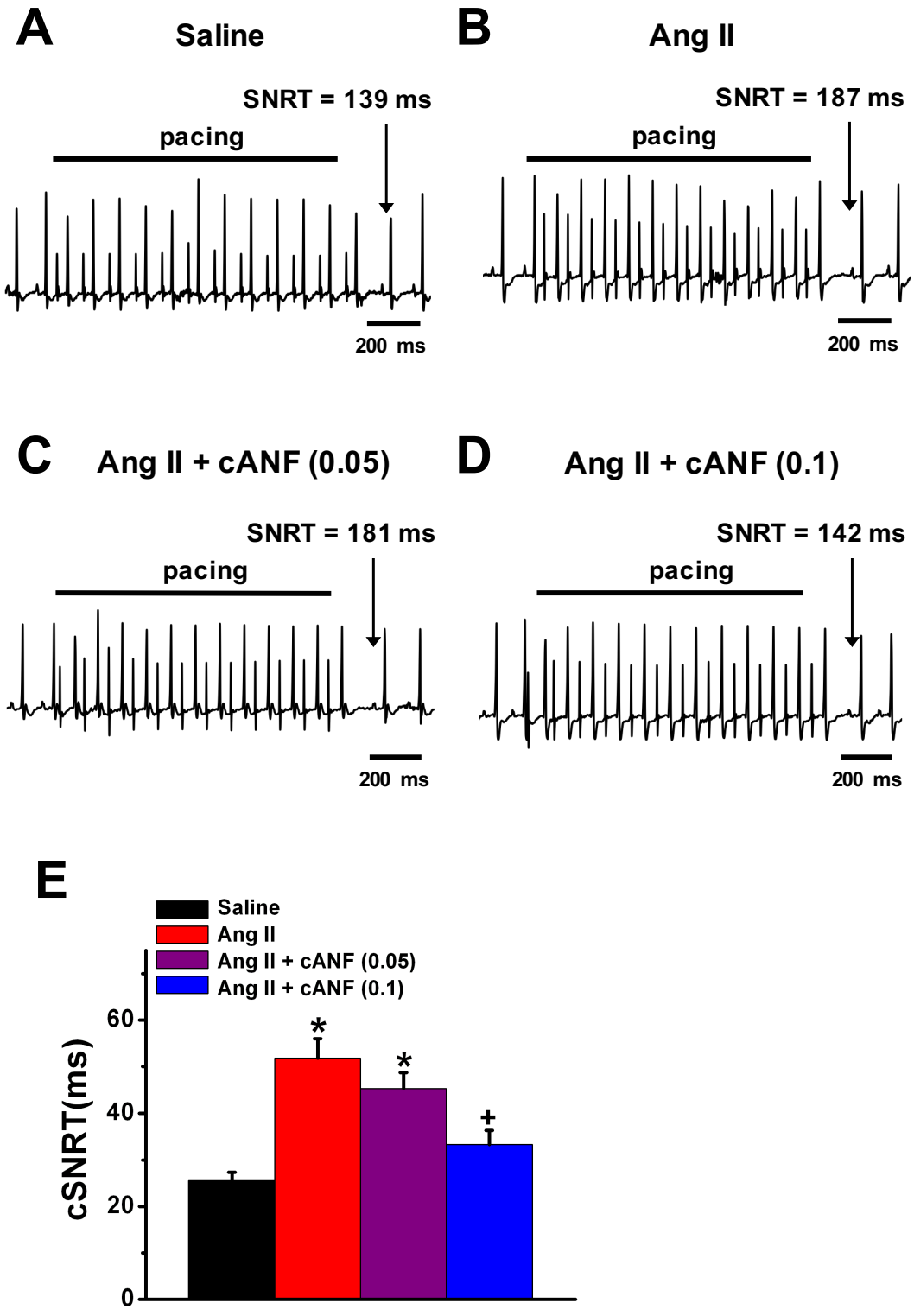
A
Saline
SNRT = 139 ms
pacing
200 ms
B
Ang II
SNRT = 187 ms
pacing
200 ms
C
Ang II + cANF (0.05)
SNRT = 181 ms
pacing
200 ms
D
Ang II + cANF (0.1)
SNRT = 142 ms
pacing
200 ms
E
Saline
Ang II
Ang II + cANF (0.05)
Ang II + cANF (0.1)
cSNRT(ms)
0
20
40
60
*
*
+

Figure 5.18

Figure 5.19. Effects of the NPR-C agonist cANF on susceptibility to induced atrial fibrillation in Ang II treated mice.

A. Summary data for the inducibility of AF in saline, Ang II, and Ang II with cANF (0.1 mg/kg/min) treated mice. Numbers in parenthesis indicate the number of mice induced into AF following burst pacing. $^{*}P < 0.05$ vs. saline. $^{+}P < 0.05$ vs. Ang II. Data analyzed by Fisher's exact test. $n = 25$ saline, 30 Ang II, 20 Ang II with cANF (0.1 mg/kg/min) treated mice. Data collected from H. Jansen and other members of the Rose laboratory.

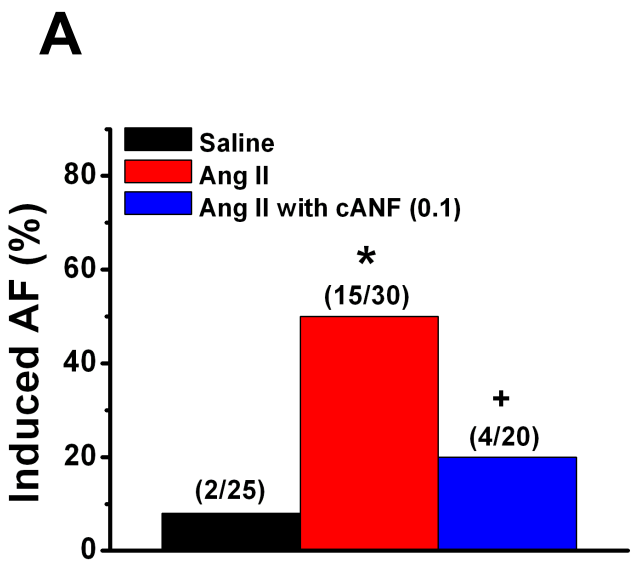
A
Saline
Ang II
Ang II with cANF (0.1)
Induced AF (%)
0
20
40
60
80
(2/25)
*
(15/30)
+
(4/20)

Figure 5.19

Table 5.2. Duration of arrhythmia in saline, Ang II, and Ang II with cANF (0.1 mg/kg/min) treated mice that were induced into atrial fibrillation.

Duration (s)	Saline	Ang II	Ang II with cANF (0.1 mg/kg/min)
< 5	100% (2/2)	60% (9/15)	100% (4/4)
5 – 25		27% (4/15)	
> 25		13% (2/15)	

Numbers in parenthesis indicate the number of mice in each group.

mg/kg/min) had a reduced incidence of AF compared to Ang II treated mice. AF was induced in 20% of Ang II with cANF (0.1 mg/kg/min) (4/20) treated mice, which is lower ($P = 0.041$) compared to Ang II alone and not different ($P = 0.38$) compared to saline treated mice. Further scrutiny of the data revealed that the duration of AF was brief and lasted less than 5 seconds in all Ang II with cANF (0.1 mg/kg/min) treated mice that were induced into AF (Table 5.2). In contrast, AF lasted longer than 5 seconds in 40% of Ang II treated mice that were induced into AF before reverting back to normal sinus rhythm. This demonstrates that Ang II with cANF (0.1 mg/kg/min) treated mice have a reduced susceptibility to induced AF and when induced, AF is brief.

Next, the effects of the NPR-C agonist cANF on P wave duration (Fig. 5.20A), P-R interval (Fig. 5.20B), and AERP (Fig. 5.20C) were assessed in anaesthetized Ang II treated mice. P wave duration ($P < 0.001$) and P-R interval ($P < 0.001$) were prolonged in Ang II with cANF (0.05 mg/kg/min) vs. saline treated mice. There were no differences in P wave duration ($P = 0.98$) or P-R interval ($P = 0.63$) between Ang II with cANF (0.05 mg/kg/min) and Ang II treated mice. In contrast, P wave duration was reduced ($P = 0.023$) in Ang II with cANF (0.1 mg/kg/min) vs. Ang II treated mice and prolonged ($P = 0.002$) in Ang II with cANF (0.1 mg/kg/min) vs. saline treated mice. This suggests a moderate improvement in atrial conduction time in Ang II with cANF (0.1 mg/kg/min) treated mice. P-R interval was reduced ($P = 0.009$) in Ang II with cANF (0.1 mg/kg/min) vs. Ang II treated mice and was not different ($P = 0.10$) in Ang II with cANF (0.1 mg/kg/min) vs. saline treated mice. Therefore, conduction time through the AV node is improved in Ang II with cANF (0.1 mg/kg/min) treated mice. There were no differences in AERP (Fig. 5.20C) in mice treated with Ang II with cANF (0.05 mg/kg/min; $P = 0.88$) or Ang II with cANF (0.1 mg/kg/min; $P = 0.97$) vs. Ang II treated mice. Compared to saline treated mice, AERP was prolonged in Ang II ($P < 0.001$), Ang II with cANF (0.05 mg/kg/min; $P < 0.001$), and Ang II with cANF (0.1 mg/kg/min; $P < 0.001$) treated mice. Combined, these data demonstrate that co-treatment with a lower dose of cANF (0.05 mg/kg/min) does not attenuate alterations in P wave duration, P-R interval, or AERP in Ang II treated mice. On the other hand, co-treatment with a higher dose of cANF (0.1 mg/kg/min) improves P wave duration and P-R interval, but not AERP, in Ang II treated mice.

Figure 5.20. Effects of the NPR-C agonist cANF on atrial and atrioventricular node conduction and atrial effective refractory period in anaesthetized wildtype mice treated with Ang II.

A. and **B.** Summary data illustrating the effects of cANF on P wave duration (A) and P-R interval (B) in Ang II treated mice. n = 23 saline, 33 Ang II, 20 Ang II with cANF (0.05 mg/kg/min), 22 Ang II with cANF (0.1 mg/kg/min) treated mice. **C**. Summary data illustrating the effects of cANF on atrial effective refractory period (AERP) in Ang II treated mice. n = 16 saline, 22 Ang II, 14 Ang II with cANF (0.05 mg/kg/min), 20 Ang II with cANF (0.1 mg/kg/min) treated mice. Mice receiving cANF were co-treated with Ang II for three weeks. $^{*}P<0.05$ vs. saline; $^{+}P<0.05$ vs. Ang II. Data analyzed by one-way ANOVA with Tukey's post hoc test.

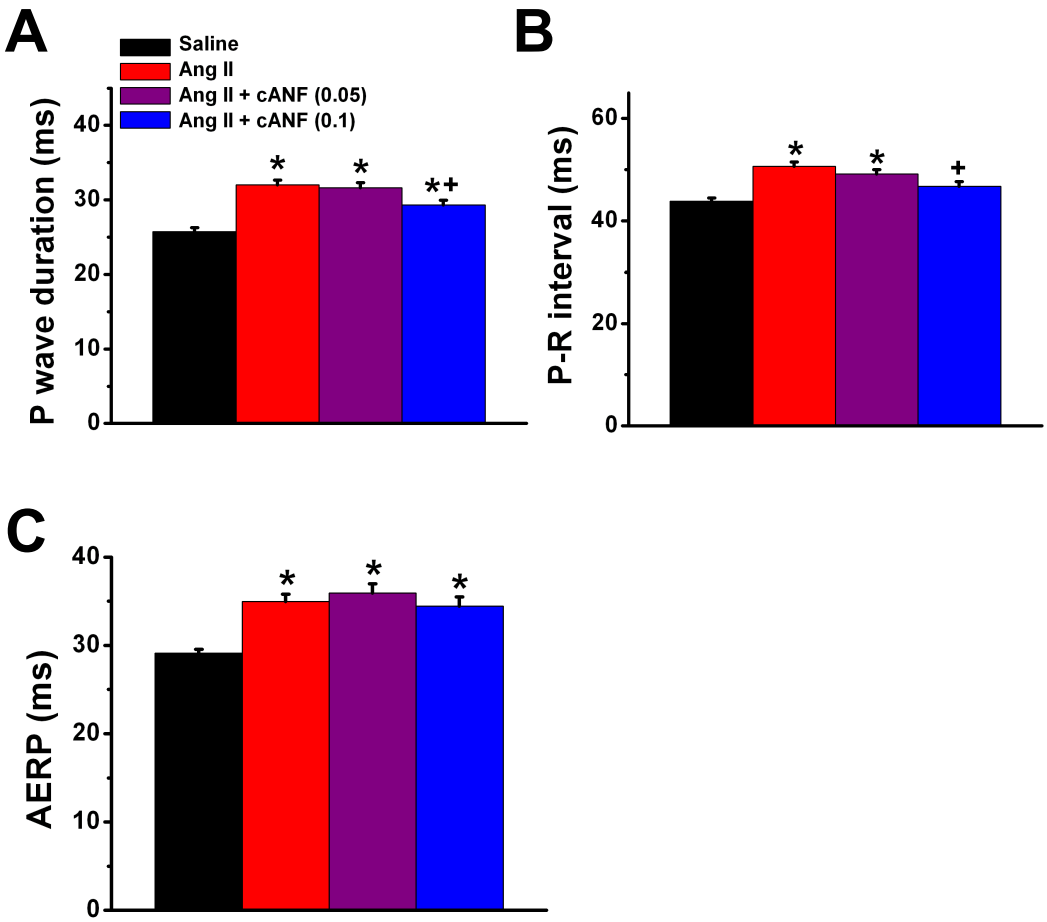
A
Saline
Ang II
Ang II + cANF (0.05)
Ang II + cANF (0.1)
P wave duration (ms)
0
10
20
30
40
*
*
*+
B
P-R interval (ms)
0
20
40
60
*
*
+
C
AERP (ms)
0
10
20
30
40
*
*
*

Figure 5.20

5.5. Effects of the NPR-C agonist cANF on action potential morphology in right and left atrial myocytes from Ang II treated wildtype mice

The data presented in section 5.4 demonstrates a clear improvement in cardiac electrophysiology *in vivo* in mice co-treated with Ang II and cANF (0.1 mg/kg/min) compared to mice treated with Ang II alone. To determine if these changes were associated with electrophysiological changes in atrial myocytes, AP morphology was characterized in right and left atrial myocytes from mice co-treated with Ang II with cANF (0.1 mg/kg/min) compared to Ang II alone. All subsequent experiments were performed on mice co-treated with the higher dose of cANF (0.1 mg/kg/min) as this is the dose that elicited improvement in cardiac electrophysiology *in vivo.*

There were no differences ($P = 0.55$) in cell capacitance between saline, Ang II, and Ang II with cANF (0.1 mg/kg/min) treated right atrial myocytes, as summarized in Fig. 5.21A. In left atrial myocytes, cell capacitance (Fig. 5.21B) was increased ($P < 0.001$) in Ang II with cANF (0.1 mg/kg/min) and Ang II treated left atrial myocytes vs. saline controls. There were no differences ($P = 0.82$) in cell capacitance between Ang II with cANF (0.1 mg/kg/min) vs. Ang II alone treated myocytes.

AP recordings in right atrial myocytes are presented in Fig. 5.22A while left atrial myocytes are presented in Fig. 5.22B. There were no differences ($P > 0.05$) in RMP (Fig. 5.22C) between treatment groups in right atrial myocytes. In right atrial myocytes, there were no differences ($P = 0.30$) in V_{max} (Fig. 5.22D) between treatment groups while AP overshoot (Fig. 5.22E) was reduced ($P = 0.010$) in Ang II with cANF (0.1 mg/kg/min) vs. saline treated right atrial myocytes. Strikingly, APD_{50} ($P = 0.012$; Fig. 5.22F), APD_{70} ($P = 0.003$; Fig. 5.22G), and APD_{90} ($P = 0.002$; Fig. 5.22H) were reduced in Ang II with cANF (0.1 mg/kg/min) vs. Ang II treated right atrial myocytes and there were no differences ($P > 0.05$) in APD between Ang II with cANF (0.1 mg/kg/min) and saline treated right atrial myocytes. In contrast, there were no differences in RMP ($P = 1.00$), V_{max} ($P = 1.00$), AP overshoot ($P = 0.73$), APD_{50} ($P = 0.45$), APD_{70} ($P = 0.39$), or APD_{90} ($P = 0.99$) between Ang II with cANF (0.1 mg/kg/min) and Ang II treated left atrial myocytes. In comparison to saline controls, V_{max} ($P= 0.036$) and AP overshoot ($P < 0.001$) were reduced in Ang II with cANF (0.1 mg/kg/min) treated left atrial myocytes.

Figure 5.21. Effects of the NPR-C agonist cANF on cell capacitance in right and left atrial myocytes from wildtype mice treated with Ang II.

A. Summary data for cell capacitance in right atrial myocytes from saline, Ang II, or Ang II with cANF (0.1 mg/kg/min) treated mice. There were no differences in cell capacitance between treatment groups ($P = 0.55$). **B.** Summary data for cell capacitance in saline, Ang II, and Ang II with cANF (0.1 mg/kg/min) treated left atrial myocytes. $^{*}P<0.05$ vs. saline; $^{+}P<0.05$ vs. Ang II. Data analyzed by one-way ANOVA with Tukey's post hoc test. Right atrium: $n = 41$ saline, 39 Ang II, 19 Ang II with cANF (0.1 mg/kg/min) treated myocytes; Left atrium: $n = 25$ saline, 30 Ang II, and 24 Ang II with cANF (0.1 mg/kg/min) treated myocytes.

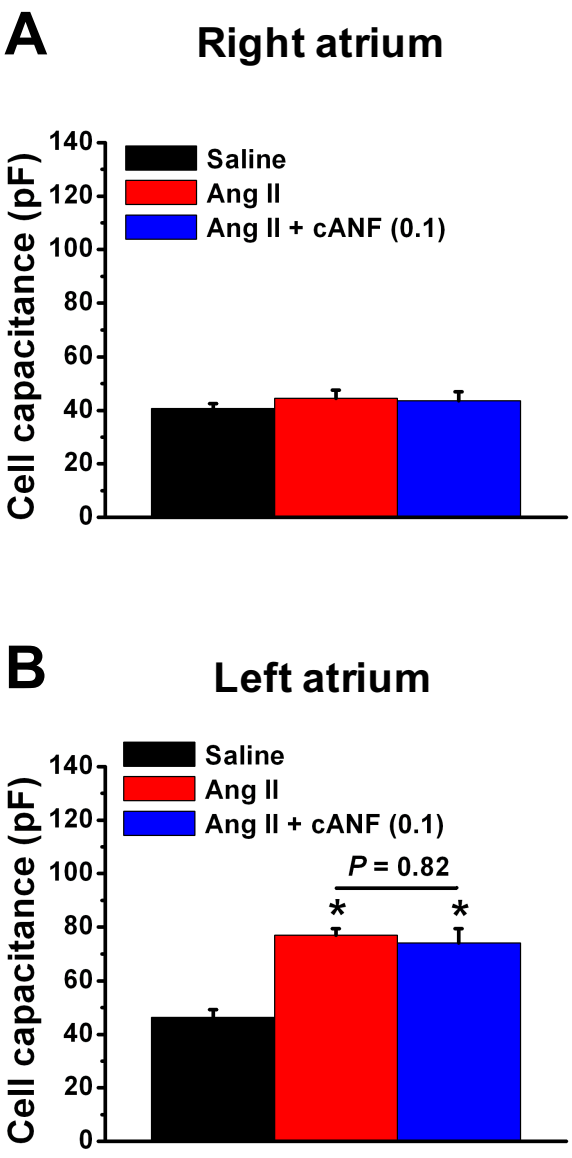
A
Right atrium
Cell capacitance (pF)
140
120
100
80
60
40
20
0
Saline
Ang II
Ang II + cANF (0.1)
B
Left atrium
Cell capacitance (pF)
140
120
100
80
60
40
20
0
Saline
Ang II
Ang II + cANF (0.1)
P = 0.82
*
*

Figure 5.21

Figure 5.22. Effects of the NPR-C agonist cANF on action potential morphology in right and left atrial myocytes from wildtype mice treated with Ang II.

A. and **B.** Representative right atrial (A) and left (B) action potentials (APs) from saline, Ang II, and Ang II with cANF (0.1 mg/kg/min) treated mice. Mice receiving cANF were co-treated with Ang II for three weeks. **C – H.** Summary data illustrating the effects of cANF on RMP (C), V_{max} (D), AP overshoot (E), APD_{50} (F), APD_{70} (G), and APD_{90} (H) in Ang II treated mice. $^{*}P<0.05$ vs. saline within atrium. $^{+}P<0.05$ vs. Ang II within atrium. Data analyzed by one-way ANOVA with Tukey's post hoc test. Right atrium: $n = 19$ saline, 15 Ang II, 17 Ang II with cANF (0.1 mg/kg/min) treated myocytes; Left atrium: $n = 14$ saline, 15 Ang II, 18 Ang II with cANF (0.1 mg/kg/min) treated myocytes.

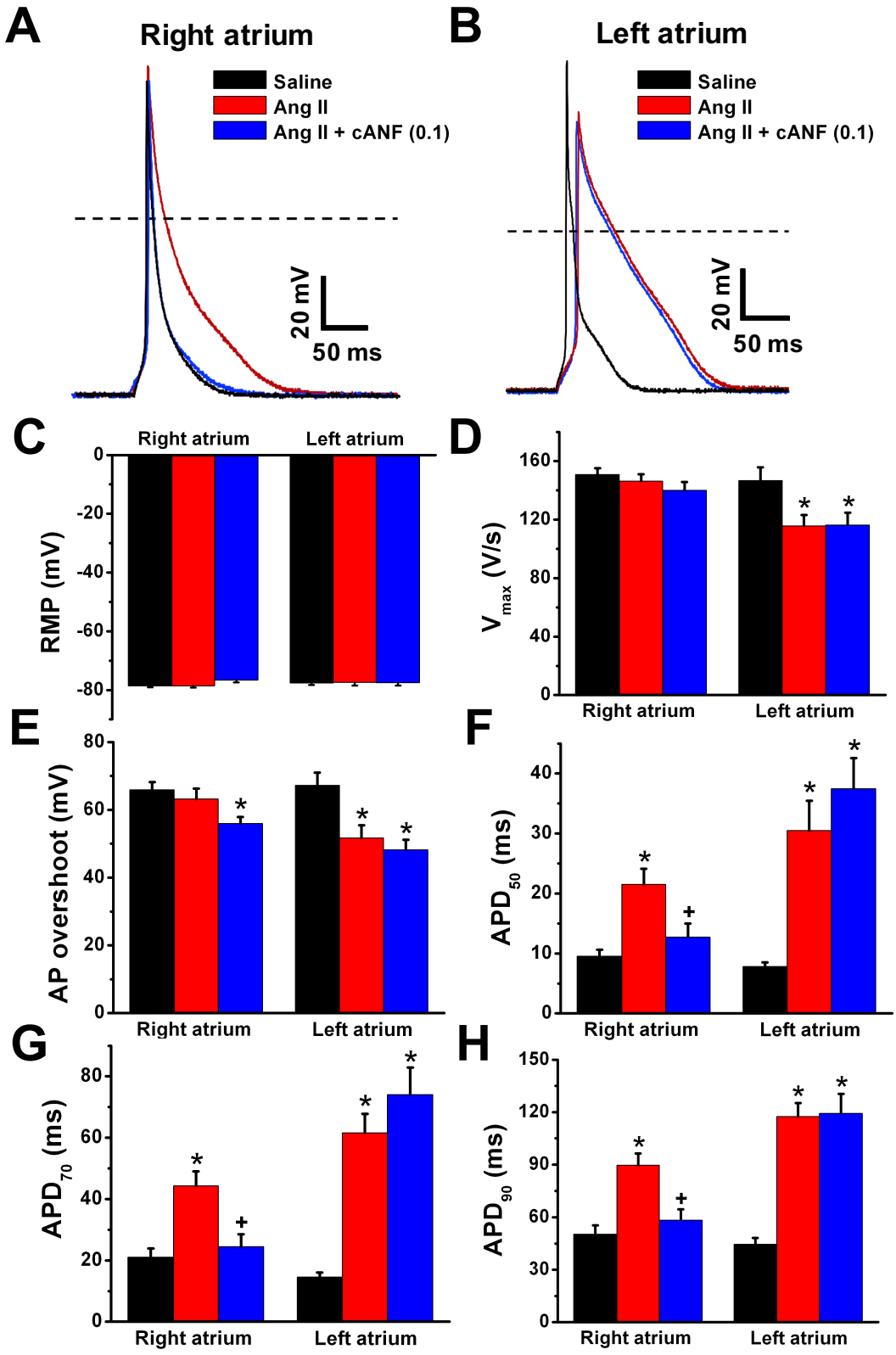
A
Right atrium
Saline
Ang II
Ang II + cANF (0.1)
20 mV
50 ms
B
Left atrium
Saline
Ang II
Ang II + cANF (0.1)
20 mV
50 ms
C
Right atrium
Left atrium
RMP (mV)
0
-20
-40
-60
-80
D
V_{max} (V/s)
160
120
80
40
0
Right atrium
Left atrium
E
AP overshoot (mV)
80
60
40
20
0
Right atrium
Left atrium
F
APD_{50} (ms)
40
30
20
10
0
Right atrium
Left atrium
G
APD_{70} (ms)
80
60
40
20
0
Right atrium
Left atrium
H
APD_{90} (ms)
150
120
90
60
30
0
Right atrium
Left atrium

Figure 5.22

Furthermore, APD_{50} ($P < 0.001$), APD_{70} ($P < 0.001$), and APD_{90} ($P < 0.001$) were prolonged in Ang II with cANF (0.1 mg/kg/min) vs. saline treated controls. Combined, these data demonstrate a substantial attenuation of electrical remodelling, as assessed by AP morphology, in right atrial myocytes from Ang II with cANF (0.1 mg/kg/min) treated mice compared to Ang II alone. In fact, AP morphology was not different in Ang II with cANF (0.1 mg/kg/min) treated right atrial myocytes compared to saline controls. However, Ang II with cANF (0.1 mg/kg/min) does not alter AP morphology in left atrial myocytes compared to Ang II alone.

5.6. Effects of the NPR-C agonist cANF on potassium currents in right and left atrial myocytes from Ang II treated wildtype mice

The AP data presented in section 5.5 demonstrates a reduction in APD at all repolarization times in Ang II with cANF (0.1 mg/kg/min) treated right atrial myocytes compared to Ang II alone. In fact, when compared to saline controls APD was not different in Ang II with cANF (0.1 mg/kg/min) treated right atrial myocytes. In contrast, there were no differences in APD in Ang II with cANF (0.1 mg/kg/min) treated left atrial myocytes compared to Ang II alone. To further elucidate the role of the NPR-C agonist cANF in Ang II treated mice, K^+ currents were characterized in right and left atrial myocytes.

Representative patch-clamp recordings showing a family of total K^+ currents (no pre-pulse) from Ang II and Ang II with cANF (0.1 mg/kg/min) treated right and left atrial myocytes are presented in Figs. 5.23A-D. Summary K^+ I-V relationships (Fig. 5.23E) demonstrate that, in right atrial myocytes, outward K^+ current is increased ($P < 0.05$) at membrane potentials positive to +10 mV in Ang II with cANF (0.1 mg/kg/min) vs. Ang II treated myocytes. Furthermore, there were no differences ($P = 0.73$) in I_K density in Ang II with cANF (0.1 mg/kg/min) vs. saline treated right atrial myocytes at all membrane potentials. In left atrial myocytes, there were no differences ($P = 0.95$) in total K^+ currents in Ang II with cANF (0.1 mg/kg/min) vs. Ang II alone as summarized in Fig. 5.23F. Compared to saline controls, outward K^+ currents were reduced ($P < 0.05$) at

Figure 5.23. Effects of the NPR-C agonist cANF on total potassium currents in right and left atrial myocytes from wildtype mice treated with Ang II.

A. and **B.** Representative patch-clamp recordings showing a family of total K^+ currents (no pre-pulse) recorded from an Ang II (A) and Ang II with cANF (0.1 mg/kg/min; B) treated right atrial myocyte. **C.** and **D.** Representative patch-clamp recordings showing a family of total K^+ currents recorded from an Ang II (C) and Ang II with cANF (0.1 mg/kg/min; D) treated left atrial myocyte. **E.** and **F**. Summary K^+ I-V relationships illustrating the effects of cANF treatment in right (E) and left (F) atrial myocytes from Ang II treated wildtype mice. Currents measured at the peak current at each membrane potential. $^{*}P<0.05$ vs. saline at the membrane potential; $^{+}P<0.05$ vs Ang II at the membrane potential. Data analyzed by two-way repeated measures ANOVA with Tukey's post hoc test. Right atrium: n = 29 saline, 28 Ang II, 14 Ang II with cANF (0.1 mg/kg/min) treated myocytes; Left atrium: n = 10 saline, 17 Ang II, 19 Ang II with cANF (0.1 mg/kg/min) treated myocytes.

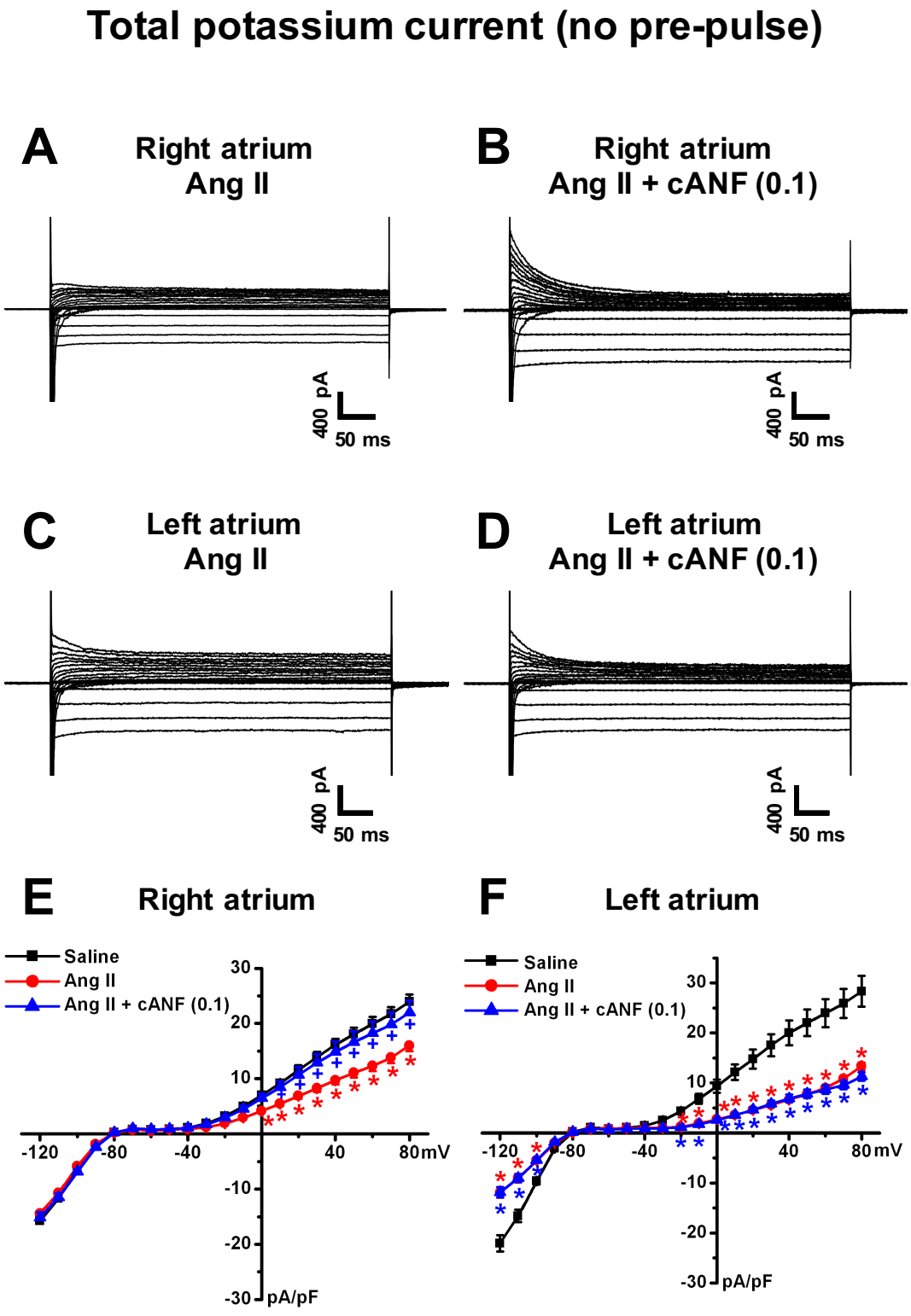
Total potassium current (no pre-pulse)
A
Right atrium
Ang II
B
Right atrium
Ang II + cANF (0.1)
400 pA
50 ms
C
Left atrium
Ang II
D
Left atrium
Ang II + cANF (0.1)
E
Right atrium
F
Left atrium
Saline
Ang II
Ang II + cANF (0.1)
30
20
10
-10
-20
-30
-120
-80
-40
40
80mV
pA/pF

Figure 5.23

membrane potentials negative to -100 mV and positive to -20 mV Ang II with cANF (0.1 mg/kg/min) treated left atrial myocytes.

Comparison of I_K density (no pre-pulse) measured at +50 mV between treatment groups is presented Figs. 5.24A and 5.24B for right and left atrial myocytes. In right atrial myocytes, I_k density is increased ($P < 0.001$) in Ang II with cANF (0.1 mg/kg/min) vs. Ang II and not different ($P = 0.73$) compared to saline controls. In left atrial myocytes, I_K density measured at +50 mV is reduced ($P < 0.001$) in Ang II with cANF (0.1 mg/kg/min) vs. saline and not different ($P = 1.00$) when compared to Ang II alone. Combined, these data demonstrate a substantial improvement in I_K density in right atrial myocytes treated Ang II with cANF (0.1 mg/kg/min). These data are consistent with the APD data presented in Fig. 5.22 for showing a reduction in APD in right atrial myocytes and no difference in left atrial myocytes from Ang II with cANF (0.1 mg/kg/min) vs. Ang II alone.

Next, K^+ currents were measured following a pre-pulse to -40 mV to inactivate I_{to}. Representative recordings from right and left atrial myocytes isolated from Ang II and Ang II with cANF (0.1 mg/kg/min) treated mice are presented in Figs. 5.25A-D. In the right atrium, I_K in Ang II with cANF (0.1 mg/kg/min) treated myocytes was increased ($P = 0.80$) compared to Ang II alone from membrane potentials positive to +40 mV, as shown in the summary K^+ I-V relationships in Fig. 5.25E. In left atrial myocytes, summary I-V relationships (Fig. 5.25F) demonstrate I_K was reduced ($P < 0.05$) between -100 mV and -120 mV and outward currents at membrane potentials positive to -20 mV in Ang II with cANF (0.1 mg/kg/min) compared to saline controls. There were no differences ($P = 0.92$) in I_K between Ang II with cANF (0.1 mg/kg/min) and Ang II treated myocytes.

Comparison of I_K density measured at +50 mV following a pre-pulse to -40 mV indicates a reduction ($P < 0.05$) in I_K in Ang II treated myocytes in right (Fig. 5.26A) and left (Fig. 5.26B) atrial myocytes compared to saline controls. In right atrial myocyte, I_K measured at +50 mV was increased ($P = 0.036$) in Ang II with cANF (0.1 mg/kg/min) vs. Ang II treated myocytes. There were no differences ($P = 0.91$) in I_K between Ang II with cANF (0.1 mg/kg/min) and saline treated right atrial myocytes. In contrast, I_K was

Figure 5.24. Comparison of the effects of the NPR-C agonist cANF on total potassium currents in right and left atrial myocytes from Ang II treated wildtype mice.

A. and **B.** Summary data illustrating the effects of cANF treatment on total K^+ currents (no pre-pulse) measured at +50 mV in saline, Ang II, and Ang II with cANF (0.1 mg/kg/min) treated right (A) and left (B) atrial myocytes. $^{*}P<0.05$ vs. saline; $^{+}P<0.05$ vs Ang II. Data analyzed by one-way ANOVA with Tukey's post hoc test. Right atrium: $n = 29$ saline, 28 Ang II, 14 Ang II with cANF (0.1 mg/kg/min) treated myocytes; Left atrium: $n = 10$ saline, 17 Ang II, 19 Ang II with cANF (0.1 mg/kg/min) treated myocytes.

Total potassium current (no pre-pulse)

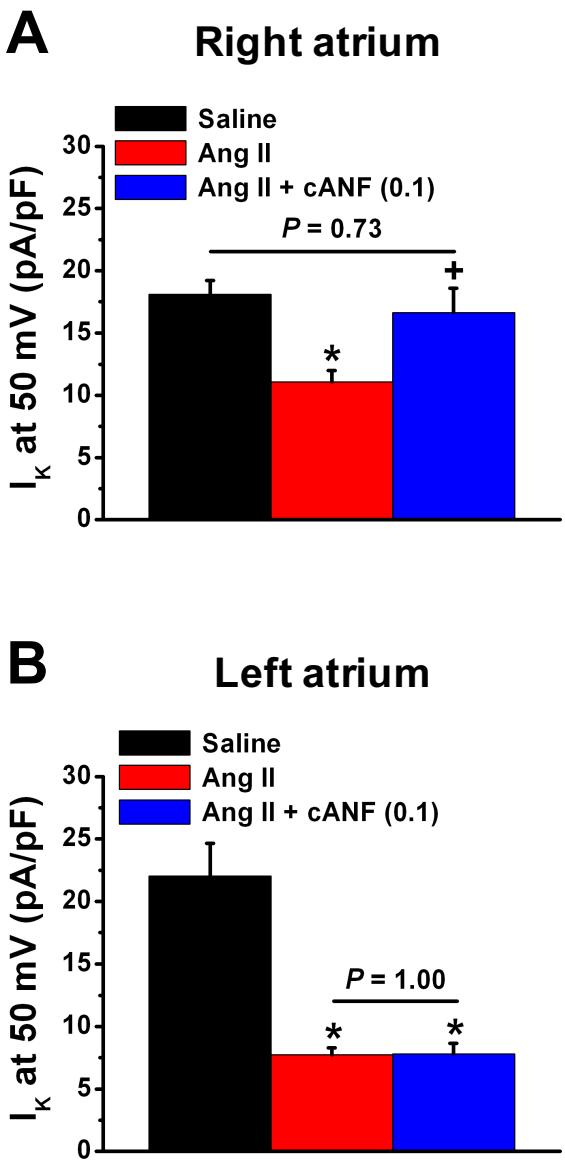

Figure 5.24

Figure 5.25. Effects of the NPR-C agonist cANF on potassium currents following a pre-pulse to -40 mV in right and left atrial myocytes from wildtype mice treated with Ang II.

A. and **B.** Representative patch-clamp recordings showing a family of K^+ currents recorded from Ang II (A) and Ang II with cANF (0.1 mg/kg/min; B) treated right atrial myocytes following a pre-pulse to -40 mV to inactivate I_{to} in wildtype mice. **C.** and **D.** Representative patch-clamp recordings showing a family of K^+ currents recorded from Ang II (C) and Ang II with cANF (0.1 mg/kg/min; D) treated left atrial myocytes following a pre-pulse to -40 mV to inactivate I_{to} in wildtype mice. **E.** and **F.** Summary K^+ I-V relationships illustrating the effects of cANF treatment in right (E) and left (F) atrial myocytes following a pre-pulse to -40 mV in Ang II treated wildtype mice. Currents measured at the peak current at each membrane potential. $^{*}P<0.05$ vs. saline at the membrane potential; $^{+}P<0.05$ vs Ang II at the membrane potential. Data analyzed by two-way repeated measures ANOVA with Tukey's post hoc test. Right atrium: n = 29 saline, 28 Ang II, 14 Ang II with cANF (0.1 mg/kg/min) treated myocytes; Left atrium: n = 10 saline, 17 Ang II, 19 Ang II with cANF (0.1 mg/kg/min) treated myocytes

Potassium current with inactivating pre-pulse

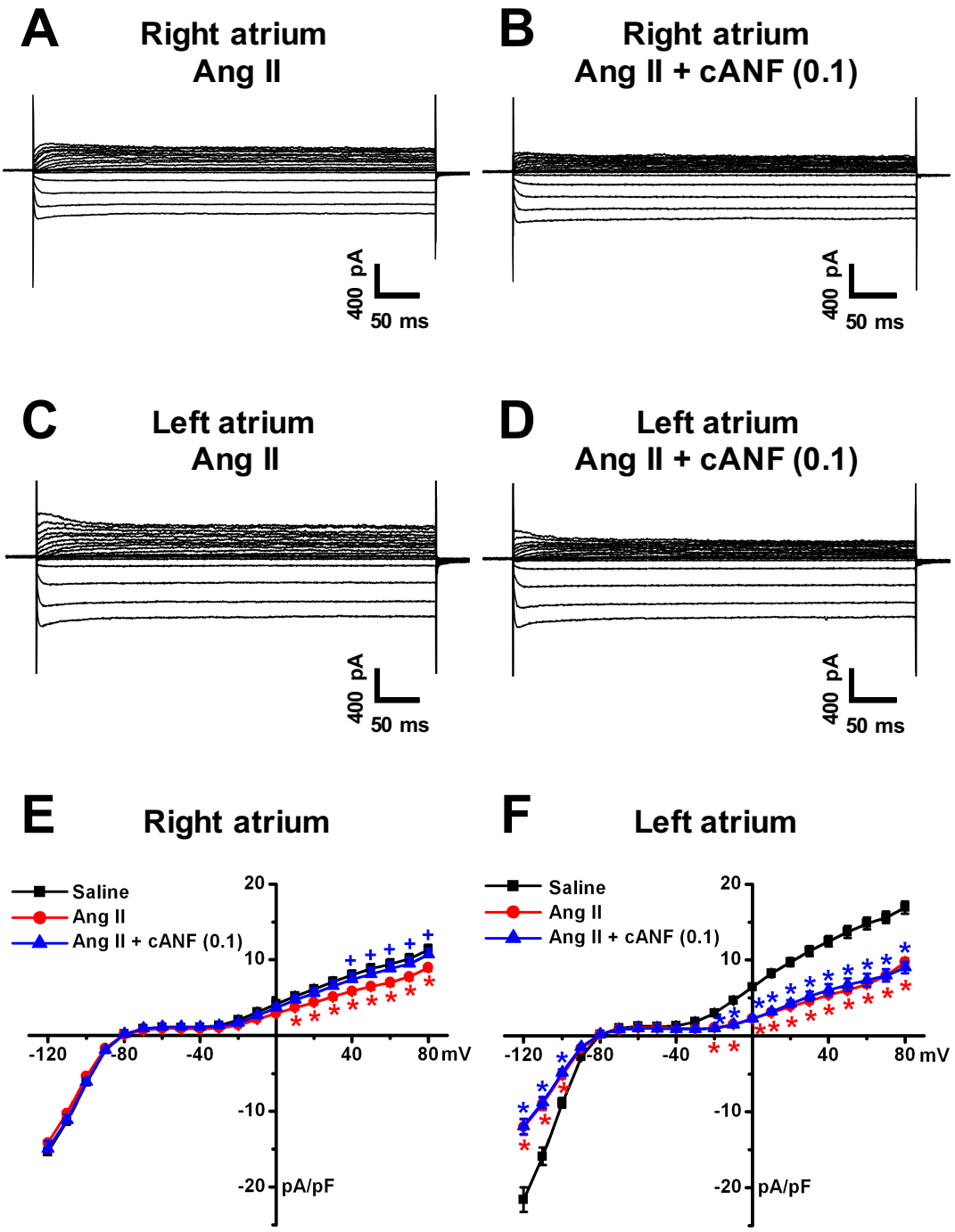

Figure 5.25

Figure 5.26. Comparison of the effects of the NPR-C agonist cANF on potassium currents following a pre-pulse to -40 mV right and left atrial myocytes from Ang II treated wildtype mice.

A. and **B.** Summary data illustrating the effects of cANF treatment on potassium currents following a pre-pulse to -40 mV to inactivate I_{to} in saline, Ang II, and Ang II with cANF (0.1 mg/kg/min) treated right (A) and left (B) atrial myocytes. $^{*}P<0.05$ vs. saline; $^{+}P<0.05$ vs Ang II. Data analyzed by one-way ANOVA with Tukey's post hoc test. Right atrium: n = 29 saline, 28 Ang II, 14 Ang II with cANF (0.1 mg/kg/min) treated myocytes; Left atrium: n = 10 saline, 17 Ang II, 19 Ang II with cANF (0.1 mg/kg/min) treated myocytes.

Potassium current with inactivating pre-pulse

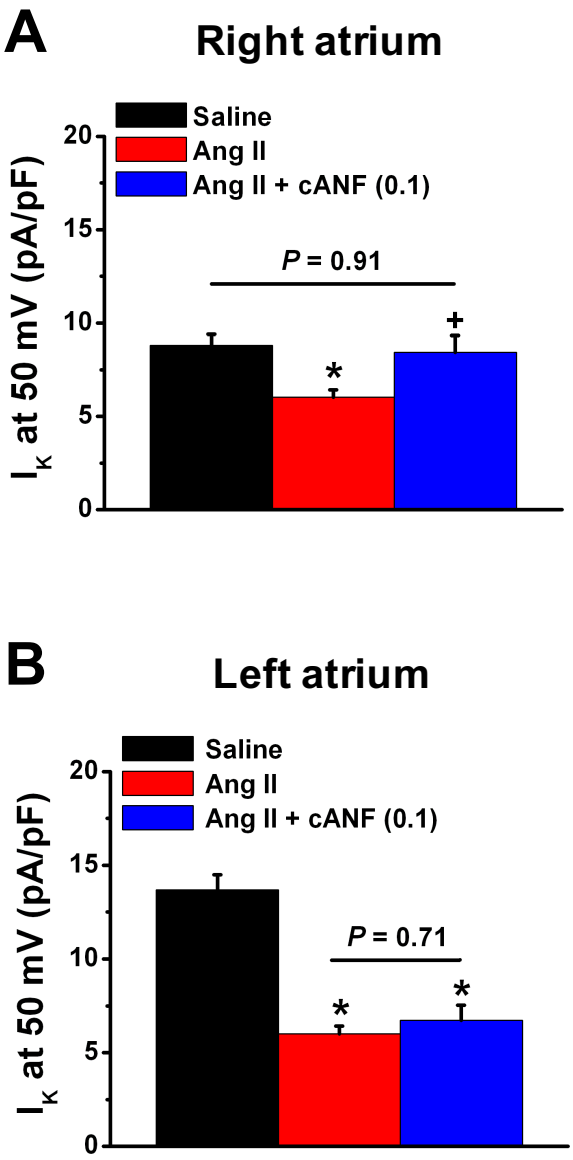

Figure 5.26

reduced ($P < 0.001$) in Ang II with cANF (0.1 mg/kg/min) vs. saline treated left atrial myocytes and was not different ($P = 0.71$) to Ang II treated myocytes.

Representative I_{to} recordings measured at +50 mV are presented in Figs. 5.27A-D for right and left atrial myocytes treated with Ang II with cANF (0.1 mg/kg/min) or Ang II alone. Summary I_{to} I-V relationships (Fig. 5.27E) demonstrate an increase in I_{to} in Ang II with cANF (0.1 mg/kg/min) right atrial myocytes compared to Ang II alone. Furthermore, there were no differences ($P= 0.87$) in I_{to} at all membrane potentials between Ang II with cANF (0.1 mg/kg/min) and saline treated right atrial myocytes. In contrast, summary I_{to} I-V relationships (Fig. 5.27F) demonstrate a reduction in I_{to} in Ang II with cANF (0.1 mg/kg/min) vs. saline controls and no differences ($P = 0.82$) vs. Ang II alone in left atrial myocytes. Comparison of I_{to} measured at +50 mV is summarized in Fig. 5.28. In right atrial myocytes (Fig. 5.28A), there were no differences ($P = 0.87$) in I_{to} between Ang II with cANF (0.1 mg/kg/min) and saline treated controls. Furthermore, I_{to} was increased ($P = 0.031$) in Ang II with cANF (0.1 mg/kg/min) compared to Ang II alone. In contrast, I_{to} remained reduced ($P < 0.001$) in left atrial myocytes from Ang II with cANF (0.1 mg/kg/min) treated mice vs. saline controls. There were no differences ($P = 0.86$) in I_{to} between Ang II with cANF (0.1 mg/kg/min) and Ang II treated left atrial myocytes. These data are consistent with the total K^+ currents presented in Fig. 5.23 that demonstrate an improvement in right, but not left, atrial myocytes treated with Ang II with cANF (0.1 mg/kg/min).

5.7. Effects of Ang II treatment on NPR expression in the right and left atrium of wildtype mice

The effects of Ang II treatment on NPR-A, NPR-B, NPR-C, and ANP mRNA expression was investigated in the right and left atrium of Ang II treated wildtype mice. Expression of NPR-A (*Npr1*; Fig. 5.29A) was not different in the right ($P = 0.46$) or left ($P = 0.14$) atrium of Ang II treated mice compared to saline controls. However, in comparison to the right atrium, *Npr1* mRNA expression was higher ($P = 0.009$) in the left atrium of Ang II treated mice. There were no differences ($P = 0.058$) in *Npr1* mRNA expression in the right vs. left atrium of saline treated mice.

Figure 5.27. Effects of the NPR-C agonist cANF on I_{to} in right and left atrial myocytes from wildtype mice treated with Ang II.

A. and **B.** Representative patch-clamp recordings showing I_{to} from Ang II (A) and Ang II with cANF (0.1 mg/kg/min; B) treated right atrial myocytes. **C.** and **D.** Representative patch-clamp recordings showing I_{to} from Ang II (C) and Ang II with cANF (0.1 mg/kg/min; D) treated left atrial myocytes. Representative recordings at +50 mV as measured from the difference current between with and without a pre-pulse to -40 mV recordings. **E.** and **F.** Summary I-V relationships illustrating the effects of cANF treatment on I_{to} in right (E) and left (F) atrial myocytes from Ang II treated wildtype mice. Currents were obtained from the difference in current between no pre-pulse and with pre-pulse recordings. $^{*}P<0.05$ vs. saline at each membrane potential; $^{+}P<0.05$ vs Ang II at each membrane potential. Data analyzed by two-way repeated measures ANOVA with Tukey's post hoc test. Right atrium: n = 29 saline, 28 Ang II, 14 Ang II with cANF (0.1 mg/kg/min) treated myocytes; Left atrium: n = 10 saline, 17 Ang II, 19 Ang II with cANF (0.1 mg/kg/min) treated myocytes.

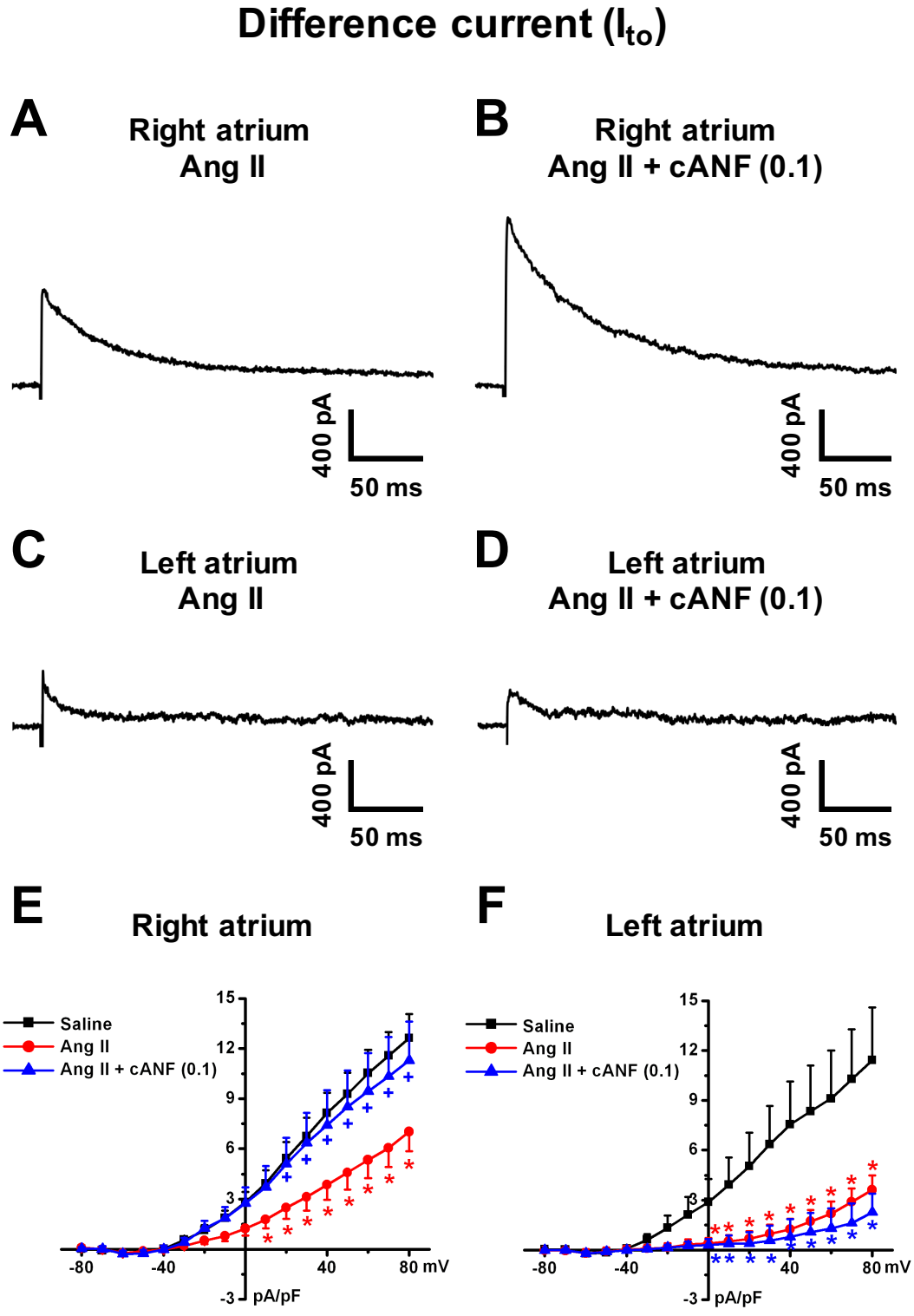
Difference current (I_{to})
A
Right atrium
Ang II
400 pA
50 ms
B
Right atrium
Ang II + cANF (0.1)
400 pA
50 ms
C
Left atrium
Ang II
400 pA
50 ms
D
Left atrium
Ang II + cANF (0.1)
400 pA
50 ms
E
Right atrium
Saline
Ang II
Ang II + cANF (0.1)
15
12
9
6
3
-3
-80
-40
40
80 mV
pA/pF
F
Left atrium
Saline
Ang II
Ang II + cANF (0.1)
15
12
9
6
3
-3
-80
-40
40
80 mV
pA/pF

Figure 5.27

Figure 5.28. Comparison of the effects of the NPR-C agonist cANF on I_{to} in right and left atrial myocytes from wildtype mice treated with Ang II.

A. and **B.** Summary data illustrating the effects of cANF treatment on I_{to} measured at +50 mV in right (A) and left (B) atrial myocytes from Ang II treated wildtype mice. $^{*}P<0.05$ vs. saline at each membrane potential; $^{+}P<0.05$ vs Ang II at each membrane potential. Data analyzed by one-way ANOVA with Tukey's post hoc test. Right atrium: $n = 29$ saline, 28 Ang II, 14 Ang II with cANF (0.1 mg/kg/min) treated myocytes; Left atrium: $n = 10$ saline, 17 Ang II, 19 Ang II with cANF (0.1 mg/kg/min) treated myocytes.

Difference current (I_{to})

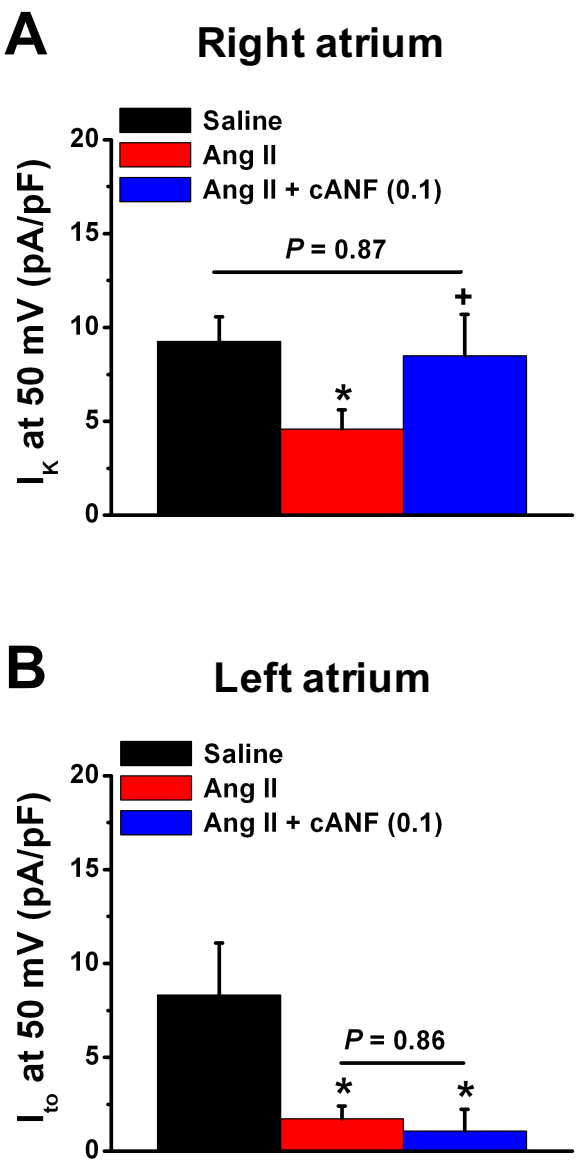

Figure 5.28

Figure 5.29. Quantitative mRNA expression of NPR-A, NPR-B, NPR-C, and ANP following Ang II treatment in the right and left atrium.

A – D. Summary data illustrating the effects of Ang II treatment on mRNA expression levels for NPR-A (*Npr1*; A), NPR-B (*Npr2*; B), NPR-C (*Npr3*; C), and ANP (*Nppa*; D) in the right and left atrium of wildtype mice. mRNA expression was normalized to GAPDH and β-actin. **P*<0.05 vs. saline within atrial region; ^{+}P<0.05 vs. right atrium within treatment group. Data analyzed by two-way ANOVA with Tukey's post hoc test. Right atrium: n = 7 saline and 8 Ang II treated hearts; Left atrium: n = 8 saline and 8 Ang II treated hearts.

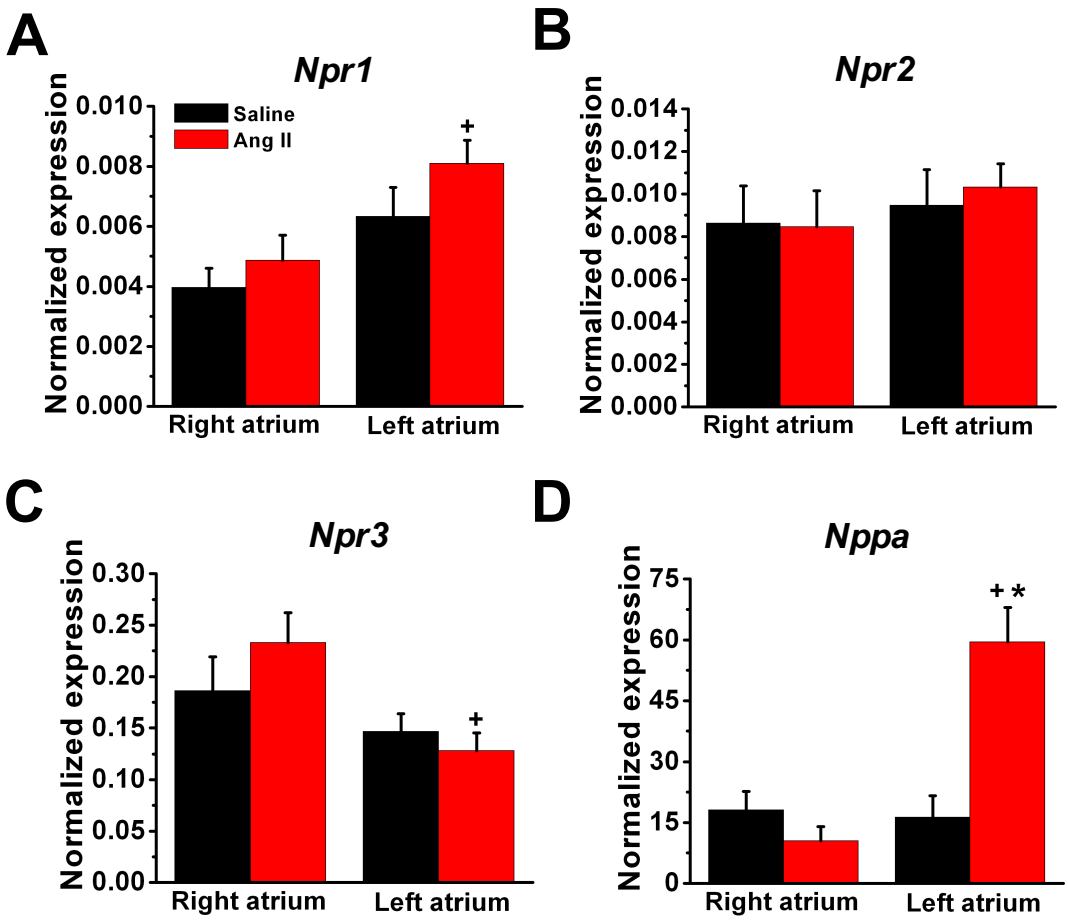
A
Npr1
Saline
Ang II
Normalized expression
0.010
0.008
0.006
0.004
0.002
0.000
+
Right atrium
Left atrium
B
Npr2
Normalized expression
0.014
0.012
0.010
0.008
0.006
0.004
0.002
0.000
Right atrium
Left atrium
C
Npr3
Normalized expression
0.30
0.25
0.20
0.15
0.10
0.05
0.00
+
Right atrium
Left atrium
D
Nppa
Normalized expression
75
60
45
30
15
0
+ *
Right atrium
Left atrium

Figure 5.29

Summary data for NPR-B (*Npr2*) is presented in Fig. 5.29B. There were no differences ($P = 0.83$) in *Npr2* mRNA expression in the right or left atrium of Ang II treated mice. In addition, there were no regional differences ($P = 0.40$) in *Npr2* mRNA expression in saline or Ang II treated mice.

NPR-C is encoded by *Npr3* and summary data is presented in Fig. 5.29C. There were no differences in *Npr3* mRNA expression in the right ($P = 0.20$) or left ($P = 0.60$) atrium of saline vs. Ang II treated mice. In addition, there were no differences ($P = 0.27$) in *Npr3* expression in the right and left atrium of saline treated mice. However, *Npr3* mRNA expression was significantly lower ($P = 0.005$) in the left vs. right atrium of Ang II treated mice.

There were no differences ($P = 0.37$) in ANP (*Nppa*; Fig. 5.29D) mRNA expression in the right atrium of saline vs. Ang II treated mice. In the left atrium, *Nppa* mRNA expression was higher ($P < 0.001$) following Ang II treatment. In addition, *Nppa* mRNA expression was not different ($P = 0.83$) in saline treated right and left atria.

CHAPTER 6
EFFECTS OF AGE AND FRAILTY ON SINOATRIAL NODE FUNCTION, ATRIAL FUNCTION, AND ARRHYTHMOGENESIS *IN VIVO*

6.1. Assessment of frailty in young and aged wildtype mice

During the natural ageing process, health deficits are accumulated and manifest as frailty. Frailty is a measure of biological age rather than chronological age, and is reflective of the overall health status of an individual (Rockwood *et al.*, 2000; Rockwood and Mitnitski, 2007; Rockwood and Mitnitski, 2011). In mice, we can quantify frailty using a non-invasive 31 index frailty assessment and generate a frailty index (FI) score (Whitehead *et al.*, 2014).

This study used young (13.0 ± 0.4 weeks) and aged (100.9 ± 1.2 weeks) mice. All young and aged mice used in this study underwent a frailty assessment immediately prior to experimental use. Fig. 6.1A summarizes FI scores in young and aged mice used in this study. Each circle represents the FI score for an individual mouse. Average FI score was increased ($P < 0.001$) in aged vs. young mice, thereby indicating a decline in overall health status in aged mice. Further scrutiny of the data revealed that FI scores ranged from 0.03 to 0.17 in young mice while aged mice had FI scores between 0.17 to 0.37. These data indicate that not only was FI score increased as a function of chronological age, but that FI scores, and therefore biological age, fell along a continuum between young and aged mice.

6.2. Effects of age and frailty on heart rate and sinoatrial node function in anaesthetized wildtype mice

Previous studies have demonstrated a decline in heart rate and SAN function with age (Dobrzynski *et al.*, 2007; Monfredi and Boyett, 2015; Csepe *et al.*, 2015), however the impacts of frailty on heart rate and SAN function is unknown. Accordingly, the goal

Figure 6.1. Frailty index in young and aged wildtype mice.

A. Summary data illustrating frailty index (FI) measurements in young (black) and aged (red) mice. Each circle represents the FI score of an individual mouse. Data analysed by Student's *t*-test. $n = 49$ young and 60 aged mice.

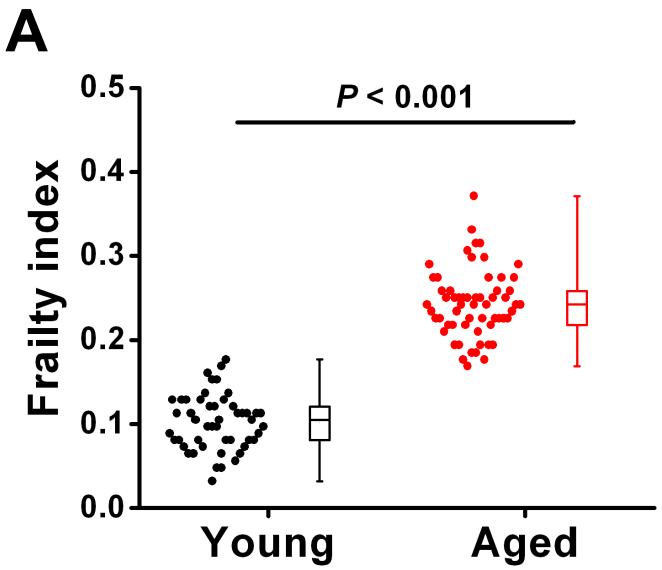

Figure 6.1

of the next set of experiments was to determine the effects of age and frailty on heart rate and SAN function in anaesthetized wildtype mice. Summary of all ECG intervals and intracardiac ECG parameters measured is located in Appendix G.

Representative ECG recordings from young and aged mice are shown in Figs. 6.2A and 6.2B. Heart rate was reduced ($P < 0.001$) in aged vs. young mice, as shown in Fig. 6.2C. Furthermore, there is a high degree of variability in heart rate measurements in aged mice compared to young mice. This indicates that factors other than chronological age are influencing heart rate in these animals. To determine if frailty (i.e. overall health status) could explain the increase in heteroscedasticity observed in aged mice, linear regression analysis was performed by plotting the heart rate for each mouse as a function of that individual's FI score as shown in Fig. 6.2D. In this figure, and all subsequent figures, each circle represents an individual mouse, young mice are shown in black circles and aged mice in red circles. Linear regression analysis indicates there is a negative correlation ($P = 0.02$) between heart rate and FI score such that heart rate declines as FI score increases.

Next, the effects of age and frailty on SAN function was assessed in anaesthetized mice by measuring cSNRT using intracardiac programmed electrical stimulation. Representative ECG recordings are presented in Figs. 6.3A and 6.3B for young and aged mice. cSNRT (Fig. 6.3C) was prolonged ($P < 0.001$) in aged vs. young mice and cSNRT in aged mice showed considerable variability compared to young mice. Fig. 6.3D illustrates the relationship between cSNRT and FI score. There was a positive correlation ($P < 0.001$) between cSNRT and FI score such that cSNRT was prolonged in mice with increasing FI scores. These data are consistent with the heart rate data demonstrating both an impairment in SAN function with chronological age and a correlation with FI score.

6.3. Effects of age and frailty on arrhythmogenesis in anaesthetized wildtype mice

The occurrence of supraventricular arrhythmias, including AF, increases with age (Mirza *et al.*, 2012; Rahman *et al.*, 2014). The goal of the next set of experiments was to determine the effects of age and frailty on inducibility to AF and incidence of AV node block in anaesthetized wildtype mice.

Figure 6.2. Effects of age and frailty on heart rate in anaesthetized wildtype mice.
A. and **B.** Representative ECG recordings in young (A) and aged (B) wildtype mice. **C.** Summary of differences in heart rate between young and aged anaesthetized mice. Data analyzed by Mann-Whitney rank sum test. n = 29 young and 34 aged mice. **D.** Linear regression analysis illustrating the relationship between heart rate and FI score for the same mice as used in panel C. Correlation coefficients obtained using Pearson's correlation. n = 63 mice.

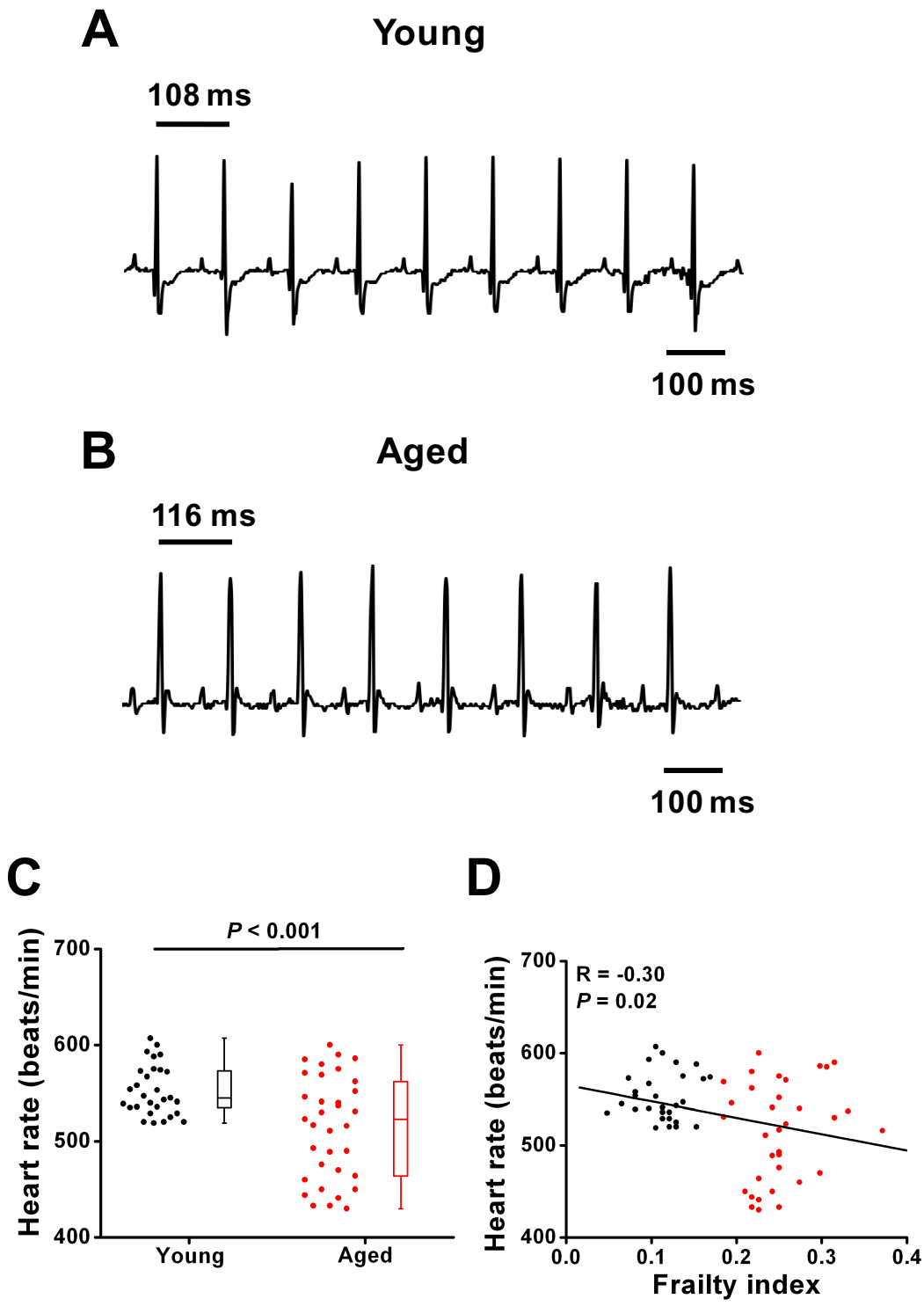
A
Young
108 ms
100 ms
B
Aged
116 ms
100 ms
C
P < 0.001
Heart rate (beats/min)
700
600
500
400
Young
Aged
D
R = -0.30
P = 0.02
Heart rate (beats/min)
700
600
500
400
0.0
0.1
0.2
0.3
0.4
Frailty index

Figure 6.2

Figure 6.3. Effects of age and frailty on sinoatrial node recovery time in anaesthetized wildtype mice.

A. and **B.** Representative ECG recordings during intracardiac programmed electrical stimulation in young (A) and aged (B) mice. **C.** Summary of differences in cSNRT between young and aged anaesthetized mice. Data analyzed by Mann-Whitney rank sum test. n = 29 young and 34 aged mice. **D.** Linear regression analysis illustrating the relationship between cSNRT and FI score for the same mice as used in panel C. Correlation coefficients obtained using Pearson's correlation. n = 63 mice.

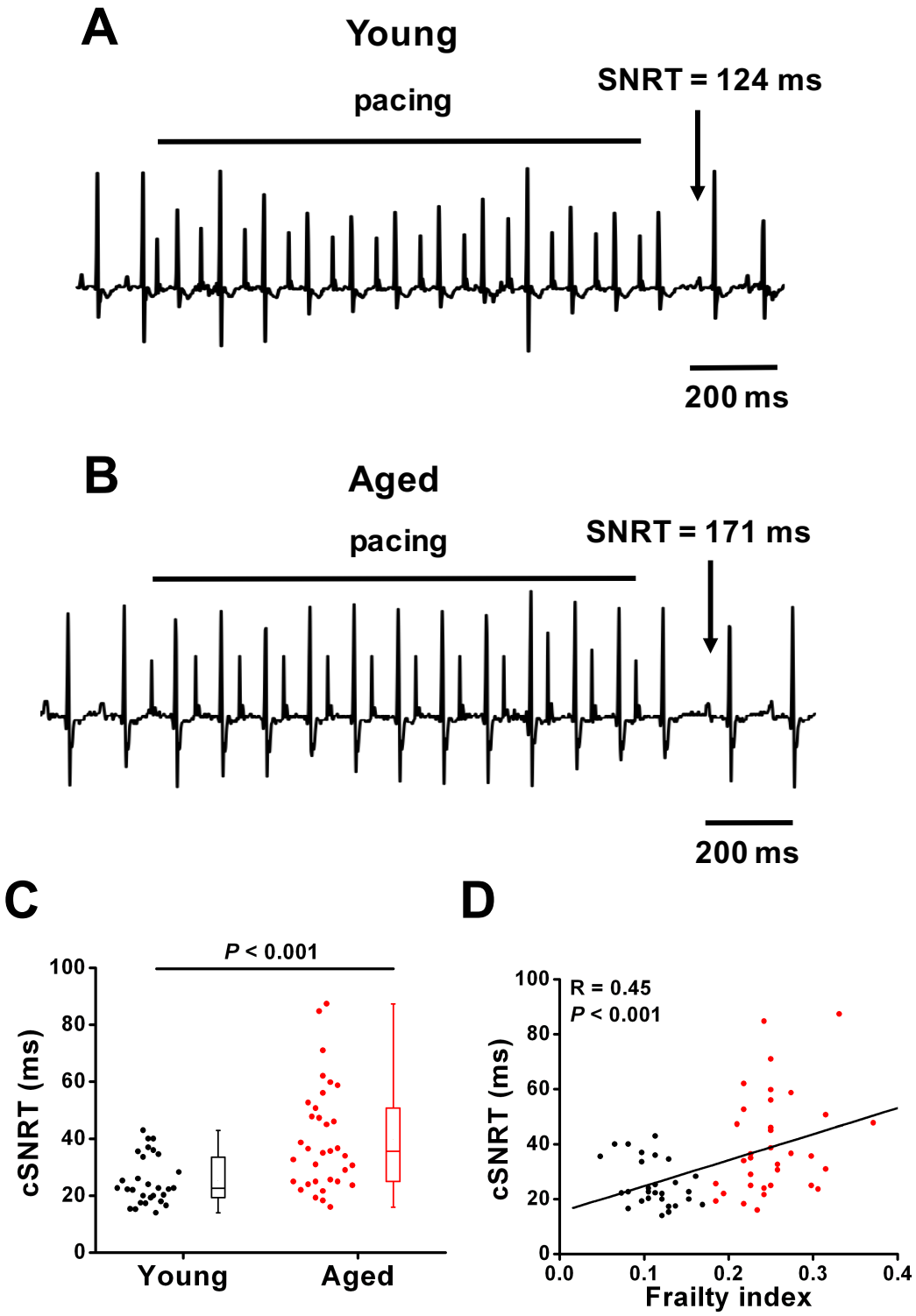
A
Young
pacing
SNRT = 124 ms
200 ms
B
Aged
pacing
SNRT = 171 ms
200 ms
C
P < 0.001
cSNRT (ms)
100
80
60
40
20
0
Young
Aged
D
R = 0.45
P < 0.001
cSNRT (ms)
100
80
60
40
20
0
0.0
0.1
0.2
0.3
0.4
Frailty index

Figure 6.3

Fig. 6.4A and 6.4B show representative surface and atrial ECG recordings of a young and aged mouse induced into AF following burst pacing of the right atrium. There were no differences ($P = 0.71$) in inducibility to AF (Fig. 6.4C) in young (4/20) vs. aged (4/26) mice. However, further scrutiny of the data revealed a difference in AF duration (Fig. 6.4D and Table 6.1) such that AF duration was considerably longer ($P = 0.03$) in aged mice compared to young mice. In young mice, AF was non-sustained and lasted less than 5 seconds before spontaneously reverting back into normal sinus rhythm in all cases. In contrast, AF duration was sustained and lasted longer than 25 seconds in 75% of aged mice that were induced into AF. The duration of AF was 21.3 seconds in the other aged mouse that was induced into AF. These data demonstrate that although the incidence of induced AF is not different in young vs. aged mice, there is a considerable increase in AF duration in aged mice. In addition, Fig. 6.4E demonstrates that aged mice induced into AF had a higher ($P < 0.001$) FI score compared to young mice induced into AF, thereby demonstrating that mice with higher FI scores are more likely to have sustained AF whereas and mice with lower FI scores are more likely to have transient AF when induced into AF.

Next, the occurrence of spontaneous AV node block was assessed in a subset of young and aged anaesthetized mice under baseline conditions. An example of an aged mouse in 2:1 AV node block is presented in Fig. 6.5A and complete AV node block in Fig. 6.5B. Summary data (Fig. 6.5C) demonstrates that no young mice (0/26) had spontaneous AV node block whereas 27% (4/26) of aged mice displayed AV node block. In this subset of mice, the average FI score (Fig. 6.5D) was higher ($P < 0.001$) in aged vs. young mice. These data demonstrate the occurrence of spontaneous AV node block increases with age and FI score.

6.4. Effects of age and frailty on P wave duration and P-R interval in anaesthetized wildtype mice

The data presented in section 6.3 demonstrates that the severity of AF and incidence of spontaneous AV node block is increased in aged and frail mice, which is indicative of impaired function in the atrium and the AV node. Accordingly, the goal of

Figure 6.4. Susceptibility to induced atrial fibrillation in young and aged mice.

A. and **B.** Representative surface (top) and intracardiac atrial (bottom) ECG recordings from young (A) and aged (B) mice that were induced into atrial fibrillation (AF) following burst pacing of the right atrium. The young mouse was in AF for 1.1 seconds following burst pacing before spontaneously reverting back to normal sinus rhythm whereas the aged mouse remained in AF for 21.3 seconds. **C.** Summary data for the inducibility of AF in young and aged mice following burst pacing. Numbers in parenthesis indicate the number of mice induced into AF following burst pacing. Data analyzed by Fischer's exact test. n = 20 young and 26 aged mice. **D.** Summary of differences in AF duration in young and aged mice that were induced into AF. n = 4 young and 4 aged mice. Data analyzed by Student's t-test. **E.** Summary data illustrating the FI scores of mice that were induced into AF following burst pacing. $^{*}P < 0.05$ vs. young. Data analyzed by Student's t-test. n = 4 young and 4 aged mice.

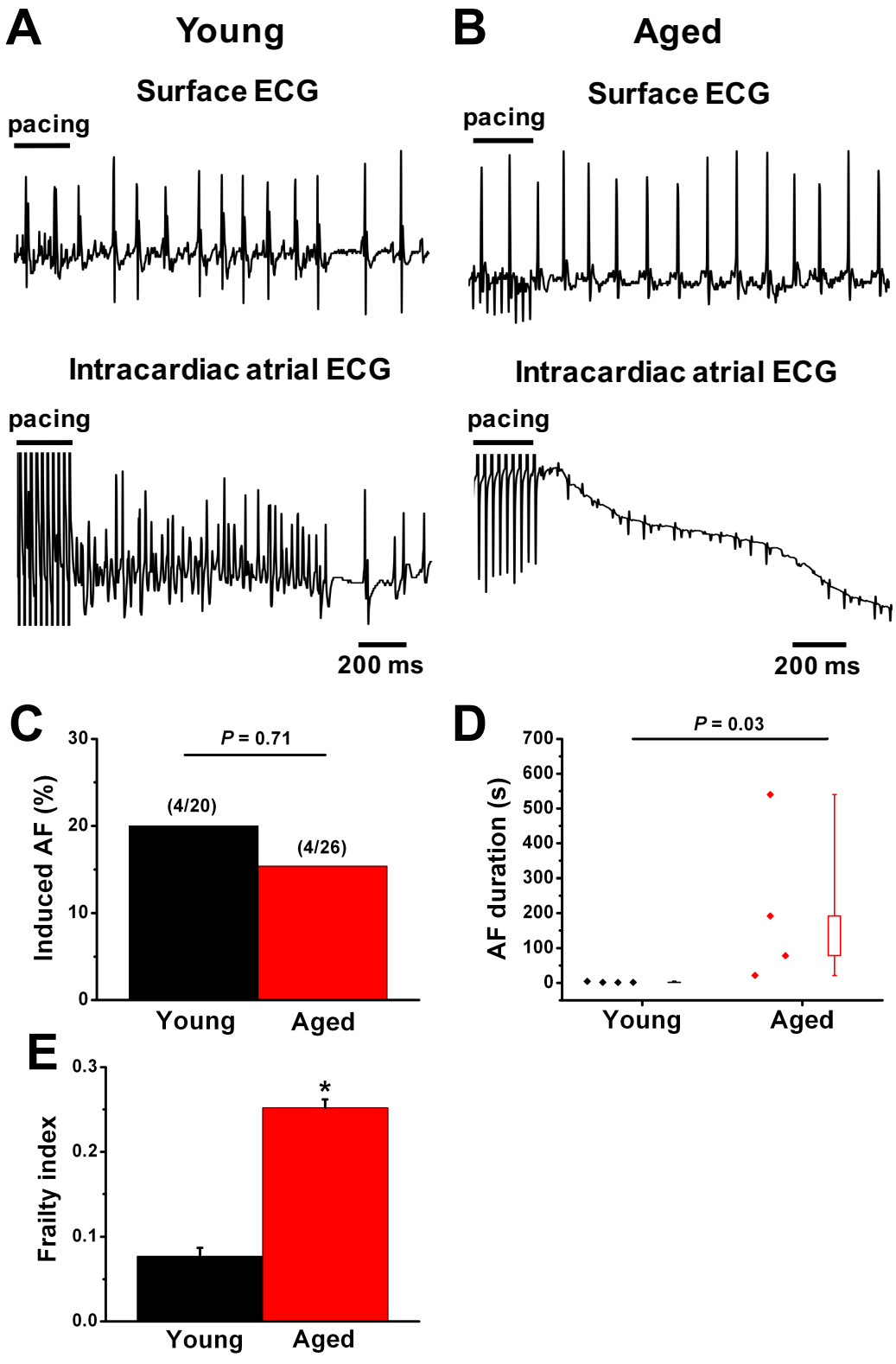
A
Young
Surface ECG
pacing
Intracardiac atrial ECG
pacing
200 ms
B
Aged
Surface ECG
pacing
Intracardiac atrial ECG
pacing
200 ms
C
P = 0.71
(4/20)
(4/26)
Induced AF (%)
30
20
10
0
Young
Aged
D
P = 0.03
AF duration (s)
700
600
500
400
300
200
100
0
Young
Aged
E
Frailty index
0.3
0.2
0.1
0.0
*
Young
Aged

Figure 6.4

Table 6.1. Duration of arrhythmias in young and aged mice that were induced into atrial fibrillation

Duration (s)	Young	Aged
< 5	100% (4/4)	
5 – 25		25% (1/4)
> 25		75% (3/4)

Numbers in parenthesis indicate the number of mice in each group.

Figure 6.5. Incidence of atrioventricular node block in young and aged mice.

A. and **B.** Representative ECG recordings from aged mice showing examples of 2:1 atrioventricular node (AV node) block (A) and complete AV node block (B). **C.** Summary data for the frequency of spontaneous AV node block in young and aged mice. Numbers in parenthesis indicate the number of mice with spontaneous AV node block. Data analyzed by Fischer's exact test. **D.** FI scores for the young and aged mice used to determine the occurrence of spontaneous AV node block. Data analyzed by Student's *t*-test. $^{*}P < 0.05$ vs. young. $n = 20$ young and 26 aged mice.

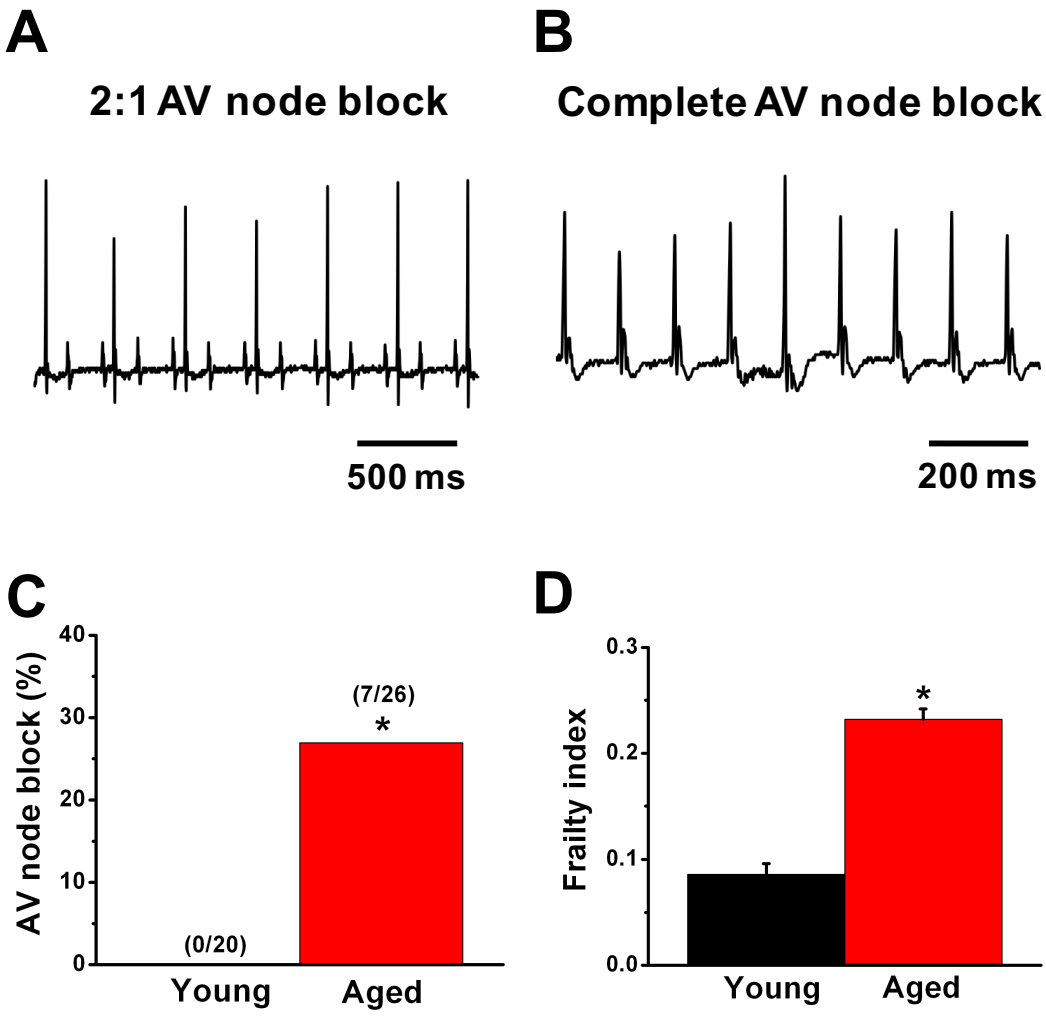
A
2:1 AV node block
500 ms
B
Complete AV node block
200 ms
C
AV node block (%)
40
30
20
10
0
(7/26)
*
(0/20)
Young
Aged
D
Frailty index
0.3
0.2
0.1
0.0
*
Young
Aged

Figure 6.5

the next set of experiments was to characterize P wave duration and P-R interval in anaesthetized young and aged mice.

Atrial conduction time was assessed in young and aged mice by measuring P wave duration. As summarized in Fig. 6.6A, average P wave duration was prolonged ($P < 0.001$) in aged vs. young mice; however, there is considerable heterogeneity in the two age groups. Next, P wave duration was plotted as a function of FI score for each mouse, as shown in Fig. 6.6B. These data demonstrate a positive correlation ($P < 0.001$) between P wave duration and FI score such that P wave duration is graded by FI score. Combined, these data indicate that atrial conduction time is slowed in aged and frail animals, which could contribute to increased occurrence of atrial arrhythmias.

Next, P-R interval was measured in anaesthetized young and aged wildtype mice. P-R interval (Fig. 6.6C) was prolonged ($P < 0.001$) in aged vs. young mice. Furthermore, there was considerable variability in P-R interval measurements in aged mice, which indicates that variables other than chronological age are contributing to the prolongation in P-R interval observed in aged mice. Linear regression analysis (Fig. 6.6D) demonstrates a positive correlation ($P = 0.002$) between P-R interval and FI score such that animals with higher FI scores have longer P-R intervals. Combined, these data demonstrate a prolongation in AV node conduction time in aged animals and as a function of FI score.

Prolongation of P wave duration and P-R interval indicates slowed conduction in the atrium and through the AV node which can contribute to a substrate for AF (Magnani *et al.*, 2013; Censi *et al.*, 2016; Conte *et al.*, 2017; Smith *et al.*, 2017). Accordingly, P wave duration and P-R interval were plotted as a function of AF duration in young and aged mice that were induced into AF. Linear regression analysis shown in Fig. 6.7A demonstrates a positive correlation ($P = 0.04$) between AF duration and P wave duration. Similarly, increased AF duration was correlated with prolongation of the P-R interval ($P = 0.003$; Fig. 6.7B). These data demonstrate that slowed conduction times are associated with an increase in AF duration.

Figure 6.6. Effects of age and frailty on P wave duration and P-R interval in anaesthetized wildtype mice.

A. Summary of differences in P wave duration in young and aged anaesthetized mice. Data analyzed by Student's *t*-test. $n = 22$ young and 24 aged mice. **B.** Linear regression analysis illustrating the relationship between P wave duration and FI score for the same mice as used in panel A. **C.** Summary of the differences in P-R interval in young and aged anaesthetized mice. Data analyzed by Mann-Whitney rank sum test. $n = 22$ young and 24 aged mice. **D.** Linear regression analysis illustrating the relationship between P-R interval and FI score for the same mice used in panel C. Correlation coefficients for panels B and D obtained by Pearson's correlation. $n = 46$ mice.

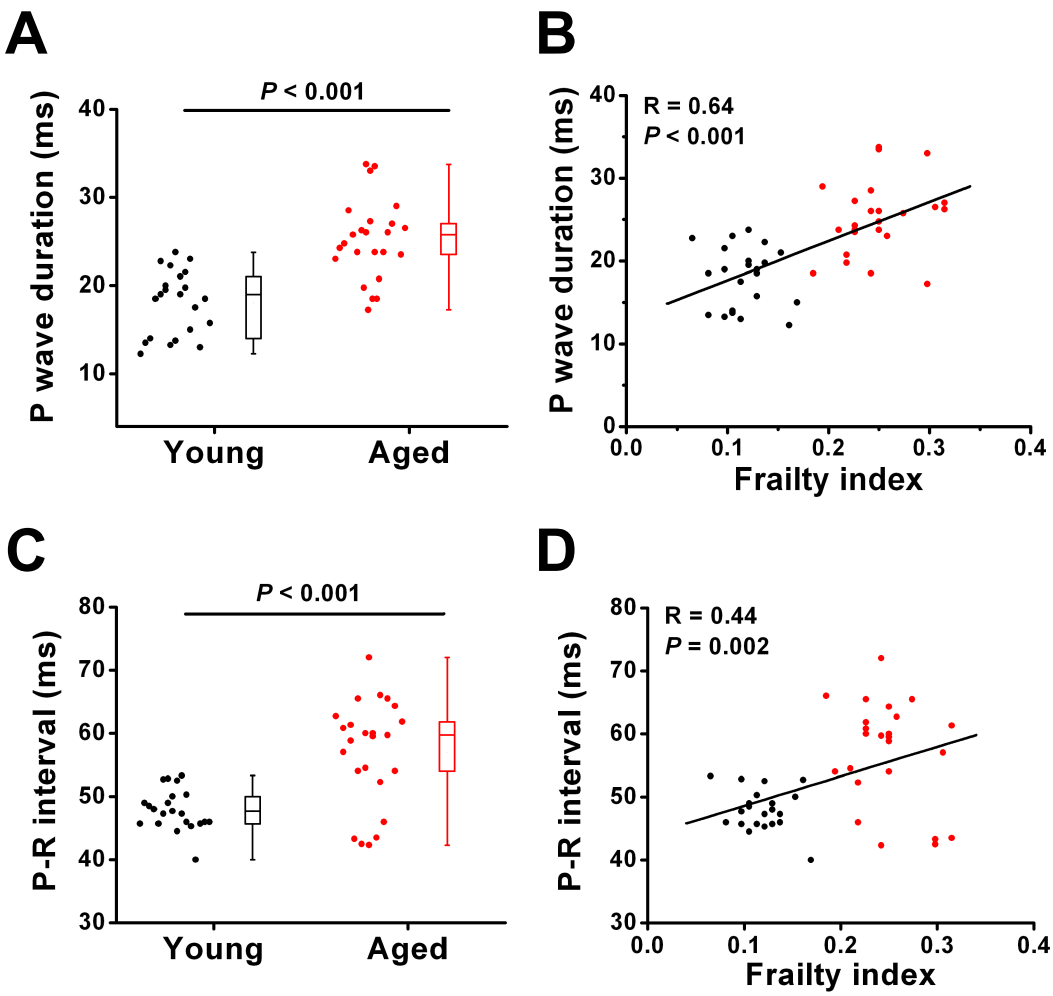
A
P < 0.001
P wave duration (ms)
40
30
20
10
Young
Aged
B
R = 0.64
P < 0.001
P wave duration (ms)
40
30
20
10
0
0.0
0.1
0.2
0.3
0.4
Frailty index
C
P < 0.001
P-R interval (ms)
80
70
60
50
40
30
Young
Aged
D
R = 0.44
P = 0.002
P-R interval (ms)
80
70
60
50
40
30
0.0
0.1
0.2
0.3
0.4
Frailty index

Figure 6.6

Figure 6.7. Correlation between P wave duration or P-R interval and AF duration in young and aged mice that were induced into AF.

A. Linear regression analysis illustrating the relationship between P wave duration and AF duration in young and aged mice induced into AF. **B.** Linear regression analysis illustrating the relationship between P-R interval and AF duration in young and aged mice induced into AF. Correlation coefficients obtained using Pearson's correlation. $n = 4$ young and 4 aged mice.

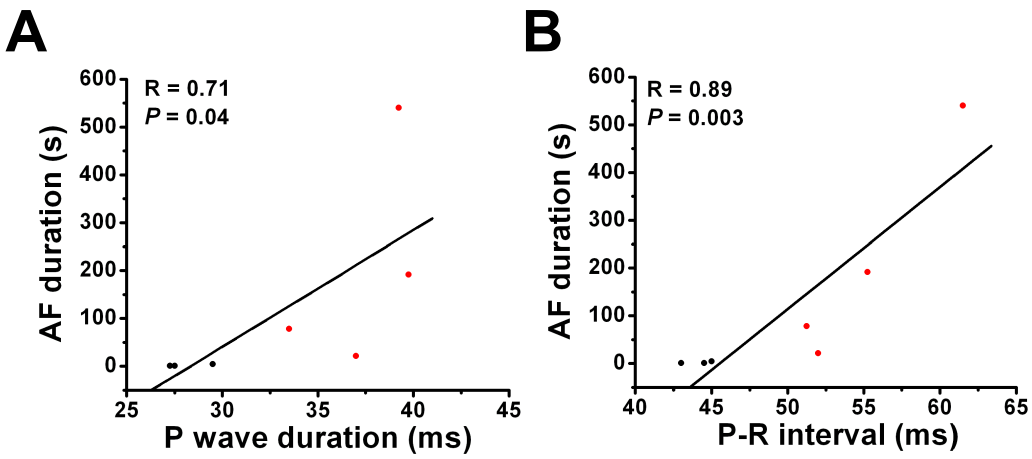
A
R = 0.71
P = 0.04
AF duration (s)
P wave duration (ms)
B
R = 0.89
P = 0.003
AF duration (s)
P-R interval (ms)

Figure 6.7

6.5. Effects of age and frailty on heart rate, P wave duration, and P-R interval following autonomic nervous system blockade in anaesthetized wildtype mice

The goal of the next set of experiments was to determine the effects of age and frailty on heart rate, P wave duration, and P-R interval in the presence of autonomic nervous system blockade. In this set of experiments, a subset of young and aged mice were subjected to a combined intraperitoneal injection of atropine and propranolol (10 mg/kg) to block muscarinic and β-adrenergic receptors, respectively.

Representative surface ECG recordings at baseline and following autonomic nervous system blockade in a young and aged mouse are presented in Figs. 6.8A and 6.8B. Summary data (Fig. 6.8C) demonstrates that application of atropine and propranolol reduces ($P < 0.001$) heart rate in young and aged mice compared to baseline measurements. Furthermore, heart rate remained lower ($P = 0.006$) in aged vs. young mice following autonomic nervous system blockade. When plotted as a function of FI score, heart rate was graded by FI score at baseline ($P = 0.003$; Fig. 6.8D) and in the presence of autonomic nervous system blockade ($P = 0.05$; Fig. 6.8E). Combined, these data demonstrate intrinsic SAN function is impaired in aged mice and an increase in FI score is correlated with a decline in SAN function.

Next, the effects of autonomic nervous system blockade on P wave duration and P-R interval were assessed in young and aged mice. P wave duration was increased in the presence of autonomic nervous system blockade in young ($P < 0.001$) and aged ($P < 0.001$) mice (Fig. 6.9A) compared to baseline measurements. Furthermore, P wave duration remained prolonged ($P < 0.001$) in the presence of autonomic nervous system blockade in aged mice vs. young mice. When plotted as a function of each individual's FI score, it was apparent that P wave duration was graded by FI score at baseline ($P < 0.001$, Fig. 6.9B) and in the presence of autonomic nervous system blockade ($P = 0.02$; Fig. 6.9C). P-R interval was prolonged in the presence of atropine and propranolol ($P < 0.001$) in young ($P = 0.018$) and aged ($P < 0.001$) mice, as summarized in Fig. 6.10A. In addition, P-R interval was prolonged to a greater extent ($P < 0.001$) in aged mice compared to young mice in the presence of autonomic nervous system blockade. When

Figure 6.8. Effects of age and frailty on heart rate following autonomic nervous system blockade in anaesthetized mice.

A. and **B.** Representative ECG recordings at baseline and following a combined intraperitoneal injection of atropine and propranolol (10 mg/kg) to block the autonomic nervous system in young (A) and aged (B) mice. **C.** Summary data illustrating the effects of autonomic nervous system blockade on heart rate in young and aged mice. $^{*}P < 0.05$ vs. baseline, $^{+}P < 0.05$ vs. young. Data analysed by two-way repeated measures ANOVA with Tukey's post hoc test. $n = 17$ young and 16 aged mice. **D** and **E.** Linear regression analysis of heart rate at baseline (D) and following autonomic blockade (E) as a function of FI score for the same mice as used in panel C. Correlation coefficients obtained using Pearson's correlation. $n = 33$ mice.

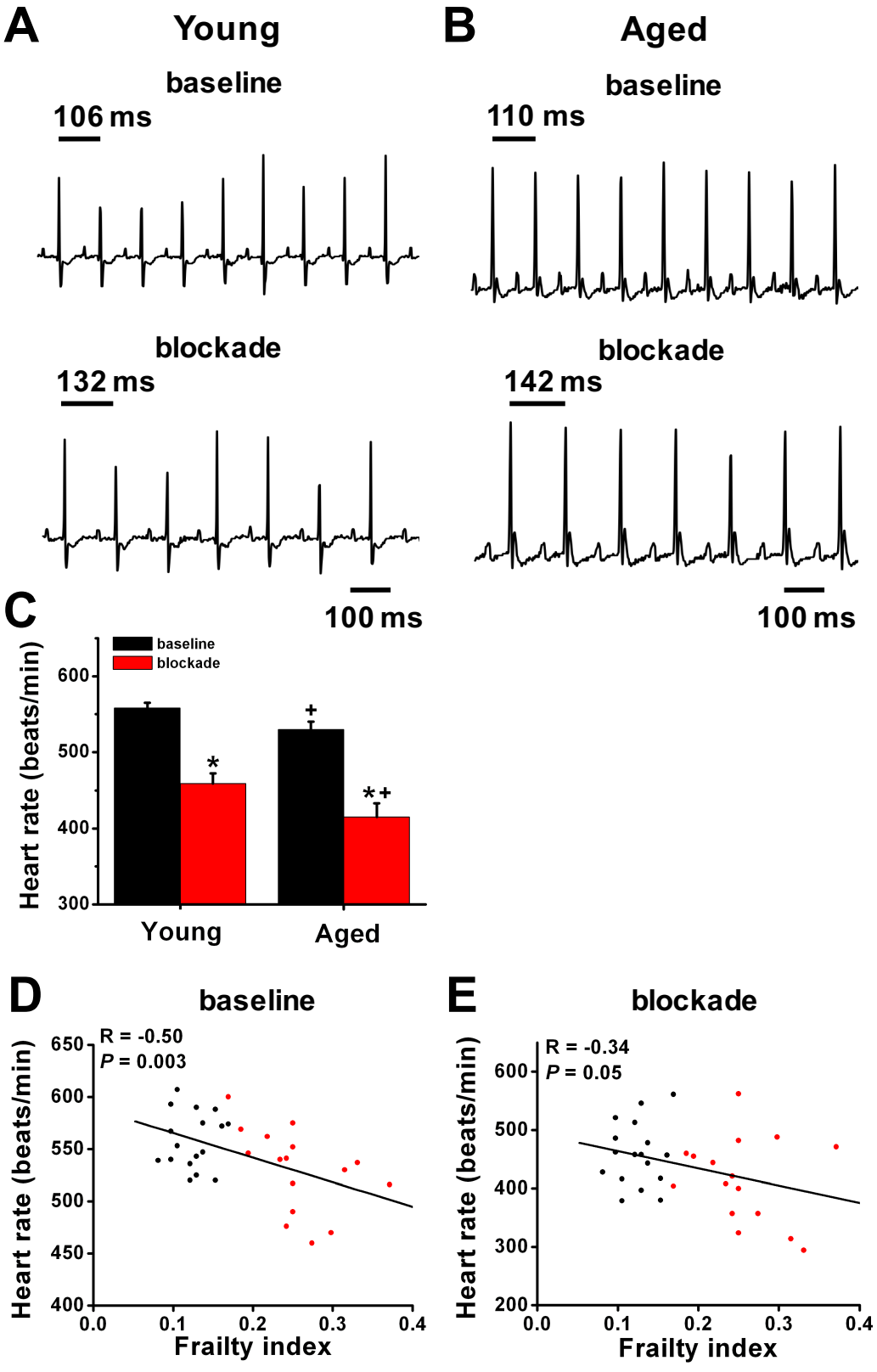
A
Young
baseline
106 ms
blockade
132 ms
100 ms
B
Aged
baseline
110 ms
blockade
142 ms
100 ms
C
baseline
blockade
Heart rate (beats/min)
600
500
400
300
*
+
*+
Young
Aged
D
baseline
R = -0.50
P = 0.003
Heart rate (beats/min)
650
600
550
500
450
400
0.0
0.1
0.2
0.3
0.4
Frailty index
E
blockade
R = -0.34
P = 0.05
Heart rate (beats/min)
600
500
400
300
200
0.0
0.1
0.2
0.3
0.4
Frailty index

Figure 6.8

Figure 6.9. Effects of age and frailty on P wave duration following autonomic nervous system blockade in anaesthetized mice.

A. Summary data illustrating the effects of autonomic nervous system blockade on P wave duration in young and aged mice. $^{*}P < 0.05$ vs. baseline, $^{+}P < 0.05$ vs. young. Data analysed by two-way repeated measures ANOVA with Tukey's post hoc test. $n = 11$ young and 11 aged mice. **B.** and **C.** Linear regression analysis of P wave duration at baseline (B) and following autonomic nervous system blockade (C) for the same mice as used in panel A. Correlation coefficients obtained using Pearson's correlation. $n = 22$ mice.

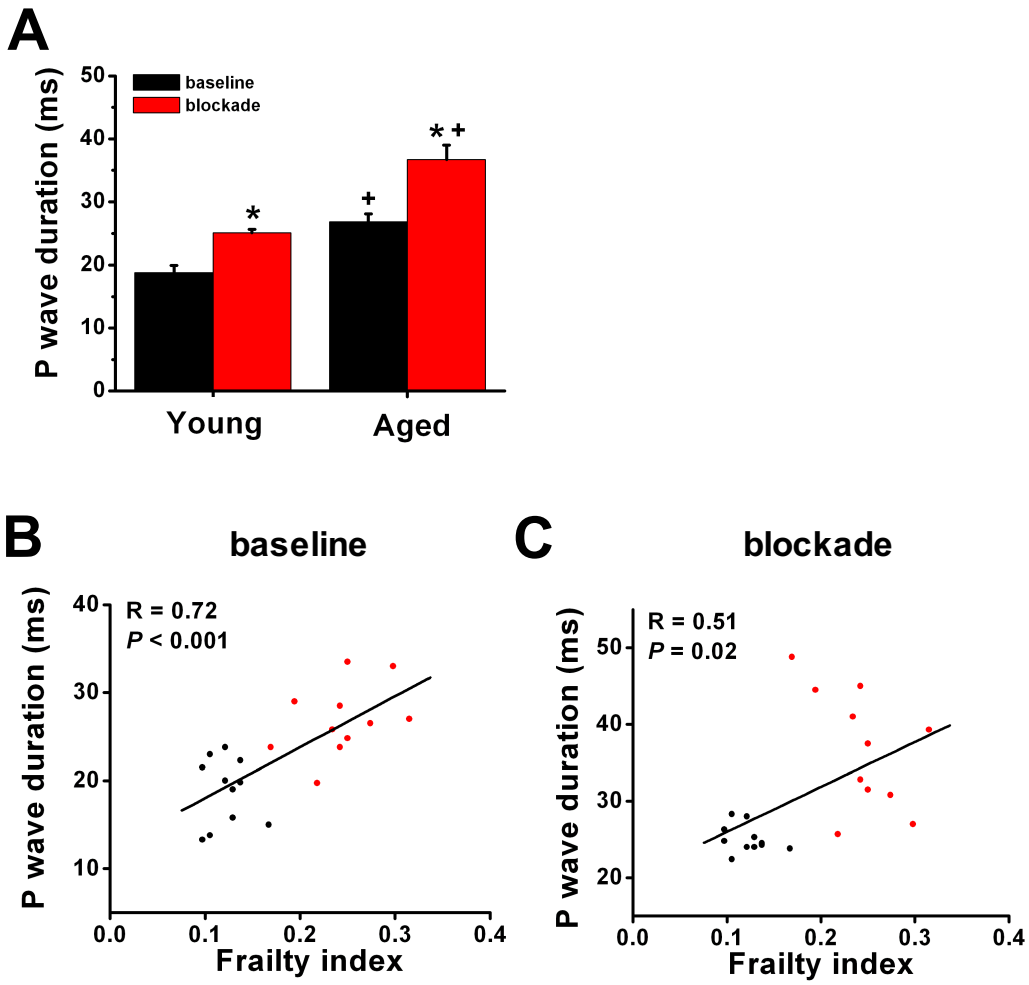
A
baseline
blockade
P wave duration (ms)
50
40
30
20
10
0
*
+
* +
Young
Aged
B
baseline
R = 0.72
P < 0.001
P wave duration (ms)
40
30
20
10
0.0
0.1
0.2
0.3
0.4
Frailty index
C
blockade
R = 0.51
P = 0.02
P wave duration (ms)
50
40
30
20
0.0
0.1
0.2
0.3
0.4
Frailty index

Figure 6.9

Figure 6.10. Effects of age and frailty on P-R interval following autonomic nervous system blockade in anaesthetized mice.

A. Summary data illustrating the effects of autonomic nervous system blockade on P-R interval in young and aged mice. $^{*}P < 0.05$ vs. baseline, $^{+}P < 0.05$ vs. young. Data analysed by two-way repeated measures ANOVA with Tukey's post hoc test. $n = 11$ young and 11 aged mice. **B.** and **C.** Linear regression analysis of P-R interval at baseline (B) and following autonomic blockade (C) as a function of FI score for the same mice as used in panel A. Correlation coefficients obtained using Pearson's correlation. $n = 22$ mice.

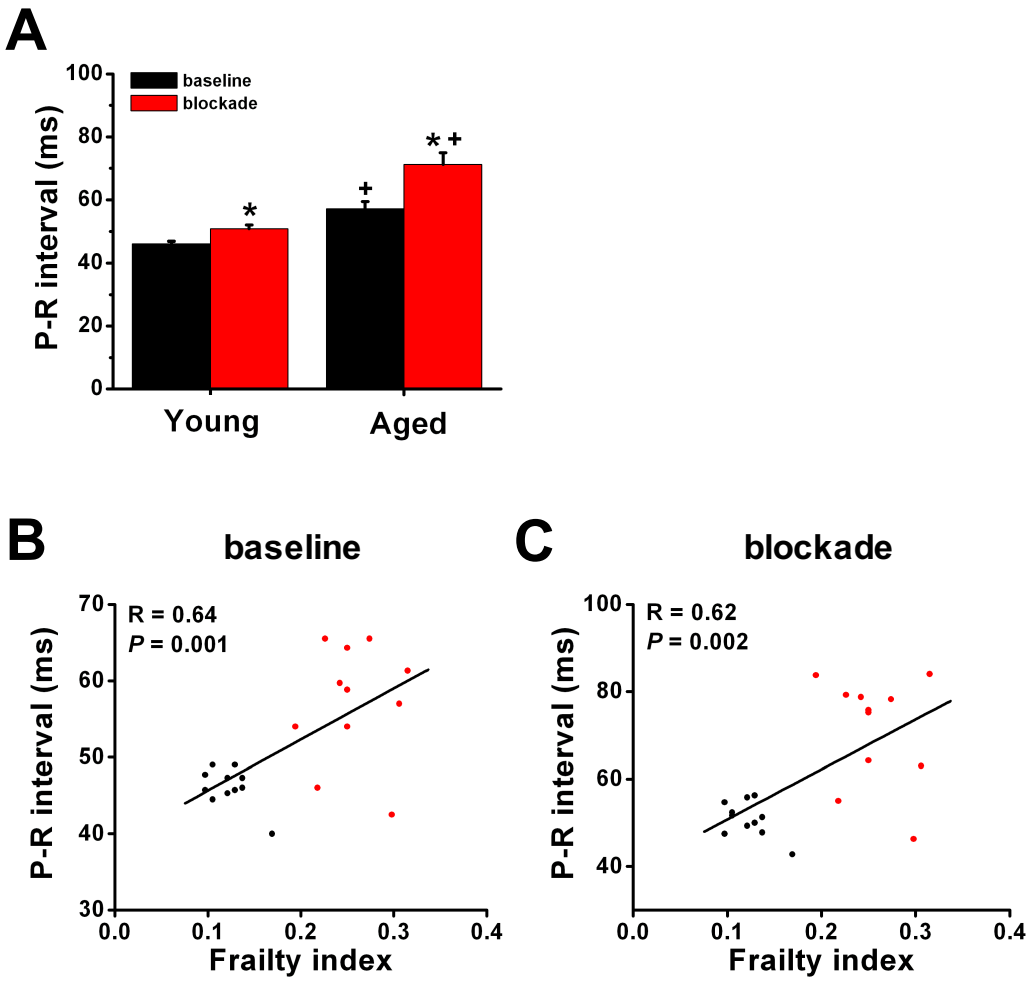
A
baseline
blockade
P-R interval (ms)
100
80
60
40
20
0
*
*+
+
Young
Aged
B
baseline
R = 0.64
P = 0.001
P-R interval (ms)
70
60
50
40
30
0.0
0.1
0.2
0.3
0.4
Frailty index
C
blockade
R = 0.62
P = 0.002
P-R interval (ms)
100
80
60
40
0.0
0.1
0.2
0.3
0.4
Frailty index

Figure 6.10

analyzed as a function of FI score, P-R interval was graded by FI score under baseline conditions ($P = 0.001$; Fig. 6.10B) and in the presence of autonomic blockade ($P = 0.002$; Fig. 6.10C). Taken together, these data demonstrate that independent of the autonomic nervous system, there is a slowing of conduction across the atrium and through the AV node. Furthermore, this slowing occurs in association with increasing frailty, and therefore an increase in biological age, such that mice with higher FI scores have a greater prolongation in conduction times in these regions compared to mice with lower FI scores, regardless of chronological age.

CHAPTER 7
DISCUSSION

7.1. Overview of key findings

My studies demonstrate that Ang II treatment is associated with SAN dysfunction and increased susceptibility to sustained forms of AF. These occurred in association with a reduction in heart rate, prolongation in atrial and AV node conduction times as well as prolongations in AERP and AVERP measurements. Patch-clamp studies revealed that the atrial AP is prolonged in association with reductions in I_{to} and I_{Kur} in Ang II treated right atrial myocytes. Strikingly, V_{max} and AP overshoot were reduced and AP was prolonged to a greater extent in Ang II treated left atrial myocytes. This occurred in association with reductions in I_{Na}, I_{to}, and I_{Kur}.

My experiments also show that Ang II treatment in NPR-$C^{-/-}$ mice was associated with more severe SAN dysfunction and susceptibility to more severe forms of AF. In fact, 82% of Ang II treated NPR-$C^{-/-}$ mice were induced into AF and when induced, AF lasted longer than 5 seconds in 56% of mice. P wave duration, P-R interval, AERP, and AVERP were prolonged to a greater extent in Ang II treated NPR-$C^{-/-}$ mice compared to Ang II treated NPR-$C^{+/+}$ mice. In right atrial myocytes, the extent of electrical remodelling was the same in Ang II treated NPR-$C^{-/-}$ and NPR-$C^{+/+}$ mice, based on AP morphology and K^+ current recordings. In contrast, left atrial myocytes exhibited a greater reduction in V_{max} and greater AP prolongation in NPR-$C^{-/-}$ mice treated with Ang II, whereas the reduction in K^+ currents was comparable to Ang II treated NPR-$C^{+/+}$ mice.

Concomitant treatment with the NPR-C agonist cANF (0.1 mg/kg/min) substantially improved SAN and atrial function *in vivo* in Ang II treated wildtype mice. In addition, mice co-treated with Ang II and cANF (0.1 mg/kg/min) had a lower susceptibility to AF, and when induced, AF was transient and lasted less than 5 seconds in all cases. Right atrial AP morphology and K^+ currents were normalized in mice co-treated with Ang II and cANF (0.1 mg/kg/min) compared to saline controls, indicating an attenuation in Ang II induced electrical remodelling in the setting of chronic NPR-C activation. In contrast,

there were no improvements in left atrial AP morphology or K^+ currents in mice co-treated with Ang II and cANF (0.1 mg/kg/min).

The effects of age and frailty on SAN and atrial function were investigated using a mouse model of ageing. My experiments demonstrate an age-related decline in heart rate and SAN function. When assessed as a function of frailty, it was observed that both heart rate and cSNRT were graded by FI score. In addition, AF was more severe when induced in frail mice and frail mice had an increased prevalence of AV node block. This occurred in association with prolonged conduction times across the atrial myocardium and through the AV node. Importantly, these measures were positively correlated with FI score. These findings demonstrate that FI score is a powerful predictor of SAN and atrial function *in vivo*.

7.2. Effects of Ang II treatment on SAN and atrial function in wildtype mice

In the present study, Ang II treatment reduced heart rate and prolonged cSNRT under baseline conditions. To directly assess intrinsic SAN function *in vivo*, heart rate was measured in the presence of autonomic nervous system blockade, as we have done previously (Egom *et al.*, 2015). Intraperitoneal injection of atropine and propranolol resulted in a decline in heart rate throughout the time course of the experiment. In addition, heart rate was lower in Ang II treated mice at all time points compared to saline treated mice. This further demonstrates that intrinsic SAN function is impaired in Ang II treated mice. In addition, Ang II treatment significantly increased systolic blood pressure during the three-week treatment period. Collectively, these results are highly consistent with previous studies demonstrating bradycardia, SAN dysfunction, and hypertension in Ang II treated mice (Ji *et al.*, 2010; Swaminathan *et al.*, 2011; Purohit *et al.*, 2013).

These *in vivo* data demonstrate that intrinsic function of the SAN is impaired in Ang II treated mice. SAN dysfunction can arise from structural and electrical remodelling within the SAN. In a previous study, Ang II treatment was associated with increased SAN myocyte apoptosis and increases fibrosis (Swaminathan *et al.*, 2011), indicating the presence of structural remodelling in the SAN. In addition, a reduction in heart rate can also result from a reduction in SAN automaticity that arises from electrical remodelling

in SAN myocytes. This can include a downregulation in several ion currents including I_f, $I_{Ca,T}$, and $I_{Ca,L}$ (Mangoni and Nargeot, 2008; Choudhury *et al.*, 2015). Reductions in these currents are consistent with a reduction in diastolic depolarization slope, AP firing rate, and slowing of SAN conduction velocity. The underlying mechanisms for SAN dysfunction in Ang II treated mice is currently being investigated in the Rose laboratory.

In the present study, Ang II treated mice had an increased susceptibility to AF. AF was induced in 8% of saline treated mice and when induced, AF lasted less than 5 seconds before reverting back to spontaneous sinus rhythm in all cases. In contrast, 50% of Ang II treated wildtype mice were induced into AF. AF durations were longer in Ang II treated mice and lasted longer than 5 seconds in 40% of mice induced into AF. These findings are consistent with previous studies demonstrating that Ang II treated mice have an increased susceptibility to more severe forms of AF (Fukui *et al.*, 2013; Swaminathan *et al.*, 2011; Westermann *et al.*, 2012; Purohit *et al.*, 2013). This data is also highly consistent with clinical data showing that AF is highly prevalent in patients with hypertensive heart disease (Verkerk *et al.*, 2003; Sanders *et al.*, 2003; Medi *et al.*, 2011).

P wave duration and P-R interval are powerful predictors of both the severity and susceptibility to AF (Magnani *et al.*, 2013; Censi *et al.*, 2016; Conte *et al.*, 2017; Smith *et al.*, 2017). In the present study, P wave duration and P-R interval were prolonged in Ang II treated animals. This is consistent with clinical data demonstrating slowed conduction times in patients with hypertension as well as animal models of hypertension and hypertrophy (Kistler *et al.*, 2006; Lau *et al.*, 2010; Medi *et al.*, 2011; Cooley *et al.*, 2013; Parikh *et al.*, 2013; Vaidean *et al.*, 2016). Autonomic nervous system blockade increased P wave duration and P-R interval in both saline and Ang II treated mice compared to baseline measurements. Furthermore, Ang II treated mice exhibited a greater prolongation in atrial and AV node conduction times in the presence of autonomic nervous system blockade compared to saline treated mice. These data demonstrate the prolongation in P wave duration and P-R interval in Ang II treated mice is attributed, at least in part, to alterations occurring within the atria and AV node, respectively. These prolonged conduction times also create a substrate for AF. Prolonged conduction times allow the refractory pathway to recover from activation and become re-excitable (Nattel

et al., 2007). Therefore, the propagating wave front or triggered activity could re-excite the tissue and sustain fibrillatory activities in the atria.

Slowed conduction across the atrial myocardium and through the AV node can result from electrical remodelling (Allessie *et al.*, 2001; Milnes *et al.*, 2012). In the present study, measures of both AERP and AVERP were prolonged in Ang II treated mice, indicating electrical remodelling in both the atria and the AV node. These findings are consistent with observations made in patients with hypertension and in animal models (Lau *et al.*, 2010; Medi *et al.*, 2011). Consistent with the increase in AERP, AP was prolonged in right and left atrial myocytes. Mechanistically, AP prolongation can contribute to the generation of triggers for AF. Excessive AP prolongation allows ion channels to recover from inactivation and can result in the generation of EADs. Adverse electrical remodelling can also generate DADs. Although not assessed in this study, a previous study demonstrated that DADs are present in atrial myocytes from Ang II treated mice (Purohit *et al.*, 2013). Functional requirements, including a vulnerable substrate, unidirectional block, and slowed conduction, are required to sustain re-entrant circuits during AF (Van Wagoner and Nerbonne, 2000; Schmitt *et al.*, 2014). In the present study, atrial conduction is slowed, as determined by a prolongation in P wave duration. In addition, AERP and APD are prolonged, which can create regions of unidirectional block. Combined, these mechanisms can underly the increased susceptibility to AF in Ang II treated mice.

Alterations in atrial electrophysiology was characterized by recording APs and ion currents in right and left atrial myocytes from Ang II treated mice. Strikingly, measures of both V_{max} and AP overshoot were significantly reduced in left atrial myocytes following Ang II treatment but remained unchanged in right atrial myocytes. I_{Na} is a critical determinant of V_{max} and AP overshoot (Kleber and Rudy, 2004). In agreement with this, I_{Na} was reduced in left, but not right, atrial myocytes from Ang II treated mice. Furthermore, I_{Na} and V_{max} are key determinants of conduction velocity (Kleber and Rudy, 2004; Nerbonne and Kass, 2005; Rook *et al.*, 2012; Detta *et al.*, 2015). Accordingly, reductions in I_{Na} and V_{max} can contribute to a greater reduction in conduction velocity specifically in the left atrium of Ang II treated mice. A regional difference in conduction velocity has been demonstrated in a previous study on Ang II treated mice using optical

mapping (Swaminathan *et al.*, 2011). In this study, the authors observed a greater reduction in conduction velocity across the left atrium compared to the right atrium of Ang II treated mice. Reductions in conduction velocity in the atria will contribute to the prolongation of the P wave duration (a measure of atrial conduction time) observed *in vivo*.

The reduction in I_{Na} density in Ang II treated left atrial myocytes occurred in association with a reduction in G_{max}. Analysis of activation kinetics revealed that $V_{1/2(act)}$ and the slope factor remained unchanged in Ang II treated left atrial myocytes. *SCN5a* (encodes $Na_V1.5$) mRNA expression remained unchanged in left atrial myocytes from Ang II treated mice, indicating that a reduction in mRNA expression does not account for the reduction in I_{Na} density or G_{max} in the left atria of Ang II treated mice. However, it is possible that mRNA transcripts are degraded post transcriptionally and therefore $Na_V1.5$ protein expression would be reduced independently of *SCN5a* mRNA expression. Alternatively, $Na_V1.5$ protein folding or insertion into the cellular membrane may be impaired in Ang II treated mice. Accordingly, additional experiments are required to quantify $Na_V1.5$ protein expression and characterize cellular localization in Ang II treated mice. In addition, it is possible that the reduction in I_{Na} density is attributed to cell hypertrophy. Cell capacitance is an indirect measure of cell size and is associated with cellular hypertrophy (Nattel, 2008). Current densities can therefore be reduced if cell capacitance increases without changes in ion channel expression. This could explain the observation that I_{Na} density is reduced in Ang II treated left atrial myocytes without a change in *SCN5a* mRNA expression.

Several post-translational modifications have been shown to reduce I_{Na}. In the Ang II type 1 receptor (AT1R) overexpression model, AT1R expression is driven by an α-MHC promoter and results in an increase in AT1R expression that is specifically restricted to cardiomyocytes (Paradis *et al.*, 2000; Rivard *et al.*, 2008, Rivard *et al.*, 2011; Mathieu *et al.*, 2016). This results in a cardiac specific increase in Ang II signalling that occurs independently of hypertension. 50 day old mice lack cardiac hypertrophy and structural remodelling, whereas cardiac hypertrophy is present in AT1R mice by the age of 6 months. Therefore, observations made in 50 day old AT1R mice are a direct result of increased Ang II/AT1R signalling. In ventricular myocytes isolated from AT1R mice,

V_{max} was reduced at 50 days and 6 months and was associated with a reduction in I_{Na} (Mathieu *et al.*, 2016). In 50 day mice, the reduction in I_{Na} occurred independently of alterations in *SCN5a* mRNA expression or $Na_V1.5$ protein expression. However, in 6 month old mice, both *SCN5a* mRNA and $Na_V1.5$ protein expression were reduced. It is important to note that the magnitude of reduction in I_{Na} was the same in 50 day and 6 month old mice. Therefore, it occurred independently of altered $Na_V1.5$ protein expression and cellular hypertrophy (Mathieu *et al.*, 2016). In this study, the reduction in I_{Na} was attributed to increased PKCα signalling, which is increased by enhanced Ang II signalling (Mathieu *et al.*, 2016). Additional experiments are required to determine if the reduction in I_{Na} observed in Ang II treated left atrial myocytes is attributed to PKCα signalling. $Na_V1.5$ also contains multiple phosphorylation sites for CaMKII. Ang II signalling increases the activity of ox-CaMKII, which is a constitutively active form of CaMKII (Swaminathan *et al.*, 2011; Purohit *et al.*, 2013). In addition, previous studies have demonstrated that CaMKII mediated phosphorylation of $Na_V1.5$ can reduce peak I_{Na} (Abriel, 2010; Wagner *et al.*, 2011; Detta *et al.*, 2015). Accordingly, additional experiments are required to determine if the reduction in peak I_{Na} observed in left atrial myocytes from Ang II mice is attributed to CaMKII activity.

In recent years, it has become evident that the late I_{Na} plays a role in arrhythmogenesis and cardiac disease. Late I_{Na} plays a role in creating a window current that can contribute to AP prolongation and the generation of EAD and DADs (Song *et al.*, 2008; Belardinelli *et al.*, 2015). It is important to note that although peak I_{Na} and late I_{Na} are conducted by $Na_V1.5$, the currents are not mutually exclusive (Makielski, 2016). Therefore, it is possible that late I_{Na} is increased in Ang II treated myocytes from the right atria as well as the left atria where peak I_{Na} is reduced. Previous studies have indicated that Ang II is associated with an increase in late I_{Na}, and enhanced late I_{Na} density has been documented in patients and animal models of cardiac hypertrophy, heart failure, and AF (Coppini *et al.*, 2013; Belardinelli *et al.*, 2015; Makielski, 2016). In addition, a study has shown that late I_{Na} is increased specifically in left atrial myocytes and not altered in right atrial myocytes from rabbits with ventricular hypertrophy (Guo *et al.*, 2010). The authors also observed EADs in left atrial myocytes. Accordingly, additional experiments

to elucidate the role of the late I_{Na} in right and left atrial myocytes from Ang II treated mice will be insightful.

Ang II treatment resulted in a prolongation in AP duration in right and left atrial myocytes and is consistent with the increase in AERP observed *in vivo.* AP prolongation was attributed to reductions in outward K^+ current densities recorded in the presence and absence of an inactivating pre-pulse in right and left atrial myocytes from Ang II treated mice. The reduction in total outward K^+ currents was attributed to reductions in both I_{to} and I_{Kur} densities in Ang II treated right and left atrial myocytes. The reduction in I_{Kur} was comparable between right and left atrial myocytes. These data are consistent with previous studies demonstrating that Ang II signalling reduces peak K^+ current, I_{to}, and I_{Kur} in ventricular myocytes (Rivard *et al.*, 2008; Tozakidou *et al.*, 2010). In addition, AP prolongation and a reduction in I_{to} density have been observed in animal models of hypertension, hypertrophy, and heart failure (Perrier *et al.*, 2004; Rose *et al.*, 2005; Marionneau *et al.*, 2008; Zhang *et al.*, 2014; Kim *et al.*, 2017).

Strikingly, Ang II treatment was associated with a greater reduction in outward K^+ currents and I_{to} in left atrial myocytes compared to right atrial myocytes. This is consistent with the greater AP prolongation observed in Ang II treated left atrial myocytes. A regional difference in AP duration has been demonstrated in previous studies (Cabellero *et al.*, 2010; Sirish *et al.*, 2016). In a pressure overload model in mice, one study demonstrated a greater prolongation of APD and ERP in the left atria compared to the right atria in optical mapping experiments (Sirish *et al.*, 2016). In another study, I_{to} was reduced to a greater extent in left atrial myocytes compared to right atrial myocytes from patients with chronic AF (Cabellero *et al.*, 2010). The significance of these regional differences requires further investigation.

In addition to outward K^+ currents, inward K^+ currents negative to -100 mV were reduced specifically in Ang II treated left atrial myocytes. Sensitivity to $BaCl_2$ was used to ascertain if this was associated with a reduction in I_{K1} in left atrial myocytes from Ang II treated mice. However, there were no differences in sensitivity to $BaCl_2$ which indicates that I_{K1} is not altered in Ang II treated mice and is consistent with the AP data that demonstrated RMP is unaltered in Ang II treated mice. This indicates these

reductions in inward K^+ currents (negative to -100 mV) in left atrial myocytes are attributed to a different, yet to be identified current.

Alterations in background K^+ currents could partially explain the regional differences in K^+ currents observed in Ang II treated mice. Two-pore-domain K^+ channels, including the stretch-sensitive $K_{2P}2.1$(TREK-1) and $K_{2P}10.1$ (TREK-2) and $K_{2P}3.1$ (TASK-1) channels, are expressed in the atria in humans and mice (Goldstein *et al.*, 2001; Limberg *et al.*, 2011; Schmidt *et al*., 2017). In addition, $K_{2P}2.1$ protein expression is higher in the left atrium compared to the right atrium, and expression is reduced in patients with heart failure and AF, as well as in animal models of AF. In addition, $K_{2P}3.1$ (TASK-1) is expressed in the human and mouse heart (Goldstein *et al*., 2001; Limberg *et al.*, 2011). Pharmacological blockade of this channel is associated with an increase in APD_{50} and APD_{90} in isolated human atrial myocytes (Limberg *et al.*, 2011). Accordingly, reductions in these background currents could contribute to the greater prolongation in AP observed in the left atria of Ang II treated mice compared to the right atria.

Increased systemic blood pressure increases pressures exerted on the left atrium and is associated with atrial remodelling (Mensah *et al.,* 2003; Prisant, 2005; Abhayaranta *et al.*, 2006; Beigel *et al.*, 2014). In addition, ANP expression is increased in response to atrial distension (Pandey, 2005; Volpe *et al.*, 2016). Studies presented in this thesis demonstrate that cell capacitance is specifically increased in left atrial myocytes from Ang II treated mice and *Nppa* (encodes ANP) mRNA expression is substantially increased in the left atrium. In contrast, neither cell capacitance nor *Nppa* mRNA expression were altered in the right atrium of Ang II treated mice. This indicates an increase in left atrial pressure in Ang II treated mice. Accordingly, the increased pressures exerted on the left atrium in Ang II treated mice can further contribute to the regional differences in atrial electrophysiological remodelling observed in the present study.

In the Ang II treated left atrium, qPCR experiments revealed important reductions in *KCND2* (encodes $K_V4.2$)*, KCND3* (encodes $K_V4.3$), and *KCNIP2* (encodes KChIP2) mRNA levels compared to saline treated controls. The reductions in mRNA expression of these genes correlates with the reduction in I_{to} density in the left atria of Ang II treated mice. Additional experiments are needed to quantify protein expression. It is also

possible that cell capacitance, which is specifically increased in Ang II treated left atrial myocytes, contributes to the greater reduction in I_{to} density observed in left atrial myocytes.

In this study, gene expression patterns did not always correlate with current densities in Ang II treated mice. In the right atria, I_{to} and I_{Kur} densities were reduced however *KCND2* (encodes $K_V4.2$), *KCND3* (encodes $K_V4.3$), *KCNIP2* (encodes KChIP2), and *KCNA5* (encodes $K_V1.5$) mRNA expression remained unaltered in Ang II treated mice. In the left atria, *KCNA5* mRNA expression was increased in Ang II treated mice, but I_{Kur} was reduced. It is important to note that mRNA expression does not always correlate with protein expression. This has been demonstrated in previous studies where a reduction in I_{to} and I_{Kur} density was observed without alterations in *KCND2, KCND3,* or *KCNA5* mRNA expression. In these studies, $K_V4.2$, $K_V4.3$, and $K_V1.5$ protein expression was reduced in the diseased heart, indicating post transcriptional regulation of these mRNA transcripts (Rose *et al.*, 2005; Marionneau *et al.*, 2008; Rivard *et al.*, 2008). Accordingly, it is possible that protein expression, rather than mRNA expression, is altered for $K_V4.2$, $K_V4.3$, KChIP2, and $K_V1.5$ in Ang II treated mice and would result in a reduction in I_{to} and I_{Kur}. Furthermore, there is evidence to suggest that AT1R regulates surface expression of $K_V4.3$ (Doronin *et al.*, 2004; Ehrlich *et al.*, 2006). Following Ang II activation, it is thought that the AT1R-$K_V4.3$ complex is internalized. This may be a mechanism by which Ang II reduces I_{to} without altering *KCND3* mRNA expression. These are areas requiring further investigation.

In the current study, I_{to} and I_{Kur} were reduced in right and left atrial myocytes from Ang II treated wildtype mice. In addition, the reductions in the right atria occurred independent of a change in cell capacitance or gene expression patterns for ion channel subunits. This indicates that the reductions in I_{to} and I_{Kur} may be attributed to alterations in signalling pathways in Ang II treated mice. The C-terminal domains of $K_V4.2$ and K_V-4.3 contain phosphorylation sites for PKA, PKC, PKG, CaMKII, and ERK (van der Heyden *et al.*, 2006; Niwa and Nerbonne, 2010). PKC isoforms also reside in a macromolecular complex that contains $K_V1.5$ (David *et al.*, 2012). Although poorly understood, there is evidence to suggest PKA, PKC, endothelin-1 and CaMKII activity inhibit I_{to} (Hagiwara *et al.*, 2003; van der Heyden *et al.*, 2006; Udyavar *et al.*, 2008;

Wagner *et al.*, 2009). Future experiments are required to determine whether any of these candidate pathways contributes to the reductions in I_{to} and I_{Kur} density observed in Ang II treated atrial myocytes.

Impaired AP repolarization can arise from reductions in outward K^+ currents and/or increased Ca^{2+} currents (Nattel *et al.*, 2007; Grant, 2009; Amin *et al.*, 2010). In the present study, neither $I_{Ca,L}$ density nor activation kinetics were altered in Ang II treated right or left atrial myocytes. In addition, *CACNA1c* (encodes $Ca_V1.2$) and *CACNA1d* (encodes $Ca_V1.3$) mRNA expression remained unchanged in both the right and left atria of Ang II treated mice. This is consistent with a previous study that demonstrated chronic Ang II treatment does not affect $I_{Ca,L}$ in ventricular myocytes (Markandeya *et al.*, 2015). Taken together, these findings demonstrate that AP prolongation observed in Ang II treated right and left atrial myocytes is attributed to reductions in outward K^+ currents and occurs independently of Ca^{2+} currents.

The NP system has numerous cardioprotective roles in the heart. In the present study, *Npr1* (encodes NPR-A), *Npr2* (encodes NPR-B), and *Npr3* (encodes NPR-C) mRNA expression was not different in the right or left atrium of Ang II treated mice compared to saline treated mice within the same region. However, when compared to the right atrium of Ang II treated mice, *Npr1* mRNA expression was increased and *Npr3* mRNA expression was reduced in the left atrium of Ang II treated mice. A reduction in NPR-C expression has been described in heart homogenates extracted from spontaneously hypertensive rats and mice with dilated cardiomyopathy (Li *et al.*, 2014; Wang *et al.*, 2014). In addition, *Nppa* (encodes ANP) expression was increased specifically in the left atrium of Ang II treated mice. An increase *Nppa* mRNA expression has been documented in the left atria of dogs with heart failure and in the heart of mice with dilated cardiomyopathy (Ichiki *et al.*, 2012; Wang *et al.*, 2014). Combined, the altered NPR expression can have drastic effects on downstream signalling cascades that are modulated by NPR-A and NPR-C. Additional experiments are required to measure cGMP (increased with NPR-A activation) and cAMP (reduced with NPR-C activation) levels in Ang II treated mice as well as crosstalk between these two signalling pathways in the diseased heart.

Although not the focus of my thesis, structural remodelling can also contribute to the prolongation in atrial and AV node conduction times as well as the increased susceptibility to AF observed *in vivo.* In the present study, cell capacitance was increased in left atrial myocytes from Ang II treated mice, which is indicative of hypertrophy. Cellular hypertrophy can contribute to a delay in the electrical impulse propagation between adjacent myocytes and can prolong conduction time across the atrial myocardium (Kleber and Rudy, 2004). In addition, increased cell capacitance and a prolongation in the P wave duration is indicative of atrial enlargement (Hill, 2003; Kirchhof and Schotten, 2006). Accordingly, it is likely that Ang II treatment is associated with atrial enlargement, especially in the left atrial appendage, and can be confirmed in a series of echocardiography experiments.

Previous studies have demonstrated that Ang II treatment is associated with increased interstitial fibrosis (Erickson *et al.*, 2008; Tsai *et al.*, 2008; Wakui *et al.*, 2010; Wei *et al.*, 2017). Increased fibrosis can also contribute to the prolongation in conduction time across the atrial myocardium and can create a substrate for AF (Allessie *et al.*, 2001; Eckstein *et al.*, 2008; Schotten *et al.*, 2011). Increased levels of interstitial fibrosis can also facilitate the perpetuation of fibrillatory activity in the atria as fibrotic lesions create anatomical obstacles that impede conduction and promote the formation of re-entrant circuits (Iwasaki *et al.*, 2011; Schotten *et al.*, 2011; Jalife and Kaur, 2015). The mechanisms underlying increased atrial fibrosis in Ang II treated mice is currently under investigation in the Rose laboratory.

7.3. Effects of Ang II treatment on electrical remodelling in NPR-C$^{-/-}$ mice

Consistent with our previous work (Egom *et al.*, 2015), heart rate was not different and cSNRT was prolonged in saline treated NPR-C$^{-/-}$ mice compared to saline treated NPR-C$^{+/+}$ mice. Ang II treatment in NPR-C$^{-/-}$ mice resulted in greater SAN dysfunction compared to Ang II treatment in NPR-C$^{+/+}$ mice, as indicated by a greater reduction in baseline heart rate and a greater prolongation in cSNRT in Ang II treated NPR-C$^{-/-}$ mice compared to NPR-C$^{+/+}$ mice. Although not investigated in this thesis, these findings are indicative of a greater level of electrical and/or structural remodelling of the SAN in

NPR-C$^{-/-}$ mice compared to NPR-C$^{+/+}$ mice treated with Ang II. For example, there could be differences in electrical remodelling in SAN myocytes from Ang II treated NPR-C$^{-/-}$ mice compared to NPR-C$^{+/+}$ Ang II treated mice that may involve distinct alterations in ionic currents such as in I_f, $I_{Ca,L}$, $I_{Ca,T}$, and I_{Na}. Reductions in these currents could reduce the diastolic depolarization slope and reduce SAN automaticity (Mangoni and Nargeot, 2008). In addition, SAN dysfunction can occur in association with enhanced SAN fibrosis (Morris and Kalmna, 2014; Choudhury *et al.*, 2015). It is therefore possible that Ang II treated NPR-C$^{-/-}$ mice have higher levels of SAN fibrosis compared to Ang II treated NPR-C$^{+/+}$ mice, which could result in a greater reduction in SAN conduction velocity and fragmentation of the propagating wave front (Fedorov *et al.*, 2012). This would contribute to a prolongation in cSNRT. These areas are currently being investigated in the Rose laboratory.

Ang II treated NPR-C$^{-/-}$ mice had an increased susceptibility to AF. Saline treated NPR-C$^{-/-}$ mice had an increase in susceptibility to induced AF compared to saline treated NPR-C$^{+/+}$ mice, which is consistent with our previous work (Egom *et al.*, 2015). In particular, AF was induced in 56% of saline treated NPR-C$^{-/-}$ mice compared to 8% of saline treated NPR-C$^{+/+}$ mice. Strikingly, 82% of Ang II treated NPR-C$^{-/-}$ mice were induced into AF compared to 50% of Ang II treated NPR-C$^{+/+}$ mice. In addition, Ang II treated NPR-C$^{-/-}$ mice were induced into more severe forms of AF. For example, AF lasted less than 5 seconds in 60% of Ang II treated NPR-C$^{+/+}$ mice and 44% of Ang II treated NPR-C$^{-/-}$ mice. On the other hand, the duration of AF exceeded 25 seconds in 30% of Ang II treated NPR-C$^{-/-}$ mice before spontaneously reverting into normal sinus rhythm. In contrast, 13% of Ang II treated NPR-C$^{+/+}$ mice and 17% of saline treated NPR-C$^{-/-}$ mice were induced into AF that lasted longer than 25 seconds. Collectively, these data demonstrate that Ang II treatment in NPR-C$^{-/-}$ mice results in a more severe AF phenotype compared to NPR-C$^{+/+}$ mice. In addition, it suggests that NPR-C is cardioprotective against AF in disease settings.

The increase in AF susceptibility and severity was associated with a greater prolongation of P wave duration and P-R interval in Ang II treated NPR-C$^{-/-}$ mice compared to Ang II treated NPR-C$^{+/+}$ mice. This is in agreement with the concept that prolongations in P wave duration and P-R intervals correspond with an increased severity

of AF (Magnani *et al.* 2009; Weinsaft *et al.*, 2014; Conte *et al.*, 2017; Smith *et al.*, 2017). In NPR-$C^{+/+}$ mice, cell capacitance was specifically increased in left atrial myocytes from Ang II treated mice. In contrast, cell capacitance was increased in both right and left atrial myocytes from Ang II treated NPR-$C^{-/-}$ mice. This could contribute to the greater prolongation of P wave duration observed in Ang II treated NPR-$C^{-/-}$ mice compared to Ang II treated NPR-$C^{+/+}$ mice. Cell capacitance is an indirect measure of cell size and is indicative of hypertrophy (Dobrzynski *et al.*, 2013; Nattel, 2008). Accordingly, Ang II treatment in NPR-$C^{-/-}$ mice may be associated with global changes to atrial structure, including atrial dilation and hypertrophy. These global changes could contribute to the greater prolongation in conduction times observed in Ang II treated NPR-$C^{-/-}$ mice and is an area currently under investigation in the Rose laboratory. Increased patterns of interstitial fibrosis in the atria would result slowing of conduction across the atrial myocardium in Ang II treated NPR-$C^{-/-}$ mice. In addition, atrial fibrosis will result in increased dispersion of electrical signals within the atria that would fragment the propagating wave front (Nattel, 2002; King *et al.*, 2013). This would reduce atrial conduction time and increase the perpetuation of AF by increasing the number of re-entrant circuits. The underlying mechanisms of atrial fibrosis and patterns of conduction in Ang II treated NPR-$C^{-/-}$ mice are currently under investigation in the Rose laboratory.

Conduction velocity is dependent on cardiomyocyte coupling and V_{max} (Boyett, 2009). Accordingly, the greater reduction in V_{max} in Ang II treated left atrial myocytes from NPR-$C^{-/-}$ mice compared to Ang II treated NPR-$C^{+/+}$ mice can contribute to the greater prolongation in P wave duration observed *in vivo*. Although not statistically significant ($P = 0.08$), there was a trend towards a lower AP overshoot in NPR-$C^{-/-}$ mice compared to NPR-$C^{+/+}$ mice treated with Ang II. It is possible that I_{Na} is reduced to a greater extent in Ang II treated NPR-$C^{-/-}$ mice compared to Ang II treated NPR-$C^{+/+}$ mice and would explain the greater reduction in V_{max} observed in left atrial myocytes. Additional patch-clamp experiments are required to confirm this. In addition, it is also possible that gap junctions are altered in Ang II treated NPR-$C^{-/-}$ mice, which would further contribute to the prolongation in conduction times, although this would need to be confirmed.

Prolongations in P wave duration and P-R interval can occur in association with electrical remodelling. In this study, measures of both AERP and AVERP were prolonged to a greater extent in Ang II treated NPR-$C^{-/-}$ mice compared to NPR-$C^{+/+}$ mice treated with Ang II. This indicates a greater extent of electrical remodelling refractoriness in Ang II treated NPR-$C^{-/-}$ mice. AERP is a function of APD and post-repolarization refractoriness, which is determined by RMP (Milnes *et al.*, 2012). In the present study, left atrial myocytes from Ang II NPR-$C^{-/-}$ mice had a greater AP prolongation and a depolarized RMP compared to left atrial myocytes from Ang II treated NPR-$C^{+/+}$ mice. These alterations in AP morphology will contribute to the prolongation in AERP measured in Ang II treated NPR-$C^{-/-}$ mice.

The magnitude of AP prolongation was greater in Ang II treated left atrial myocytes from NPR-$C^{-/-}$ mice compared to NPR-$C^{+/+}$ mice. Analysis of K^+ currents revealed that outward K^+ currents and I_{to} were reduced to a similar extent in Ang II treated left atrial myocytes from NPR-$C^{-/-}$ mice and to NPR-$C^{+/+}$ mice. Only K^+ currents (measured with no pre-pulse and with pre-pulse protocols) and I_{to} were measured in the present study. However, it is possible that other ion currents are altered specifically in left atrial myocytes from Ang II treated NPR-$C^{-/-}$ mice that are not altered in Ang II treated NPR-$C^{+/+}$ mice. This could include an increase in $I_{Ca,L}$ that would prolong the AP or a reduction in I_{K1} that would prolong late repolarization and depolarize the RMP. In addition, an increase in late I_{Na} could increase the APD. Furthermore, AP prolongation is also associated with the generation of EADs that could create triggers that initiate AF (Nattel *et al.*, 2008). This could explain the increased susceptibility and severity of AF observed in Ang II treated NPR-$C^{-/-}$ mice. Needless to say, these are areas requiring further investigation.

Electrical remodelling in right atrial myocytes was comparable in Ang II treated NPR-$C^{-/-}$ and NPR-$C^{+/+}$ mice. Consistent with prior work (Egom *et al.*, 2015), AP morphology was not different in right atrial myocytes between saline treated NPR-$C^{-/-}$ and NPR-$C^{+/+}$ mice. In right atrial myocytes, Ang II treatment prolonged the AP without altering RMP, V_{max}, and AP overshoot in both NPR-$C^{-/-}$ and NPR-$C^{+/+}$ mice. Interestingly the magnitude of AP prolongation was comparable in Ang II treated NPR-$C^{-/-}$ and NPR-$C^{+/+}$ mice. In addition, patch-clamp recordings revealed that outward K^+ currents

(measured with no pre-pulse and with pre-pulse protocols) and I_{to} densities were not different in Ang II treated NPR-$C^{-/-}$ and NPR-$C^{+/+}$ mice. Taken together, these data demonstrate that the magnitude of Ang II induced electrical remodelling is the same in right atrial myocytes from NPR-$C^{-/-}$ and NPR-$C^{+/+}$ mice.

Collectively, these data demonstrate that Ang II treatment in results in a more severe phenotype in NPR-$C^{-/-}$ mice compared to NPR-$C^{+/+}$ mice. In addition, these data demonstrate that NPR-C signalling is protective against cardiovascular disease. To our knowledge, this is the first study to characterize electrical remodelling in isolated right and left atrial myocytes from NPR-$C^{-/-}$ mice in the setting of cardiovascular disease.

7.4. Effects of the NPR-C agonist cANF on Ang II treatment in wildtype mice

Co-treatment with the selective NPR-C agonist cANF elicited numerous protective effects in Ang II treated wildtype mice. In Ang II with cANF (0.1 mg/kg/min) treated mice, measures of heart rate and cSNRT were not different compared to saline treated controls. Additional experiments are required to determine the effects of cANF on SAN electrical and structural remodelling in the SAN. AF susceptibility was not different in mice co-treated with Ang II and cANF (0.1 mg/kg/min) compared to saline treated mice, and was significantly lower compared to mice treated with Ang II alone. In fact, 20% of mice co-treated with Ang II and cANF (0.1 mg/kg/min) were induced into AF and in each case the duration of AF was transient, lasting less than 5 seconds. In contrast, 50% of mice treated with Ang II alone were induced into AF. AF durations were between 5 and 25 seconds in 27% of mice and exceeded 25 seconds in 13% of Ang II treated mice that were induced into AF. Additional experiments are required to assess the susceptibility to AF in Ang II with cANF (0.05 mg/kg/min) treated mice. Collectively, these data demonstrate that co-treatment with cANF (0.1 mg/kg/min) attenuates Ang II induced SAN dysfunction and susceptibility to AF in Ang II treated mice. Furthermore, these data demonstrate that NPR-C plays a critical role in preserving *in vivo* cardiac electrophysiology during cardiac disease.

P wave duration was shortened in mice co-treated with Ang II and cANF (0.1 mg/kg/min) compared to mice treated with Ang II alone and remained prolonged

compared to saline treated mice. Therefore, co-treatment with cANF (0.1 mg/kg/min) in Ang II treated mice can partially improve conduction time across the atrial myocardium. In the present study, AERP was not altered in mice co-treated with Ang II and cANF (0.1 mg/kg/min) compared to mice treated with Ang II alone. In isolated myocytes, APD was normalized in right atrial myocytes from mice co-treated with Ang II and cANF (0.1 mg/kg/min). In contrast, AP remained prolonged in left atrial myocytes from mice co-treated with Ang II and cANF (0.1 mg/kg/min). As both atria contribute to AERP measurements and AERP is determined by APD and P wave duration was improved, one would predict a partial improvement in AERP measurements from mice co-treated with Ang II and cANF (0.1 mg/kg/min) rather than no improvement as observed in the present study. Accordingly, this is an area requiring further investigation. In addition to an improvement in P wave duration, P-R interval was not different between mice co-treated with Ang II and cANF (0.1 mg/kg/min) and saline treated mice, demonstrating an improvement in AV node conduction time in Ang II with cANF (0.1 mg/kg/min) treated mice.

In vivo experiments demonstrate that co-treatment with cANF (0.05 mg/kg/min) did not improve cardiac function in Ang II treated mice. This was demonstrated by the observation that measures of heart rate, cSNRT, P wave duration, P-R interval, and AERP were not different in mice co-treated with Ang II and cANF (0.05 mg/kg/min) compared to mice treated with Ang II alone. Taken together, these data demonstrate that the dose of cANF plays a critical role in attenuating Ang II mediated changes in SAN and atrial function *in vivo*. It is important to note that systolic blood pressure was elevated in Ang II with cANF (0.05 mg/kg/min), Ang II with cANF (0.1 mg/kg/min), and Ang II treated mice compared to saline treated mice. This indicates that the effects of cANF result from enhanced NPR-C signalling in the heart and that they occur independently of alterations in blood pressure.

Cellular electrophysiology data can partly explain the improvements observed *in vivo*. P wave duration represents atrial conduction time and is representative of conduction across both the right and left atria. In this study, AP morphology in right atrial myocytes co-treated with Ang II and cANF (0.1 mg/kg/min) was not different compared to saline controls. However, left atrial myocyte electrophysiology was not improved in mice co-

treated with Ang II and cANF (0.1 mg/kg/min). In fact, AP morphology was not different in mice co-treated with Ang II and cANF (0.1 mg/kg/min) compared to mice treated with Ang II alone. It is therefore possible that these regional differences in myocyte electrophysiology manifest as differences in conduction velocity in the right and left atria. This could in turn result in a partial improvement in P wave duration as conduction velocity in the right atrial appendage would be faster than the left atrial appendage in mice co-treated with Ang II and cANF (0.1 mg/kg/min). In addition, mice co-treated with Ang II and cANF (0.1 mg/kg/min) may have lower levels of interstitial fibrosis compared to Ang II treated mice. This would be expected to increase conduction velocity and reduce atrial conduction time. Ongoing experiments in the Rose laboratory are investigating the effects of co-treatment with cANF on fibrosis and conduction velocity in Ang II treated mice using high resolution optical mapping. The *in vivo* studies presented in this thesis demonstrate that concomitant treatment with cANF reduces the susceptibility to AF and partially improves atrial conduction times in Ang II treated mice. In addition, electrical remodelling alone does not account for these improvements as electrical remodelling remained unaltered in left atrial myocytes from mice co-treated with Ang II and cANF (0.1 mg/kg/min) compared to Ang II alone. Accordingly, it is likely that co-treatment with cANF reduces fibrosis in Ang II treated mice. In addition, atrial conduction times were improved in Ang II with cANF treated mice. This indicates that conduction velocity within the atrial myocardium will be increased following co-treatment with cANF compared to Ang II alone.

Co-treatment with cANF completely attenuated Ang II induced changes in AP prolongation in right atrial myocytes. In fact, APD was not different in right atrial myocytes treated with saline compared to Ang II with cANF (0.1 mg/kg/min). Further to this, K^+ current densities (measured with no pre-pulse and with pre-pulse protocols) and I_{to} densities were not different between right atrial myocytes from mice treated with saline and mice co-treated with Ang II and cANF (0.1 mg/kg/min). Collectively, these data indicate that co-treatment with cANF (0.1 mg/kg/min) can prevent Ang II induced electrical remodelling in right atrial myocytes. Although *in vivo* experiments demonstrated that atrial function was not effected in mice co-treated with Ang II and cANF (0.05 mg/kg/min), it is possible that co-treatment with the lower dose of cANF can

elicit a partial improvement on Ang II induced changes in right atrial myocyte electrophysiology. This requires further investigation.

Intriguingly, cANF did not elicit protective effects in left atrial myocytes. Characterization of AP morphology demonstrated there were no differences between left atrial myocytes co-treated with Ang II and cANF (0.1 mg/kg/min) and Ang II alone. V_{max} and AP overshoot were reduced in left atrial myocytes from mice co-treated with Ang II and cANF (0.1 mg/kg/min). Although not measured, it is conceivable that I_{Na} is also reduced in left atrial myocytes co-treated with Ang II and cANF (0.1 mg/kg/min). In addition, AP duration was prolonged in left atrial myocytes co-treated with Ang II and cANF (0.1 mg/kg/min) compared to saline controls, and was not different compared to left atrial myocytes treated with Ang II alone. Consistent with these findings, both K^+ current densities (measured with no pre-pulse and with pre-pulse protocols) and I_{to} densities were not different between left atrial myocytes co-treated with Ang II and cANF (0.1 mg/kg/min) and Ang II alone.

Npr3 (encodes NPR-C) mRNA expression was lower in the left atrium of mice treated with Ang II compared to the right atrium of mice treated with Ang II. Although additional experiments are required to determine if NPR-C protein expression is altered in mice treated with Ang II with cANF (0.1 mg/kg/min), it is conceivable that this could result in a regional difference in the efficacy of cANF treatment. Accordingly, it would be insightful to quantify intracellular cAMP levels in right and left atrial myocytes treated with Ang II and co-treated with Ang II and cANF (0.1 mg/kg/min) as a measure of the level of NPR-C signalling.

As demonstrated in the *in vivo* experiments, the dose of cANF is critical in eliciting a protective effect on cardiac function in Ang II treated mice. Accordingly, it is conceivable that the 0.1 mg/kg/min dose of cANF was not sufficient to attenuate Ang II induced electrical remodelling in left atrial myocytes. Accordingly, a series of experiments should be performed where Ang II treated mice are concomitantly treated with a higher dose of cANF. However, it is also conceivable that increasing the dose of cANF will not alter left atrial electrophysiology. Evidence to support this comes from two observations. The first is that cell capacitance is increased in left atrial myocytes co-treated with Ang II and cANF (0.1 mg/kg/min) and Ang II alone compared to saline

controls. If cellular hypertrophy is contributing to the alterations in left atrial myocyte electrophysiology, then increasing the dose of cANF might not elicit an effect unless cell capacitance is also reduced. The second observation is that blood pressure remained elevated in mice co-treated with Ang II and cANF (0.1 mg/kg/min) compared to mice treated with Ang II alone. Increased blood pressure will increase the pressure exerted on the left ventricle and can alter atrial function (Mensah *et al.*, 2003; Prisant, 2005; Abhayaratna *et al.*, 2006; De Jong *et al.*, 2013). Accordingly, if the increase in blood pressure is contributing to electrical remodelling in left atrial myocytes from Ang II treated mice, then increasing the dose of cANF will not attenuate these changes unless it occurs in conjunction with a reduction in blood pressure.

In the present study, concomitant treatment with cANF elicited critical protective effects against Ang II induced SAN and atrial remodelling. The exact mechanisms through which cANF antagonized Ang II induced electrical remodelling in the heart remains unknown. The effects are most likely multifaceted and could include crosstalk between Ang II and NPR-C intracellular signalling pathways as well as other mechanisms, such as a reduction in inflammation and reactive oxygen species in the heart. This is an area requiring further investigation. An important question that stems from these novel findings is whether cANF (or NPR-C activation) can elicit beneficial effects in the setting of already progressing or established disease. Therefore, it will be insightful to determine the effects of cANF treatment following the onset of disease by performing a series of experiments where Ang II treatment precedes cANF treatment, rather than occurring concomitantly. In this context, enhanced NPR-C signalling will occur following the onset of disease and therefore in the presence of electrical (and structural) remodelling. Although pure speculation, it is possible that enhanced NPR-C signalling will reverse electrical remodelling that occurred or prevent further electrical remodelling from occurring. Either result would be interesting and warrants further investigation.

Previous studies have demonstrated a therapeutic potential for NPs. One study used an AAV9 viral vector to overexpress pro-BNP in spontaneously hypertensive rats. Pro-BNP treatment resulted in increased plasma BNP levels, a reduction in blood pressure, improved diastolic function, and reduced hypertrophy compared to untreated controls

(Cataliotti *et al.*, 2011). In a pilot study in patients with heart failure, subcutaneous BNP treatment resulted in an improvement in left ventricular function and a reduction in left atrial volume (Chen *et al.*, 2012). This was attributed to enhanced NPR-A signalling as plasma cGMP levels were increased following BNP administration. The effects on cardiac electrophysiology were not assessed in these studies. Recently, a new synthetic NP, C_NAA_C, was created by fusing the ring and C-terminus of ANP with the N-terminus of CNP. C_NAA_C increases cGMP more potently than ANP or CNP alone and has potent relaxant, diuretic, and hypotensive properties (Zhang *et al.*, 2015; Zhang *et al*., 2017). C_NAA_C was administered to rats for four weeks following myocardial infarction and prevented left ventricular hypertrophy and reduced the infarct size (Zhang *et al.*, 2017). The effects on electrophysiology were not examined in these studies; however, they are broadly consistent with my experiments showing that NPs are cardioprotective in several models of heart disease.

In contrast to previous studies, the data presented in this thesis are the first to characterize the effects of chronic NPR-C activation on atrial electrophysiology in a disease model. The experiments presented in Chapter 5 demonstrate that co-treatment with Ang II and cANF (0.1 mg/kg/min) results in drastic improvements in cardiac function *in vivo* and atrial electrophysiology. In addition, the susceptibility to AF in mice co-treated with Ang II and cANF (0.1 mg/kg/min) was significantly reduced compared to mice treated with Ang II alone, and was not different to saline treated mice. This demonstrates that chronic activation of NPR-C can be used as a therapeutic target for preventing adverse electrical remodelling in addition to preserving SAN and atrial function. These powerful novel findings indicate that NPR-C should be considered as a possible new therapeutic target and that it's activation can be highly protective against major contributors to electrical dysfunction and atrial arrhythmogenesis in the setting of hypertension and cardiac remodelling.

7.5. Effects of age and frailty on sinoatrial node function

Frailty, and therefore overall health status, was quantified in young and aged mice using a 31 item non-invasive frailty index (Whitehead *et al.*, 2014). FI scores were higher

in aged mice compared to young mice. This is consistent with previous studies demonstrating an increase in frailty with chronological age (Whitehead *et al.*, 2014; Rockwood *et al.*, 2017). Importantly, FI scores fell along a continuum between young and aged mice, demonstrating that individuals age at different rates.

In the present study, chronological age was associated with a decline in SAN function. This was demonstrated by a reduction in heart rate under baseline conditions and in the presence of autonomic nervous system blockade in aged mice. In addition, cSNRT was prolonged in aged mice. These data are consistent with an age-related decline in heart rate and SAN function observed in both humans and animal models of ageing (Anyukhovsky *et al.*, 2002; Jones *et al.*, 2004; Kistler *et al.*, 2004; Tellez *et al.*, 2011; Larson *et al.*, 2013; Huang *et al.*, 2015). Remarkably, measures of heart rate and cSNRT displayed significant heteroscedasticity, indicating that factors in addition to chronological age affect SAN function. When assessed as a function of each individual's FI score (i.e. overall health status) it was evident that measures of heart rate and cSNRT were correlated with FI score whereby SAN function declined as FI score increased. In fact, mice with the same FI score can have similar measures of heart rate and cSNRT, independent of chronological age. This demonstrates that overall health status impacts SAN function independently of chronological age. In addition, these data indicate that FI score can be used as a powerful predictor of intrinsic SAN function.

The effects of age and frailty on SAN function was further investigated by other members of the Rose laboratory. In particular, the effects of age and frailty on electrical conduction and structural remodelling was examined and will be described below. Electrical conduction in aged and frail mice was assessed in optical mapping experiments and revealed important distinctions in SAN function in aged and frail mice. The location of the leading pacemaker site was more inferior in aged hearts compared to young hearts and was associated with slower conduction velocities across the SAN in aged mice (Moghtadaei *et al.*, 2016b). Strikingly, the location of the leading pacemaker site was associated with FI score such that frail hearts had leading pacemaker sites that were at a more inferior location whereas the leading pacemaker site was at a more superior location in less frail hearts. In addition, there was increased beat to beat variability in the location of the leading pacemaker site in frail mice compared to less frail mice. Optical mapping

experiments demonstrated that cycle length was not different in aged hearts and SAN conduction velocity was reduced in aged hearts (Moghtadaei *et al.*, 2016b). However, when assessed as a function of frailty, measures of both cycle length and conduction velocity were correlated with FI score. There was a positive correlation between cycle length and FI score, and a negative correlation between conduction velocity and FI score. SAN conduction velocity is critical determinant of SAN function and heart rate (Fedorov *et al.*, 2010; Fedorov *et al.*, 2012). Accordingly, these data are consistent with the reduction in heart rate and prolongation in cSNRT observed *in vivo.* Taken together, these data demonstrate that frailty affects SAN electrophysiology and that frailty enables the identification of changes in SAN function that occur independently of chronological age.

The effects of age and frailty on SAN electrical function were further investigated by characterizing optical AP morphology in SAN preparations. Diastolic depolarization slope was reduced in aged hearts and was negatively correlated with FI score (Moghtadaei *et al.*, 2016b). In addition, APD_{50} was not different in aged heart whereas APD_{70} was shorter in aged hearts compared to young hearts. When assessed as a function of FI score, both APD_{50} and APD_{70} were correlated with FI score such that a reduction in APD was associated with an increase in FI score (Moghtadaei *et al.*, 2016b). This provides further evidence that frailty can discriminate changes in SAN function that do not occur as a function of chronological age. Although specific ion currents were not assessed in this study, previous studies have demonstrated reductions in I_f, $I_{Ca,L}$, $I_{Ca,T}$, and I_{Na} in aged SAN myocytes (Mangoni and Nargeot, 2008; Dobrzynski *et al.*, 2013). Additional experiments are required to determine the effects of frailty on these ion currents.

In addition to electrical remodelling, aged and frail hearts have increased levels of interstitial fibrosis in the SAN. Fibrosis was assessed by staining for collagen in histological sections of the SAN and by quantifying total collagen content using hydroxyproline assays. Both of these approaches demonstrated that SAN fibrosis increases in with age and is positively correlated with frailty (Moghtadaei *et al.*, 2016b). In addition, increased fibrosis in the SAN can contribute to the alterations in SAN conduction observed in aged and frail mice (Csepe *et al.*, 2015). Interestingly, collagen

mRNA expression was not different in aged mice, neither did it correlate with FI score (Moghtadaei *et al.*, 2016b). This indicates that collagen is not being actively deposited at an increased rate in aged or frail mice. Rather, the increase in fibrosis levels was attributed to alterations in TIMP and MMP mRNA expression that will alter the balance of extracellular matrix turnover in aged and frail hearts (Moghtadaei *et al.*, 2016b).

Collectively, these studies demonstrate there is a decline in SAN function that occurs not only with chronological age, but is also highly correlated with frailty. In fact, in some cases frailty was better able to discriminate changes in SAN function than chronological age. These data also demonstrate that health status affects SAN function *in vivo* and that frailty is a powerful predictor of changes at the tissue and molecular levels using the FI. In addition, these findings demonstrate that FI score is a powerful tool that can be used to investigate cellular and molecular function.

7.6. Effects of age and frailty on atrial function and arrhythmogenesis

The prevalence and severity of AF increases with chronological age (Polidoro *et al.*, 2013; Maden *et al.*, 2016; Nguyen *et al.*, 2016; Kim *et al.*, 2017). In the present study, aged mice were induced into more long lasting forms of AF compared to young mice, even though the susceptibility to AF was similar. In fact, all young mice that were induced into AF had transient forms of AF that lasted less than 5 seconds before spontaneously reverting back to sinus rhythm. In contrast, AF lasted longer than 30 seconds in 75% of mice when induced in aged mice. These data demonstrate that aged mice are more susceptible to more severe forms of AF. In addition to AF, spontaneous AV node block was observed in aged mice and was absent in young mice. FI scores, and therefore overall health status, were higher in aged mice induced into AF and in mice with AV node block compared to young mice. Combined, these findings demonstrate that frailty is associated with an increased severity of AF and incidence of AV node bock.

Consistent with these AF data, P wave duration and P-R interval were prolonged in aged mice under baseline conditions and in the presence of autonomic nervous system blockade. The age-related prolongation of atrial and AV node conduction times is consistent with clinical data in humans and animal models (Anyukhovsky *et al.*, 2002;

Kistler *et al.*, 2004; Gan *et al.*, 2013). Similar to heart rate and cSNRT measurements, P wave duration and P-R interval displayed substantial heteroscedasticity, most notably in aged mice. To determine if frailty, and therefore overall health status, could account for this variability, P wave duration and P-R interval were assessed as a function of FI score. This analysis demonstrates that both P wave duration and P-R interval are highly correlated with FI score such that mice with higher FI scores had prolonged conduction times across the atrial myocardium and through the AV node. This correlation was observed under baseline conditions and in the presence of autonomic nervous system blockade. In fact, mice with comparable FI scores can have similar P wave durations and P-R intervals. In addition, prolonged atrial and AV node conduction times are associated with an increase in severity of AF (Magnani *et al.*, 2013; Censi *et al.*, 2016; Conte *et al.*, 2017; Smith *et al.*, 2017). Consistent with this concept, both P wave duration and P-R interval were positively correlated with AF duration in mice that were induced into AF. Collectively, these data demonstrate that frailty (i.e. health status) impacts atrial and AV node conduction times independently of chronological age. In addition, these data demonstrate that frailty is a powerful tool that can be used to predict atrial function and severity of AF, independently of chronological age.

Although beyond the scope of this thesis, the effects of age and frailty on atrial electrophysiology and structure were further investigated by other members of the Rose laboratory. Electrical function was assessed in aged and frail mice using high resolution optical mapping. Conduction velocity was reduced in both the right and left atria in aged mice, which is consistent with the prolongation in P wave duration observed *in vivo* (Jansen *et al.*, 2017b). In addition, conduction velocity in the right and left atria was negatively correlated with frailty demonstrating that factors other than chronological age can affect atrial electrical function. Characterization of optical AP morphology revealed that APD_{90} is reduced both the right and left atria whereas APD_{50} remained unchanged (Jansen *et al.*, 2017b). Interestingly, APD_{50} and APD_{90} in the right atria and APD_{90} in the left atria were negatively correlated with frailty. This demonstrates that frailty can identify changes in atrial electrophysiology that cannot be identified by chronological age. In addition, these findings further demonstrate that frailty is a powerful tool that can be used to identify changes in atrial electrophysiology.

Reductions in conduction velocity and APD will shorten the wavelength of re-entry which creates a substrate for AF (Allessie *et al.*, 2002; Nattel and Dobrev, 2016). Both of these measures were correlated with frailty and are consistent with the observation that frail mice were induced into more severe forms of AF. Although not assessed in the present study, alterations in optical AP morphology are indicative of changes in ion current density in aged and frail mice. Previous studies have demonstrated that $I_{Ca,L}$ is reduced whereas I_{to} is increased with age (Dun *et al.*, 2003; Dun and Boyden, 2009; Gan *et al.*, 2013). Accordingly, a series of experiments to determine the effects of age and frailty on ion channel function in isolated atrial myocytes will vastly improve our knowledge on electrical remodelling in the aged population. In addition, further studies are required to determine the relationship between frailty and ion current density.

Slowed atrial conduction time and a reduction in conduction velocity are also indicative of structural remodelling in the atria. Indeed, aged mice had increased levels of interstitial fibrosis, as assessed by histological sections staining for collagen as well as total collagen content (Jansen *et al.*, 2017b). In addition, there was a positive correlation between levels of fibrosis and FI score. Further scrutiny of the data demonstrated that in some cases FI score was better able to predict collagen content than chronological age. In addition, these data indicate that overall health status has an impact on molecular function and structural remodelling in the atria. Mechanistically, increased levels of atrial fibrosis will contribute to a slowing of conduction across the atria as fibrosis interferes with electrical conduction (Heijman *et al.*, 2014; Jalife and Kaur, 2015; Nattel and Dobrev, 2016). This can create a substrate for AF and could explain the increased susceptibility to more severe forms of AF observed in frail mice.

Collectively, these studies demonstrate that frailty is a powerful predictor of atrial structure, function, and arrhythmogenesis. In fact, in some cases frailty was better able to identify changes in atrial electrophysiology and molecular function than chronological age alone. Furthermore, we have demonstrated that FI score can be used as a powerful tool to predict electrical and structural changes in the atria that create a substrate for AF, independent of chronological age. These findings have important clinical applications as frail patients are more susceptible to adverse outcomes, including mortality (McNallan *et al.*, 2013; Singh *et al.*, 2014; Forman *et al.*, 2016). By quantifying a patient's overall

health status to generate an FI score, physicians will be able to predict the degree of structural and electrical remodelling in the atrium. This has important implications in determining a patient's risk of developing AF as well as designing treatment options that will be better tolerated by the individual. Therefore, factoring frailty in the decision-making process in the clinical setting will allow for a personalized approach to generating therapeutic interventions that could promote longevity and reduce adverse outcomes.

Our work clearly demonstrates that there is a decline in SAN and atrial function that occurs during the natural ageing process. Furthermore, we have demonstrated that by quantifying health status to generate an FI score one can predict the level of structural and electrical remodelling in the atria and SAN. Epidemiology studies have demonstrated that cardiovascular disease is highly prevalent in the aged population (Mizra *et al.*, 2012; Rahman *et al.*, 2014; Monfredi and Boyett, 2015). In addition, frail patients have an increased risk in developing heart failure and AF (McNallen *et al.*, 2013; Frisoli *et al.*, 2015). In fact, frailty is an independent risk factor for morbidity and mortality in patients with cardiovascular disease and AF (Frisoli *et al.*, 2015; Nguyen *et al.*, 2016; Maden *et al.*, 2016; Kim *et al.*, 2017). The findings presented in this thesis demonstrate that Ang II treatment in adult mice results in SAN dysfunction and an increased susceptibility to AF. In addition, the data presented in this thesis demonstrates that Ang II treatment is associated with electrical remodelling in isolated right and left atrial myocytes. It is likely that frail mice treated with Ang II will have a more severe impairment in SAN and atrial function compared to less frail mice. Accordingly, it will be important to characterize the effects of Ang II treatment in aged and frail mice. In addition, the studies presented in this thesis demonstrate that cANF exhibits protective effects on cardiac function *in vivo* and reduces arrhythmogenesis in the diseased heart. I have also demonstrated there is a decline in SAN and atrial function in aged and frail mice, as well as increase in the susceptibility to supraventricular arrhythmias. Accordingly, it is possible that administration of cANF in aged and frail mice can improve cardiac function *in vivo* in aged and frail mice.

7.7. Limitations

The intracardiac programmed electrical stimulation is a powerful technique used to determine SAN and atrial function as well as susceptibility to arrhythmias. However, it is an invasive procedure that requires the use of anaesthetic. Previous studies have demonstrated that anesthetics can reduce heart rate (Constantinides *et al.*, 2011; Yang *et al.*, 2014) and it is possible that this may influence the measures of cardiac function assessed in the current study. It would be insightful to add to the data acquired in anesthetized mice by performing a series of experiments in awake, conscious mice using a telemetry system. This approach will provide valuable insight into the presence of SAN dysfunction by possibly observing SAN pauses as well as enable the detection of spontaneous arrhythmias, including AF, in Ang II treated mice.

cANF is a synthetic peptide that was infused into the interstitial space using a miniosmotic pump for the duration of the experiment. Accordingly, the beneficial effects observed in this study might not be limited to the heart as cANF can affect other organ systems. Future studies should investigate the effects of cANF in other organ systems.

The present study used the mouse model of chronic Ang II treatment to investigate alterations in electrophysiology in the setting of hypertension and hypertrophy. Although powerful and insightful, there are differences in ion channel expression in the mouse and human heart. Most notably, I_{Ks} and I_{Kr} play an important role in repolarization in larger mammals and humans (Nerbonne and Kass, 2005; Bartos *et al.*, 2015). Performing experiments in larger mammals will be insightful in determining the effects of Ang II treatment on these ion channels, as well as the effects of co-treatment with cANF in modulating ion channel function. In addition, it is important to note that patch-clamp experiments were performed at room temperature rather than the physiological temperature of 37ºC. Performing experiments at physiological temperature will exclude the possibility of temperature dependent effects on ion channel function.

All experiments were performed on male mice. However, there are differences in the structure and electrophysiological function of the healthy and diseased male and female heart (Trepanier-Boulay *et al.*, 2001; Blenck *et al.*, 2016; Harrington *et al.*, 2017). In addition, studies have shown that there is a difference in how male and female mice

respond to Ang II treatment (Harrington *et al.*, 2017). It is therefore important to perform experiments in both male and female mice in future studies.

7.8. Future Directions

The data presented in this thesis demonstrate that Ang II treatment has profound effects on atrial electrophysiology and arrhythmogenesis that can be attenuated by concomitant treatment with the NPR-C agonist cANF (0.1 mg/kg/min). However, these beneficial effects were observed *in vivo* and in right atrial myocytes and not in left atrial myocytes. It is possible that targeted delivery of cANF to the specific regions of the heart will elicit additional protective effects. In addition, NPR-C mRNA expression was lower in the diseased left atria compared to the right atria. A combination of targeted delivery of NPR-C, using nanoparticles or viral vectors, in conjunction with cANF could elicit a beneficial effect in the left atrium.

In the present study, chronic NPR-C activation elicited protective effects against Ang II induced electrical remodelling *in vivo* and in right atrial myocytes. In addition, these effects occurred independently of a reduction in blood pressure in Ang II treated mice. NPR-A and NPR-B signalling is involved in the regulation of blood pressure, hypertrophy, and cardiac fibrosis (Kishimoto *et al.*, 2000; Franco *et al.*, 2004; Potter *et al.*, 2006; Rubattu *et al.*, 2008; Potter *et al.*, 2009; Kishimoto *et al.*, 2011). Therefore, therapeutic approaches that targets multiple NPRs (NPR-C and NPR-A or NPR-B) may provide additional benefits in the treatment of hypertensive and hypertrophic heart disease. Accordingly, additional studies are required to characterize the effects of activating multiple NPRs in the setting of cardiac disease.

7.9. Conclusions

In conclusion, this thesis demonstrates that Ang II treatment is associated with SAN dysfunction and an increased susceptibility to longer lasting forms of AF. In right and left atrial myocytes, Ang II treatment was associated with distinct patterns of electrical remodelling that included reductions in I_{to} and I_{Kur} in right atrial myocytes and I_{Na}, I_{to},

and I_{Kur} in left atrial myocytes. This creates a substrate for the genesis of AF. Ang II treatment in NPR-$C^{-/-}$ mice results in a more severe phenotype, as demonstrated by a greater impairment in SAN function, increased susceptibility and severity of AF, and greater prolongations in atrial and AV node conduction times. This occurred in association with more severe electrical remodelling in left, but not right, atrial myocytes. Strikingly, concomitant treatment with the NPR-C agonist cANF (0.1 mg/kg/min) attenuated Ang II induced SAN dysfunction, atrial arrhythmogenesis, and impairments in atrial function. In isolated myocytes, AP morphology and K^+ currents were not different between Ang II with cANF (0.1 mg/kg/min) and saline treated right atrial myocytes. In contrast, co-treatment with cANF (0.1 mg/kg/min) did not attenuate Ang II induced electrical remodelling in left atrial myocytes. Collectively, these data demonstrate that NPR-C signalling has protective effects in Ang II treated mice and has the potential for as a treatment strategy for patients.

In addition, the effects of age and frailty on SAN and atrial function was assessed *in vivo*. There is an age-related decline in SAN and atrial function as well as an increase in the incidence of atrial arrhythmias. Importantly, measures of SAN and atrial function were highly correlated with FI score (i.e. overall health status). In addition, long lasting forms of AF as well as spontaneous AV node block was demonstrated in frail mice. Therefore, the quantification of health status gives valuable insight into SAN and atrial physiology. Cardiovascular disease is highly prevalent in the aged population. Accordingly, frailty can be used as a powerful predictor of SAN and atrial function, which has important therapeutic implications when designing treatment strategies for patients.

In conclusion, the studies presented in this thesis new provide mechanistic insight into the distinct patterns of electrical remodelling that occur in right and left atrial myocytes from Ang II treated mice. These findings substantially advance our knowledge of the underlying mechanisms responsible for electrical remodelling in the diseased atria that contribute to the creation of a substrate for AF. The data presented in this thesis has advanced our understanding of the role of NPR-C in the diseased heart. In fact, these studies indicate that enhanced NPR-C signalling can preserve SAN and atrial electrophysiological function in the diseased heart. Accordingly, targeting NPR-C can be

used as a therapeutic target for the treatment and prevention of AF and should be considered when designing new therapeutic interventions for cardiac disease. Cardiovascular disease is more prevalent in the elderly population. The findings presented in this thesis demonstrate that frailty (i.e. overall health status) can be used as a predictor of SAN and atrial function *in vivo* as well as the susceptibility to atrial arrhythmias. In addition, frailty can identify changes in SAN and atrial function independently of chronological age. Accordingly, frailty should be considered when designing therapeutic interventions for elderly patients with AF and/or cardiovascular disease.

APPENDIX A. ECG intervals and intracardiac ECG parameters in anaesthetized saline and Ang II treated wildtype mice.

	Saline	Ang II
Heart rate (beats/min)	547.8 ± 6.3	517.3 ± 8.7 *
cSNRT (ms)	25.5 ± 1.9	51.9 ± 4.2 *
P wave duration (ms)	25.7 ± 0.5	32.0 ± 0.7 *
P-R interval (ms)	43.8 ± 0.7	50.6 ± 0.9 *
AERP (ms)	29.1 ± 0.4	35.0 ± 0.9 *
AVERP (ms)	49.4 ± 1.6	57.3 ± 2.5 *

Data are means ± SEM; Heart rate, P wave duration, and P-R interval: n = 23 saline and 33 Ang II treated mice; cSNRT: n = 23 saline and 24 Ang II treated mice; AERP: n = 16 saline and 22 Ang II treated mice; AVERP: n = 7 saline and 13 Ang II treated mice. *P<0.05 vs. saline. Data analyzed by Student's t-test. Abbreviations: AERP, atrial effective refractory period; AVERP, atrioventricular node effective refractory period; cSNRT, corrected sinoatrial node recovery time. P wave duration was measured from the start to the end of the P wave. P-R interval was measured from the start of the P wave to the peak of the QRS complex.

APPENDIX B. Effects of Ang II treatment on systolic blood pressure in saline and Ang II treated wildtype mice.

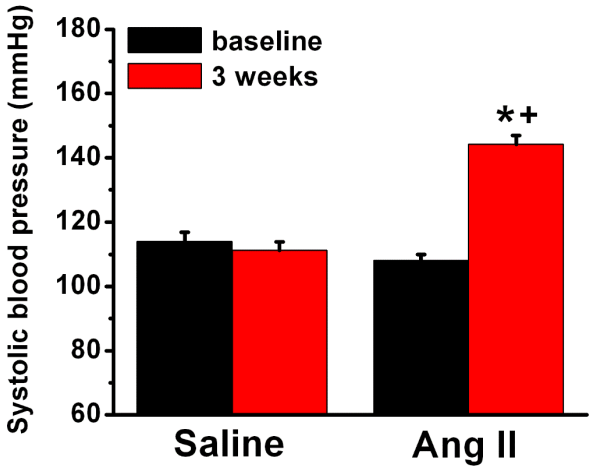

Summary data illustrating the effects of Ang II treatment on systolic blood pressure at baseline (before surgery) and after 3 weeks of treatment with saline or Ang II in wildtype mice. *P<0.05 vs. baseline within treatment group; ^{+}P<0.05 vs. saline within time point. Data analyzed by two-way repeated measures ANOVA with Tukey's post-hoc test; n = 17 saline and 18 Ang II treated mice. Data provided by the Rose laboratory.

APPENDIX C. Effects of Ang II treatment on systolic blood pressure in NPR-C$^{+/+}$ and NPR-C$^{-/-}$ mice.

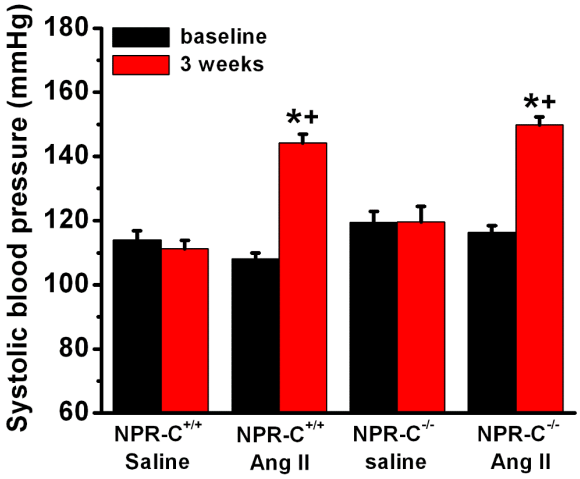

Summary data illustrating the effects of Ang II treatment on systolic blood pressure in NPR-C$^{+/+}$ and NPR-C$^{-/-}$ mice measured at baseline (before surgery) and after 3 weeks of treatment with saline or Ang II. *P<0.05 vs. baseline in treatment group; ^{+}P<0.05 vs. saline within genotype. Data analyzed by two-way repeated measures ANOVA with Tukey's post hoc test; NPR-C$^{+/+}$: n = 17 saline and 18 Ang II treated mice; NPR-C$^{-/-}$: n = 13 saline and 11 Ang II treated mice. Data provided by the Rose laboratory.

APPENDIX D. ECG intervals and intracardiac ECG parameters in anaesthetized NPR-C$^{+/+}$ and NPR-C$^{-/-}$ mice treated with saline and Ang II.

	NPR-C$^{+/+}$ saline	NPR-C$^{+/+}$ Ang II	NPR-C$^{-/-}$ saline	NPR-C$^{-/-}$ Ang II
Heart rate (beats/min)	547.8 ± 6.3	517.3 ± 8.7 *	535.3 ± 10.4	488.3 ± 14.3 *$^{+}$
cSNRT (ms)	25.5 ± 1.9	51.9 ± 4.2 *	49.7 ± 4.4 $^{+}$	78.1 ± 7.8 *$^{+}$
P wave duration (ms)	25.7 ± 0.5	32.0 ± 0.7 *	29.8 ± 0.7 $^{+}$	39.6 ± 2.2 *$^{+}$
P-R interval (ms)	43.8 ± 0.7	50.6 ± 0.9 *	48.8 ± 0.9 $^{+}$	58.9 ± 3.3 *$^{+}$
AERP (ms)	29.1 ± 0.4	35.0 ± 0.9 *	33.4 ± 0.7 $^{+}$	39.0 ± 2.1 *$^{+}$
AVERP (ms)	49.4 ± 1.6	57.3 ± 2.5 *	52.4 ± 1.2	65.0 ± 2.8 *$^{+}$

Data are means ± SEM; NPR-C$^{+/+}$: Heart rate, P wave duration, and P-R interval: n = 23 saline and 33 Ang II treated mice; cSNRT: n = 23 saline and 24 Ang II treated mice; AERP: n = 16 saline and 22 Ang II treated mice; AVERP: n = 7 saline and 13 Ang II treated mice. NPR-C$^{-/-}$: Heart rate, P wave duration, and P-R interval: n = 14 saline and 15 Ang II treated mice; cSNRT: n = 14 saline and 12 Ang II treated mice; AERP: n = 11 saline and 8 Ang II treated mice; AVERP: n = 9 saline and 8 Ang II treated mice. *P<0.05 vs. saline within genotype. ^{+}P<0.05 vs. NPR-C $^{+/+}$ within treatment group. Data analyzed by two-way ANOVA with Tukey's post hoc test. Abbreviations: AERP, atrial effective refractory period; AVERP, atrioventricular node effective refractory period; cSNRT, corrected sinoatrial node recovery time. NPR, natriuretic peptide receptor. P wave duration was measured from the start to the end of the P wave. P-R interval was measured from the start of the P wave to the peak of the QRS complex.

APPENDIX E. Effects of the NPR-C agonist cANF on systolic blood pressure in wildtype mice treated with Ang II.

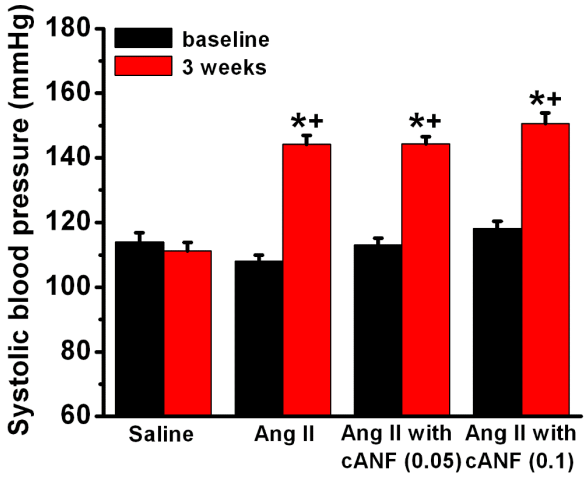

Summary data illustrating the effects of Ang II treatment on systolic blood pressure in saline, Ang II, Ang II with cANF (0.05 mg/kg/min), and Ang II with cANF (0.1 mg/kg/min) treated mice measured at baseline (before surgery) and after 3 weeks of treatment. *P<0.05 vs. baseline within treatment group; ^{+}P<0.05 vs. saline within time point. Data analyzed by two-way repeated measures ANOVA with Tukey's post hoc test; n = 17 saline, 18 Ang II, 14 Ang II with cANF (0.05 mg/kg/min), and 13 Ang II with cANF (0.1 mg/kg/min) treated mice. Data provided by the Rose laboratory.

APPENDIX F. ECG intervals and intracardiac ECG parameters in anaesthetized saline, Ang II, Ang II with cANF (0.05 mg/kg/min), and Ang II with cANF (0.1 mg/kg/min) treated wildtype mice.

	Saline	Ang II	Ang II with cANF (0.05 mg/kg/min)	Ang II with cANF (0.1 mg/kg/min)
Heart rate (beats/min)	547.8 ± 6.3	517.3 ± 8.7 *	507.0 ± 9.3 *	549.2 ± 6.8 $^{+}$
cSNRT (ms)	25.5 ± 1.9	51.9 ± 4.2 *	45.4 ± 3.4 *	33.3 ± 3.0 $^{+}$
P wave duration (ms)	25.7 ± 0.5	32.0 ± 0.7 *	31.6 ± 0.7 *	29.3 ± 0.6 *$^{+}$
P-R interval (ms)	43.8 ± 0.7	50.6 ± 0.9 *	49.1 ± 0.9 *	46.7 ± 0.9 $^{+}$
AERP (ms)	29.1 ± 0.4	35.0 ± 0.9 *	35.9 ± 1.0 *	34.5 ± 1.0 *

Data are means ± SEM; Heart rate: n = 23 saline, 33 Ang II, 20 Ang II with (cANF 0.05 mg/kg/min), 22 Ang II with cANF (0.1 mg/kg/min) treated mice; cSNRT: n = 23 saline, 24 Ang II, 19 Ang II with cANF (0.05 mg/kg/min), 22 Ang II with cANF (0.1 mg/kg/min) treated mice; P wave duration and P-R interval: n = 23 saline, 33 Ang II, 20 Ang II with cANF (0.05 mg/kg/min), 22 Ang II with cANF (0.1 mg/kg/min) treated mice; AERP: n = 16 saline, 22 Ang II, 14 Ang II with cANF (0.05 mg/kg/min), 20 Ang II with cANF (0.1 mg/kg/min) treated mice. *P<0.05 vs. saline; ^{+}P<0.05 vs. Ang II. Data analyzed by one-way ANOVA with Tukey's post hoc test. Abbreviations: AERP, atrial effective refractory period; cSNRT, corrected sinoatrial node recovery time. P wave duration was measured from the start to the end of the P wave. P-R interval was measured from the start of the P wave to the peak of the QRS complex.

APPENDIX G. ECG intervals and intracardiac ECG parameters in anaesthetized young and aged mice.

	Young	Aged
Heart rate (beats/min)	552.7 ± 4.9	514.3 ± 9.2 *
cSNRT (ms)	25.2 ± 1.6	39.8 ± 3.2 *
P wave duration (ms)	18.0 ± 0.8	25.2 ± 0.9 *
P-R interval (ms)	47.9 ± 0.7	57.0 ± 1.7 *

Data are means ± SEM; Heart rate and cSNRT: n = 29 young and 34 aged mice; P wave duration and P-R interval: n = 22 young and 24 aged mice. *P<0.05 vs. young. Data analyzed by Student's t-test. Abbreviations: cSNRT, corrected sinoatrial node recovery time. P wave duration was measured from the start to the end of the P wave. P-R interval was measured from the start of the P wave to the peak of the QRS complex.

APPENDIX H. Publications

Manuscripts:

Jansen, HJ[*], Moghtadaei, M[*], Mackasey, M, Rafferty, SA, Bogachev, O, Sapp, JL, Howlett, SE, Rose, RA (2017). Atrial structure, function and arrhythmogenesis in aged and frail mice. Scientific Reports. 7:44336. [*]co-first author

Moghtadaei, M[*], **Jansen, HJ**[*], Mackasey, M, Rafferty, SA, Bogachev, O, Sapp, JL, Howlett, SE, Rose, RA. (2016). The impacts of age and frailty on heart rate and sinoatrial node function. The Journal of Physiology. 549:7105-7126. [*]co-first author

Hua, R, MacLeod, SL, Polina, I, Moghtadaei, M, **Jansen, HJ**, Bogachev, O, O'Blenes, SB, Sapp, JL, Legare, JF, Rose, RA. (2015). Effects of wild-type and mutant forms of atrial natriuretic peptide on atrial electrophysiology and arrhythmogenesis. Circulation Arrhythmia and Electrophysiology. 8:1240-1254.

Krishnaswamy, PS, Egom, EE, Moghtadaei, M, **Jansen, HJ**, Azer, J, Bogachev, O, Mackasey, M, Robbins, C. Rose, RA. (2015). Altered parasympathetic nervous system regulation of the sinoatrial node in Akita diabetic mice. Journal of Molecular and Cellular Cardiology. 82: 125-135.

Egom, EE, Vella, K. Hua, R, **Jansen, HJ**, Moghtadaei, M, Polina, I, Bogachev, O, Hurnik, R, Mackasey, M, Rafferty, S, Ray, G, Rose, RA. (2015). Impaired sinoatrial node function and increased susceptibility to atrial fibrillation in mice lacking natriuretic peptide receptor C. The Journal of Physiology. 593:1127-1146.

Published Abstracts:

Jansen, HJ, Egom, EE, Rafferty SA, Rose, RA. (2017). Atrial Fibrillation in hypertensive heart disease is associated with distinct patterns of electrical remodelling in the left and right atria. Biophysical Journal. Biophysical Society 61st Annual Meeting, New Orleans, United States.

Jansen, HJ, Rafferty, SA, Howlett, SE, Rose, RA. (2015). Assessment of sinoatrial node function and atrial conduction as a function of age and frailty in mice. Journal of Molecular and Cellular Cardiology. International Society of Heart Research XXXV Annual Meeting of the North American Section, Seattle, United States.

Book Chapters:

Jansen, HJ, Quinn, TA, Rose, RA. (2017). Cellular Sinoatrial Node and Atrioventricular Node Activity in the Heart. In Reference Module in Biomedical Sciences, Elsevier, 2017, ISBN 9780128012383. https://doi.org/10.1016/B978-0-12-801238-3.99759-9

Jansen, HJ and Rose, RA. (2015). Natriuretic peptides: critical regulators of cardiac fibroblasts and the extracellular matrix in the heart. In: Dixon, I.M., Wigle, J.T. (Eds.), Cardiac Fibrosis and Heart Failure: Cause or Effect. Springer International Publishing, pp. 383-404.

REFERENCES

Abhayaratna, WP, Seward, JB, Appleton, CP, Douglas, PS, Oh, JK, Tajik, AJ, Tsang, TSM. (2006). Left Atrial Size: Physiologic Determinants and Clinical Applications. J Am Coll Cardiol. 47:2357-2363.

Abriel, H. (2007). Roles and regulation of the cardiac sodium channel $Na_V1.5$: recent insights from experimental studies. Cardiovascular Research 76:381-389

Abriel, H. (2010). Cardiac sodium channel Nav1.5 and interacting proteins: physiology and pathophysiology. J. Mol. Cell. Cardiol. 48:2-11

Accili, EA, Proenza, C, Baruscotti, M, DiFrancesco, D. (2002). From funny current to HCN channels: 20 years of excitation. News Physiol Sci. 17:32-37

Adam, O, Theobald, K, Lavall, D, Grube, M, Kroemer, HK, Ameling, S, Schafers, H, Bohm, M, Laufs, U. (2011). Increased lysyl oxidase expression and collagen cross-linking during atrial fibrillation. Journal of Molecular and Cellular Cardiology. 50:678-685

Afilalo, J, Karunananthan, S, Eisenberg, MJ, Alexander, KP, Bergman, H. (2009). Role of frailty in patients with cardiovascular disease. Am J Cardiol. 103:1616-1621

Agrawal, R, Agrawal, N, Koyani, CH, Singh, R. (2010). Molecular targets and regulators of cardiac hypertrophy. Pharmacological Research 61:269-280

Ahern, CA, Payandeh, J, Bosmans, F, Chada, B. (2016). The hitchhiker's guide to the voltage-gated sodium channel galaxy. J Gen Phsyiol. 147:1-25

Allessie, M, Ausma, J, Schooten, U. (2002). Electrical, contractile, and structural remodeling during atrial fibrillation. Cardiovascular Research. 54:230-246

Allessie, MA, Boyden, PA, Camm, AJ, Kleber, AG, Lab, MJ, Legato, MJ, Rosen, MR, Schwartz, PJ, Spooner, PM, Van Wagoner, DR, Waldo, AL. (2001). Pathophysiology and prevention of atrial fibrillation. Circulation. 103:769-777.

Amin, AS, Tan, HL, Wilde, AAM. (2010). Cardiac ion channels in health and disease. Heart Rhythm. 7:117-126

An, WF, Bowlby, MR, Betty, M, Cao, J, Ling, H, Mendoza, BW, Trimmer, JS, Rhodes, KJ. (2000). Modulation of A-type potassium channels by a family of calcium sensors. Nature. 403:553-556

Anand-Srivastava, MB, Sairam, MR, Cantin, M. (1990). Ring-deleted analogs of atrial natriuretic factor inhibit adenylyl cyclase/cAMP system. Possible coupling of clearance atrial natriuretic factor receptors to adenlyly cyclase/cAMP signal transduction system. The Journal of Biological Chemistry. 265:8566-8572.

Anand-Srivastava, MB, Trachte, GJ, (1993). Atrial natriuretic factor receptors and signal transduction mechanisms. Pharmacol. Rev. 45:e497.

Anand-Srivastava, MB. (2005). Natriuretic peptide receptor-C signaling and regulation. Peptides. 26:1044-1059

Anumonwo, JMB and Lopatin, AN. (2010). Cardiac strong inward rectifier potassium channels. Journal of Molecular and Cellular Cardiology. 48:45-54.

Anyukhovsky, EP, Sosunov, EA, Chandra, P, Rosen, TS, Boyden, PA, Danilo, P, Rosen, MR. (2005). Age-associated changes in electrophysiologic remodeling: a potential contributor to initiation of atrial fibrillation. Cardiovasc Res. 66:353–363

Anyukhovsky, EP, Sosunov, EA, Plotnikov, A, Gainullin, RZ, Jhang, JS, Marboe, CC, Rosen, MR. (2002). Cellular electrophysiologic properties of old canine atria provide a substrate for arrhythmogenesis. Cardiovasc Res. 54:462-469

Azer, J, Hua, R, Krishnaswamy, PS, Rose, RA. (2014). Effects of natriuretic peptides on electrical conduction in the sinoatrial node and atrial myocardium of the heart. J. Physiol. 592:1025-1045.

Azer, J, Hua, R, Vella, K, Rose, RA. (2012). Natriuretic peptides regulate heart rate and sinoatrial node function by activating multiple natriuretic peptide receptors. J. Mol. Cell. Cardiol. 53:715-724.

Baba, S, Dun, W, Hirose, M, Boyden, PA. (2006). Sodium current function in adult and aged canine atrial cells. Am J Physiol Heart Circ Physiol. 291:H756-H761

Barbee, RW, Perry, BD, Re, RN, Murgo, JP, Field LJ. (1994). Hemodynamics in transgenic mice with overexpression of atrial natriuretic factor. Circ Res 74:747-751.

Barold, SS. (2002). Centennial of Einthoven's first recording of the human electrocardiogram with the string galvanometer. Journal of Pacing and Clinical Electrophysiology. 25:399-401

Barry, SP, Davidson, SM, Townsend, PA. (2008). Molecular regulation of cardiac hypertrophy. The International Journal of Biochemistry & Cell Biology. 40:2023-2039

Bartos, DC, Grandi, E, Ripplinger, CM. (2015). Ion channels in the heart. Compr Physiol. 5:1423-1464

Becker, DE. (2006). Fundamentals of electrocardiography interpretation. Anesth Prog 53:53-64

Beigel, R, Wunderlich, NC, Ho, SY, Arsanjani, R, Siegel, RJ. (2014). The Left Atrial Appendage: Anatomy, Function, and Noninvasive Evaluation. Journal Am Coll Cardiol Img. 7:1251-1265

Belardinelli, L, Giles, WR, Rajamani, S, Karagueuzian, HS, Shryock, JC. (2015). Cardiac late Na^+ current: Proarrhythic effects, roles in long QT syndromes, and pathological relationship to CaMKII and oxidative stress. Heart Rhythm. 12:440-448

Berenfel, O and Jalife, J. (2016). Mechanisms of atrial fibrillation: Rotors, ionic determinants, and excitation frequency. Heart Failure Clin 12:167-178.

Berger, R, Huelsman, M, Strecker, K, Bojic, A, Moser, P, Stanek, B, Pacher, R. (2002). B-type natriuretic peptide predicts sudden death in patients with chronic heart failure. Circulation. 105:2392-2397.

Bernardo, BC, Weeks, KL, Pretorius, L, McMullen, JR. (2010). Molecular distinction between physiological and pathological cardiac hypertrophy: Experimental findings and therapeutic strategies. Pharmacology & Therapeutics. 128:191-227

Birnbaum, SG, Varga, AW, Yuan, L, Anderson, AW, Sweatt, JD, Schrader, LA. (2004). Structure and function of Kv4-family transient potassium channels. Phsyiol Rev. 84:803-833.

Bleeker, WK, MacKaay, AJ, Masson-Pevet, M, Bouman, LN, Becker, AE (1980). Functional and morphological organization of the rabbit sinus node. Circ Res. 46:11-20

Blenck, CL, Harvey, PA, Reckelhoff, JF, Leinwand, LA. (2016). The importance of biological sex and estrogen in rodent models of cardiovascular disease. Circ Res. 118:1294-1312.

Bodi, I, Mikala, G, Kock, SE, Akhter, SA, Schwartz, Z. (2005). The L-type calcium channel in the heart: the beat goes on. JCI. 115:3306-3317

Boerrigter, G, Costello-Boerrigter, LC, Burnett, JC. (2009). Natriuretic peptides in the diagnosis and management of chronic heart failure. Heart Failure Clin. 5:501-514.

Boixel, C, Gonzalez, Q, Louedec, L, Hatem, SN. (2001). Mechanisms of L-Type Ca^{2+} current downregulation in rat atrial myocytes during heart failure. Circ Res. 89:607-613

Bond, RC, Bryant, SM, Watson, JJ, Hancox, JC, Orchard, CH, James, AF (2017). Reduced density and altered regulation of rat atrial L-type Ca^{2+} current in heart failure. Am J Physiol Heart Circ Physiol. 312:H384-H391

Bosch RF, Zeng, X, Grammer, JB, Popovic, K, Mewis, C, Kuhlkamp, V. (1999). Ionic mechanisms of electrical remodeling in human atrial fibrillation. Cardiovasc Res 44:121-131.

Bosch, RF, Scherer, CR, Rub, N, Worhl, S, Steinmeyer, K, Hasse, H, Busch, AE, Seipel, L, Kuhlkamp, V. (2003). Molecular mechanisms of early electrical remodeling: Transcriptional downregulation of ion channel subunits reduces $I_{Ca,L}$ and I_{to} in rapid atrial pacing in rabbits. Journal of the American Collage of Cardiology. 41:858-869

Boswell-Smith, V, Spina, D, and Page, CP. (2006). Phosphodiesterase inhibitors. British Journal of Pharmacology. 147:S252-S257

Boyett, MR, Bobrzynski, H, Lancaster, MK, Jones, SA, Honjo, H, Kodama, I. (2003). Sophisticated architecture is required for the sinoatrial node to perform its normal pacemaker function. J Cardiovasc Electrophysiol. 14:104-106.

Boyett, MR, Honjo, H, Kodama, I. (2000). The sinoatrial node, a heterogeneous pacemaker structure. Cardiovasc Res. 47:658-87.

Boyett, MR. (2009). ‘And the beat goes on’ The cardiac conduction system: the wiring system of the heart. Exp Physiol. 94:1035-1049

Bricca, G and Lantelme, P. (2011). Natriuretic peptides: Ready for prime-time in hypertension? Archives of Cardiovascular Disease. 104:403-409

Brundel, BJJM, Van Gelder, IC, Henning, RH, Tieleman, RG, Tuinenburg, AE, Wietses, M, Grandjean, JG, Van Gilst, WH, Crijns, HJGM. (2001). Ion channel remodeling is related to intraoperative atrial effective refractory periods in patients with paroxysmal and persistent atrial fibrillation. Circulation. 103:684-690.

Burashnikov, A and Antzelevitch, C. (2006). Late-Phase 3 EAD. A unique mechanism contributing to initiation of atrial fibrillation. Pacing Clin Electrophysiol. 29:290-295.

Burley, DS, Cox, CD, Zhang, J, Wann, KT, Baxter, GF. (2014). Natriuretic peptides modulate ATP-sensitive K^+ channels in rat ventricular cardiomyocytes. Basic Res. Cardiol. 109:402.

Caballero, R, Gomez, R, Moreno, I, Nunez, L, Gonzalez, T, Arias, C, Guizy, M, Valenzuela, C, Tamargo, J, Delpon, E. (2004). Interaction of angiotensin II with the angiotensin type 2 receptor inhibits the cardiac transient outward potassium current. Cardiovascular Research. 62:86-95

Calloe, K, Nof, E, Jespersen, T, Diego, J, Chlus, N, Olesen, S, Antzelevitch, C, Cordeiro, JM. (2011). Comparison of the effects of a transient outward potassium channel activstor on currents recorded from atrial and ventricular cardiomyocytes. J Cardiovasc Electrophysiol. 22:1057-1066

Calveieri, C, Rubattu, S, Volpe, M. (2012). Molecular mechanisms underlying cardiac antihypertrophic and antifibrotic effects of natriuretic peptides. J Mol Med. 90:5-13

Calzetta, L, Orlandi, A, Page, C, Rogliani, P, Rinaldi, B, Rosano, G, Cazzola, M, Matera, MG. (2016). Brain natriuretic peptide: Much more than a biomarker. International Journal of Cardiology. 221:1031-1038

Camelliti, P, Borg, TK, Kohl, P. (2005). Structural and functional characterisation of cardiac fibroblasts. Cardiovascular Research. 65:40-51

Cao, L and Gardner, DG. (1995). Natriuretic peptides inhibit DNA synthesis in cardiac fibroblasts. Hypertension. 25:227–234

Cataliotti, A, Tonne, JM, Bellavia, D, Martin, FL, Oehler, EA, Harders, GE, Campbell, JM, Peng, K, Russell, SJ, Malatino, LS, Burnett, JC, Ikeda, Y. (2011). Long-Term Cardiac pro-B-Type Natriuretic Peptide Gene Delivery Prevents the Development of Hypertensive Heart Disease in Spontaneously Hypertensive Rats. Circulation. 123:1297-1305

Catterall, WA. (2000). Voltage-Gated Calcium Channels. Cold Spring Harb Perspect Biol. 3:a003947

Censi, F, Corazza, I, Reggiani, E, Calcagnini, G, Mattei, E, Triventi, M, Boriani, G. (2016). P-wave Variability and Atrial Fibrillation. Scientific Reports 6:26799

Cha, T, Ehrlich, JR, Zhang, L, Nattel, S. (2004). Atrial ionic remodeling induced by atrial tachycardia in the presence of congestive heart failure. Circulation. 110:1520-1526.

Cha, Y, Dzeja, PP, Shen, WK, Jahangir, A, Hart, CYT, Terzic, A, Redfield, MM. (2003). Failing atrial myocardium: energetic deficits accompany structural remodeling and electrical instability. Am J Physiol Circ Phsyiol. 284:H1313-H1320

Chandler, NJ, Greener, ID, Tellez, JO, Inada, SMusa, H, Molenaar, P, DiFrancesco, D, Baruscotti, M, Longhi, R, Anderson, RH, Billeter, R, Sharma, V, Sigg, DC, Boyett, MR, Dobrzynski, H. (2009). Molecular architecture of the human sinus node. Circulation. 119:1562-1575

Chen, HH, Glockner, JF, Schirger, JA, Caraliotti, A, Redfield, MM, Burnett, JC. (2012). Novel protein therapeutics for systolic heart failure: Chronic subcutaneous B-type natriuretic peptide. J Am Coll Cardiol. 60:2305-2312.

Choudhury, M, Boyett, MR, Morris, GM. (2015). Biology of the sinus node and its disease. Arrhythmia and Electrophysiology Review 4:28-34

Cody, RJ, Atlas, SA, Laragh, JH, Kubo, SH, Covit, AB, Ryman, KS, Shaknovich, A, Pondolfino, K, Clark, M, Camargo, MJ, Scarborough, RM, Lewicki, JA. (1986). Atrial natriuretic factor in normal subjects and heart failure patients. Plasma levels and renal, hormonal, and hemodynamic responses to peptide infusion. J Clin Invest. 78:1362-1374.

Constantinides, C, Mean, R, Janssen, BJ. (2011). Effects of isoflurane anaesthesia on cardiovascular function of the C57BL/6 mouse. ILAR Journal. 52:e21-e31

Conte, G, Luca, A, Yazdani, S, Caputo, ML, Regoli, F, Moccetti, T, Kappenberger, L, Vesin, J, Auricchio, A. (2017). Usefulness of P-wave duration and morphologic variaibility to identify patients prone to paroxysmal atrial fibrillation. Am J Cardiol 119:275-279

Cooley, N, Ouyang, K, McMullen, JR, Kiriazis, H, Sheikh, F, Wu, W, Mu, Y, Du, X, Chen, J, Woodcock, EA. (2013). No contribution of IP_3-R(2) to disease phenotype in models of dilated cardiomyopathy or pressure overload hypertrophy. Circ Heart Fail. 6:318-325

Coppini, R, Ferrantini, C, Yao, L, Fan, P, Del Luango, M, Stillitano, F, Sartiani, L, Tosi, B, Suffredini, S, Tesi, C, Yacoub, M, Olivotto, I, Belardinelli, L, Poggesi, C, Cerbai, E, Mugelli, A. (2013). Late Sodium Current Inhibition Reverses Electromechanical Dysfunction in Human Hypertrophic Cardiomyopathy. Circulation. 127:575-578

Csepe, TA, Kalyanasundaram, A, Hansen, BJ, Zhao, J, Fedorov, VV. (2015). Fibrosis: a structural modulator of sinoatrial node physiology and dysfunction. Frontiers in Physiology. 6:37

D'Souza, SP, Davis, M, Baxter, GF. (2004). Autocrine and paracrine actions of natriuretic peptides in the heart. Pharmacology & Therapeutics. 101:113-129

David, M, Macias, A, Moreno, C, Prieto, A, Matrinez-Marmol, R, Vicente, R, Gonzalez, T, Felipe, A, Tamkun, MM, Valenzuela, C. (2012). Protein Kinase C (PKC) Activity Regulates Functional Effects of Kv 1.3 Subunit on KV1.5 Channels. Identification of a cardiac Kv1.5 channelosome. The Journal of Biological Chemistry. 287:21416-21428

de Bold, AJ, Borenstein, HB, Veress, AT, Sonnenberg, H. (1981). A rapid and potent natriuretic response to intravenous injection of atrial myocardial extract in rats. Life Sci. 28:89-94

De Jong, AM, Van Gelder, IC, Vreeswijk-Baudoin, I, Cannon, MV, Van Gilst, WH, Maass, AH. (2013). Atrial Remodeling Is Directly Related to End-Diastolic Left Ventricular Pressure in a Mouse Model of Ventricular Pressure Overload. PLoS ONE 8: e72651.

De Mello, W and Danser, AJH. (2000). Angiotensin II and the heart: on the intracrine renin-angiotensin system. Hypertension. 35:1183-1188.

De Mello, WC. (2011). Novel aspects of angiotensin II action in the heart. Implications to myocardial ischemia and heart failure. Regulatory Peptides. 166:9-14

Del Ry, S, Cabiati, M, Clerico, A. (2013). Recent advances on natriuretic peptide system: New promising therapeutic targets for the treatment of heart failure. Pharmocological Research. 76:190-198

Detta, N, Frisso, G, Salvatore, F. (2015). The multi-faceted aspects of the complex cardiac $Na_v1.5$ protein in membrane function and pathophysiology. Biochimica et Biophysica Acta 1854:1502-1509

Dhamoon, AS and Jalife, J. (2005). The inward rectifier current (I_{K1}) controls cardiac excitability and is involved in arrhythmogenesis. Heart Rhythm. 2:316-324.

Dickey, DM, Yoder, AR, Potter, LR. (2009). A familial mutation renders atrial natriuretic Peptide resistant to proteolytic degradation. J Biol Chem. 284:19196–19202.

DiFrancesco, D and Tortora, P. (1991). Direct activation of cardiac pacemaker channels by intracellular cyclic AMP. Nature. 351:145-7.

DiFrancesco, D. (2010). The role of the funny current in pacemaker activity. Circ Res. 106:434-446

DiFrancesco, D. and Borer, JS. (2007). The funny current: Cellular basis for the control of heart rate. Drugs. 67:15-24.

Dirkx, E, da Costa Martins, PA, De Windt, LJ. (2013). Regulation of fetal gene expression in heart failure. Biochimica et Biophysica Acta. 1832:2414-2424.

Dobrev, D and Ravens, U. (2003). Remodeling of cardiomyocyte ion channels in human atrial fibrillation. Basic Res Cardiol. 98:137-148

Dobrzynski, H. (2009). Molecular architecture of the human sinus node: insights into the function of the cardiac pacemaker. Circulation. 119:1562-1575.

Dobrzynski, H, Anderson, RH, Atkinson, A, Borbas, Z, D'Souza, A, Fraser, JF, Inada, S, Logantha, SJRJ, Monfredi, O, Morris, GM, Moorman, AFM, Nikolaidou, T, Schneider, H, Szuts, V, Temple, IP, Yanni, J, Boyett, MR. (2013). Structure, function and clinical relevance of the cardiac conduction system including the atrioventricular ring and outflow tract tissues. Pharmacology & Therapeutics. 139:260-288

Dobrzynski, H, Boyett, MR, Anderson, RH. (2007). New insights into pacemaker activity: promoting understanding of sick sinus syndrome. Circulation. 115:1921-1932

Doronin, SV, Potapova, IA, Lu, Z, Cohen, IS. (2004). Angiotensin receptor type 1 forms a complex with the transient outward potassium channel Kv4.3 and regulates its gating properties and intracellular localization. The Journal of Biological Chemistry. 279:48231-48237

Dun, W, Yagi, T, Rosen, MR, & Boyden, PA (2003). Calcium and Potassium currents in cells from adult and aged canine right atria. Cardiovascular Research. 58:526–534.

Dun, W. and Boyden, PA. (2009). Aged atria: electrical remodelling conducive to atrial fibrillation. J Interv Card Electrophysiol. 25:9-18.

Eckstein, J, Verheule, S, de Groot, N, Allessie, M, Schotten, U. (2008). Mechanisms of perpetuation of atrial fibrillation in chronically dilated atria. Progress in Biophysics and Molecular Biology. 97:435-451.

Egom, EE, Vella, K. Hua, R, Jansen, HJ, Moghtadaei, M, Polina, I, Bogachev, O, Hurnik, R, Mackasey, M, Rafferty, S, Ray, G, Rose, RA. (2015). Impaired sinoatrial node function and increased susceptibility to atrial fibrillation in mice lacking natriuretic peptide receptor C. J. Physiol. 593:1127-1146.

Ehrlich, JR, Hohnloser, SH, Nattel, S. (2006). Role of angiotensin system and effects of its inhibition I atrial fibrillation: clinical and experimental evidence. European Heart Journal. 27:512-518

Elvan, A, Wylie, K, Zipes, DP. (1996). Pacing-induced chronic atrial fibrillation impairs sinus node function in dogs: electrophysiological remodeling. Circulation. 94:2953–2960.

Erickson, JR, Joiner, MA, Guan, X, Kutschke, W, Yang, J, Oddis, CV, Barlett, RK, Lowe, JS, O'Donnell, SE, Aykin-Burns, N, Zimmerman, MC, Zimmerman, K, Ham, AL, Weiss, RM, Spitz, DR, Shea, MA, Colbran, RJ, Mohler, PJ, Anderson, ME. (2008). A Dynamic Pathway for Calcium-Independent Activation of CaMKII by Methionine Oxidation. Cell. 133:462-474

Fan, D, Takawale, A, Lee, J, Kassiri, Z. (2012). Cardiac fibroblasts, fibrosis and extracellular matrix remodeling in heart disease. Fibrogenesis & Tissue Repair. 5:15

Fedorov, VV, Chang, R, Glukhov, AV, Kostechki, G, Janks, D, Schuessler, RB, Efimov, IR. (2010). Complex interactions between the sinoatrial node and atrium during reentrant arrhythmias in the canine heart. Circulation. 122:782-789

Fedorov, VV, Glukhov, AV, Chang, R. (2012). Conduction barriers and pathways of the sinoatrial pacemaker complex: their role in normal rhythm and atrial arrhythmias. Am J Physiol Heart Circ Physiol. 302: H1773-1783.

Fedorov, VV, Schuessler, RB, Hemphill, M, Ambrosi, CM, Chang, R, Voloshina, AS, Brown, K, Hucker, WJ, Efimov, IR. (2009). Structural and functional evidence for discrete exit pathways that connect the canine sinoatrial node and atria. Circ Res. 104:915-923

Feng, JA, Perry, G, Mori, T, Hayashi, T, Oparil, S, Chen, Y. (2003). Pressure-independent enhancement of cardiac hypertrophy in atrial natriuretic peptide-deficient mice. Clinical and Experimental Pharmacology and Physiology. 30:342-349

Feridooni, HA, Sun, MH, Rockwood, K. Howlett, S.E. (2015). Reliability of a Frailty Index Based on the Clinical Assessment of Health Deficits in Male C57BL/6J Mice. J Gerontol A Biol Sci Med Sci 70:686–693

Ferrario, CM and Mullick, AE. (2017). Renin angiotensin aldosterone inhibition in the treatment of cardiovascular disease. Pharmacol Res. 125(Pt A):57-71

Fischmeister, R, Castro, LRV, Abi-Gerges, A, Rochais, F, Jurevicius, J, Leroy, J, Vandecasteele, G. (2006). Compartmentation of Cyclic Nucleotide Signaling in the Heart. The Role of Cyclic Nucleotide Phosphodiesterases. Circ Res. 99:816-828

Foeger, NC, Wang, W, Mellor, RL, NErbonne, JM. (2013). Stabilization of Kv4 protein by the accessory K^+ channel interacting protein 2 (KChIP2) subunit is required for the generation of native myocardial fast transient outward K^+ currents. J Physiol. 591:4149-4166

Franciosi, S, Perry, FKG, Roston, TM, Armstrong, KR, Claydon, VE, Sanatani, S. (2017). The role of the autonomic nervous system in arrhythmias and sudden cardiac death. Autonomic Neuroscience: Basic and Clinical. 205:1-11.

Franco, V, Chen, Y, Oparil, S, Feng, JA, Wang, D, Hage, F and Perry, G. (2004). Atrial natriuretic peptide dose-dependently inhibits pressure overload-induced cardiac remodeling. Hypertension. 44:746-750

Frisoli, A, Ingham, SJ, Paes, A, Tinoco, E, Greco, A, Zanata, N, Pintarelli, V, Elber, I, Borges, J, Camargo Carvalho, AC. (2015). Fraily predictors and outcomes among older patients with cardiovascular disease: Data from Fragicor. Archives of Gerontology and Geriatrics. 61:1-7

Fukui, A, Takahashi, N, Nakada, C, Masaki, T, Kume, O, Shinohara, T, Teshima, Y, Hara, M, Saikawa, T. (2013). Role of leptin signaling in the pathogenesis of angiotensin II-mediated atrial fibrosis and fibrillation. Circ Arrhythm Electrophysiol. 6:402-409.

Fye, WB. (1994). A history of the origin, evolution, and impact of electrocardiography. The American Journal of Cardiology. 73:937-949.

Gan, T, Qiao, W, Xu, G, Zhou, X, Tang, B, Song, J, Li, Y, Zhang, J, Li, F, Mao, T, Jiang, T. (2013). Aging-associated changes in L-type calcium channels in the left atria of dogs. Experimental and Therapeutic Medicing. 6:919-924

Gandhi, PU, and Pinney, S. (2014). Management of chronic heart failure: Biomarkers, monitors, and disease management programs. Annals of Global Health. 80:46-54.

Gassanov, N, Brandt, MC, Michels, G, Lindner, M, Er, F, Hoppe, UC. (2006). Angiotensin II-induced changes of calcium sparks and ionic currents in human atrial myocytes: Potential role for early remodeling in atrial fibrillation. Cell Calcium. 39:175-186

Gehrmann, J, Hammer, PE, Maguire, CT, Wakimoto, H, Triedman, JK, Berul, CI. (2000). Phenotypic screening for heart rate variability in the mouse. Am J Physiol 279:H733-H740.

Georgiopoulou, VV, Kalogeropolous, AP, Raggi, P, Butler, J. (2010). Prevention, diagnosis, and treatment of hypertensive heart disease. Cardiol Clin 28:675-691.

Geske, JB, McKie, PM, Ommen, SR, Sorajja, P. (2013). B-Type natriuretic peptide and survival in hypertrophic cardiomyopathy. Journal of the American College of Cardiology. 61:2456-2460

Glenn, DJ, Rahmutula, D, Nishimoto, M, Liang, F, Gardner, DG. (2009). Atrial natriuretic peptide suppresses endothelin gene expression and proliferation in cardiac fibroblasts through a GATA4-dependent mechanism. Cardiovasc Res 84:209–217.

Goldstein, SAN, Bockenhauer, D, O'Kelly, I, Zilberberg, N. (2001). Potassium leak channels and the KCNK family of two-P-domain subunits. Nature Reviews Neuroscience. 2:175-184.

Gradman, AH and Alfayoumi, F. (2006). From Left Ventricular Hypertrophy to Congestive Heart Failure: Management of Hypertensive Heart Disease. Progress in Cardiovascular Diseases. 48:326-341

Grant, O. (2009). Cardiac ion channels. Circ Arrhythmia Electrophysiology. 2:185-194

Grubb, S, Aistrup, GL, Koivumaki, JT, Speerschneider, T, Gottlieb, LA, Mutsaers, NAM, Olesen, S, Calloe, K, Thomsen, MB. (2015). Preservation of cardiac function by prolonged action potentials in mice deficient of KChIP2. 309:H481-H489

Grubb, S, Calloe, K, Thomsen, MB. (2012). Impact of KChIP2 on cardiac electrophysiology and the progression of heart failure. Frontiers of Physiology. 3:118

Grubb, S, Speerschneider, T, Occhipinti, D, Fiset, C, Olesen, S, Thomsen, MB, Calloe, K. (2014). Loss of K+ Currents in Heart Failure Is Accentuated in KChIP2 Deficient Mice. J Cardiovasc. Electrophsyiol. 25:896-904

Grunnet, M, Bentzen, BH, Sørensen, US, Diness, JG. (2011). Cardiac Ion Channels and Mechanisms for Protection Against Atrial Fibrillation. In: Nilius B. et al. (eds) Reviews of Physiology, Biochemistry and Pharmacology. Reviews of Physiology, Biochemistry and Pharmacology, vol 162. Springer, Berlin, Heidelberg

Gu, J, Liu, X, Wang, Q, Guo, M, Liu, F, Song, Z, Zhang, D. (2013). Beneficial effects of pioglitazone on atrial structural and electrical remodeling in vitro cellular models. Journal of Molecular and Cellular Cardiology. 65:1-8

Guo, D, Young, L, Wu, Y, Belardinelli, L, Kowey, PR, Yan, G. (2010). Increased late sodium current in left atrial myocytes of rabbits with left ventricular hypertrophy: its role in the genesis of atrial arrhythmias. Am J Physiol Heart Circ Physiol. 298: H1375-H1318.

Guo, W, Li, H, Aimond, F, Johns, DC, Phodes, KJ, Trimmer, JS, Nerbonne, JM. (2002). Role of Heteromultimers in the Generation of Myocardial Transient Outward K Currents. Circ Res. 90:586-593

Hadian, D, Zipes, DP, Olgin, JE, Miller, JM (2002). Short-term rapid atrial pacing produces electrical remodeling of sinus node function in humans. J Cardiovasc Electrophysiol. 13:584–586.

Hagiwara, K, Nunoki, K, Ishii, K, Abe, T, Yanagisawa, T. (2003). Differential inhibition of transient outward currents of Kv1.4 and Kv4.3 by endothelin. Biochemical and Biophysical Research Communications. 310:634-640.

Harrington, J, Fillmore, N, Gao, S, Yang, Y, Zhang, X, Liu, P, Stoehr, A, Chen, Y, Springer, D, Zhu, J, Wang, X, Murphy, E. (2017). A systems biology approach to investigating sex differences in cardiac hypertrophy. J Am Heart Assoc. 6:e005838.

Hasegawa, K, Fujiwara, H, Doyama, K, Miyamae, M, Fujiawra, T, Suga, S, Mukoyama, M, Nakao, K, Imura, H, Sasayama, S. (1993). Ventricular expression of brain natriuretic peptide in hypertrophic cardiomyopathy. Circulation. 88:372-380.

He, J, Chen, Y, Huang, Y, Yao, F, Wu, Z, Chen, S, Wang, L, Xiao, P, Dai, G, Meng, R, Zheng, C, Tang, L, Huang, L, Ki, Z. (2009). Effect of long-term B-type natriuretic peptide treatment on left ventricular remodeling and function after myocardial infarction in rats. Eur J Pharmacol. 602:132–137.

Healey, JS, Baranchuk, A, Crystal, E, Morillo, CA, Garfinkle, M, Yusuf, S, Connolly, SJ. (2005). Prevention of atrial fibrillation with angiotensin-converting enzyme inhibitors and angiotensin receptor blockers. Journal of the American College of Cardiology. 45:1832-1839.

Heijman, J, Voigt, N, Nattel, S, Dobrev, D. (2014). Cellular and Molecular Electrophysiology of Atrial Fibrillation Initiation, Maintenance, and Progression. Circ Res. 114:1483-1499.

Hill, JA. (2003). Electrical Remodeling in Cardiac Hypertrophy. Trends Cardiovasc Med. 13:316-322

Hocini M, Sanders P, Deisenhofer I, Jais, P, Hsu, L, Scavee, C, Weerasoriya, R, Raybaud, F, Macle, L, Shah, DC, Garrigue, S, Le Metayer, P, Clementy, J, Haissaguerre, M. (2003). Reverse remodeling of sinus node function after catheter ablation of atrial fibrillation in patients with prolonged sinus pauses. Circulation. 108:1172–1175.

Hodgson-Zingman, D, Karst, ML, Zingman, LV, Heublein, DM, Darbar, D, Herron, KJ, Ballew, JD, de Andrade, M, Burnett, JC, Olson, TM. (2008). Atrial natriuretic peptide frameshift mutation in familial atrial fibrillation. The New England Journal of Medicine. 358:158-165.

Horio, T, Tokudome, T, Maki, T, Yoshihara, F, Suga, S, Nishikimi, T, Kojima, M, Kawano, Y, Kangawa, K. (2003). Gene expression, secretion, and autrocrine action of C-type natriuretic peptide in cultured adult rat cardiac fibroblasts. Endocrinology. 144:2279-2284

Hua, R, MacLeod, SL, Polina, I, Moghtadaei, M, Jansen, HJ, Bogachev, O, O'Blenes, SB, Sapp, JL, Legare, JF, Rose, RA. (2015). Effects of wild-type and mutant forms of atrial natriuretic peptide on atrial electrophysiology and arrhythmogenesis. Circ. Arrhythm. Electrophysiol. 8:1240-1254.

Huang, X, Du, Y, Yang, P, Lin, S, Xi, Y, Yang, Z, Ma, A. (2015). Age-dependent alterations of voltage-gated Na^+ channel isoforms in rat sinoatrial node. Mechanisms of Ageing and Development. 152:80-90

Huang, X, Yang, P, Du, Y, Zhang, J, Ma, A. (2007). Age-related down-regulation of HCN channels in rat sinoatrial node. Basic Res Cardiol 102:429-435

Huo, X, Zhang, Y, Zhang, X, Nirmalan, M, Davies, L, Konstantinou, D, Yin, F, Dobrzynski, H, Wang, X, Grace, A, Zhang, H, Boyett, M, Huang, C, Lei, M. (2011). TGF-β_1 Mediated Fibrosis and Ion Channel Remodeling Are Key Mechanisms Producing the Sinus Node Dysfunction Associated with SCN5A Deficiency and Aging. Circulation: Arrhythmia and Electrophysiology. 4:397-406

Ichihara, S, Senbonmatsu, T, Price, Jr, E, Ichiki, T, Gaffney, A, Inagami, T. (2001). Angiotensin II type 2 receptor is essential for left ventricular hypertrophy and cardiac fibrosis in chronic angiotensin II-induced hypertension. Circulation. 104:346-351

Ichiki, T, Boerrigter, G, Huntley, BK, Sangaralingham, SJ, KcKie, PM, Harty, GJ, Harders, GE, Burnett, JC. (2012). Differential expression of the pro-natriuretic peptide convertases corin and furin in experimental heart failure and atrial fibrosis Am J Phsyiol Regul Integr Comp Physiol. 304:R102-R109.

Inoue, S, Murakami, Y, Sano, K, Katoh, J, Shimada, T. (2000). Atrium as a source of brain natriuretic polypeptide in patients with atrial fibrillation. Journal of Cardiac Failure. 6:92-96

Irisawa, H, Brown, HF, Giles, W. (1993). Cardiac pacemaking in the sinoatrial node. Physiol Rev, 73, 197-227.

Iwai, N, Shimoike, H, Kinoshita, M. (1995). Cardiac renin-angiotensin system in the hypertrophied heart. Circulation. 92:2690-2696.

Iwasaki, Y, Nishida, K, Kato, T, Nattel, S. (2011). Atrial fibrillation pathophysiology: Implications for management. Circulation. 124:2264-2274

Izzo, JL and Grandman, AH. (2004). Mechanisms and management of hypertensive heart disease: from left ventricular hypertrophy to heart failure. Med Clin N Am. 88:1257-1271

Jackson, LR, Rathakrishnan, B, Campbell, K, Thomas, KL, Piccini, JP, Bahnson, T, Stiber, JA, Daubert, JP. (2017). Sinus Node Dysfunction and Atrial Fibrillation: A Reversible Phenomenon? PACE. 40:442-450.

Jalife, J and Kaur, K. (2015). Atrial remodeling, fibrosis, and atrial fibrillation. Trends in Cardiovascular Medicine. 25:475-484

Jansen, HJ and Rose, RA. (2015). Natriuretic peptides: critical regulators of cardiac fibroblasts and the extracellular matrix in the heart. In: Dixon, IM, Wigle, JT. (Eds.), Cardiac Fibrosis and Heart Failure: Cause or Effect. Springer International Publishing, pp. 383e404.

Jansen, HJ, Moghtadaei, M, Mackasey, M, Rafferty, SA, Bogachev, O, Sapp, JL, Howlett, SE, Rose, RA (2017b). Atrial structure, function and arrhythmogenesis in aged and frail mice. Scientific Reports. 7:44336

Jansen, HJ, Quinn, TA, Rose, RA. (2017a). Cellular Sinoatrial Node and Atrioventricular Node Activity in the Heart. In Reference Module in Biomedical Sciences, Elsevier, 2017, ISBN 9780128012383. http://dx.doi.org/10.1016/B978-0-12-801238-3.99759-9

Janssen, BJ and Smits, JF. (2002). Autonomic control of blood pressure in mice: basic physiology and effects of genetic modification. Am J Physiol Regul Integr Comp Physiol. 282:R1545-R1564.

Jaubert, J, Jaubert, F, Martin, N, Washburn, LL, Lee, BL, Eicher, EM, Guenet, J. (1999). Three new allelic mouse mutations that cause skeletal overgrowth involve the natriuretic peptide receptor C gene (Npr3). Proc Natl. Acad. Sci. 96:10278-10283

Ji, H, Zheng, W, Wu, X, Ecelbarger, CM, Watkins, R, Arnold, AP, Sandberg, K. (2010). Sex Chromosome Effects Unmasked in Angiotensin II–Induced Hypertension. Hypertension. 55:1275-1282.

John, RM and Kumar, S. (2016). Sinus node and atrial arrhythmias. Circulation. 133:1892-1900.

Jones, SA, Boyett, MR, Lancaster, MK. (2007). Declining Into Failure: The Age-Dependent Loss of the L-Type Calcium Channel Within the Sinoatrial Node. Circulation. 115:1183-1190.

Jones, SA, Lancaster, MK, Boyett, MR. (2004). Ageing-related changes to connexins and conduction within the sinoatrial node. J Physiol. 560:429-437

Joung, B, Lin, S, Chen, Z, Antoun, PS, Maruyama, M, Han, S, Piccirillo, G, Stucky, M, Zipes, DP, Chen, P, Das, MK. (2010). Mechanisms of sinoatrial node dysfunction in a canine model of pacing-induced atrial fibrillation. Heart Rhythm. 7:88-95

Just, A, Faulhaber, J, Ehmke, H. (2000). Autonomic cardiovascular control in conscious mice. Am J Physiol. 279:R2214–R2221.

Kane, AE, Ayaz, O, Ghimire, A, Feridooni, HA, Howlett, SE. (2017). Implementation of the mouse frailty index. Can. J. Physiol. Pharmacol. 95:1149-1155

Kapoun, AM, Liang, F, O'Younh, G, Damm, DL, Quon, D, White, RT, Munson, K, Lam, A, Schreiner, GF, Protter, AA. (2004). B-Type Natriuretic Peptide Exerts Broad Functional Opposition to Transforming Growth Factor- in Primary Human Cardiac Fibroblasts: Fibrosis, Myofibroblast Conversion, Proliferation, and Inflammation. Circ Res. 94:453-461.

Keith, A, Flack, M. (1907). The Form and Nature of the Muscular Connections between the Primary Divisions of the Vertebrate Heart. J Anat Physiol. 41:172-89.

Kim, S and Iwao. H. (2011). Molecular and cellular mechanisms of Angiotensin-II mediated cardiovascular and renal diseases. Pharmocological Reviews. 52:11- 34

Kim, S, Yoon, S, Choi, J, Kang, M, Cho, Y, /oh, I, Kim, C, Kim, K. (2017). Clinical implication of frailty assessment in older patients with atrial fibrillation. Archives of Gerontology and Geriatrics. 70:1-7

King, JH, Huang, CLH, Fraser, JA. (2013). Determinants of myocardial conduction velocity: implications for arrhythmogenesis. Frontiers in Physiology. 4:1-14

Kirchhof, CJ and Allessie, MA. (1992). Sinus node automaticity during atrial fibrillation in isolated rabbit hearts. Circulation. 86:263–271.

Kirchhof, P, and Schotten, U. (2006). Hypertension begets hypertrophy begs atrial fibrillation: Insights from yet another sheep model. European Heart Journal. 27:2919-2920.

Kishimoto, I, Rossi, K, Garbers, DL (2000). A genetic model provides evidence that the receptor for atrial natriuretic peptide (guanylyl cyclase-A) inhibits cardiac ventricular myocyte hypertrophy. PNAS 98:2703-2706

Kistler, PM, Sanders, P, Dodic, M, Spence, SJ, Samuel, CS, Zhao, C, Charles, JA, Edwards, GA, Kalman, JM. (2006). Atrial electrical and structural abnormalities in an ovine model of chronic blood pressure elevation after prenatal corticosteroid exposure: implications for development of atrial fibrillation. European Heart Journal. 27:3045-3056.

Kistler, PM, Sanders, P, Fynn, SP, Stevenson, IH, Spence, SJ, Vohra, JK, Sparks, PB, Kalman, JM. (2004). Electrophysiologic and electroanatomic changes in the human atrium associated with age. Journal of the American College of Cardiology. 44:109-116

Kleber, AG and Rudy, Y. (2004). Basic mechanisms of cardiac impulse propagation and associated arrhythmias. Physiol Rev. 84:431-388.

Knowles, JW, Esposito, G, Mao, L, Hagaman, JR, Fox, JE, Smithies, O, Rockman, HA, Maeda, N. (2001). Pressure-independent enhancement of cardiac hypertrophy in natriuretic peptide receptor A-deficient mice. J Clin Invest. 107:975-984

Kodama, I, and Boyett, MR. (1985). Regional differences in the electrical activity of the rabbit sinus node. Pflugers Arch. 404:214-26.

Koschak, A, Reimer, D, Huber, I, Grabner, M, Glossmann, H, Engel, J, Striessnig, J. (2001). 1D (Cav1.3) Subunits Can Form L-type Ca^{2+} Channels Activating at Negative Voltages. The Journal of Biological Chemistry. 276:22100-22106.

Kuo, H, Cheng, C, Clark, RB, Lin, JJC, Lin, JLC, Hoshijima, M, Nguyen-Tran, VTB, Gu, Y, Ikeda, Y, Chu, PH, Ross, J, Giles, WR, Chien, KR. (2001). A Defect in the K_V Channel-Interacting Protein 2 (KChIP2) Gene Leads to a Complete Loss of I_{to} and Confers Susceptibility to Ventricular Tachycardia. Cell. 107:801-813.

Larson, ED, St. Clair, JR, Sumner, WA, Bannister, RA, Proenza, C. (2013). Depressed pacemaker activity of sinoatrial node myocytes contributes to the age-dependent decline in maximum heart rate. PNAS 110:18011-18016

Lau, DH, Linz, D, Schotten, U, Mahajam, R, Sanders, P, Kalman, JM. (2017). Pathophysiology of paroxysmal and persistent atrial fibrillation: Rotors, foci and fibrosis. Heart, Lung, and Circulation. 26:887-893.

Lau, DH, MacKenzie, L, Kelly, DJ, Psaltis, PJ, Worthington, M, Rajendram, A, Kelly, DR, Nelson, AJ, Zhang, Y, Kuklik, P, Brooks, AG, Worthley, SG, Faull, RJ, Rao, M, Edwards, J, Saint, DA, Sanders, P. (2010). Short-term hypertension is associated with the development of atrial fibrillation substrate: A study in an ovine hypertensive model. Heart Rhythm. 7:396-404

Lau, DH, Schotten, U, Mahajan, R, Antic, NA, Hatem, SN, Pathak, RK, Hendriks, JML, Kalman, JM, Sanders, P. (2016). Novel mechanisms in the pathogenesis of atrial fibrillation: practical applications. European Heart Journal. 37:1573-1581.

Le Grand, B, Deroubaix, E, Couetil, JP, Coraboeuf, E. (1992). Effects of atrionatriuretic factor on Ca^{2+} current and Cai-independent transient outward K^+ current in human atrial cells. Pflugers Arch. 421:486e491.

Leung, AA, Daskalopoulou, SS, Dasgupta, K, McBrien, K, Butalia, S, Zarne, KB, Nerenberg, K, Harris, KC, Nakhla, M, Cloutier, L, Gerlfer, M, Lamarre-Cliche, M, Milot, A, Bolli, P, Tremblay, G, McLean, D, Tobe, SW, Ruzicka, M, Burns, KD, Vallee, M, Prasad, GVR, Gryn, SE, Feldman, RD, Selby, P, Pipe, A, Schiffrin, EL, McFaleane, PA, Oh, P, Hegele, RA, Khara, M, Wilson, TW, Penner, SB, Burgess, E, Sivapalan, P, Herman, RJ, Bacon, SL, Rabkin, SW, Gilbery, RE, Campbell, TS, Grover, S, Honos, G, Lindsay, P, Hill, MD, Coutts, SB, Gubitz, G, Campbell, NRC, Moe, GW, Howlett, JG, Boulanger, J, Prebtani, A, Kline, G, Leiter, LA, Jones, C, Cote, A, Woo, V, Kaczorowski, J, Trudea, L, Tsuyuki, RT, Hiremath, S, Drouin, D, Lavoie, KL, Hamet, P, Gregoire, JC, Lewanczuk, R, Dresser, GK, Sharma, M, Reid, D, Lear, SA, Moullec, G, Gupta, M, Magee, LA, Logan, AG, Dionne, J, Fournier, A, Benoit, G, Feber, J, Poirier, L, Padwal, RS, and Rabi, DM. (2017). Hypertension Canada's 2017 guidelines for diagnosis, risk assessment, prevention, and treatment of hypertension in adults. Canadian Journal of Cardiology. 33:557-576

Li, P, Wang, D, Lucas, J, Oparil, S, Xing, D, Cao, X, Novak, L, Renfrow, MB, Chen, YF (2008). Atrial natriuretic peptide inhibits transforming growth factor beta induced Smad signaling and myofibroblast transformation in mouse cardiac fibroblasts. Circ Res. 102:185–192.

Li, G, Liu, E, Liu, T, Wang, J, Dai, J, Xu, G, Korantzopoulos, P, Yang, W. (2011). Atrial electrical remodeling in a canine model of sinus node dysfunction. International Journal of Cardiology. 146:32-36

Li, H, Guo, W, Mellor, RL, Nebonne, JM. (2005). KChIP2 modulates the cell surface expression of Kv1.5-encoded K^+ channels. Journal of Molecular and Cellular Cardiology. 39:121-132

Li, Y, Sarkar, O, Brochu, M, Anand-Srivastava, MB. (2014). Natriuretic Peptide Receptor-C Attenuates Hypertension in Spontaneously Hypertensive Rats: Role of Nitroxidative Stress and Gi Protein. Hypertension. 63:846-855.

Lin, Y, Chen, Y, Lee, T, Chen, Y, Chen, C, Chen, Y. (2017). Aging modulates the substrate and triggers remodeling in atrial fibrillation. Circ J. doi:10.1253/circj.CJ-17-0242

Limberg, SH, Netter, MF, Rolfes, C, Rinne, S, Schlichthorl, G, Zuzarte, M, Vassiliou, T, Moosdorf, R, Wulf, H, Daut, J, Sachse, FB, Decher, N. (2011). TASK-1 channels may modulate action potential duration of human atrial cardiomyocytes. Cell Physiol Biochem. 28: 613-624

Lindpainter, K, Jin, M, Niedermaier, N, Wilhelm, MJ, Ganten, D. (1990). Cardiac angiotensinogen and its local activation in the isolated perfused beating heart. Circulation Research. 67:564-573

Lisy, O, Lainchbury, JG, Leskinen, H, Burnett, JC. (2001). Therapeutic Actions of a New Synthetic Vasoactive and Natriuretic Peptide, Dendroaspis Natriuretic Peptide, in Experimental Severe Congestive Heart Failure. Hypertension. 37:1089-1094.

Liu, J, Dobrzynski, H, Yanni, J, Boyett, MR, Lei, M. (2007). Organization of the mouse sinoatrial node: structure and expression of HCN channels. Cardiovasc Res, 73:729-38.

Liu, X, Wang, Y, Zhang, H, Shen, L, Xu, Y. (2017). Distinct protein kinase C isoenzyme mediates inhibitory effects of different G-protein coupled receptors on cardiac rapidly activating delayed rectifier K+ current. British Journal of Pharmacology. doi:10.1111/bph.14049

Liu, X., Jahangir, A., Terzic, A., Gersh, BJ, Hammil, SC, Shen, W. (2004). Age- and sex-related atrial electrophysiologic and structural changes. Am J Cardiol 94:373-375

Lomax, AE, Kondo, CS, Giles, WR. (2003b). Comparison of time- and voltage-dependent K currents in myocytes from left and right atria of adult mice. Am J Physiol Heart Cir Physiol. 285:H1837-H1848.

Lomax, AE, Rose, RA, Giles, WR. (2003a). Electrophysiological evidence for a gradient of G protein-gated K^+ current in adult mouse atria. British Journal of Pharmacology. 104:576-584.

London, B, Guo, W, Pan, X, Lee, JS, Shusterman, V, Rocco, CJ, Logothetis, DA, Nerbonne, JM, Hill, JA. (2001). Targeted Replacement of Kv1.5 in the Mouse Leads to Loss of the 4-Aminopyridine–Sensitive Component of IK,slow and Resistance to Drug-Induced QT Prolongation. Circ Res. 88:940-946

Lopatin, AN and Nichols, CG. (2001). Inward rectifiers in the heart: An update on I_{K1}. J Mol Cell Cardiol. 33:625-638

Lopez, MJ, Wong, SK, Kishimoto, I, Dubois, S, Mach, V, Friesen, J, Garbers, DL, Beuve, A. (1995). Salt-resistant hypertension in mice lacking the guanylyl cyclase-A receptor for atrial natriuretic peptide. Nature 378:65–68.

Lu, G, Xu, C, Tang, K, Zhang, J, Li, Q, Peng, L, Wang, Y, Huang, Z, Gao, X. (2017). H_2S inhibits angiotensin II-induced atrial Kv1.5 upregulation by attenuating Nox4-mediated ROS generation during atrial fibrillation. Biochemical and Biophysical Research Communications. 483:534-540.

Lu, G, Xu, S, Peng, L, Huang, Z, Gao, X. (2014). Angiotensin II upregulates Kv1.5 expression through ROS-dependent transforming growth factor-beta1 and extracellular signal-regulated kinase 1/2 signalings in neonatal rat atrial myocytes. Biochemical and Biophsysical Research Communications. 454:410-416

Lytwyn, J, Stammers, AN, Kehler, DS, Jung, P, Alexander, B, Hiebert, BM, Dubiel, C, Kimber, D, Hamm, N, Clarke, M, Fraser, C, Pedreria, B, Duhamel, TA, Tangri, N, Arora, RC. (2017). The impact of frailty on functional survival in patients 1 year after cardiac surgery. J Thorac Cariovasc Surg. 1-10.

Ma, Y, Kong, L, Qi, S, Wang, D. (2016). Atorvastatin blocks increased L-type Ca2+ current and cell injury elicited by angiotensin II via inhibiting oxide stress. Acta Biochim Biophys Sin. 48:378-384

Maack, T, Suzuki, M, Almeida, FA, Nussenzveig, D, Scardorough, RM, McEnroe, GA, Lewicki, JA. (1987). Physiological role of silent receptors of atrial natriuretic factor. Science. 238:675-678

Macheret, F, Heublein, D, Costello-Beorrigter, LC, Boerrigter, G, McKie, P, Bellavia, D, Mangiafico, S, Ikeda, Y, Bailey, K, Scott, CG, Sandberg, S, Chen, HH, Malatino, L, Redfield, MM, Rodeheffer, R, Burnett, J, Cataliotti, A. (2012). Hyman hypertension is characterized by a lack of activation of the antihypertensive cardiac hormones ANP and BNP. Journal of the American College of Cardiology. 60:1558-1565.

Maden, SA, Fida, N, Barman, P, Sims, D, Shin, J, Verghese, J, Pina, I, Jorde, U, Patel, SR. (2016). Frailty assessment in advanced heart failure. Journal of Cardiac Failure. 22:840-844.

Mahajan, R., Pathak, RK, Thiyagarajah, A, Lau, DH, Marchlinski, FE, Dixit, S, Day, JD, Hendriks, JML, Carrington, M, Kalman, JM, Sanders, P. (2017). Risk factor management and atrial fibrillation clinics: Saving the best for last? Heart, Lunch, and circulation. 26:990-997

Maisel, A, Xue, Y, Greene, SJ, Pang, PS, Januzzi, JL, Pina, IL, Defilippi, C, Butler, J. (2015). The potential role of natriuretic peptide – guided management for patients hospitalized for heart failure. J Cardiac Fail. 21:233-239

Maisel, WH and Stevenoson, LW (2003). Atrial Fibrillation in Heart Failure: Epidemiology, Pathophysiology, and Rationale for Therapy. Am J Cardiol. 91(suppl):2D-8D.

Makielski, JC. (2016). Late sodium current: A mechanism for angina, heart failure, and arrhythmia. Trends in Cardiovascular Medicine. 26:115-122

Mangiafico, S, Costello-Boerrigter, LC, Andersen, IA, Cataliotti, A, Burnett, JC. (2013). Neutral endopeptidase inhibition and the natriuretic peptide system: an evolving strategy in cardiovascular therapeutics. European Heart Journal. 34:886-893.

Mangoni, ME and Nargeot, J. (2008). Genesis and Regulation of the Heart Automaticity. Physiol Rev. 88:919-982

Mangoni, ME, Couette, B, Bourinet, E, Platzer, J, Reimer, D, Striessnig, J, Nargeot, J. (2003). Functional role of L-type $Ca_V1.3$ Ca^{2+}channels in cardiac pacemaker activity. PNAS. 100:5543-5548

Mangoni, ME, Couette, B, Marger, L, Bourinet, E, Striessnig, J, Nargeot, J. (2006). Voltage-dependent calcium channels and cardiac pacemaker activity: From ionic currents to genes. Progress in Biophysics and Molecular Biology. 90:38-63

Marionneau, C, Brunet, S, Flagg, TP, Pilgram, TK, Demolombe, S, Nerbonne, JM. (2008). Distinct Cellular and Molecular Mechanisms Underlie Functional Remodeling of Repolarizing K^+ Currents With Left Ventricular Hypertrophy. Circ. Res. 102:1406-1415.

Markandeya, YS, Phelan, LJ, Woon, MT, Keefe, AM, Reynolds, CR, August, BK, Hacker, TA, Roth, DM, Patel, HH, Balijepalli, RC. (2015). Caveolin-3 Overexpression Attenuates Cardiac Hypertrophy via Inhibition of T-type Ca2 Current Modulated by Protein Kinase C in Cardiomyocytes. The Journal of Biological Chemistry. 290:22085-22100

Markides, V and Schilling, RJ. (2003). Atrial fibrillation: Classification, pathophysiology, mechanisms and drug treatment. Heart. 89:939-943

Mathieu, S, Khoury, NE, Rivard, K, Gelinas, R, Goyette, P, Paradis, P, Nemer, M, Fiset, C. (2016). Reduction in Na^+ current by angiotensin II is mediated by PKCα in mouse and human-induced pluripotent stem cell-derived cardiomyocytes. Heart Rhythm. 13:1346-1354.

McKinnon, D, and Rosati, B. (2016). Transmural gradients in ion channel and auxiliary subunit expression. Progress in Biophysics and Molecular Biology. 122:165-186

McNallen, SM, Chamerlain, AM, Gerber, Y, Sing, M, Kane, RL, Weston, SA, Dunlay, SM, Jiang, R, Roger, VL (2013). Measuring frailty in heart failure: A community perspective. Am Heart J. 166:768-774

Medi, C, Kalman, JM, Spence, SJ, Teh, AW, Lee, G, Bader, I, Kaye, DM, Kistler, PM. (2011). Atrial electrical and structural changes associated with hypertension in humans: implication for the substrate for atrial fibrillation. J Cardiovasc Electprhysiol. 22:1317-1324.

Mehta, PK and Griendling, KK. (2007). Angiotensin II cell signaling: physiological and pathological effects in the cardiovascular system. Am J Physiol Cell Phsyiol. 292:C82-C97

Mensah, GA, Croft, JB, Giles, WH. (2003). The heart, kidney, and brain as target organs in hypertension. Cardiol Clin. 20:303-319

Mesirca, P, Torrente, AG, Mangoni, ME. (2015). Functional role of voltage gated Ca^{2+} channels in heart automaticity. 6:1

Messerli, FH, Rimoldi, SF, Bangalore, S. (2017). The transition from hypertension to heart failure. JACC: Heart Failure. 5:543-551

Metra, M, Carubelli, V, Ravera, A, Stweart Coats, AJ. (2016). Heart failure 2016: still more questions than answers. International Journal of Cardiology. 227:766-777

Mezzano, V and Morley, GE. (2015). New insights into the complex effects of KChIP2 on calcium transients. Am J Physiol Heart Circ Phsyiol. 309:H553-H554

Milnes, JT, Madge, DJ, Ford, JW. (2012). New pharmacological approaches to atrial fibrillation. Drug Discovery Today. 17:654-659

Mirza, M, Strunets, A, Shen, W, Jahangir, A. (2012). Mechanisms of arrhythmias and conduction disorders in older adults. Clin Geriatr Med 28:555-573

Mitnitski, A, Song, X, Rockwood, K. (2013). Assessing biological aging: the origin of deficit accumulation. Biogerentology. 14:709-717

Mitnitski, AB, Graham, JE, Mogilner, AJ, Rockwood, K. (2002). Frailty, fitness and late-life mortality in relation to chronological and biological age. BMC Geriatrics. 2:1

Miyasaka, Y, Barnes, ME, Gersh, BJ, Cha, SS, Bailey, KR, Ahbayaratna, W, Seward, JB, Iwasaka, T, Tsang, TSM. (2006). Incidence of mortality risk of congestive heart failure in atrial fibrillation patients: a community-based study over two decades. European Heart Journal. 27:936-941.

Mizra, M, Strunets, A, Shen, W, Jahangir, A. (2012). Mechanisms of Arrhythmias and Conduction Disorders in Older Adults, In Clinics in Geriatric Medicine, Volume 28, Issue 4, Pages 555-573, ISSN 0749-0690, ISBN 9781455749348

Moghtadaei, M, Jansen, HJ, Mackasey, M, Rafferty, SA, Bogachev, O, Sapp, JL, Howlett, SE, Rose, RA. (2016b). The impacts of age and frailty on heart rate and sinoatrial node function. J Physiol. 549:7105-7126

Moghtadaei, M, Polina, I, Rose, RA. (2016a). Electrophysiological effects of natriuretic peptides in the heart are mediated by multiple receptor subtypes. Progress in Biophysics and Molecular Biology. 120:37-49.

Monfredi, O and Boyett, MR. (2015). Sick sinus syndrome and atrial fibrillation in older persons – A view from the sinoatrial node myocyte. Journal of Molecular and Cellular Cardiology. 83:88-100.

Morillo, CA, Klein, GJ, Jones, DL, Guiraudon, CM. (1995). Chronic rapid atrial pacing. Structural, functional, and electrophysiological characteristics of a new model of sustained atrial fibrillation. Circulation. 91:1588-1595.

Morris, GM and Kalman, JM. (2014). Fibrosis, electrics and genetics. Perspectives in sinoatrial node disease. Circulation Journal. 78:1272

Mukoyama, M, Nakao, K, Hosoda, K, Suga, S, Saito, Y, Ogawa, Y, Shirakami, G, Jougasaki, M, Obata, K, Yasue, H, Kambayashi, Y, Inouye, K, Imura, H. (1991). Brain natriuretic peptide as a novel cardiac hormone in humans. Evidence for an exquisite dual natriuretic peptide system, atrial natriuretic peptide and brain natriuretic peptide. J Clin Invest 87:1402–1412.

Naccarelli, GV and Peacock, F. (2009). Angiotensin II receptor blockers in the prevention of complications from atrial fibrillation. Vascular Health and Risk Management. 5:783-791.

Nakao, K, Ogawa, Y, Suga, S, Imura, H. (1992). Molecular biology and biochemistry of the natriuretic peptide system. II: Natriuretic peptide receptors. Journal of Hypertension. 10:1111-1114

Nassal, DM, Wan, X, Liu, H, Maleski, D, Ramirez-Navarro, A, Moravec, CS, Ficker, E, Laurita, KR, Deschenes, I. (2017). KChIP2 is a core transcriptional regulator of cardiac excitability. eLife 2017:6:e17304

Nattel, S and Harada M. (2014). Atrial Remodeling and Atrial Fibrillation: Recent Advances and Translational Perspectives. Journal of the American College of Cardiology. 63:2335-2345

Nattel, S, Burstein, B, Dobrev, D. (2008). Atrial Remodeling and Atrial Fibrillation Mechanisms and Implications. Circ Arrhythmia Electrophsyiol. 1:62-73

Nattel, S, Maguy, A, La Bouter, S, Yeh, Y. (2007). Arrhythmogenic ion-channel remodeling in the heart: Heart failure, myocardial infarction, and atrial fibrillation. Phsyiol Rev. 87:425-456

Nattel, S, Yue, L, Wang, Z. (1999). Cardiac ultrarapid delayed rectifiers: A novel potassium current family of functional similarity and molecular diversity. Cellular Physiology and Biochemistry. 9:217-226

Nattel, S. (2002). New ideas about atrial fibrillation 50 years on. Nature. 415:219-226

Nattel, S. (2008). Effects of Heart Disease on Cardiac Ion Current Density Versus Current Amplitude: Important Conceptual Subtleties in the Language of Arrhythmogenic Ion Channel Remodeling. Circ. Res. 102:1298-1300

Nerbonne, JM and Kass, RS. (2005). Molecular physiology of cardiac repolarization. Phsyiol Rev 85:1205-1253

Nerbonne, JM, Nichols, CG, Schwarz, TL, Escande, D. (2001). Genetic Manipulation of Cardiac K Channel Function in Mice: What Have We Learned, and Where Do We Go From Here? Circ Res. 89:944-956

Nguyen, TN, Cumming, RG, Hilmer, SN. (2016). The impact of frailty on mortality, length of stay, and re-hospitalisation in older patients with atrial fibrillation. Heart, Lung, and Circulation. 25:551 – 557.

Nishikimi, T, Yoshihara, F, Morimoto, A, Ishikawa, K, Ishimitsu, T, Saito, Y, Kangawa, K, Matsuo, H, Omae, T, Matsuoka, H. (1996). Relationship between left ventricular geometry and natriuretic peptide levels in essential hypertension. Hypertension 28:22-30.

Niwa, N and Nerbonne, JM. (2010). Molecular determinants of cardiac transient outward potassium current (I_{to}) expression and regulation. JMCC 48:12

Ogawa, Y, Itoh, H, Tamura, N, Suga, S, Yoshimasa, T, Uehira, M, Matsuda, S, Shiono, S, Nishimoto, H, Nakao, K. (1994). Molecular cloning of the complementary DNA and gene that encode mouse brain natriuretic peptide and generation of transgenic mice that overexpress the brain natriuretic peptide gene. J Clin Invest. 93:1911–1921.

Ogawa Y, Nakao K, Mukoyama M, Hosoda K, Shirakami G, Arai H, Saito Y, Suga S, Jougasaki M, Imura H. (1991). Natriuretic peptides as cardiac hormones in normotensive and spontaneously hypertensive rats-The ventricle is a major site of synthesis and secretion of brain natriuretic peptide. Circ Res. 69:491-500.

Ogawa, T and de Bold, AJ. (2004). The heart as an endocrine organ. Endocrine Connections. 3:R31-R44

Oh, S, Kim, K, Ahn, H, Cho, H, Choi, Y. (2010). Remodeling of Ion Channel Expression in Patients with Chronic Atrial Fibrillation and Mitral Valvular Heart Disease. Korean J Intern Med. 25:377-385

Oliver, PM, Fox, JE, Kim, R, Rockman, HA, Kim, HS, Reddick, RL, Pandey, KN, Milgram, SL, Smithies, O, Maeda, N. (1997). Hypertension, cardiac hypertrophy, and sudden death in mice lacking natriuretic peptide receptor A. Proc Natl Acad Sci USA. 94:14730-14735

Olivotto, I, Cecchi, F, Casey, SA, Dolara, A, Traverse, H, Maron, BJ. (2001). Impact of atrial fibrillation on the clinical course of hypertrophic cardiomyopathy. Circulation. 104:2517-2524.

Opthof, T. (1988). The mammalian sinoatrial node. Cardiovasc Drugs Ther, 1, 573-97.

Ozdemir, O. (2004). P-wave durations as a predictor for atrial fibrillastion development in patients with hypertrophic cardiomyopathy. International Journal of Cardiology. 94:163-166

Padfield, GJ, Steinberg, C, Swampillai, J, Qian, H, Connology, SJ, Dorian, P, Green, MS, Humphries, KH, Klein, GJ, Sheldon, R, Taljic, M, Kerr, CR. (2017). Progression of paroxysmal to persistent atrial fibrillation:10-year follow-up in the Canadian Registry of Atrial Fibrillation. Heart Rhythm, 14:801- 807.

Pandey, KN. (2005). Biology of natriuretic peptides and their receptors. Peptides. 26:901-932.

Pandey, A, Kim, S, Moore, C, Thomas, L, Gersh, B, Allen, LA, Kowey, PR, Mahaffey, KW, Hylek, E, Peterson, ED, Piccini, JP, Fonarow, GC. (2017). Predictors and prognostic implications of incident heart failure in patients with prevalent atrial fibrillation. JACC: Heart Failure. 5:44-52

Pandey, KN. (2008). Emerging roles of natriuretic peptides and their receptors in pathophysiology of hypertension and cardiovascular regulation. Journal of the American Society of Hypertension 2:210-226

Paradis, P, Dali-Youcef, N, Paradis, FW, Thibault, G, Nemer, M. (2000). Overexpression of angiotensin II type I receptor in cardiomyocytes induces cardiac hypertrophy and remodeling. Proc Natl Acad Sci USA. 97:931–936.

Parikh, A, Patel, D, McTiernan, CF, Xiang, W, Haney, J, Yang, L, Lin, B, Kaplan, AD, Bett, GCL, Rasmusson, RL, Shroff, SG, Schwatzman, D, Salama, G. (2013). Relaxin Suppresses Atrial Fibrillation by Reversing Fibrosis and Myocyte Hypertrophy and Increasing Conduction Velocity and Sodium Current in Spontaneously Hypertensive Rat Hearts. Circ Res. 113:313-321

Park, BH, Kim, SY, Kim, SM, Noh, HJ, Cho, CG, Kim, SZ. (2015). Characteristics of dendroaspis natriuretic peptide and its receptor in streptozotocin-induced diabetic rats. Molecular Medicine Reports. 12:2969-2976

Park, J, Shim, J, Uhm, J, Joung, B, Lee, M, Pak, H. (2013). Post-shock sinus node recovery time is an independent predictor of recurrence after catheter ablation of longstanding persistent atrial fibrillation. International Journal of Cardiology. 168:1937-1942.

Parks, RJ, Fares, E, MacDonald, JK, Ernst, MC, Sinal, CJ, Rockwood, K, Howlett, SE. (2012). A Procedure for Creating a Frailty Index Based on Deficit Accumulation in Aging Mice. J Gerentol A Biol Sci Med Sci. 67A:217-227

Parthasarathy, A, Gopi, V, Umadevi, S, Simna, A, Sheik, MJ, Divya, H, Vellaichamy, E. (2013). Suppression of atrial natriuretic peptide/natriuretic peptide receptor-A-mediated signaling upregulates angiotensin-II-induced collagen synthesis in adult cardiac fibroblasts. Mol Cell Biochem. 378:217-228.

Patel, S, Raug, A, Khan, H, Abu-Izneid, T. (2017). Renin-angiotensin-aldosterone (RAAS): The ubiquitous system for homeostasis and pathologies. Biomedicine & Pharmacotherapy. 94:317-325.

Pauza, DH, Rysevaite, K, Inokaitis, H, Jokubauskas, M, Pauza, AG, Brack, KE, Pauziene, N. (2014). Innervation of sinoatrial nodal cardiomyocytes in mouse. A combined approach using immunofluorescent and electron microscopy. J Mol Cell Cardiol. 75:188-197.

Pauza, DH, Saburkina, I, Rysevaite, K, Inokaite, K, Inokaitis, H, Jokubauskas, M, Jalife, J, Pauzeine, N. (2013). Neuroanatomy of the murine cardiac conduction system: a combined stereomicroscopic and fluorescence immunohistochemical study. Auton Neurosci. 176:32-47.

Perrier, E, Kerfant, B, Lalevee, N, Bideaux, P, Rossier, MF, Richard, S, Gomez, AM, Benitah, J. (2004). Mineralocorticoid Receptor Antagonism Prevents the Electrical Remodeling That Precedes Cellular Hypertrophy After Myocardial Infarction. Circulation. 110:776-783

Polidoro, A, Stefanelli, F, Ciacciarelli, M, Pacelli, A, Di Sanzo, D, Alessandri, C. (2013). Frailty in patients affected by atrial fibrillation. Archives of Gerontology and Geriatrics. 57:325- 327.

Potter, LR, Abbey-Hosch, S, Dickey, DM. (2006). Natriuretic Peptides, Their Receptors, and Cyclic Guanosine Monophosphate-Dependent Signaling Functions. Endocrine Reviews. 27:47-72

Potter, LR, Yoder, AR, Flora, DR, Antos, LK, Dickey, DM. (2009). Natriuretic Peptides: Their Structures, Receptors, Physiologic Functions and Therapeutic Applications. Handb Exp Pharmacol. 191:341-366

Prabhu, S, Voskoboinik, A, Kaye, DM, and Kistler, PM. (2017). Atrial fibrillation and heart failure – cause or effect? Heart, Lung and Circulation. 26:967-974.

Prisant, LM. (2005). Hypertensive heart disease. The Journal of Cliical Hypertension. 4:231-238.

Purohit, A, Rokita, AG, Guan, X, Xhen, B, Koval, OM, Voigt, N, Neef, S, Sowa, T, Gao, Z, Luczak, ED, Stefansdottir, H, Behunin, AC, Li, N, El-Accaoui, RN, Yang, B, Swaminathan, PD, Weiss, RM, Wehrens, XHT, Song, L, Dobrev, D, Maier, LS, Anderson, ME. (2013). Oxidized Ca^{2+}/Calmodulin-Dependent Protein Kinase II Triggers Atrial Fibrillation. Circulation. 128:1748-1757

Rahman, F, Kwan, GF, Benjamin, EJ. (2014). Global epidemiology of atrial fibrillation. Nat. Rev. Cardiol. 11:639- 654

Ravens, U, and Odening, KE. (2017). Atrial fibrillation: Therapeutic potential of atrial K^+ channel blockers. Pharmacology & Therapeutics. 176:13-21.

Ravens, U, and Wettwer, E. (2011). Ultra-rapid delayed rectifier channels: molecular basis and therapeutic implications. Cardiovasc Res. 89:776-785.

Redondo, J, Bishop, JE, Wilkins, MR. (1998). Effect of atrial natriuretic peptide and cyclic GMP phosphodiesterase inhibition on collagen synthesis by adult cardiac fibroblasts. Br J Pharmacol 124:1455–1462.

Rivard K, Grandy SA, Douillette A, Paradis P, Nemer M, Allen BG, Fiset C. (2011). Overexpression of type 1 angiotensin II receptors impairs excitation-contraction coupling in the mouse heart. Am J Physiol Heart Circ Physiol. 301: H2018–H2027.

Rivard, K, Paradis, P, Nemer, M, Fiset, C. (2008). Cardiac-specific overexpression of the human type 1 angiotensin II receptor causes delayed repolarization. Cardiovasc Res 78:53–62.

Rockwood, K and Mitnitski, A. (2011). Frailty defined by deficit accumulation and geriatric medicine defined by frailty. Clin Geriatr Med. 27:17-26

Rockwood, K and Mitnitski, A. (2007). Frailty in relation to the accumulation of deficits. Journal of Gerontology: Medical Sciences. 62A:722-727

Rockwood, K, Blodgett, JM, Theou, O, Sun, MH, Feridooni, HA, Mitnitski, A, Rose, RA, Godin, J, Gregson, E, Howlett, SE. (2017). A frailty index based on deficit accumulation quantifies mortality risk in humans and in mice. Scientific Reports. 7:43068.

Rook, MB, Evers, MM, Vos, MA, Bierhuizen, MFA. (2012). Biology of cardiac sodium channel $Na_V1.5$ expression. Cardiovascular Research. 93:12-23

Rosati, B, Pan, Z, Lypen, S, Wang, HS, Cohen, I, Dixon, JE, McKinnon, D. (2001). Regulation of KChIP2 potassium channel beta subunit gene expression underlies the gradient of transient outward current in canine and human ventricle. The Journal of Physiology. 533:119–125.

Rosati, B, Grau, F, Rodriguez, S, Li, H, Nerbonne, JM, McKimmon, D. (2003). Concordant expression of KChIP2 mRNA, protein and transient outward current through the canine ventricle. J Physiol. 548:815-822

Rose, J, Armoundas, AA, Tian, Y, DiSilvestre, D, Burysek, M, Halperin, V, O'Rourke, B, Kass, DA, Marban, E, Tomaselli, GF. (2005). Molecular correlates of altered expression of potassium currents in failing rabbit myocardium. Am J Physiol Heart Circ Physiol. 288:H2077-H2087

Rose, RA and Giles, WR. (2008). Natriuretic peptide C receptor signalling in the heart and vasculature. J Physiol. 2:353-366

Rose, RA, Lomax, AE, Kondo, CS, Anand-Srivastava, MB, Giles, WR. (2004). Effects of C-type natriuretic peptide on ionic currents in mouse sinoatrial node: a role for the NPR-C receptor. Am J Physiol Heart Circ Phsyiol. 286:H1970-H1977

Rubattu, S, Sciarretta, S, Valenti, V, Stanzione, R, Volpe, M. (2008). Natriuretic Peptides: An Update on Bioactivity, Potential Therapeutic Use, and Implication in Cardiovascular Diseases. American Journal of Hypertension. 21:733-741

Sadoshima, J, Xu, Y, Slayter, HS, Izumo, S. (1993). Autocrine release of Angiotensin II mediates stretch-induced hypertrophy of cardiac myocytes in vitro. Cell. 75:977-984.

Sanders, P, Morton, JB, Davidson, NC, Spence, SJ, Vohra, JK, Sparks, PB, Kalman, JM (2003). Electrical remodeling of the atria in congestive heart failure: Electrophysiological and electroanatomic mapping in humans. Circulation. 108:1461–1468.

Schirger, JA, Heublein, DM, Chen, HH, Lisy, O, Jougasaki, M, Wennberg, PW, Burnett, JC. (1999). Presence of Dendroaspis Natriuretic Peptide-like Immunoreactivity in Human Plasma and its Increase During Human Heart Failure. Mayo Clin Proc. 74:126-130

Schmidt, C, Wiedmann, F, Kallenberger, SM, Ratte, A, Schulte, JS, Scholz, B, Ulrich Muller, F, Voigt, N, Zafeiriou, M, Ehrlich, JR, Tochtermann, U, Veres, G, Ruhparwar, A, Karck, M, Katus, HA, Thomas, D. (2017). Stretch-activated two-pore-domain (K_{2P}) potassium channels in the heart: Focus on atrial fibrillation and heart failure. Progress in in Biophysics and Molecular Biology.
http://dx.doi.org/10.1016/j.pbiomolbio.2017.05.004

Schmitt, N, Grunnet, M, Olsen, S. (2014). Cardiac potassium channel subtypes: new roles in repolarization and arrhythmia. Phsyiol Rev. 94:609-653

Schoonderwoerd, BA, Van Gelder, IC, Van Veldhiusen, DJ, Van den Berg, MP, Crijns, HJGM. (2005). Electrical and structural remodeling: Role in the genesis and maintenance of atrial fibrillation. Progress in Cardiovascular Diseases. 48:153-168.

Schotten, U, Verheule, S, Kirchhof, P, Goette, A. (2011). Pathophysiological mechanisms of atrial fibrillation: A translational appraisal. Physiol Rev. 91:265-325

Schram, G, Pourrier, M, Melnyk, P, Nattel, S. (2002). Differential Distribution of Cardiac Ion Channel Expression as a Basis for Regional Specialization in Electrical Function. Circ Res. 90:939-950

Schweitz, H, Vigne, P, Moinier, D, Frelin, C, Lazdunski, M (1992). A new member of the natriuretic peptide family is present in the venom of the green mamba (Dendroaspis angusticeps). J Biol Chem. 267:13928–13932

Searle, SD, Mitnitski, A, Gahbauer, EA, Gill, TM, Rockwood, K. (2008). A standard procedure for creating a frailty index. BMC Geriatrics. 8:24

Seccia, TM, Caroccia, B, Muiesan, ML, Rossi, GP. (2016). Atrial fibrillation and arterial hypertension: A common duet with dangerous consequences where the renin angiotensin-aldosterone system plays an important role. International Journal of Cardiology. 206:71-76.

Sergeeva, IA and Christoffels, VM. (2013). Atrial fibrillation and arterial hypertension: A common duet with dangerous consequences where the renin angiotensin-aldosterone system plays an important role. Biochemica et Biophysica Acta. 1832:2403-2413.

Shang, LL, Sanyal, S, Pfahnl, AE, Jiao, Z, Allen, J, Liu, H, Dudley, SC. (2008). NF-κB-dependent transcriptional regulation of the cardiac scn5a sodium channel by angiotensin II. Am J Physiol Cell Physiol. 294:C372-C379

Sharpe, EJ, Larson, ED, Proenza, C. (2017). Cyclic AMP reverses the effects of aging on pacemaker activity and I_f in sinoatrial node myocytes. The Journal of General Physiology. 149:237-247

Shimizu, I and Minamino, T. (2016). Physiological and pathological cardiac hypertrophy. Journal of Molecular and Cellular Cardiology. 97:245-262

Si, M, Xu, J, Zhang, F, Wang, C, Du, X, Zhang, H. (2013). Involvement of Protein Kinase A and C in Norepinephrine- and Angiotensin II-Induced Modulation of Cardiac IKs. Pharmacology. 92:217-226

Siontis, KC, Geske, JB, Ong, K, Nishimura, RA, Ommen, SR, Gersh, BJ. (2014). Atrial fibrillation in hypertrophic cardiomyopathy: prevalence, clinical corrections, and mortality in a large high-risk population. J Am Heart Assoc. 3:e001002

Sirish, P, Li, N, Timofeyev, V, Zhang, X, Wang, L, Yang, J, Lee, KSS, Bettaieb, A, Ma, SM, Lee, JK, Su, D, Lau, VC, Meyers, RE, Lieu, DK, Lopez, JE, Young, JN, Yamoah, EN, Haj, F, Ripplinger, CM, Hammock, BD, Chiamvimonvat, N. (2016). Molecular mechanisms and new treatment paradigm for atrial fibrillation. Circ Arrhythm Electrophsyiol. 9:e003721.

Smith, JW, O'Neal, WT, Shoemaker, MB, Chen, LY, Alonso, A, Whalen, SP, Soliman, EZ. (2017). PR-interval components and atrial fibrillation risk (from the atherosclerosis risk in communities study). Am J Cardiol. 119:466-472

Smith, MW, Espiner, EA, Yandle, TG, Charles, CJ, Richards, AM. (2000). Delayed metabolism of human brain natriuretic peptide reflects resistance to neutral endopeptidase. J Endocrinol 167:239-246

Soeki, T, Kishimoto I, Okumura, H, Tokudome, T, Horio T, Mori, K, Kangawa, K (2005). C- type natriuretic peptide, a novel antifibrotic and antihypertrophic agent, prevents cardiac remodeling after myocardial infarction. J Am Coll Cardiol 45:608–616.

Song, Y, Shryock, JC, Belardinelli, L, (2008). An increase of late sodium current induces delayed afterdepolarizations and sustained triggered activity in atrial myocytes. Am J Physiol Heart Circ Physiol. 294:H2031-H2039.

Souders, CA, Bowers, SLK, Baudino, TA. (2009). Cardiac fibroblast: The renasissance cell. Circ Res. 105:1164-1176

Springer, J, Azer, J, Hua, R, Robbins, C, Adamczyk, A, McBoyle, S, Bissell, MB, Rose, R.A. (2012). The natriuretic peptides BNP and CNP increase heart rate and electrical conduction by stimulating ionic currents in the sinoatrial node and atrial myocardium following activation of guanylyl cyclase-linked natriuretic peptide receptors. J. Mol. Cell. Cardiol. 52, 1122e1134.

Stambler, BS, Fenelon, G, Shepard, RK, Clemo, HF, Guiraudon, CM. (2003). Characterization of sustained atrial tachycardia in dogs with rapid ventricular pacing-induced heart failure. J Cardiovasc Electrophysiol. 14:499-507.

Steinhelper, ME, Cochrane, KL, Field, LJ. (1990). Hypotension in transgenic mice expressing atrial natriuretic factor fusion genes. Hypertension 16:301–307.

Sudoh, T, Kangawa, K, Minamino, N and Matsuo, H. (1998). A new natriuretic peptide in porcine brain. Nature 332:78-81

Sudoh, T, Minamino, N, Kangawa, K and Matsuo, H. (1990). C-type natriuretic peptide (CNP): a new member of natriuretic peptide family identified in porcine brain. Biochem Biophys Res Commun 168:863-870

Swaminathan, PD, Purohit, A, Soni, S, Voigt, N, Singh, MV, Glukhov, AV, Gao, Z, He, BJ, Luczak, ED, Joiner, MA, Kutschke, W, Yang, J, Donahue, JK, Weiss, RM, Grumbach, IM, Ogawa, M, Chen, P, Efimov, I, Dobreb, D, Mohler, PJ, Hund, TJ, Anderson, ME. (2011). Oxidized CaMKII causes cardiac sinus node dysfunction in mice. J Clin Invest. 121:3277-3288.

Tadevosyan, A, Xiao, J, Surinkaew, S, Naud, P, Merlen, C, Harada, M, Qi, X, Chatenet, D, Fournier, A, Allen, BG, Nattel, S. (2017). Intracellular Angiotensin-II Interacts With Nuclear Angiotensin Receptors in Cardiac Fibroblasts and Regulates RNA Synthesis, Cell Proliferation, and Collagen Secretion. J Am Heart Assoc. 6:e004965

Takemura, G, Fujiwara, H, Mukoyama, M, Saito, Y, Nakao, K, Kawamura, A, Ishida, M, Kida, M, Uegaito, T, Tanaka, M, Matsumori, A, Fujiwara, T, Imura, H, Kawai, C. (1991). Expression and distribution of atrial natriuretic peptide in human hypertrophic ventricle of hypertensive hearts and hearts with hypertrophic cardiomyopathy. Circulation. 83:181-190.

Tamura, N, Ogawa, Y, Chusho, H, Nakamura, K, Nakao, K, Suda, M, Kasahara, M, Hashimoto, R, Katsuura, G, Mukoyama, M, Itoh, H, Saito, Y, Tanaka, I, Otani, H, Katsuki, M. (2000). Cardiac fibrosis in mice lacking brain natriuretic peptide. Proc Natl Acad Sci U S A 97:4239–4244.

Tellez, JO, Dobryzinski, H, Greener, ID, Graham, GM, Laing, E, Honjo, H, Hubbard, SJ, Boyett, MR, Billeter, R. (2006). Differential expression of ion channel transcripts in atrial muscle and sinoatrial node in rabbit. Circ Res. 99:1384-1393.

Tellez, JO, Maczewski, M, Yanni, J, Sutyagin, P, Mackiewicz, U, Atkinson, A, Inada, S, Beresewicz, A, Billeter, R, Dobrzynski, H, Boyett, MR. (2011). Ageing-dependent remodelling of ion channel and Ca^{2+} clock genes underlying sino-atrial node pacemaking. Exp Physiol. 96:1163-1178

Thomsen, MB, Sosunov, EA, Anyukhovsky, EP, Ozgen, N, Boyden, PA, Rosen, MR. (2009b). Deleting the accessory subunit KChIP2 results in loss of $I_{to,f}$ and increased $I_{K,slow}$ that maintains normal action potential configuration. Heart Rhythm. 6:370-377

Thomsen, MB, Wang, C, Ozgen, N, Wang, H, Rosen, MR, Pitt, GS. (2009a). Accessory subunit KChIP2 modulates the cardiac L-type calcium current. Circ. Res. 104:1382-1389

Tilman, V. (2014). Atrial fibrillation and heart failure: Is atrial fibrillation a disease? Medical Hypotheses 83:299-301

Titus, JL. (1973). Anatomy of the conduction system. Circulation. 47:170-177

Tozakidou, M, Boltz, D, Hagenstrom, T, Budack, MK, Vitzthum, H, Szlachta, K, Bahring, R, Ehmke, H. (2010). Molecular and functional remodeling of Ito by angiotensin II in the mouse left ventricle. Journal of Molecular and Cellular Cardiology. 48: 140-151.

Trepanier-Boulay, V, St-Michel, C, Tremblay, A, Fiset, C. (2001). Gender-based differences in cardiac repolarization in mouse ventricle. Circ Res. 89:437-444.

Triposkiadis, F, Karayannis, G, Giamouzis, G, Skoularigis, J, Lourdis, G, and Butler, J. (2009). The sympathetic nervous system in heart failure. Physiology, pathophysiology, and clinical implications. J Am Coll Cardiol 54:1747-1762

Tsai, C, Lai, L, Kuo, K, Hwang, J, Hsieh, C, Hsu, K, Tseng, C, Tseng, Y, Chiang, F, Lin, J. (2008). Angiotensin II activates signal transducer and activators of transcription 3 via Rac1 in atrial myocytes and fibroblasts. Circulation. 117:344-355.

Tsai, C, Wang, DL, Chen, W, Hwang, J, Hsieh, C, Hsu, K, Tseng, C, Lai, L, Tseng, Y, Chiang, F, Lin, J. (2007). Angiotensin II Increases Expression of 1C Subunit of L-Type Calcium Channel Through a Reactive Oxygen Species and cAMP Response Element–Binding Protein–Dependent Pathway in HL-1 Myocytes. Circ Res. 100:1476-1485.

Tsai, EJ and Kass, DA. (2009). Cyclic GMP signaling in cardiovascular pathophysiology and therapeutics. Pharmacology & Therapeutics. 122:216-238.

Tsukamoto, Y, Mano, T, Sakata, Y, Ohtani, T, Takeda, Y, Tamaki, S, Omiri, Y, Ikeya, Y, Saito, Y, Ishii, R, Higashimori, M, Kaneko, M, Miwa, T, Yamomoto, K, and Komuro, I. (2013). A novel heart failure mice model of hypertensive heart disease by angiotensin II infusion, nephrectomy, and salt loading. AM J Physiol Heart Circ Physiol. 305: H1658-H1667.

Udyavar, AR, Chen, Y, Chen, Y, Cheng, C, Lin, C, Chen, S. (2008). Endothelin-1 modulates the arrhythmogenic activity of pulmonary veins. J Cardiovasc Electrophysiol. 19:285-292

Vaidean, GD, Manczuk, M, Magnani, JW. (2016). Atrial electrocardiography in obesity and hypertension: Clinical insights from the Polish-Norwegian Study (PONS). Obesity. 24:2608 – 2614

Vaidya, K, Semsarian, C, Chan, KH. (2017). Atrial Fibrillation in Hypertrophic Cardiomyopathy. Heart, Lung and Circulation. 26:975-982

van der Heyden, MAG, Wijnhoven, TJM, Opthof, T. (2006). Molecular aspects of adrenergic modulation of the transient outward current. Cardiovascular Research. 71:430-442

van Kats, JP, Methot, D, Parsdis, P, Silversides, DW, and Reudelhuber, TL. (2001). Use of a biological peptide pump to study chronic peptide hormone action n transgenic mice. The Journal of Biological Chemistry. 276:44012-44017

Van Wagoner, DR and Nerbonne, JM. (2000). Molecular basis of electrical remodelling in atrial fibrillation. J Mol Cell Cardiol. 32:1101-1117

Van Wagoner, DR, Pond, AL, Lamorgese, M, Rossie, SS, McCarthy, PM, Nerbonne, JM. (1999). Atrial L-type Ca2+ currents and human atrial fibrillation. Circ Res. 85:428-436.

Van Wagoner, DR, Pond, AL, McCarthy, PM, Trimmer, JS, Nerbonne, JM. (1997). Outward K+ current densities and Kv1.5 expression are reduced in chronic human atrial fibrillation. Circ Res. 80:772-81.

Veerman, CC, Wilde, AAM, Lodder, EM. (2015). The cardiac sodium channel gene SCN5A and its gene product $Na_v1.5$: Role in physiology and pathophysiology. Gene. 573:177-187

Verkerk, AO, Wilders, R, Coronel, R, Ravesloot, JH, Verheijck, EE. (2003). Ionic Remodeling of Sinoatrial Node Cells by Heart Failure. Circulation. 108:760-766

Voigt, N, Trausch, A, Knaut, M, Matschke, K, Varro, A, Van Wagoner, DR, Nattel, S, Ravens, U, Dobrev, D. (2010). Left-to-right atrial inward rectifier potassium current gradients in patients with paroxysmal verses chronic atrial fibrillation. Circ Arrhythm Electrophysiol. 3:472-480

Volpe, M, Carnovali, M, Mastromarino, V. (2016). The natriuretic peptides system in the pathophysiology of heart failure: from molecular basis to treatment. Clinical Science. 130:57-77

Wagner, S, Dantz, C, Flebbe, H, Azizian, A, Sag, CM, Engels, S, Mollencamp, J, Dybkova, N, Islam, T, Shah, AM, Maier, LS. (2014). NADPH oxidase 2 mediates angiotensin II-dependent cellular arrhythmias via PKA and CaMKII. Journal of Molecular and Cellular Cardiology. 75:206-215.

Wagner, S, Hacker, E, Grandi, E, Weber, SL, Dybkova, N, Sossalla, S, Sowa, T, Fabritz, L, Kirchhof, P, Bers, DM, Maier, LS. (2009). Ca/Calmodulin kinase II differentially modulate potassium currents. Cir Arrhythmia Electrophysiol. 2:285-294.

Wagner, S, Ruff, HM, Weber, SL, Bellmann, S, Sowa, T, Schulte, T, Anderson, ME, Grandi, E, Bers, DM, Backs, J, Belardinelli, L, Maier, LS. (2011). Reactive Oxygen Species–Activated Ca/Calmodulin Kinase II Is Required for Late I_{Na} Augmentation Leading to Cellular Na and Ca Overload. Circ Res. 108:555-565

Wakili, R, Voigt, N, Kaab, S, Dobrev, D, Nattel, S. (2011). Recent advances in the molecular pathophysiology of atrial fibrillation. J Clin Invest. 121:2955–2968.

Wakisaka, O, Takahashi, N, Shinohara, T, Ooie, T, Nakagawa, M, Yonemochi, H, Hara, M, Shimada, T, Saikawa, T, Yoshimatsu, H. (2007). Hyperthermia treatment prevents angiotensin II-mediated atrial fibrosis and fibrillation via induction of heat-shock protein 72. Journal of Molecular and Cellular Cardiology. 43:616-626.

Wakui, H, Tamura, K, Tanaka, Y, Matsuda, M, Bai, Y, Dejima, T, Masuda, S, Shigenaga, A, Maeda, A, Mogi, M, Ichihara, N, Kobayashi, Y, Hirawa, N, Ishigami, T, Toya, Y, Yabana, M, Horiuchi, M, Minamisawa, S, Umemura. (2010). Cardiac-Specific Activation of Angiotensin II Type 1 Receptor–Associated Protein Completely Suppresses Cardiac Hypertrophy in Chronic Angiotensin II–Infused Mice. Hypertension. 55:1157-1164

Wang, D, Gladysheva, IP, Fan, TM, Sullivan, R, Houng, AK, Reed, GL. (2014). Atrial natriuretic peptide affects cardiac remodeling, function, heart failure, and survival in a mouse model of dilated cardiomyopathy. Hypertension. 63:514-519

Wang, D, Oparil, S, Feng, JA, Li, P, Perry, G, Chen, LB, Dai, M, John, SWM, Chan, Y. (2003). Effects of pressure overload on extracellular matrix expression in the heart of the atrial natriuretic peptide-null mouse. Hypertension. 42:88-95.

Wang, YH, Shi, CX, Dong, F, Sheng, JW, Xu, YF. (2008). Inhibition of the rapid component of the delayed rectifier potassium current in ventricular myocytes by angiotensin II via the AT1 receptor. British Journal of Pharmacology. 154:429-439.

Wang, Z, Fermini, B, Nattel, S. (1993). Sustaiined Depolarization-Induced Outward Current in Human Atrial Myocytes Evidence for a Novel Delayed Rectifier K' Current Similar to Kvl.5 Cloned Channel Currents. Circ Res. 73:1061-1076.

Wei, CM, Heublein DM, Perrella, MA, Lerman, A, Rodeheffer, RJ, McGregor, CG, Edwards, WD, Schaff, HV, Burnett JC Jr. (1993). Natriuretic peptide system in human heart failure. Circulation 88:1004-1009

Wei, T, Huang, G, Gao, J, Huang, C, Sun, M, Wu, J, Bu, J, Shen, W. (2017). Sirtuin 3 Deficiency Accelerates Hypertensive Cardiac Remodeling by Impairing Angiogenesis. J Am Heart Assoc. 6:e006114

Weinsaft, JW, Kochav, JD, Kim, J, Gurevich, S, Volo, SC, Afroz, A, Petashnick, M, Kim, A, Devereux, RB, Okin, PM (2014). P Wave Area for Quantitative Electrocardiographic Assessment of Left Atrial Remodeling. PLoS ONE. 9:e99178

Weiss, JN, Garfinkel, A, Karagueuzian, HS, Chen, P, Qu, Z. (2010). Early afterdepolarizations and cardiac arrhythmias. Heart Rhythm. 7:1891-1899.

Westermann, D, Becher, PM, Lindner, D, Savvatis, K, Xia, Y, Frohlich, M, Hoffmann, S, Schultheiss, K, Tschope, C. (2012). Selective PDE5A inhibition with sildenafil rescues left ventricular dysfunction, inflammatory immune response and cardiac remodeling in angiotensin II-induced heart failure in vivo. Basic Res Cardiol. 107:308

Wettersten, N and Maisel, AS. (2016). Biomarkers for heart failure: An update for practitioners of internal medicine. The American Journal of Medicine. 129:560-567.

Whitehead, JC, Hildebrand, BA, Sun, M, Rockwood, MR, Rose, RA, Rockwood, K, Howlett, SE. (2014). A Clinical Frailty Index in Aging Mice: Comparisons With Frailty Index Data in Humans. J Gerentol A Biol Sci Med Sci. 69:621-632

Wijffels, MC, Kirchhof, CJ, Dorland, R, Allessie, MA. (1995). Atrial fibrillation begets atrial fibrillation. A study in awake chronically instrumented goats. Circulation. 92:1954-1968.

Wollert, KC and Drexler, H. (1999). The renin-angiotensin system and experimental heart failure. Cardiovascular Research. 43:838-849

Wongcharoen, Q, Chen, Y, Chen, Y, Lin, C, Chen, S. (2007). Effects of Aging and Ouabain on Left Atrial Arrhythmogenicity. J Cardiovasc Electrophysiol. 18:526-531
Woodrow, P. (2009). An introduction to electrocardiogram interpretation: part 1. Nursing Standard. 24:50-57

Woods, RL. (2004). Cardioprotective functions of atrial natriuretic peptide and B-type natriuretic peptide: A brief review. Clinical and Experimental Pharmacology and Physiology. 31:791-794

Wozakowska-Kaplon, B. (2009). Changes in plasma natriuretic peptide levels in patients with atrial fibrillation after cardioversion. International Journal of Cardiology. 144:436-437.

Wright, GA and Struthers, AD. (2006). Natriuetic peptides as a prognostic marker and therapeutic target in heart failure. Heart. 92:149-151.

Xu, G, Gan, T, Tang, B, Chen, Z, Jiang, T, Song, J, Guo, X, Li, J. (2013). Age-related changes in cellular electrophysiology and calcium handling for atrial fibrillation. J Cell Mol Med 17:1109-1118

Xu, W and Lipscombe, D. (2001). Neuronal $Ca_V1.3_{\alpha1}$ L-type channels activate at relatively hyperpolarized membrane potentials and are incompletely inhibited by dihydroprydines. The Journal of Neuroscience. 21:5944-5951

Yang, C, Chen, MY, Chen, T, Cheng, C. (2014). Dose-dependent effects of isoflurane on cardiovascular function in rats. Tzu Chi Medical Journal. 26:119-122

Yang, K and Nerbonne, JM. (2016). Mechanisms contributing to myocardial potassium channel diversity, regulation and remodeling. Trends in Cardiovascular Medicine. 26:209-218

Yeh, YH, Burstein, B, Qi, XY, Sakabe, M, Chartier, D, Comtois, P, Wang, Z, Kuo, C, Nattel, S. (2009). Funny current downregulation and sinus node dysfunction associated with atrial tachyarrhythmia: a molecular basis for tachycardia- bradycardia syndrome. Circulation. 119:1576–1585.

Yue, L, Melnyk, P, Gaspo, R, Wang, Z, Nattel, S. (1999). Molecular mechanisms underlying ionic remodeling in a dog model of atrial fibrillation. Circ Res. 84:776-784

Yue, L, Xie, J, Nattel, S. (2011). Molecular determinants of cardiac fibroblast electrical function and therapeutic implications for atrial fibrillation. Cardiovascular Research. 89:744-753

Zaccolo, M, and Movsesian, MA. (2007). cAMP and cGMP signaling cross-talk: role of phosphodiesterases and implications for cardiac pathophysiology. Circ Res. 100:1569-1578.

Zaza, A, Belardinelli, L, Shyrock, JC. (2008). Pathophysiology and pharmacology of the cardiac “late sodium current”. Pharmacology and Therapeutics. 119:326-339

Zegkos, T, Efthimiadis, GK, Parcharidou, DG, Gossios, TD, Giannakoulas, G, Ntelios, D, Ziakas, A, Paraskevaidis, S, Karvounis, HI. (2017). Atrial fibrillation in hypertrophic cardiomyopathy: a turning point towards increased morbidity and mortality. Hellenic Journal of Cardiology. in press.

Zhang, S, Geng, X, Zhao, L, Li, J, Tian, F, Wang, Y, Fan, R, Feng, N, Liu, J, Cheng, L, Pei, J. (2015). Cardiovascular and renal effect of C_NAA_C: An innovatively designed natriuretic peptide. European Journal of Pharmacology. 761:180-188

Zhang, S, Zhoa, H, Gu, X, Li, J, Feng, N, Wang, Y, Fan, R, Chen, W, Pei, J. (2017). A new chimeric natriuretic peptide, C_NAA_C, for the treatment of left ventricular dysfunction after myocardial infarction. Scientific Reports. 7:10099.

Zhang, Z, He, Y, Tuteja, D, Xu, D, Timofeyev, V, Zhang, Q, Glatter, KA, Xu, Y, Shin, H, Low, R, Chiamvimonvat, N. (2005). Functional roles of $Ca_v1.3(\alpha_{1D})$ calcium channels in atria: Insights gained from gene-targeted null mutant mice. Circulation. 112:1936-1964

Zhao, J, Liu, T, Li, G. (2014). Relationship between two arrhythmias: Sinus node dysfunction and atrial fibrillation. Archives of Medical Research 45:351-355

Zhou, H and Murthy, KS. (2003). Identification of the G protein-activating sequence of the single-transmembrane natriuretic peptide receptor C (NPR-C). Am J Physiol Cell Physiol. 284:C1255-C1261

Ziaeian, B and Fonarow, GC. (2016). Epidemiology and aetiology of heart failure. Nature. 13:368-378